The WDR5 interaction network

By

Alissa duPuy Guarnaccia

Dissertation

Submitted to the Faculty of the

Graduate School of Vanderbilt University

in partial fulfillment of the requirements

for the degree of

DOCTOR OF PHILOSOPHY

in

Cell & Developmental Biology

February 28, 2021

Nashville, Tennessee

Approved:

Stephen J. Brandt, M.D.

Vivian Gama, Ph.D.

Ian G. Macara, Ph. D.

William P. Tansey, Ph.D.

P. Anthony Weil, Ph.D.

Acknowledgments

I am immensely grateful for all the support I have received throughout my graduate career and there are many collaborators, colleagues, and mentors I must acknowledge.

First I would like to thank my PhD advisor, Dr. Bill Tansey. Since practically my first week at Vanderbilt Bill has been a superb mentor, first as my FOCUS leader, next as a rotation mentor, and finally as my thesis advisor. Bill pointed me in the right direction as I learned new techniques, guided me in tackling an exciting and daunting project, and helped me succeed in obtaining a pre-doctoral fellowship. I am grateful for the freedom he allowed me in pursuing research in his lab and for his time and accessibility as a mentor. Thank you, Bill, for your mentorship and for encouraging me to work at the bleeding edge of discovery. Next, thank you to Dr. April Weissmiller. April is immensely generous with her time, expertise, and laughter, and her mentorship was formative to my graduate school experience. It was such a privilege to get to work next to such a brilliant scientist and mentor for nearly five years. April encouraged and inspired me to attend conferences, mentor others, and pay attention to my dreams. Shelly Lorey, lab manager extraordinaire: thank you for cheering me on and always making sure everything I needed to succeed was ordered. Tessa Popay: thank you for friendship, enthusiasm, crucial assistance during my manuscript revision, and for always reminding me to "just try." I am also incredibly grateful to the students I had the chance of training in the lab: Christina Wang, Kiana Guerrazzi, and Tyler Hansen. Training them was perhaps the most enjoyable part of my time in graduate school. Doing science with such outstanding students made our discoveries even more exciting and gratifying. Additionally, thank you to all members of the Tansey Lab, past and present; I have learned new things from each one of you.

Thank you to the all the professors outside the Tansey Lab who have been mentors to me. In particular I would like to thank Dr. Angelika Amon, Dr. Vivian Gama, and Dr. Rebecca Alexander for their time and mentorship, and for inspiring me. They encouraged me to keep going at times when I wasn't sure I could. Thank you also to the members of my thesis committee, Dr. Ian Macara, Dr. Vivian Gama, Dr. Tony Weil, and Dr. Steve Brandt who

challenged and encouraged me throughout my graduate career. Every committee meeting helped me gain a better sense of direction in my project and motivated me. I am grateful for their time, their recommendation letters, and their support—I value all of it.

Thank you to the core facilities at Vanderbilt that enabled my research. In particular, thanks to the Vanderbilt Cell Imaging Shared Resource and Nikon Center of Excellence for the microscope training and access. Thanks to the VANTAGE (Vanderbilt Technologies for Advanced Genomics) core for deep sequencing expertise for my RNA-seq and ChIP-Seq experiments. Thanks to the Vanderbilt Flow Cytometry Shared Resource, especially David Flaherty, Brittany Matlock, and Laura Warren who were so helpful and cheerful in assisting me with my flow analysis and sorting. I always looked forward to visiting the flow core and knew my samples were in the best hands. Finally, thanks most especially to the Mass Spectrometry Research Center where all the mass spectrometry data for my project was collected. Dr. Kristie Rose and Salisha Hill are excellent mass spectrometry collaborators and assisted me over the years in experimental design, sample processing, data analysis, and more.

I also want to acknowledge some of the other people and labs at Vanderbilt who collaborated with me Thank you to my bioinformatic collaborators, Dr. Jing Wang and Dr. Qi Liu, who assisted me with analyzing and presenting my RNA-Seq data. Thank to the members of the Fesik team working on WDR5 drug discovery, in particular the people who contributed to my paper: Dr. Bin Zhao and William Payne for contributing to the structural studies, J. Grace Shaw for performing TR-FRET affinity measurements, and Dr. Ed Olejniczak and Dr. Steve Fesik for project oversight. And thank you to the other collaborative labs at Vanderbilt who facilitated my research by providing key reagents and training, in particular the Cortez Lab, the Hodges Lab, the Hiebert Lab, and the Gama Lab.

Additionally, I acknowledge my funding from the NIH/NCI. I was incredibly lucky to be supported by two Ruth L. Kirschstein National Research Service Awards (NRSA): for two years by the Vanderbilt Biochemical and Chemical Training for Cancer Research institutional NRSA (T32 CA009582), and for three years by an individual NRSA (F31 CA225065). I am grateful not

only for this funding support, but also to the mentors who enabled me to successfully compete for these training awards by writing recommendation letters and helping me write my proposal.

For professional and career development opportunities and resources I am grateful to the Vanderbilt Biomedical Research Education and Training (BRET) office. In particular, thank you to Dr. Ashley Brady for guidance as I sought and secured post-graduation plans. Her help with CV review, job applications, and interview preparation was invaluable as I navigated a 2020 pandemic-era job search. Additionally, thank you to Kristi Hargrove, Susan Walker, and Lorie Franklin not only for their proficient administrative support, but also for smiles and encouragement in my time in CDB.

On a personal note, I am immensely grateful to my friends and family for believing in me and supporting me. Thank you to my dear friends all over the country for being there for me. I am so lucky to call so many smart and beautiful souls my friends. And of course, thank you to my family: my parents, sister, aunts, uncles, cousins. Your love and support means more than you know.

Table of Contents

List of Tables

List of Figures

List of Abbreviations

AML — acute myelogenous leukemia

APC/C — anaphase promoting complex/cyclosome

ATAC — Ada2a-containing

BFP — blue fluorescent protein

BIG-3 — BMP-2 Induced Gene 3 kb

BMP — bone morphogenic protein

CHAPS — 3-((3-cholamidopropyl) dimethylammonio)-1-propanesulfonate

ChIP — chromatin immunoprecipitation

ChIP-Seq — chromatin immunoprecipitation coupled to deep sequencing

co-IP — coimmunoprecipitation

COMPASS — Complex of Proteins Associated with SET1

Cryo-EM — cryogenic electron microscopy

EGFP — enhanced green fluorescent protein

H3 — histone H3

H3K4 — histone H3 lysine 4

H3K4me3 — trimethylation of lysine 4 on histone h3

H3R2me2a — asymmetrical dimethylation of arginine 2 on histone H3

H3R2me2s — symmetrical dimethylation of arginine 2 on histone H3

H4 — histone H4

HELB — helicase B

HMT — histone methyltransferase

IB — immunoblot

IGF-1 — insulin-like growth factor 1

IP — immunoprecipitation

KMT — lysine methyltransferase

lncRNA — long non-coding RNA

Mb — MYC box

mESC — mouse embryonic stem cell

MLL — mixed lineage leukemia

MLLr — mixed lineage leukemia rearranged

MOF — males absent on the first

MS — mass spectrometry

MSL — male-specific lethal

mTOR — mechanistic target of rapamycin

mTORC1 — mTOR complex 1

mTORC2 — mTOR complex 2

NSL — non-specific lethal

NuRD — nucleosome remodeling and deacetylase

PDB — Protein Data Bank

PDPK1 — 3-phosphoinositide-dependent protein kinase 1

PH — pleckstrin homology

PI3K — phosphoinositide 3-kinase

PTM — post-translational modification

RCSB — Research Collaboratory for Structural Bioinformatics

reChIP — two step (re-) chromatin immunoprecipitation

RPG — ribosome protein gene

SET1/MLL — abbreviation for the six histone methyltransferase complexes (KMT2A, KMT2B, KMT2C, KMT2D, SETD1A, and SETD1B)

TF — transcription factor

TGF-β — transforming growth factor β

TR-FRET — time-resolved fluorescence resonance energy transfer

tRNA — transfer RNA

WBM — WDR5 Binding Motif

WD40 — tryptophan-aspartic acid (WD) motif of 40 residues

WDR5 — WD Repeat-Containing Protein 5

Wdr5 — WD Repeat-Containing Protein 5 (mouse variant)

WHHERE — Wdr5, Hdac1, Hdac2, and Rere complex

WIN — WDR5 INteracting

WRAD — WDR5, RBBP5, ASH2L, and DPY30

Chapter I[1]

Introduction

Overview

Increased understanding of the complexity of eukaryotic life has led to growing awareness of the phenomenon of 'moonlighting', in which a protein characterized in one context is found to play roles in other, often quite diverse, cellular processes [2, 3]. That proteins defy neat and simple labeling is not surprising, but the mechanisms through which this occurs, and the implications it creates, are often intriguing and profound. WDR5 is a highly conserved WD40 repeat-containing protein that has proved to be a preeminent cellular multitasker. The moonlighting roles of WDR5 are impressive because it is small, highly-conserved, and highly-structured, meaning that WDR5 has had to evolve functional diversity within a constrained set of sequence and structural parameters. In this introduction, I review the current understanding of WDR5, from its canonical role in histone methylation through to functions outside the nucleus. I describe how WDR5 is able to manage its range of activities in light of extraordinary conservation, and argue that its moonlighting roles need to be carefully considered when interpreting experimental findings. I also describe how its structure and biological connections create opportunities for small molecule-mediated inhibition of WDR5, and how its multiple roles can influence the application of these inhibitors for anti-cancer therapeutics. The potential for WDR5 inhibitors as therapy urges a more complete understanding of the diverse interaction partners and moonlighting functions of WDR5.

WDR5: Beginnings and basics

WDR5 first came into focus through the lens of development. Mammalian WDR5 was

---

[1] Parts of Chapter I were adapted with permission from the following publication:

1. Guarnaccia A.D., Tansey W.P. Moonlighting with WDR5: A Cellular Multitasker. J Clin Med. 2018;7(2). PMID: 29385767. © Alissa D. Guarnaccia and William P. Tansey

identified via studies of bone formation, where differential display analysis revealed induction of a ~3 kb mRNA during osteoblastic differentiation [4]. This gene was termed *BIG-3*, for BMP-2 Induced Gene 3 kb, and was accurately predicted to encode a WD40 repeat-containing protein that folds into a seven-bladed β-propeller structure (**Figure 1-1**). Some years later, as the prevalence of WD40 repeat proteins was becoming clear, *BIG-3* was renamed *WDR5* [5], better reflecting the architecture of the protein product.

In 2001, studies of skeletal development in mice showed that Wdr5 promotes cellular differentiation and proper bone formation [4, 6]. (Mouse Wdr5 is denoted with lowercase letters). Further studies later showed that overexpression of Wdr5 in osteoblasts and odontoblasts of a developing embryo promotes growth and results in a larger than average skeletal structure [5, 7], while silencing *Wdr5* in limbs of a developing embryo severely impairs bone development [8]. In the same year that BIG-3/WDR5 was identified, its *Saccharomyces cerevisiae* homologue, Swd3, was recognized as a member of a newly-characterized histone methyltransferase complex, COMPASS (Complex of Proteins Associated with SET1), the homolog of the mammalian SET1 and MLL (mixed lineage leukemia) protein complexes that catalyze histone H3 lysine 4 (H3K4) di- and tri-methylation [9, 10]. It was seminal work from the Allis laboratory, however, that connected the WDR5 developmental phenotypes to epigenetics. In 2005 the Allis group showed that WDR5 directly associates with methylated histone H3, the mark catalyzed by the SET1/MLL protein complexes [11]. They showed that depletion of WDR5 in human cells decreases expression of developmentally-essential *HOX* genes, and that whole organism depletion of WDR5 in *Xenopus* embryos causes not only a decrease in H3K4 methylation, but also severe developmental defects [11]. Further work in mouse embryonic stem cells (mESCs) cemented the connection between WDR5 and development, showing that Wdr5 expression is high in mESCs but is decreased as cells differentiate [12]. Thus within the first few years of its research, WDR5 became associated with H3K4 methylation and developmental *HOX* gene expression, setting up a framework that to this day to influences assumptions made about WDR5 and the experimental approaches used in studying WDR5 cellular functions.

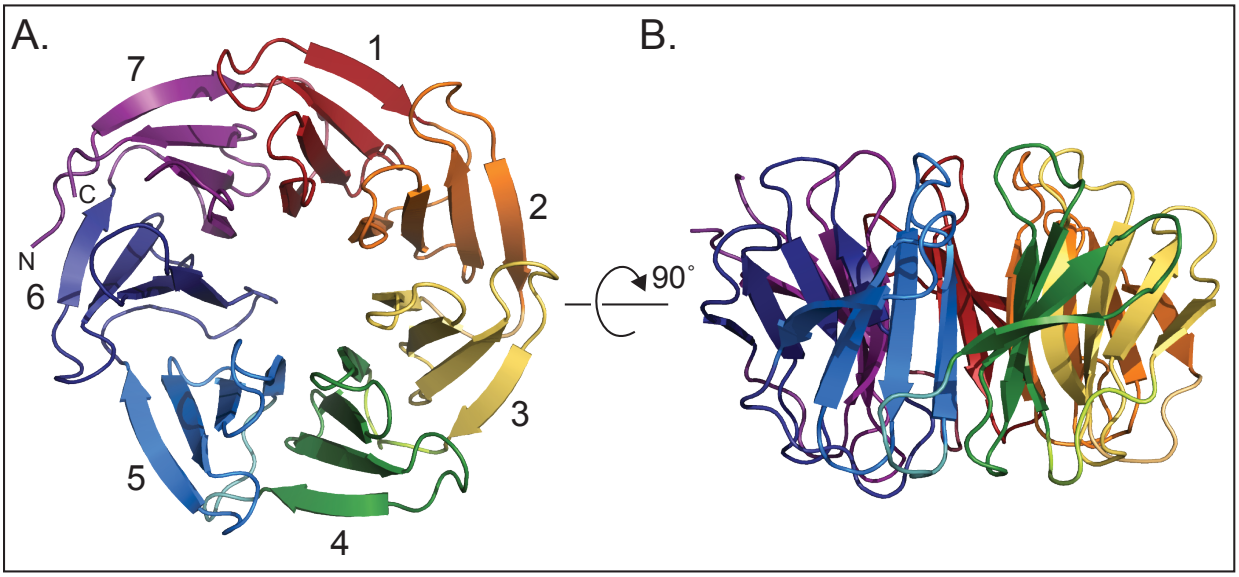

Figure 1-1: WDR5 is a seven bladed β-propeller protein
(A) This orientation of WDR5 displays the seven β-propeller blades of WDR5 each in a different color. The blades are numbered one to seven from the N-terminus starting with the first full blade.
(B) Side view of the orientation of the structure in A. (PDB: 2H14)

Three basic facts about WDR5 are worth noting here. First, WDR5 is an extraordinarily highly-conserved protein. Among vertebrates, WDR5 proteins share over 90% sequence identity over their entire length [13]. Human and mouse WDR5 are identical, and venturing further afar on the evolutionary scale, basal metazoa such as *Trichoplax* have a WDR5 homologue that is ~90% identical to human WDR5 within the WD40 repeat region (**Figure 1-2**). Because of this conservation, therefore, it is safe to assume that the structure presented in Figure 1-1 is an accurate depiction of all extant WDR5 proteins. Second, WDR5 has been particularly amenable to structural interrogation. Since 2006, more than 100 unique structures of WDR5 have been deposited into the Research Collaboratory for Structural Bioinformatics (RCSB) Protein Data Bank (PDB) [14], capturing WDR5 alone and in complex with co-factors and inhibitors. The extent to which WDR5 has been studied in this way reflects the importance of structural biology in deepening understanding of functions of WDR5 and in developing novel inhibitors that can block interactions at the surface of the protein. And finally, although WDR5 probably has at least two dozen primary direct interaction partners [15], all of the interactions that have been mapped with precision to date bind to one of two sites on WDR5 (**Figure 1-3**): a shallow cleft on one surface known as the “WDR5-binding motif” (WBM) site, and an arginine-binding cavity on the other surface referred to as the “WDR5-interacting” (WIN) site. Each site engages a particular motif in partner proteins. The consensus sequence for the WBM motif, present in proteins such as MYC and RBBP5, is [ED]-[ED]-[IVL]-D-V-[VT] [16]; and the consensus sequence for the WIN motif, present in SET1/MLL proteins as well as histone H3, KANL1, and KIF2A, is [GV]-[SCA]-A-R-[AST]-[EKR] [17-19] (**Figure 1-4 A**). Only one motif-containing protein can bind at each site on WDR5 at any given time (**Figure 1-4 B**), and it is possible that what is bound at one site influences what can bind at the other site. Large proteins bound at one site may inhibit—or promote—protein interactions at the other site and might help coordinate multi-protein complex assembly. The repeated use of these two sites by various WDR5-interaction partners appears to be one of the ways that WDR5 can function discriminately in different molecular contexts and is a theme I shall return to as I discuss the multitude of WDR5 activities.

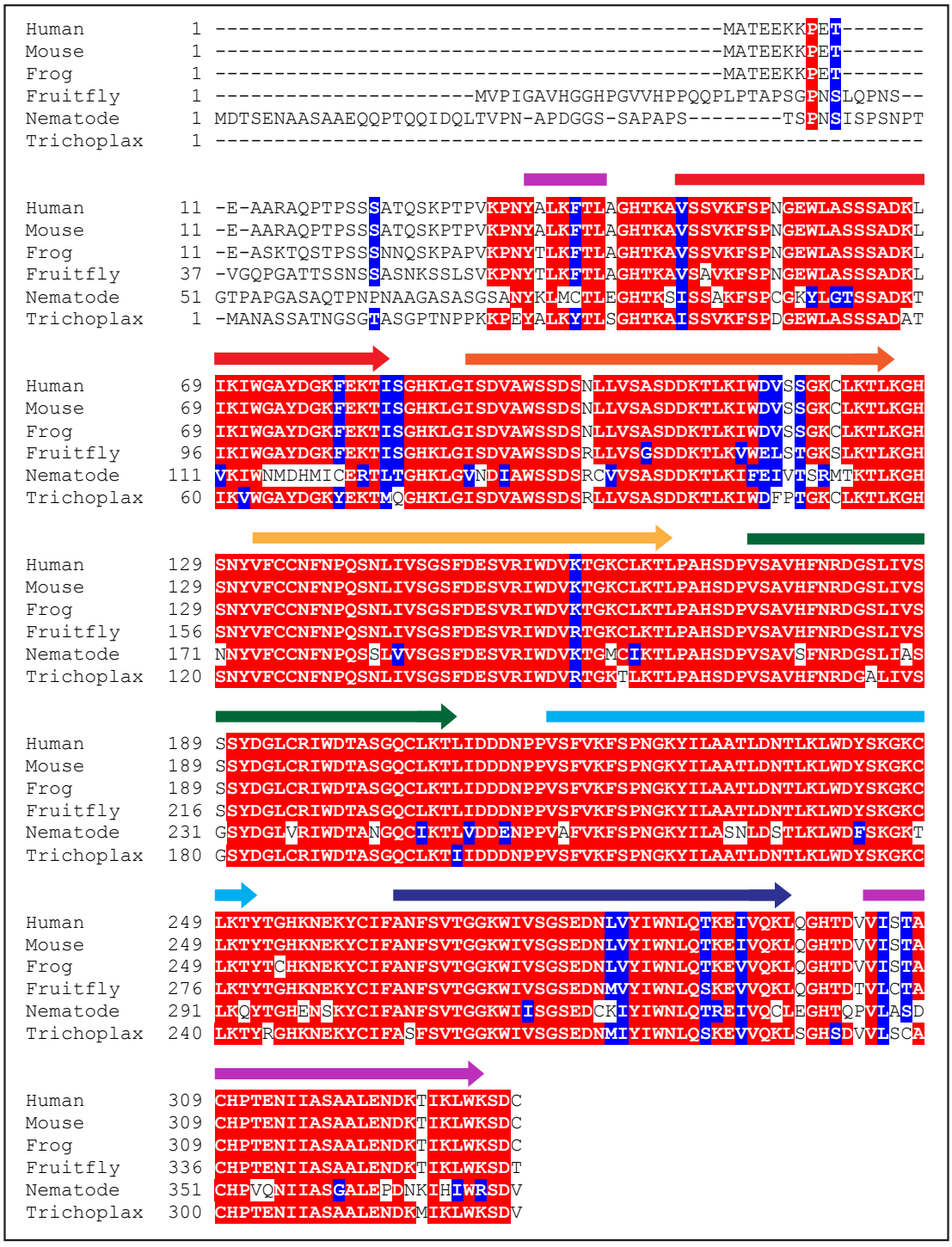

Figure 1-2: Alignment of WDR5 amino acid sequences

Analysis of the sequence alignments from several different species demonstrates high conservation of WDR5 proteins among multicellular organisms. Colored arrows above the sequences indicate the residues involved in each of the seven β-propellers and match the colors in Figure 1-1. Residues highlighted in red are identical. Residues highlighted in blue are homologous. *Homo sapiens* (NP_438172.1), *Mus musculus* (NP_543124.1), *Xenopus tropicalis* (NP_001011411.1), *Drosophila melanogaster* (NP_524984.1), *Caenorhabditis elegans* (Q17963.1), *Trichoplax adhaerens* (XP_002109498.1).

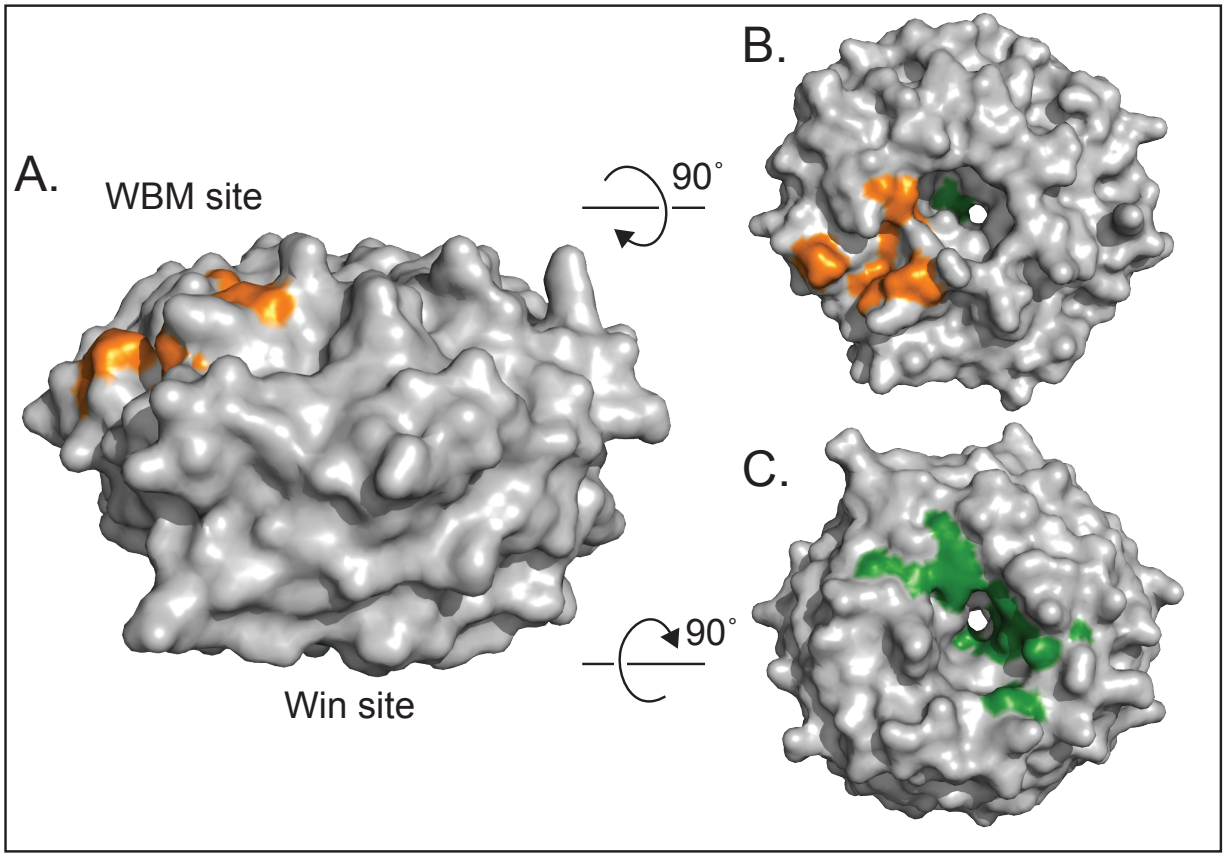

Figure 1-3: Two surfaces mediate all known direct interactions with WDR5
(A) Surface structure of WDR5 shown from the side. In this orientation, the top face contains the WBM site, and the bottom face contains the WIN site.
(B) Top view of the WBM site of WDR5. Residues involved in binding the WBM site are highlighting in orange: Asn225, Tyr228, Leu240, Phe266, Val268, Gln289. **(C)** Bottom view of WDR5 with residues involved in binding at the WIN site highlighted in green: Ala65, Ser91, Asp107, Phe133, Tyr191, Tyr260, Phe263. (PDB: 2H14)

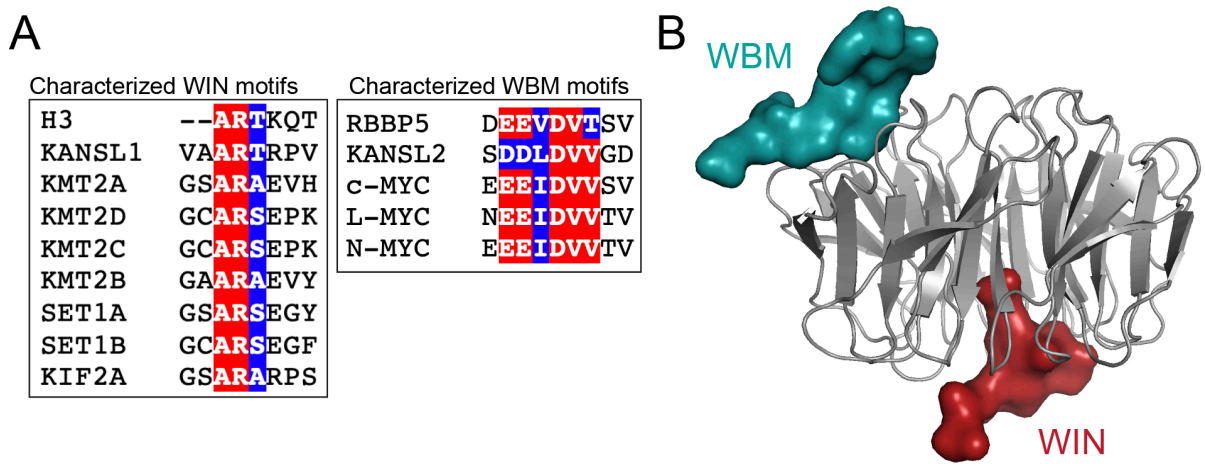

Figure 1-4: Characterized direct interacting partners of WDR5 have similar motifs and binding modes
(A) The WIN motif and WBM motif sequences for WDR5-interacting proteins mentioned in this introduction are shown. The WIN motifs are all centered on an arginine, while the WBM motifs are a specific combination of acidic and hydrophobic residues. Residues highlighted in red are identical. Residues highlighted in blue are similar.
(B) Co-crystal structure demonstrating the modes of binding at the WBM site (teal) and WIN site (red). Here WDR5 (grey) is bound by KMT2A peptide (red) at the WIN site and RBBP5 peptide (teal) at the WBM site (PDB: 3P4F).

Function of WDR5 as a component of histone H3 lysine 4 methyltransferases

Post-translational modifications (PTMs) on histones contribute to the regulation of gene expression by altering chromatin to promote active or repressive epigenetic states. Depending on the combination of marks at a particular region of the genome, different proteins are able to engage chromatin to drive processes such as transcriptional activation, transcriptional repression, and chromatin remodeling. Histone marks come in various forms including methylation, acetylation, phosphorylation, and ubiquitylation, and typically decorate the tails of histone proteins to convey an active or repressive epigenetic status. As mentioned, H3K4 di- and tri-methylation (H3K4me2 and H3K4me3) are marks of transcriptionally active chromatin, laid down by the SET1/MLL family of histone methyltransferases (HMT), also called trithorax group (TrxG), MLL-like, or COMPASS complexes [20]. WDR5 is a core component of these enzymatic complexes and this HMT association is perhaps the most well-known function of WDR5.

There are six non-redundant mammalian SET1/MLL HMT complexes, each with a distinct regulatory role [21-26] and each defined by the presence of a unique catalytic SET1/MLL subunit: SET1A, SET1B, KMT2A (MLL1), KMT2D (MLL2), KMT2C (MLL3), and KMT2B (MLL4). Besides the unique SET domain catalytic subunit, SET1/MLL HMTs are comprised of a common core set of proteins known as “WRAD”—WDR5, RBBP5, ASH2L, and DPY30 (reviewed [27], **Figure 1-5**)—which stimulate HMT activity above a weak basal level [28-30]. WDR5 plays a central scaffolding role in these complexes via its two key binding sites (**Figure 1-3**), interacting with RBBP5 via the WBM site [16], and the SET1/MLL protein via the WIN site [31-33] (**Figure 1-4 B**). The WIN site is notable here because it engages a conserved arginine central to WIN motifs [17, 31, 33-35] that are present in all six SET1/MLL family members [31-33] (**Figure 1-4 A**). Indeed, WDR5 is crucial for complex assembly of most SET1/MLL complexes (all but KMT2C) [36], however, most do not require WDR5 for their *in vitro* activity. Only for KMT2A—and perhaps also for SET1A [37]—is the presence of WDR5 in an *in vitro* histone methyltransferase assay critical for robust HMT activity; for the other HMT enzymes,

WDR5 is dispensable [30]. Thus even within this single functional context, WDR5 demonstrates different contributions to HMT activity. These observations led to the concept that small molecule inhibition of the WIN site will selectively inhibit H3K4 methylation by KMT1A (MLL1) histone methyltransferase complexes and inhibit cancers that rely on these enzymes. Indeed WIN site inhibitors selectively inhibit the *in vitro* activity of KMT2A reconstituted complexes and not other methyltransferases [38, 39]. However, it is important to note that these *in vitro* assays use recombinant fragments of the histone methyltransferase enzymes complex members, and it is possible that protein fragments behave differently from full-length proteins in complex assembly and activation. I shall discuss pharmacological inhibition of WDR5 in more depth later in this introduction.

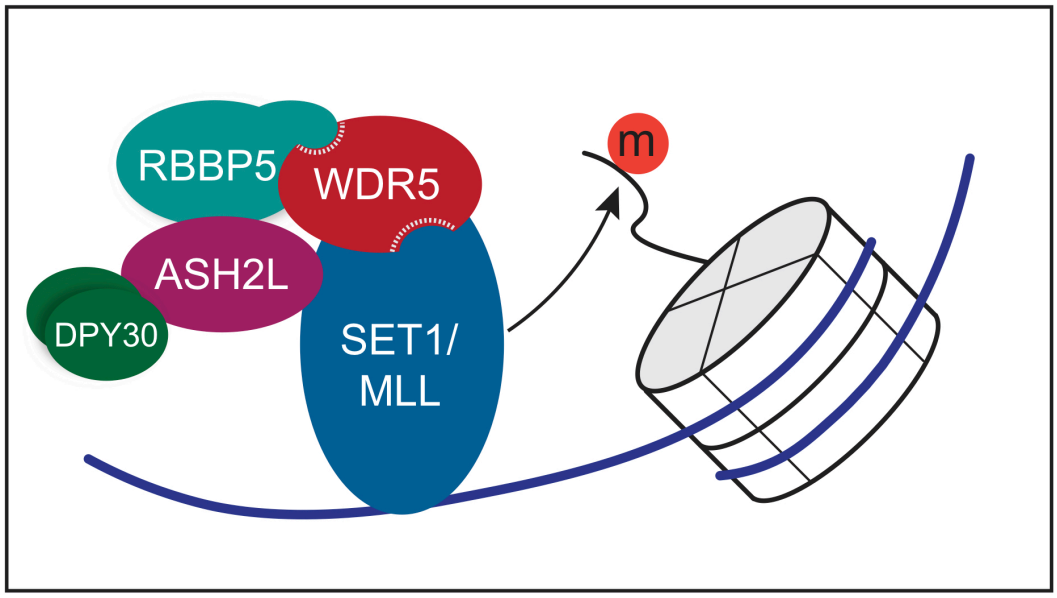

Figure 1-5: WDR5 is as a component of the SET1/MLL histone methyltransferase complexes
WDR5 functions to scaffold six distinct histone methyltransferase complexes, which catalyze the epigenetic marks of mono-, di-, or tri-methylation at lysine 4 of the peptide tails of histone H3. Two binding sites on WDR5 are required for efficient scaffolding of these complexes. These six complexes differ mainly in the identity of the SET1/MLL protein they carry.

Moonlighting in the nucleus

Although the action of WDR5 in scaffolding the assembly of SET1/MLL HMT complexes is perhaps its most studied function, there is ample evidence that WDR5 functions in a multitude of other processes, both in and out of the nucleus. Indeed, WDR5 associates (directly or indirectly) with nearly 200 different proteins in HeLa cell nuclear extracts and is roughly ten times more abundant than other WRAD proteins [40], suggesting that just a small part of what WDR5 does is devoted to H3K4 methylation. Because so much of the biology of WDR5 is filtered through the lens of its HMT connection, it is important to be cognizant of its diversity of function when considering how, for example, gene knock outs or knock downs may exert their phenotypes, or how and where small molecule inhibitors may have therapeutic benefit. In this section, I will discuss moonlighting roles for WDR5 in the nucleus.

WDR5 is a histone tail reader

Studies of chromatin reveal a complicated interplay between the genetic code, regulatory proteins, and PTMs on histones, observations that were unified by the “Histone Code” hypothesis. Put forward by Strahl and Allis, the histone code hypothesis proposes that by being “written,” “read”, and “erased” by various regulatory proteins, histone PTMs enable regulation of the transcriptional state of a piece of chromatin [41, 42]. Histone H3 is home to some of the most well-studied PTMs, in particular within the first four residues of the histone tail that projects outward from the nucleosome core (Ala1–Arg2–Thr3–Lys4 or A1–R2–T3–K4). Intriguingly, as well as scaffolding the assembly of H3K4 writer complexes, WDR5 is also an H3 tail binding protein, capable of recognizing modified and unmodified H3 tail sequences via its WIN site.

WDR5 interaction with H3 can be modulated by methylation both on lysine 4 (K4) and on arginine 2 (R2), leading to the notion that WDR5 is a histone tail reader. Pulldown assays with immobilized H3 peptides and HeLa cell nuclear extracts provided compelling evidence that WDR5 in this context preferentially binds dimethylated H3K4 sequences [11]. How this occurs,

however, is not yet resolved. Structural analyses clearly show that the histone H3 tail engages the WIN site of WDR5, but that Lys4 (K4) does not contact the core of the WIN site of WDR5 [13, 43-45], making direct recognition of methylation status at this site unlikely. It is possible that the mode of recognition is yet to be discovered, or that other proteins in complex with WDR5 in cells mediate methylated lysine specificity. What this structural data does show, however, is that Arg2 (R2) of the H3 tail anchors the H3 peptide into the WIN site of WDR5, where the guanidinium group of the arginine binds by π-π stacking interactions with phenylalanine residues of WDR5, F133, and F263 [43-45]. This “phenylalanine clamp” [43] on R2 of H3 is precisely the same mechanism through which WDR5 binds all known WIN motifs including SET1/MLL proteins [31-33]. And methylation on R2 can influence binding to WDR5 (**Figure 1-6 A**). R2 of H3 is dimethylated in two distinct ways—asymmetrically, in which two methyl groups are placed on one of the terminal nitrogen atoms of the guanidino group, and symmetrically, in which one methyl group is placed on each of the terminal guanidino nitrogens. Asymmetrical dimethylation (H3R2me2a) is negatively correlated with the transcriptional activation [46-48] and WDR5 clearly cannot bind H3 tails that carry this repressive modification [43, 48, 49]. Symmetrical dimethylation (H3R2me2s), however, marks regions of the genome that are poised for active transcription and can be bound by WDR5. H3R2me2s with WDR5 was initially reported to be a high affinity interaction (~100 nM) by surface plasmon resonance [48], however a more recent analysis found similar affinities of WDR5 for unmodified and modified H3 variants: H3R2me0, H3R2me1, and H3R2me2s all have K_d measurements between 8 and 11 μM measured by isothermal calorimetry [49]. Structural data is consistent with this affinity data as WDR5 crystal structures in complex with L-arginine, monomethyl arginine, and symmetrical dimethyl arginine show little variation between structures [49]. These results suggests a binary switch for the histone H3 reader activity of WDR5, where H3R2me0, -me1, and -me2s permits and H3R2me2a restricts WDR5 interaction.

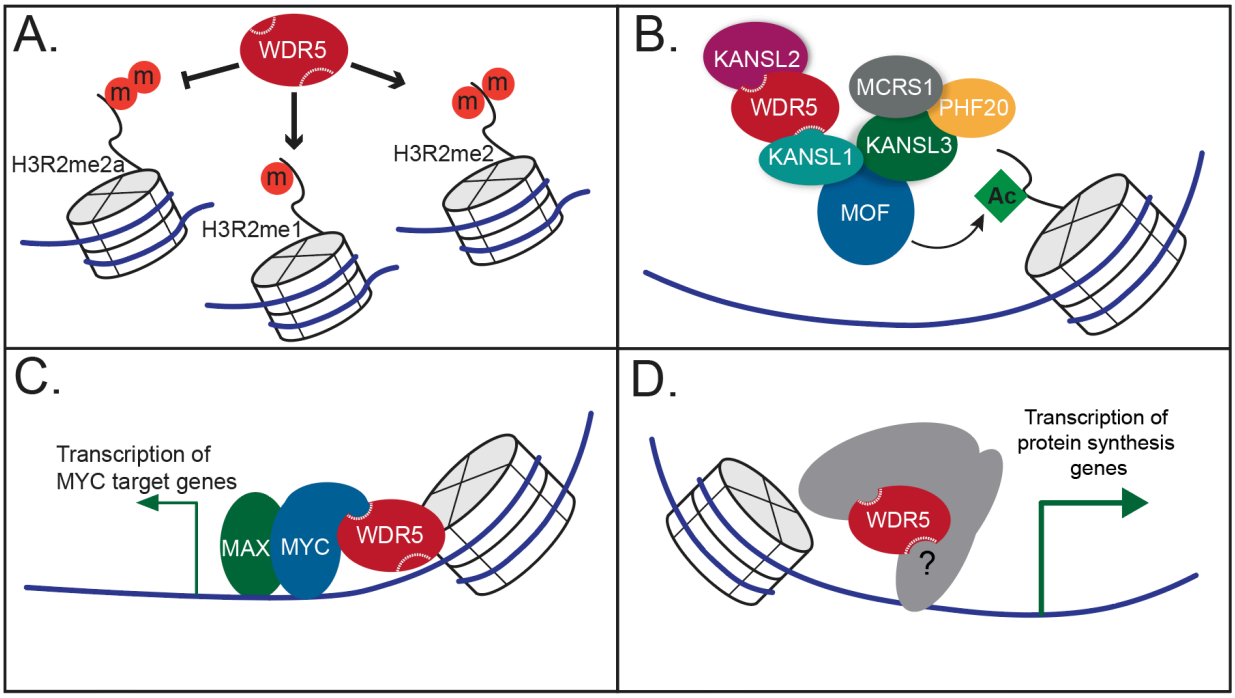

Figure 1-6: WDR5 has various roles at chromatin
(A) WDR5 binds directly to tails of histone H3 that are monomethylated or symmetrically dimethylated on Arg2. WDR5 binding is inhibited by asymmetrical dimethylation on Arg2.
(B) WDR5 assembles in the non-specific lethal (NSL) complex, which acetylates histones.
(C) WDR5 directly interacts with the transcription factor MYC to facilitate its chromatin binding and its transcriptional activation.
(D) WIN site-dependent binding of WDR5 to chromatin promotes the expression of protein synthesis genes, including half of all ribosome protein genes.

WDR5 is part of the NSL complex

MOF (males absent on the first) is a histone H4 acetyltransferase that assembles into two distinct functional complexes, the MSL (male-specific lethal) complex and the non-specific lethal (NSL) complex [50]. WDR5 associates with MOF only within the NSL complex [51-54], which also includes five other subunits: KANL1, KANL2, KANL3, PHF20, and MCRS1 [52-54] (**Figure 1-6 B**). A structural interrogation of NSL from the Akhtar laboratory revealed direct interactions with WDR5 that are parallel and mutually exclusive with direct interactions in the SET1/MLL complexes [18]. WDR5 directly interacts with KANL2 and with KANL1 at the same exact binding sites that bind RBBP5 (WBM site) and SET1/MLL enzymes (WIN site), respectively [18]. The region of KANL2 that binds WDR5 is highly conserved and contains a WBM motif that is parallel to the WBM motif of RBBP5 [18] (**Figure 1-4 A**). Similarly, KANL1 binds to WDR5 through a conserved arginine-containing WIN motif, analogous to the WIN motifs within H3 and the SET1/MLL proteins [18] (**Figure 1-4 A**). At least in *Drosophila*, the WIN site dependent KANL1–WDR5 interaction appears to be required for efficient recruitment of the NSL complex to chromatin, as mutations that disrupt this interaction reduce its chromatin binding [18]. Notably, the NSL complex provides a clear example of a multi-protein WDR5-containing complex that, like SET1/MLL, complexes engages both WIN and WBM sites.

WDR5 works with MYC

The MYC family (N-MYC, L-MYC, and c-MYC) of transcription factors features prominently in human cancer [55]. Overexpression of MYC proteins occurs in a majority of cancers and contributes to the deaths of at least 100,000 Americans each year [55]. In mice, a variety of experimental models have shown that inactivating MYC in the context of a preformed cancer promotes tumor regression [56-59] highlighting the value of MYC inhibition for cancer therapy. However, MYC itself is unstructured and considered “undruggable,” positioning MYC as a highly validated yet challenging anti-cancer target.

MYC proteins are composed of an amino-terminal transcriptional activation domain (TAD), a carboxy-terminal DNA binding domain (DBD), and an intervening “central portion.” Additionally there are six short segments (~10-20 residues each) called MYC boxes (Mb) distributed throughout the MYC protein: Mb0, MbI, MbII, MbIIIa, MbIIIb, and MbIV (**Figure 1-7**). These regions are conserved in MYC proteins across species, and experiments deleting or mutating these sequences have shown repeatedly that MYC boxes are important for MYC function [60-62]. Many cofactors for MYC require one or more MYC boxes for interaction with MYC.

MYC relies on a variety of cofactors facilitate and regulate its DNA binding. To bind DNA in cells, MYC first heterodimerizes with MAX to form a DNA-binding module that recognizes “E-box” (CACGTG) DNA sequences [63, 64]. E-box sequences occur on average every 4 kb throughout the genome [55], yet MYC–MAX dimers only bind to a small fraction of these sites. Interaction with additional cofactors imparts specificity in MYC–DNA binding and contributes to its transcriptional repression and activation. MYC transcriptional repression is influenced by interactions including with DNMT3A [65], MIZ-1 [66-68], SNF5 [69, 70], and HDAC3 [71]. MYC transcriptional activation is influenced by interactions including with TRRAP [72, 73], BPTF [74], LEO1 [75], TFIIF [61], HCF-1 [76, 77], Cyclin T1 (pTEFb) [78] (**Figure 1-7**). Most important for this discussion, MYC interacts with WDR5 to activate gene expression [62, 79].

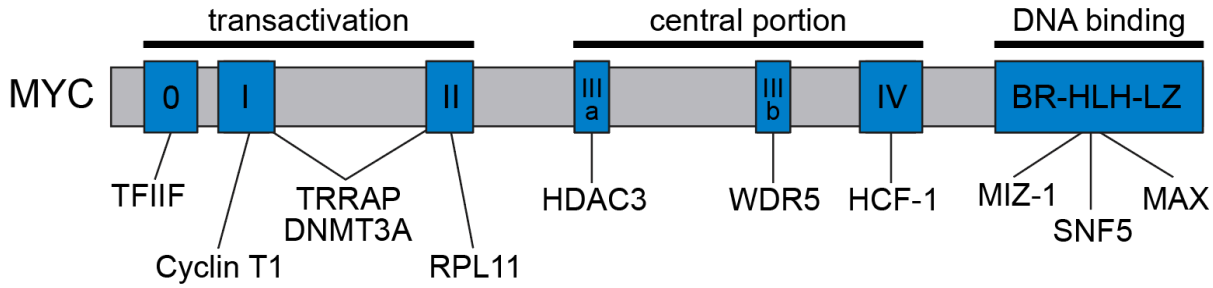

Figure 1-7: MYC boxes and MYC interacting proteins
A schematic of c-MYC (MYC) is shown indicating the regions that comprise the transcriptional activation domain, the central portion, and the DNA binding domain. Some of the cofactors that influence MYC transcriptional activation or repression are indicated.

The MYC–WDR5 interaction, first reported by our laboratory [79], forms the basis of yet another molecular function for WDR5. MYC binds directly to WDR5 via an invariant sequence motif present in MbIIIb of all MYC proteins. This motif is similar to the WBM sequences of RBBP5 and KANL2 (**Figure 1-4 A**), and indeed structural analyses show that MYC interacts with WDR5 via the WBM site and in a way that is virtually identical to RBBP5 and KANL2 [79]. WDR5 and MYC co-localize on chromatin, demonstrating extensive overlap by ChIP-Seq [62, 79, 80]. And in my unpublished experiments using sequential ChIP (reChIP) assays I found simultaneous binding of MYC and WDR5 (**Figure 1-8**). Mutating the WBM motif within MbIIIb of MYC prevents MYC—but not WDR5—from stably associating with its target genes [62, 79]. And chemical blockade of the WIN site of WDR5 does not block interaction with MYC, but does prevent both WDR5 and MYC from associating with target genes [62]. Together these results indicate that WIN site-dependent binding of WDR5 to chromatin facilitates MYC recruitment chromatin, and WDR5 functions to guide MYC to certain regions of the genome over others (**Figure 1-6 C**). Additionally, many of the genes where WDR5 facilitates MYC recruitment are ribosome protein genes. This binding pattern is significant since one of the core pro-tumorigenic MYC functions is driving a transcriptional program toward biomass accumulation. Regulation of biomass accumulation genes is also a fundamental function for WDR5 (described in the next subsection). Because inhibiting even a fraction of the tumorigenic function of MYC has tremendous anti-cancer potential, impeding MYC at a subset of its binding sites through inhibiting WDR5 may be a viable strategy for targeting MYC therapeutically [81].

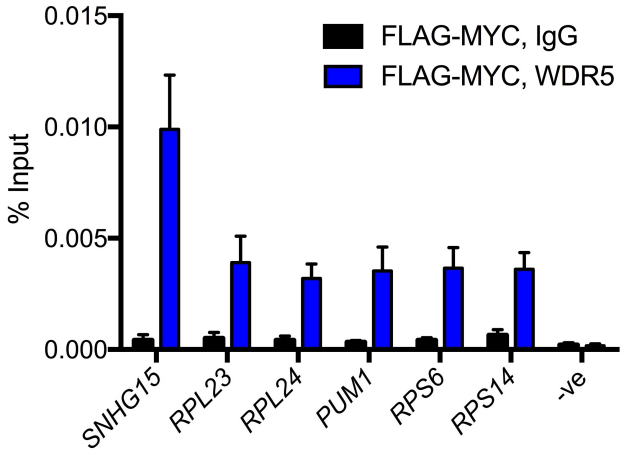

Figure 1-8: MYC and WDR5 bind together at chromatin
Re-ChIP assay from HEK293 cells expressing FLAG-MYC. FLAG ChIP was performed followed by elution and a second IP with either IgG or WDR5 antibody. Results were quantified by qPCR . *n=3*.

WDR5 is a regulator of protein synthesis gene expression

Focused genomic analyses of WDR5 have revealed a conserved function in regulating protein synthesis gene expression (**Figure 1-6 D**). This pattern was first observed in MV4;11 cells where ChIP-Seq identified ~160 sites of WDR5 chromatin binding. Among these binding sites there is clear enrichment for genes linked to protein synthesis, including half of ribosome protein genes (RPGs) [39]. Inhibition of the WIN site of WDR5 reduces WDR5 chromatin binding and is accompanied by reduced expression of these RPGs. Notably, these transcriptional changes occur before any changes in H3K4me3 are observed, indicating that an H3K4me3 epigenetic mechanism is not the cause for these gene expression changes. A subsequent study extended analysis of WDR5 chromatin binding to other cell types, comparing WDR5 ChIP-Seq datasets for a panel of human and mouse cell lines. Across all cell types tested, WDR5 is bound to a consistent set of protein synthesis genes, as observed in MV4;11 cells [82] (**Figure 1-9 A**). And again, treating cells with WIN site inhibitor decreases WDR5 chromatin binding and reduces protein synthesis gene expression in all cell types tested (**Figure 1-9 B**) [39, 82]. The same decrease in RPG transcription is phenocopied by WDR5 depletion, further supporting that this transcriptional regulation is a fundamental function of WDR5 [82]. As mentioned above, many of the WDR5-bound RPGs are also bound by MYC [62], indicating that MYC is a component of WDR5-dependent transcriptional activation of biomass accumulation. Overall, these studies establish WDR5 as a conserved regulator of protein synthesis gene expression.

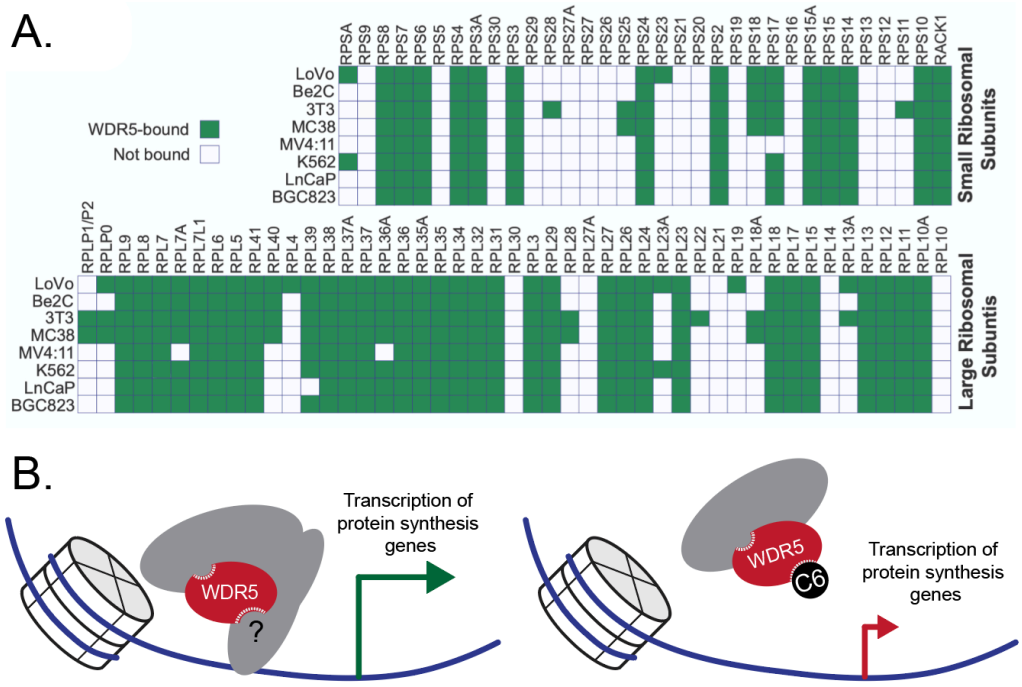

Figure 1-9: WDR5 is a conserved regulator of protein synthesis gene expression
(A) WDR5 is invariantly bound to a core set of ribosome protein genes. Figure is from [82].
(B) Function of WDR5 as a regulator of protein synthesis gene expression. Model of WDR5 at chromatin promoting the transcription of ribosome protein genes (left), a process that is impaired when the WIN site of WDR5 is inhibited (right).

WDR5 interacts with APC/C on chromatin

WDR5 also has a mitosis-specific interaction with APC/C on chromatin. In early mitosis WDR5 recruits APC/C to certain promoter regions, initiating histone ubiquitylation and priming these chromatin regions for proteasome-dependent turnover [83]. This histone ubiquitylation "bookmarks" these genes and enables them to be open and ready for transcriptional reactivation upon mitotic exit (**Figure 1-10 A**). Mutation of the WIN site or the WBM site in WDR5 disrupts interaction with APC/C, indicating that both binding sites contribute to interaction with APC/C. Specific WIN or WBM motifs in APC/C subunits that directly bind WDR5 have not yet been identified, and although a cryoEM structural model of WDR5 in complex with APC/C was determined, its ~20Å resolution reveals few details. A higher resolution structural analysis is needed to glean meaningful surface contacts between the members of this complex.

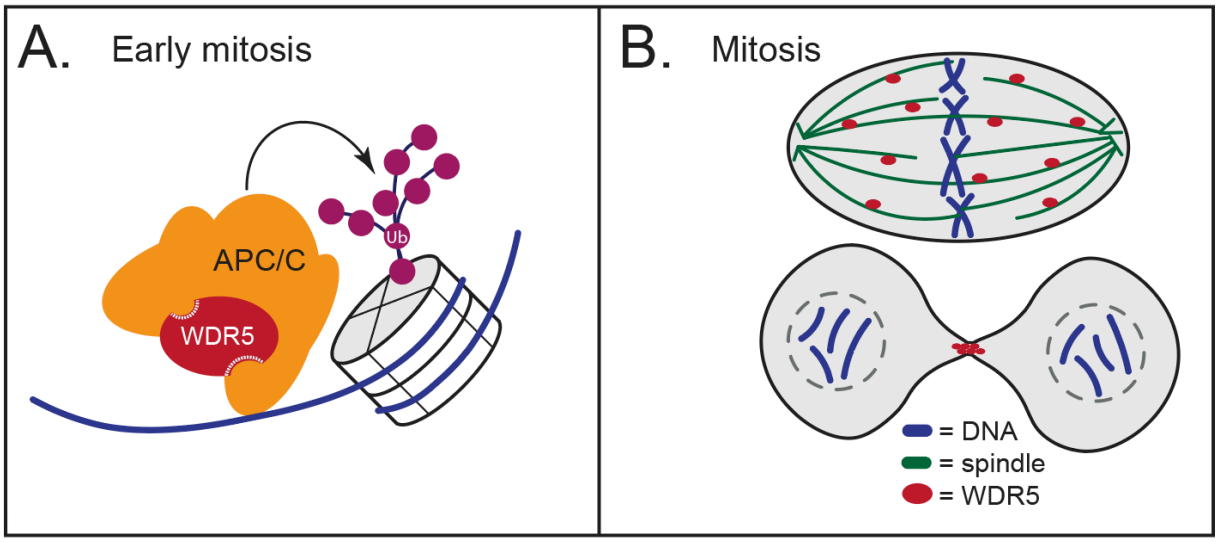

Figure 1-10: WDR5 has roles in mitosis
(A) In early mitosis WDR5 recruits APC/C to chromatin for histone ubiquitylation to prime cells for gene reactivation upon mitotic exit.
(B) In mitosis WDR5 functions at the spindle and midbody to facilitate the integrity of mitosis and cytokinesis.

The ever-expanding nuclear WDR5 interactome

Besides the moonlighting activities mentioned above, there is a growing body of evidence, less mechanistically developed, suggesting that the functions described above might just be the tip of the WDR5 iceberg. In addition to MYC, WDR5 directly interacts with several other sequence-specific transcription factors—Oct4 [12], Twist1 [84, 85], and HSF2 [86]. Most of these WDR5 interactions have been implicated in promoting the activity of the specific transcription factor. WDR5 also associates with chromatin remodelers including CHD8 [87-89], INO80 [53, 90], and CHD7 [91, 92]. WDR5 has been found to associate with the nucleosome remodeling and deacetylase (NuRD) complex [93, 94], a chromatin-associated protein complex that performs the dual-roles of chromatin remodeling and histone deacetylation [95]. WDR5 is part of the ATAC (Ada2a-containing) complex, which is an H4-specific histone acetyltransferase [96, 97]. WDR5 is a member of the repressive histone methyltransferase complex, PRC1.6 (also called E2F6.com) ([98-100] reviewed [101]), and forms part of the WHHERE complex (complex containing Wdr5, Hdac1, Hdac2, and Rere) [102] that functions as a retinoic acid receptor cofactor and contributes to embryonic development. In breast cancer cells, WDR5 interacts with the canonical PRC1 protein CBX8 to maintain oncogenic NOTCH signaling [103]. WDR5 is capable of interacting with longer translational variants of PTEN (PTEN-L) via an N-terminal extension not present in canonical PTEN, and this WDR5–PTEN-L interaction is implicated in supporting pro-tumorigenic transcriptional and epigenetic cellular programs [104]. WDR5 does not just complex with proteins, but also may be able to selectively interact with long non-coding RNAs (lncRNAs), such as HOTTIP, which is implicated in the recruitment of WDR5 to *HOXA* genes [105, 106]. Other WDR5-interacting lncRNAs include NeST [107], GClnc1 [108], and HOXD-AS1 [109], although how WDR5 recognizes these RNA species has not been determined. Clearly, the multitude of interactions centered around WDR5 is large and, although a lot of work needs to be done to tease apart these many interactions, we can reasonably conclude that WDR5 is a highly-networked protein that will continue to fascinate researchers for years ahead.

WDR5 moonlights off chromatin

There is a growing realization that many transcription factors, splicing factors, and epigenetic regulators have evolved additional chromatin-independent roles [3], and WDR5 is no exception. WDR5 is found outside of the nucleus [110-112] and exhibits functional importance in processes including cell division, cilia formation, viral replication, and cellular signaling. These associations portray WDR5 as a versatile cellular multitasker. Here I describe some of the current understandings of moonlighting functions for WDR5 off of chromatin.

WDR5 and mitosis

WDR5 localizes to the mitotic spindle and to the midbody in dividing human cells (**Figure 1-10 B**) [19, 111]. This localization depends on the integrity of the WIN site, as mutations in this site of WDR5 prevent its stable association with the midbody [111]. Every indication is that binding of WDR5 to the midbody and mitotic spindle is functionally relevant, as these WDR5 WIN site mutants also fail to rescue mitotic defects associated with WDR5 knock-down [113]. Proteomic screening for cytoplasmic partners of WDR5 led to the identification of KIF2A, a kinesin-like protein, as a direct WDR5 interaction partner [19]. KIF2A carries a WIN motif that appears to directly bind the WIN site on WDR5 [19] (**Figure 1-4 A**). Interestingly, both the WIN motif of KIF2A and the WIN site of WDR5 are required for KIF2A recruitment to the midbody, suggesting that interaction with WDR5 is required for midbody localization of KIF2A. Again, the sheer volume of traffic at the WIN site of WDR5 makes interpreting these kind of mutational results challenging. But these mitotic functional implications, together with the WDR5–APC/C interaction at chromatin, indicate that WDR5 is a player in regulating mitotic processes. Further mechanistic understanding of such functions is needed to fully elucidate the importance of WDR5 in mitosis.

WDR5 and cilia

Another chromatin-independent role for WDR5 is in cilia formation. Cilia are important for cellular motility, signaling, and sensing, as well as developmental patterning. A connection between WDR5 and cilia was discovered by examining a disease-specific missense mutation in WDR5. Exome sequencing of congenital heart disease patients identified an individual carrying a K7Q mutation in WDR5 [114], and using *Xenopus tropicalis* to study developmental consequences of perturbing WDR5, the authors found that WDR5 depletion causes defects in left-right patterning and a decrease in number of cilia [112, 115]. These phenotypes were rescued by re-expression of wild-type WDR5 and WIN site mutant WDR5 (S91K), but not by the N-terminal K7Q mutant [112]. Wild-type and K7Q mutant WDR5 both localize to ciliary basal bodies, but only wild-type WDR5 stabilizes cilia formation, indicating that the N-terminal region of WDR5 is necessary for productive cilia. These studies are the first to indicate any functional significance for the N-terminus of WDR5, an unstructured region that is separate from the WIN and WBM sites and is not conserved in non-vertebrate WDR5 proteins (**Figure 1-2**). Intriguingly, LC-MS/MS analysis found that K7 of WDR5 is acetylated in lung and thymus tissues of mouse and rat [116]. Since lower order species do not contain this sequence, perhaps WDR5 has evolved extranuclear roles in vertebrate organisms, and perhaps these roles are regulated by acetylation.

WDR5 and viruses

WDR5 is also found outside the nucleus during viral infections. Studies to date have used various viruses with different genomes—Sendai virus, measles virus, human cytomegalovirus, hepatitis B virus—but identify some consistent findings. Viral infection causes WDR5 to accumulate in the cytoplasm and to co-localize with viral proteins [110, 117, 118]. Viral infection also causes reduced ubiquitylation and stabilization of cellular WDR5 [119, 120]. WDR5 also seems to be necessary for viral replication since knockdown of WDR5 decreases viral yields [117-119] and overexpression of WDR5 enhances viral yields [119]. As of yet, no

direct interactions between WDR5 and specific viral proteins have been demonstrated. However, surely such interactions are possible, and as an example of this concept, *in vitro* binding and structural analysis demonstrates that the influenza viral protein NS1 has an internal WIN sequence that is capable of binding the WIN site of WDR5 [121]. The NS1 viral WIN sequence is proposed to act as a histone mimic that serves to hijack WDR5 for viral replication purposes [121]. Further research into what kind of viral proteins are capable of interacting with WDR5 and what surfaces of WDR5 are used will reveal if one day WDR5 inhibitors might be useful as antivirals.

WDR5 and signaling

Since its discovery in 2001 *WDR5* has been recognized as a gene connected to cellular signaling [4]. The original name for *WDR5*, *BIG-3*, is a reference to this signaling connection: *BIG-3* stands for 'BMP2-induced gene 3 kb.' Bone morphogenetic proteins (BMPs), including BMP2, are part of the TGF-β superfamily and initiate signaling cascades that promote specific gene expression programs [122]. Further connection between TGF-β signaling and WDR5 have been found in liver cells [123], in lung cells [124], and in breast cells [125] WDR5 is implicated as an important player in mediating the transcriptional response to TGF-β signaling. Correspondingly, in a mouse model of chronic kidney disease, inhibition of the WIN site of WDR5 reduces TGF-β–induced gene expression patterns [126]. Because TGF-β signaling can drive epithelial to mesenchymal transition, WDR5 is a promising target for preventing a more metastatic state in cancer [124, 125]. The mechanistic details of this longstanding connection between TGF-β signaling and WDR5 has yet to be thoroughly interrogated.

WDR5 is linked to other signaling pathways as well. In colon cancer cells WDR5 expression increases upon IGF-1 growth factor stimulation, and inhibition of the PI3K/AKT signaling pathway with LY294002 causes a decrease in WDR5 expression [127]. Similarly, in esophageal cancer, knockdown of WDR5 induces a decrease in active PI3K/AKT signaling [128]. Together, these data point to a connection between AKT signaling and cellular levels of

WDR5. WDR5 also contributes to retinoic acid signaling as part of the WHHERE complex [102], and in breast cancer WDR5 is implicated in positively regulating Notch signaling [103]. Finally, in myoblast differentiation WDR5 has been shown to be phosphorylated by PASK downstream of mTORC1 signaling, and this phosphorylation is necessary for transcriptional outputs that promote myoblast differentiation [129, 130]. Association of WDR5 with so many cellular signaling networks emphasizes the cellular importance for WDR5 and hints at moonlighting interactions that are undiscovered.

Conclusion

WDR5 has many cellular functions and interactions, on and off chromatin, and obviously all of these functions are not yet fully understood. As WDR5 research progresses, it is important to keep in mind that any manipulation made on WDR5 will impact multiple facets of WDR5 function, not all of which are currently known or understood. Thus, experiments must be carefully designed and interpreted. Because WDR5 is a major hub for protein interactions and a protein essential for cell growth [131, 132], RNAi knockdown or CRISPR knockout will more than likely impact multiple processes and make results difficult to interpret. In terms of assessing the impact of inhibiting one of the other binding sites on WDR5, it is also important to consider that inhibition may not be accurately modeled by depletion. Presently, WDR5 is beginning to be appreciated as more than just an epigenetic protein and the molecular tools for studying WDR5 are advancing. Future experimentation will enable a deeper understanding of the importance of the moonlighting activities and therapeutic potential for WDR5.

WDR5 in cancer

Studying WDR5 has importance for human health because WDR5 is frequently overexpressed in a wide variety of cancers. Increased expression of WDR5 is correlated with poor prognosis and disease progression in a litany of malignancies: glioma [133], papillary thyroid carcinoma [134], colon cancer [127, 135], head and neck squamous cell carcinoma

[136], breast cancer [125, 137], hepatacellular carcinoma [138], glioblastoma [139], neuroblastoma [139, 140], bladder cancer [141], gastric cancer [142], esophageal cancer [128], leukemia [143]. WDR5 is also found to be highly expressed in prostate cancer [144] and in hepatitis B virus (HBV)-induced hepatocellular carcinoma [120]. WDR5 is implicated in cancer-promoting processes such as epithelial to mesenchymal transition [84, 127, 133, 145] and cell migration and metastasis [125, 127, 133, 146]. Such connections between WDR5 activity and cancer progression make WDR5 an appealing candidate for targeted inhibition.

The relationship between high levels of WDR5 and malignant growth is consistent across many cancer types. Experiments in parallel systems that compare 'normal' and 'high' WDR5 levels find that WDR5 overexpression promotes cancer progression [103, 127, 141, 146]. Reciprocally, reducing WDR5 levels dramatically reduces cancer cell growth. A caveat of these depletion experiments is that they often rely on knockdown of WDR5, usually by shRNA, to demonstrate that WDR5 is important [103, 128, 133, 138-144, 147], and because WDR5 is a common essential gene [132], WDR5 knockdown in any cell type is likely to cause viability defects. Clearly WDR5 promotes cancer, but there are many more mechanistic details that needs to be elucidated to fully understand *how* WDR5 promotes cancer. We know that WDR5 interacts with MYC, but what other cancer-specific functions of WDR5 exist, and can they, like MYC, be targeted by small molecule inhibitors of WDR5? What protein interactions with WDR5 are essential for cancer cell growth? If these kind of questions can even begin to be answered, we can more rapidly begin to advance WDR5 small molecule inhibitors as cancer therapy.

WDR5 and drug discovery

In the last decade, it has become apparent that epigenetic regulatory proteins can be targeted by small molecule inhibitors for therapeutic benefit. There are currently dozens of small molecule epigenetic inhibitors in various stages of clinical trial in the United States [148] targeting histone code writers, readers, and erasers, and it is likely that this number will continue to blossom in the years ahead. For WDR5, inhibitor discovery efforts center on the two focused

binding sites on WDR5: the WBM site and the WIN site. WBM site inhibitors may have utility as anti-cancer agents by virtue of their ability to directly block the MYC–WDR5 interaction, thwarting MYC function in cancer cells [79, 81]. This concept was explored by the Tansey Lab [62, 79] and by Draetta and colleagues [149], who showed that the MYC–WDR5 interaction is a critical determinant of cancer growth. Because the WBM site is a shallow cleft and not a deep pocket, this binding surface is not overtly amenable to drug targeting. However, recently the development of such inhibitors has successfully begun through a collaboration between the Tansey and Fesik labs at Vanderbilt University. Initial high throughput screening and structure-guided optimization resulted in identification of a series of small molecules that bind to the WBM site and disrupt the MYC–WDR5 interaction [150]. Compounds in this initial series possess nanomolar affinities for WDR5, however these molecules have poor cell permeability and only disrupt the MYC–WDR5 interaction in cell lysates [150]. Subsequent NMR-based fragment screening and structure-guided optimization improved the drug-like properties of these WBM inhibitor molecules and resulted in a molecule that disrupts the MYC–WDR5 interaction in cells with ~100 nM affinity for WDR5 [151]. This molecule also decreases MYC occupancy at chromatin, indicating effective targeting of MYC through blocking the WBM site of WDR5. Further optimization will be required to make these compounds truly bioavailable, but this drug discovery effort establishes the proof of concept that small molecule inhibition of the WBM site of WDR5 is possible.

Most WDR5 drug discovery efforts focus on the WIN site, and several types of WIN site inhibitors have been discovered. An early approach to inhibiting the WIN site stemmed from the observation that a short acetylated WIN peptide based on the KMT2A (MLL1) WIN motif (Ac-ARA-NH_2) binds tightly to the WIN site of WDR5, with an affinity of 120 nM [34]. Modification and optimization of this tripeptide sequence resulted in cell permeable peptidomimetic tool compounds—MM-101 and MM-102—which (as the description implies) engage the WIN site of WDR5 by mimicking the arginine of the WIN motif [152]. Further structure-based development and optimization of this series resulted in macrocyclic peptidomimetic WIN site inhibitors

MM-401 [38] and MM-589 [153] (**Figure 1-11 A**). MM-401 binds the WIN site with relatively high affinity (~1 nM) and inhibits the HMT function of KMT2A complexes *in vitro*, consistent with the requirement of the KMT2A–WDR5 interaction for robust methyltransferase activity [30, 37]. Dou and co-workers originally proposed that WIN-site inhibitors would have efficacy against tumors bearing rearrangements of the KMT2A (MLL1) gene (abbreviated MLLr), a common occurrence in acute myelogenous leukemia (AML). This concept was, in turn, based on the idea that MLLr cancers almost always retain one wild-type copy of KMT2A, and are uniquely dependent on the HMT activity of wild-type KMT2A complexes for survival [154]. And indeed MM-401 appears to be highly selective against MLLr cancer cells and cell lines in vitro [38], where it depletes H3K4 trimethylation at *HOXA* genes, driving cellular differentiation and apoptosis. Subsequently, however, it became clear that MLLr cancers are not dependent on KMT2A, but instead rely on KMT2B (MLL2) [155]. Research in the Tansey Laboratory has provided evidence for a different, p53-dependent mechanism for sensitivity to WIN site inhibitors, described below. Given the frequent overexpression of WDR5 in a variety of cancers (see “WDR5 in cancer” section) and the various moonlighting functions of WDR5, it is likely that WDR5 inhibitors could be effective in a variety of cancer contexts.

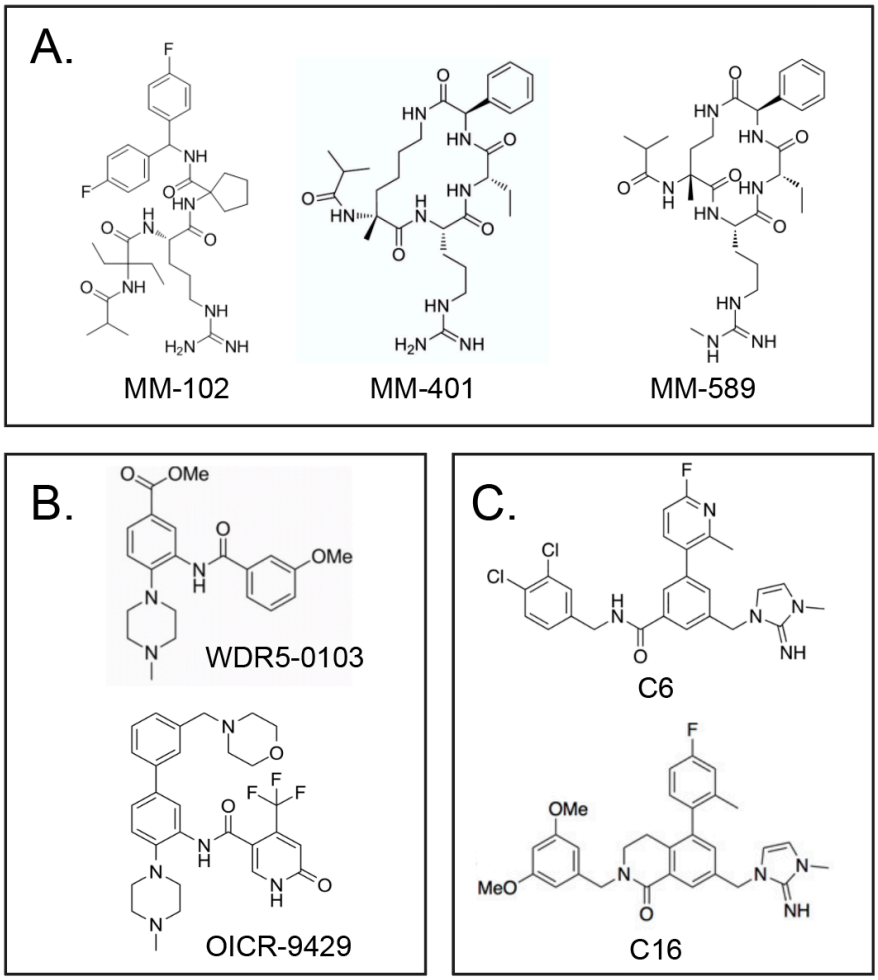

Figure 1-11: WDR5 WIN site inhibitors
(A) Peptidomimetic series of WIN site inhibitors. MM-102 K_i < 1 nM [152], MM-401 K_i = 0.9 nM [38], MM-589 K_i = 0.9 nM [153], measured by fluorescence-polarization displacement assay.
(B) Small molecule WIN site inhibitors developed by the Structural Genomics Consortium. WDR5-0103, K_d = 0.45 μM measured by isothermal calorimetry [156], and OICR-9429, K_d = 93 ± 28 nM measured by isothermal calorimetry [147].
(C) Small molecule WIN site inhibitors developed by Fesik and colleagues; C6 K_i = 0.1 nM and C16 K_i < 0.02 nM measured by TR-FRET displacement assay.

The Structural Genomics Consortium has generated a set of more traditional small molecule inhibitors of the WIN site by Fluorescence Polarization (FP) based high-throughput screening followed by structure-based optimization [147, 156-161]. An initial lead compound, WDR5-0103 (K_d ~450 nM) [156] was further optimized to produce OICR-9429 (K_d ~100 nM) (**Figure 1-11 B**), a compound that inhibits KMT2A HMT activity *in vitro* and shows inhibition of cancer cell lines in culture [135, 140, 147, 158]. The impact of OICR-9429 on MLLr cancer cells has not been reported, but it has been shown to inhibit AML cells that carry a mutant p30 isoform of the transcription factor C/EBPα [147]. The rationale for inhibition in this context is that the oncogenic p30 isoform of C/EBPα binds better to WDR5 and WDR5-containing complexes than non-oncogenic isoforms, but how p30 C/EBPα binds WDR5, whether this is through WIN site engagement, and how this connects to HMT activity are all unknown. A second use for OICR-9429 was demonstrated in seminal work from the Berger laboratory [162], who showed that cells expressing gain-of-function (oncogenic) p53 mutants—which comprise the largest group of *TP53* mutations in human cancer—are uniquely sensitive to OICR-9429. Here, there is no direct contact between oncogenic p53 variants and WDR5, but rather sensitivity to the compound appears to result from selective induction of KMT2A expression by the oncogenic p53 variants, the impact of which is mitigated by WIN site blockade and inhibition of KMT2A HMT activity. Given the magnitude of involvement of p53 gain of function mutants in cancer, these findings open the door to a potentially huge therapeutic impact of a drug-like WIN site inhibitor outside of MLLr cancers.

Cancer is not the only disease state where WIN site inhibitors may be effective, and at least four studies have applied the WIN site inhibitors described above to other disease states. First, in a rat model of neuropathic pain, treatment with WDR5-0103 was found to reduce markers of neuropathic allodynia, indicating an analgesic effect of WIN site inhibitor [163]. Second, treatment with WDR5-0103 in a mouse model of Alzheimer's disease led to better performance of memory-oriented tasks [164]. Third, in a mouse model of chronic kidney disease MM-102 and OICR-9429 were both found to reduce markers of disease advancement, possibly

through muting the transcriptional response to TGF-β stimulation [126]. And finally, studies of *in vitro* fertilization techniques found that WIN site inhibitor MM-102 enhanced the efficiency of bovine and mouse *in vitro* fertilization protocols [165]. It is unclear if these findings are mediated by on-target mechanisms, but they paint an intriguing picture that WDR5 inhibitors might be useful for other applications.

A third avenue of WIN site inhibitor drug discovery is underway at Vanderbilt University led by Steve Fesik and Bill Tansey. This effort began by using NMR-based fragment screening and a library of >13,800 compounds to identify chemical moieties that bind the WIN site of WDR5. Several classes of hits were taken forward for structure-based optimization resulting in lead compounds including C6 [39, 166] and more recently C16 [167] (**Figure 1-11 C**). Cellular studies of C6 have revealed important insights into WDR5 function and the action of WIN site inhibitors. These studies uncovered the conserved function of WDR5 in regulating protein synthesis gene expression. Treating MLLr leukemia cells with C6 causes a loss of WDR5 chromatin binding and decreased expression of WDR5-bound ribosome protein genes (RPGs) [39]. This decreased RPG expression causes translational defects and nucleolar stress as well as induction of p53 that leads to p53-mediated apoptosis. Cellular sensitivity to C6 is p53-dependent, as MLLr cell lines that are mutant or null for p53 are largely insensitive to C6 treatment. Notably, these cellular responses to C6 occur before any changes in H3K4me3 are detected, indicating that the mechanism of sensitivity and cell killing is independent of H3K4 HMT activity. Because this response does not overtly involve MLLr fusion proteins, and instead relies on decreases in RPG expression, susceptibility to WDR5 inhibitors is likely to extend to other cancer contexts.

To explore the effectiveness of WIN site inhibitors in a cancer context separate from MLLr leukemias, experiments were performed in neuroblastoma cell lines. Cell growth response curves revealed that C6 WIN site inhibitor is only effective at inhibiting cell growth in neuroblastoma cell lines where the *MYCN* gene is amplified and p53 expression is wild-type. Without high levels of N-MYC or with mutant or null p53, C6 did not impair the growth of

neuroblastoma cells. Additionally, similar to the MLLr cell lines, sensitive neuroblastoma cells exhibit decreased expression of RPGs and activation of p53 leading to apoptosis [82]. The similar effect of C6 in MLLr leukemias and *MYCN*-amplified neuroblastoma cells clearly demonstrates that the anti-proliferative action of WIN site inhibitors is not specific to MLL fusion cancers. Cells with wild-type p53 and MYC deregulation are also sensitive. Notably, C6 does not disrupt the interaction between MYC and WDR5, but does disrupt WDR5 and MYC binding to chromatin at ribosome protein genes [62, 82], which reduces the efficiency of MYC-driven biomass accumulation. Thus, WIN site inhibitors might be a useful therapeutic strategy for a variety of MYC-driven cancers [81].

The WIN site of WDR5 is a major hub for protein interactions, however, which interactions are affected by blocking the WIN site is unclear. Studies to date have done little to clarify this issue. C6 shows patterns of selectivity to MLLr and N-MYC-amplified cells, but sensitivity involves downstream activation of p53 and does not significantly MLL/SET1 HMT marks in cells. Targeting the WIN site of WDR5 can inhibit cells bearing the oncogenic p30 C/EBPα variant, but it is unclear if or how this C/EBPα protein directly binds to WDR5. And there is no direct contact between p53 gain-of-function mutants and WDR5, yet OICR-9429 appears highly effective in that setting. Potent WIN site inhibitors likely impact all proteins that engage the WIN site on WDR5, but particular proteins that tether WDR5 to chromatin at RPGs, or that dominate in certain cancer contexts, have yet to be identified. In order to understand the full potential of WIN site inhibitors, and the mechanistic details of their actions in cells, an unbiased analysis of the effect of WIN site inhibitors on the WDR5 interactome is needed.

Conclusion

The extensive moonlighting capabilities of WDR5 are enabled by the repeated use of two binding sites on WDR5. The WIN site, in particular, is a key interaction hub for WDR5 and a prime target for anti-cancer drug discovery efforts. WIN site inhibitors can selectively inhibit certain cancer cells, but the specifics of how these inhibitors act in cells are unclear leading to

two important questions. First, are there undiscovered moonlighting functions for WDR5 that rely on the WIN site? And second, what protein interactions are affected by the WIN site? Defining the WIN site interactome has potential to reveal undiscovered moonlighting functions for WDR5 and identify the protein interactions that are impacted by WIN site inhibitors.

Chapter II

Materials and Methods

Plasmid constructions

Molecular cloning was performed using XL1Blue (Agilent) or NEB 5-alpha Competent *E. coli*. PCR amplifications were performed using Q5 High-Fidelity DNA Polymerase (NEB). pcDNA3.1 containing the PDPK1 ORF and a C-terminal FLAG epitope tag was purchased from Genscript. Point mutations were generated by reverse mutagenesis or Gibson assembly modification. The PDPK1-FLAG sequences were then amplified and cloned into pBabe-puro [168] by Gibson assembly. PDPK1-EGFP fusions were similarly constructed by Gibson assembly.

Targeting vectors for endogenous FKBP(F36V) tagging were modified from pUC19-based targeting vectors that were a gift from Richard Young (Addgene #104370 and #104371) [169]. Vectors contain FKBP12(F36V)-P2A-BFP or FKBP12(F36V)-P2A-mCherry, and were modified by Gibson Assembly to include asymmetrical homology arms. Homology arms were amplified from U2OS genomic DNA purified with Purelink genomic DNA mini prep kit (Invitrogen). Homology arms used for PDPK1 are 200 bp 5' and 900 bp 3' surrounding and not including the stop codon. Homology arms used for WDR5 are 200 bp 5' (up to the stop codon) and 800 bp 3' (starting 17bp after the stop codon to ensure deletion of PAM sequence). Plasmids were verified by Sanger sequencing and prepped with the QIAGEN Midi-prep kit.

Cell lines

HEK293 (RRID:CVCL_0045), HEK293T (RRID:CVCL_1926), and U2OS (RRID:CVCL_0042) cells were cultured in DMEM with 10% FBS and 10 U/ml Penicillin-Streptomycin (Gibco 15140122). CHP134 cells (RRID:CVCL_1124) were cultured in RPMI with 10% FBS and 10 U/ml Penicillin-Streptomycin (Gibco 15140122). All cells were cultured at 37˚C and 5% CO2 and split every 2-4 days. HEK293, HEK293T, and U2OS were purchased from

ATCC. CHP134 cells were purchased from Sigma. All cell lines were tested for mycoplasma. HEK293, HEK293T, and U2OS are female. CHP134 cells are male.

Bacteria

The *E. coli* strain used for protein expression for biochemical assays is Rosetta 2-BL21; for protein purification for crystallization we used BL21-Gold (DE3) *E. coli*.

Generation of stable cell lines

HEK293T (approximately 500,000) cells were plated in 60 mm dishes and the next day cells were transfected by the calcium phosphate method. For retroviral vectors, pBabe vector of interest and pCL10A vector were co-transfected. For lentiviral transfections, lentiviral vector of interest, psPAX2, and pMD2 were co-transfected. Transfected cells were grown overnight, media replaced with fresh media and grown for 24 hours. Virus-containing media was collected by filtering through 0.45 μm filter and either immediately applied to target cells or stored in aliquots at -80˚C. To transduce target cells, 1 mL viral media and 2 mL fresh media were mixed with 8 μg/ml polybrene, incubated for 5 minutes, then applied to 1-2 million target cells. This was repeated with new virus the next day. After two rounds of transduction, cells were selected with 1 μg/ml puromycin. Proper expression was confirmed by western blotting.

Re-ChIP assay

ReChIP assays were performed in hygromycin-resistant retroviral stable HEK293 cells expressing C-terminally tagged c-MYC (pBabe-IGH-MYC-FLAG). Approximately $2x10^7$ cells were used per reChIP sample. Cells were cross linked with 0.75% formaldehyde for 10 min at room temperature. Crosslinking was quenched by adding glycine to a final concentration of 0.125 M and incubating for 10 minutes. Cells were washed twice in PBS, then each plate was scraped into 1.5 mL FALB (50 mM HEPES pH 7.5, 140 mM NaCl, 1 mM EDTA, 1% Triton X-100) supplemented 0.1% SDS, 1 mM PMSF, and Roche cOmplete Protease Inhibitor tablet. Lysates were incubated on ice for at least 10 minutes and then sonicated in 15 mL polystyrene tubes (Falcon 352099) using a Diagenode Bioruptor with approximately 1.8 mL lysate per tube,

50% power, 30s on/30s off, for 25 minutes. After sonicating in the Bioruptor, debris was spun out for 10 min at maximum speed, pooled, and aliquoted into 1.5 mL aliquots. Before proceeding to ChIPs, shearing efficiency was checked by decrosslinking a small fraction of chromatin and running it on a 1.5% agarose gel, and 2% was set aside as input. For the first ChIP a 20µl bed volume of BSA-blocked M2 agarose (Sigma) was added to the chromatin and rotated at 4˚C overnight. The next day the beads were pelleted and washed 5 minutes each with Low Salt ChIP Wash Buffer (20 mM Tris pH 8.0, 150 mM NaCl, 2 mM EDTA, 1% Triton X-100), High Salt ChIP Wash Buffer (20 mM Tris pH 8.0, 500 mM NaCl, 2 mM EDTA, 1% Triton X-100), LiCl ChIP Wash Buffer (10 mM Tris pH 8.0, 250 mM LiCl, 1 mM EDTA, 1% Triton X-100), and then twice with TE (10 mM Tris pH 8.0, 1 mM EDTA). DNA-protein complexes were eluted for 10 minutes at 65˚C in Elution Buffer (50 mM Tris-HCl pH 7.4, 10 mM EDTA, 1% SDS). The elution was brought up to 1 mL volume with FALB supplemented with 5 mg/ml BSA, 200 µg/ml sheared salmon sperm DNA (Invitrogen), 1 mM PMSF, and Roche cOmplete Protease Inhibitor tablet and taken forward to a second ChIP. For the second ChIP, 800ng IgG (Cell Signaling Normal Rabbit IgG #2729) or anti-WDR5 antibody (Cell Signaling D9E1I) was rotated overnight at 4˚C. The next day protein A beads (Roche) blocked with BSA and salmon sperm DNA were added to each ChIP and incubated for at least 2 hours before washing 5 minutes each with Low Salt ChIP Wash Buffer, High Salt ChIP Wash Buffer, LiCl ChIP Wash Buffer, and then twice with TE. Samples (ChIPs and inputs) were then brought to 50 µl in TE supplemented with 0.1% SDS and 20 µg proteinase K and decrosslinked overnight at 65˚C. Proteinase K was heat-inactivated at 95˚C for 20 minutes before proceeding to qPCR. Reactions were brought up to 200 µl with TE and qPCR was performed in triplicate using SYBR Fast 2x mastermix (Kapa Biosystems), gene specific primers (see **Table 2-1**), and 1µl diluted ChIP DNA and normalized to input.

Table 2-1: Primers for re-ChIP qPCR

Primer name	Primer sequence
SNHG15_ChIP	cgccactgaacccaatcc
SNHG15_ChIP	tctagtcatccaccgccatc
RPL23_ChIP	GCCTGAAGGAGAGCAAAG
RPL23_ChIP	AGGTTTTGTTTCTGGAGGAT
RPL24_ChIP	GGACGACAGAGAGGAGTTCT
RPL24_ChIP	CTTTTGTCTTTCCGTGGAG
PUM1_ChIP	TATGAAGGGACAATCTGCTC
PUM1_ChIP	AATCCATCTTCATCCTACCG
RPS6_ChIP	GAGACCCTTCTCCACCTAAA
RPS6_ChIP	CGAGTGTTAGACTGGGTTTG
RPS14_ChIP	GAAAGACCCCCGTCTCTCGT
RPS14_ChIP	GAGACGACGTGCAGGTAGGAG
SNHG15 GB_ChIP (-ve)	agatccgtgccatctaatgt
SNHG15 GB_ChIP (-ve)	tgatcatctgaaatgtggcta

Genome editing for knock-in of degradable tag

Targeting vectors were constructed as described under “Plasmid constructions.” The gRNA targeting PDPK1 for C-terminal tagging binds the sense strand and cuts 5 bases upstream of the stop codon: CAGGCCACGTCACTGCACAG. The gRNA targeting WDR5 for C-terminal tagging binds the antisense strand and cuts 8 bases downstream of the stop codon: CTCTCGCGGGCAGGAGCAAA. Chemically modified sgRNAs were synthesized (Synthego) and CRISPR reagents and targeting vectors were delivered to cells using the Neon Electroporation Transfection System (Invitrogen). Reactions of Cas9-sgRNA ribonucleoprotein (RNP) complexes were formed three at a time by combining recombinant Cas9 (Synthego) and sgRNA at a 1:3 ratio in Neon buffer R (Invitrogen) and incubating at room temperature for 10 min. RNP complexes were stored at 4˚C until use. Electroporation reactions were performed in triplicate so that each triplicate of reactions included 10 pmol Cas9 with 30 pmol sgRNA, ~900,000 U2OS cells or ~600,000 CHP134 cells, 12.5 µg targeting vectors (1:1 BFP:mCherry) brought to approximately 35 µl with Neon buffer R. Using this mixture, three electroporation rounds were performed using 10 µl Neon tips. Conditions for U2OS cells were 1230 V, 10 ms pulse width, and 4 pulses. Conditions for CHP134 cells were 1200 V, 20 ms pulse width, and 3 pulses. Cells were immediately placed into warm, antibiotic-free media (DMEM for U2OS and RPMI for CHP134) supplemented with 10% FBS and allowed to recover for two days. After expansion and at least five days in culture, cells were analyzed by flow cytometry for expression of fluorescent markers as a proxy for proper integration. Cells were counter stained with Zombie NIR viability dye and resuspended in 0.5% BSA in PBS. Cells were analyzed using a BD LSRII Fortessa (BD Biosciences-US) instrument for expression of BFP and mCherry fluorescent markers. After confirmation of BFP/mCherry positive cells, a population of double positive cells was sorted using a BD FACSAria III (BD Biosciences-US) and analyzed by western blotting.

Genome editing for R3A point mutation

Plasmid pX459 containing Cas9 linked to puromycin resistance marker was a gift from Feng Zhang (Addgene # 62988) [170] and was modified by digesting with BbsI and ligation of

annealed gRNA sequences. Three gRNAs targeting the N-terminus of PDPK1 were inserted into pX459 using BbsI sites, and proper insertion was confirmed by Sanger sequencing. The sequences of the gRNAs are:

CCGACGCGGGGCCCATGGCCAGG

TGGCTGGTGGTCCTGGCCATGGG

CACCAGCTGGCTGGTGGTCCTGG

A 200 bp single stranded oligonucleotide targeting the N-terminal region of PDPK1 was designed to mutate the third codon from AGG to GCG (R3A) and silence the PAM sequences. Proper repair with this ssODN also introduced a SpeI site in codons 5 and 6 for screening purposes. The 200 bp oligo was ordered from IDT with the sequence (start codon is bold; Spec site is underlined):

GGCCATTGCTGGGGCTCCGCTTCGGGGAGGAGGACGCTGAGGAGGCGCCGAGCCGCGC
AGCGCTGCGGGGGAGGCGCCCGCGCCGACGCGGGGGCC**atg**GCTGCGACCACTAGTCAG
CTGGTGAGCGCGCGGCGGCGGACTGGACGCGCCGGTTTGTTACCCTGCCGGGTCCGGC
GGCCGCCCGGGTCCGGCGAGGCGGG

For transfections, ~500,000 HEK293 cells were plated one day prior, and then transfected using Lipofectamine 3000 to deliver 0.5 µg pMAX-GFP, 0.5 µg pX459 with gRNA, 1 µg pBluescript empty vector and 1 µl 10µM ssODN template. One day after transfection cells were selected for 48 hours with 1 µg/ml puromycin to enrich for cells expressing Cas9. Individual genetic variants were isolated by single cell dilutions and analyzed for introduction of the SpeI restriction marker. Genomic DNA from the individual clones was purified with the Purelink genomic DNA mini kit (Invitrogen), and DNA was analyzed by PCR amplification with OneTaq (NEB) using GC Buffer and 10% GC enhancer. Primers for this amplification are: ACTAGCAAAGTTGCGCCTCTGAGT and CGCCAAGCCGAAAACAAACTTTC. PCR products were then analyzed by SpeI digest to screen for cells with homozygous integration. Clones carrying the R3A mutation were confirmed by Sanger sequencing and analyzed by western blotting.

Density Sedimentation Analyses

For stably expressing samples, FLAG-WDR5 HEK293 cells were plated one day prior to analysis. For treated samples, HEK293 cells were plated one day prior and then treated with DMSO or 30 μM C6 for five hours prior to analysis. Cells were washed twice in cold PBS and then lysed in Kischkel buffer (50 mM Tris pH 8.0, 150 mM NaCl, 5 mM EDTA, 1% Triton X-100) supplemented with Roche cOmplete Protease Inhibitor Cocktail and 1 mM PMSF. Protein concentrations of the lysates were measured by Bio-Rad Protein Assay Dye Reagent and normalized. Equal amounts of lysates were carefully loaded onto 5-40% sucrose gradients prepared in 5mL, 13 x 51 mm polypropylene centrifuge tubes (Cat# 326819, Beckman Coulter). Samples were centrifuged in a Beckman L-90K ultracentrifuge with a SW 55 Ti rotor at 4˚C for 14 hr at 50,000 rpm (accelerate max; decelerate no brake). 0.5 mL fractions were collected and resuspended in SDS sample buffer supplemented with β-mercaptoethanol. Samples were heated at 95˚C for five minutes and then analyzed by western blotting.

Generating lysates for western blotting

Cells were collected by scraping into PBS. Cell pellets were lysed in RIPA buffer (10mM Tris pH 8.0, 0.5 mM EDTA, 1% NP-40, 0.1% deoxycholate, 0.1% SDS, 140 mM NaCl) supplemented fresh with Roche cOmplete Protease Inhibitor Cocktail, 1 mM PMSF, and Roche PhosSTOP inhibitor tablet. Lysates were incubated on ice for at least 20 minutes and insoluble material was cleared by 10 minutes of centrifugation at 4˚C. Protein concentrations were measured by Bio-Rad Protein Assay Dye Reagent, normalized, and taken forward for western blotting analysis.

Western blotting analysis

Samples were boiled in SDS sample buffer supplemented with β-mercaptoethanol and run on homemade acrylamide gels. After transferring proteins to PVDF membrane (PerkinElmer), the membranes were blocked in 5% non-fat dry milk and TBST solution for at least one hour, and then incubated with primary antibodies overnight. The antibodies used are

detailed in the Figures and the Key Resources Table in my paper [171]. Membranes were washed three times with TBST and incubated with HRP-conjugated secondary antibodies. Blots were developed by ECL with an appropriate dilution of Supersignal West Pico Plus Chemiluminescent Substrate (Thermo Fisher Scientific).

FLAG immunoprecipitations

For transient transfections, cells were transfected by the calcium phosphate method three days prior to experiments. Stable pBabe HEK293 cells were plated two days prior to experiments. To treat cells prior to IPs, media was removed and replaced with media containing DMSO, 30 μM C6, or 30 μM C6nc for 4 hours unless otherwise indicated in the figure legend. Cells were washed twice in cold PBS, then scraped into cold Kischkel buffer (50 mM Tris pH 8.0, 150 mM NaCl, 5 mM EDTA, 1% Triton X-100) or CHAPS buffer (40 mM HEPES pH 7.5, 120 mM NaCl, 1 mM EDTA, 0.3% CHAPS) supplemented with Roche cOmplete Protease Inhibitor Cocktail and 1 mM PMSF. Whole cell extracts were sonicated for 15 seconds and then clarified by 10 minutes of centrifugation at 4˚C. For ethidium bromide treatment, ethidium bromide was added to lysates at 200 μg/ml prior to sonication and maintained at 200 μg/ml for the duration of the IP. Anti-FLAG M2 affinity gel was equilibrated in lysis buffer and blocked at room temperature for at least 20 minutes with 1 mg/ml BSA in lysis buffer. Protein concentrations of lysates were measured with Bio-Rad Protein Assay Dye Reagent and normalized, and then a 20 μl bed volume of BSA-blocked anti-FLAG M2 affinity gel was added to each sample. For FLAG IPs from treated lysates, treatments were added to the lysates and incubated simultaneous with the overnight FLAG IP. IPs were incubated on a rotator overnight at 4˚C. The next day, IPs were centrifuged at 2500 rpm, and washed four times for five minutes in cold lysis buffer. After last wash, the remaining liquid was aspirated with a 27 gauge needle and bead samples were boiled in SDS sample buffer supplemented with β-mercaptoethanol. Samples were taken forward for western blotting.

SILAC media and cell culture conditions

Heavy and light media for SILAC was prepared using DMEM for SILAC (Thermo Scientific) and adding 0.79 mM heavy or light ($^{13}C_6$; $^{15}N_2$) lysine, 0.39 mM heavy or light ($^{13}C_6$;$^{15}N_4$) arginine, and 3.5 mM light proline. Media was then sterile filtered and supplemented with 10% dialyzed FBS and 10 U/ml Penicillin-Streptomycin.

SILAC sample preparation

For each sample three plates of $3x10^6$ heavy or light amino acid-labeled HEK293 cells were plated. The next day cells were transfected with 5 µg pFLAG-WDR5 (or pcDNA3.1 PDPK1-FLAG or pFGH-MYC) and 1 µg pMAX-GFP using the calcium phosphate method. When cells were confluent (2-3 days), cells were lysed in Kischkel buffer supplemented with Roche cOmplete Protease Inhibitor Cocktail and 1 mM PMSF. Whole cell extracts were sonicated for 15 seconds and then clarified by 10 minutes of centrifugation. Anti-FLAG M2 affinity gel (Sigma) was equilibrated in Kischkel buffer and blocked at room temperature for at least 20 minutes with 1 mg/ml BSA in Kischkel buffer. Protein concentrations were measured by Bio-Rad Protein Assay Dye Reagent. Lysates were rotated overnight at 4˚C with 5 µM C6 or C6nc and 20 µl bed volume of BSA-blocked anti-FLAG M2 affinity gel. The next day IPs were washed four times for five minutes with cold Kischkel buffer. Samples were transferred to new tubes and eluted twice with 30 µl 100 ng/µl FLAG peptide in TBST by agitation on low speed mixer for 15 minutes at room temperature. Samples were analyzed by western blotting for equivalent levels of heavy and light samples before being taken forward for mass spectrometry.

SILAC-based quantitative mass spectrometry

This sample processing was performed by Dr. Kristie Rose and Salisha Hill at the Vanderbilt University Mass Spectrometry Research Center. SILAC samples were mixed 1:1 and partially separated by SDS-PAGE. For PDPK1-FLAG samples were fully separated by SDS-PAGE. Gel regions were excised and cut into $1mm^3$ cubes and treated with 45 mM DTT for 30 minutes. Available Cys residues were carbamidomethylated with 100mM iodoacetamide for 45

minutes. After destaining with 50% MeCN in 25mM ammonium bicarbonate, proteins were digested with trypsin (10ng/uL) in 25mM ammonium bicarbonate overnight at 37°C. Peptides were then extracted by gel dehydration with 60% MeCN, 0.1% TFA, vacuum dried, and reconstituted in 0.1% formic acid.

Peptides were analyzed by LC-coupled tandem mass spectrometry (LC-MS/MS) using MudPIT analysis with an 8 step salt pulse gradient. Peptides were loaded onto a self-packed biphasic C18/SCX MudPIT column using a Helium-pressurized cell. The MudPIT column consisted of 360 x 150µm i.d. fused silica, which was fritted with a filter-end fitting (IDEX Health & Science) and packed with 5 cm of Luna SCX material (5 µm, 100 Å) followed by 4 cm of Jupiter C18 material (5 µm, 300 Å, Phenomenex). Once the sample was loaded, the MudPIT column was connected using an M-520 microfilter union (IDEX Health & Science) to an analytical column (360µm x 100µm i.d.), equipped with a laser-pulled emitter tip and packed with 20 cm of C18 reverse phase material (Jupiter, 3 µm beads, 300 Å, Phenomenex). Using a Dionex Ultimate 3000 nanoLC and autosampler, MudPIT analysis was performed with an 8-step salt pulse gradient (25, 50, 100, 200, 300, 500, 750, and 1M ammonium acetate). Following each salt pulse, peptides were gradient-eluted from the reverse analytical column at a flow rate of 350 nL/min, and the mobile phase solvents consisted of 0.1% formic acid, 99.9% water (solvent A) and 0.1% formic acid, 99.9% acetonitrile (solvent B). For the peptides from the first 7 SCX fractions, the reverse phase gradient consisted of 2% to 50% B in 83 min, 50% B from 83-84 min, 50% down to 2% B from 84-85 min, and column equilibration at 2% B from 85-95 min. For the last SCX-eluted peptide fraction, the peptides were eluted from the reverse phase analytical column using a gradient of 2% to 98%B in 83 min, 98% B from 83-84 min, 98 to 2% B from 84-85 min, and 2% B from 85-95 min. Peptides were introduced via nanoelectrospray into a Q Exactive mass spectrometer (Thermo Scientific) operating in a data-dependent mode. The instrument method consisted of MS1 using an MS AGC target value of $3x10^6$, followed by up to 20 MS/MS scans of the most abundant ions detected in the preceding MS scan. The MS2

intensity threshold was set to $5x10^4$, dynamic exclusion was set to 20s, and peptide match and isotope exclusion were enabled.

SILAC MS data analysis

This analysis was performed by Dr. Kristie Rose and Salisha Hill at the Vanderbilt University Mass Spectrometry Research Center. For peptide and protein identification, data were analyzed using the Maxquant software package [172]. MS/MS spectra were searched against a human subset of the UniprotKB protein database. Precursor mass tolerance was set to 6ppm, and variable modifications included oxidation of methionine and carbamidomethylation of cysteine. Enzyme specificity was set to trypsin/P, and a maximum of 2 missed cleavages were allowed. The target-decoy false discovery rate (FDR) for peptide and protein identification was set to 1% for both peptides and proteins. A multiplicity of 2 was used, and Arg10 and Lys8 heavy labels were selected. For SILAC protein ratios, a minimum of 2 unique peptides and a minimum H/L ratio count of 2 were required, and normalized ratios were considered for all presented analysis. In total, 754 proteins are quantified by these criteria in both replicates. The label swap revealed seven contaminating keratinous proteins (included in Table S1 from [171]) which were removed before further analysis. SILAC data were also assembled in Scaffold to view protein sequence coverage and assigned spectra for identified peptides. Heatmaps of these data were generated using Seaborn. Pearson correlation analysis one sample *t*-test of the SILAC data was performed using Perseus software package [173].

Immunoprecipitations of endogenous proteins

HEK293 or U2OS cells were plated to be confluent two days later. If cells were treated, media was changed to media containing the appropriate treatment for the indicated time. Each plate was rinsed twice with PBS, and then scraped into Kischkel buffer supplemented with Roche cOmplete Protease Inhibitor Cocktail, 1 mM PMSF, and Roche PhosSTOP inhibitor tablet. For suspension cells, cells were pelleted, washed twice in PBS, and then resuspended in lysis buffer. Lysates were sonicated for 15 seconds and cleared by centrifugation for 10 minutes

at 4˚C. Protein concentrations were measured by Bio-Rad Protein Assay Dye Reagent. For each IP 1-5 mg of lysate was used as total input and 3-10 µg of antibody. Antibodies used for IPs were anti-WDR5 (Bethyl A302-429A), anti-PDPK1 (Bethyl A302-130A), anti-FAM91A1 (Bethyl A301-588A), anti-WDR11 (Bethyl A302-632A), and an equivalent amount of Normal Rabbit IgG (Cell Signaling Technologies #2729S). Antibodies and lysates were rotated at 4˚C overnight, and the next day a 20 µl bed volume of Roche Protein A agarose, blocked for at least 20 minutes with 1 mg/ml BSA in Kischkel buffer, was added to each sample. IPs were incubated with protein A agarose for 2-6 hours and then washed four times for five minutes with 1 ml cold Kischkel buffer, transferring to new tubes before last wash. Samples were eluted with SDS sample buffer supplemented with β-mercaptoethanol and taken forward for western blotting analysis.

Subcellular fractionation

Subcellular fractionation was performed similar to as described [174]. A confluent plate of U2OS cells was washed twice in PBS, scraped into PBS and pelleted. Cells were resuspended in 200 ml Buffer A (10 mM HEPES, pH 7.9, 10 mM KCl, 1.5 mM MgCl2, 0.34 M sucrose, 10% glycerol, 1 mM DTT, Roche cOmplete Protease Inhibitor Cocktail and 1 mM PMSF) and incubated on ice for 8 minutes. Samples were centrifuged at 1,300 x g at 4˚C for five minutes. The supernatant (S1 fraction) and pellet (P1 fraction) were separated and S1 was clarified by high-speed centrifugation at 4˚C for 10 minutes. The resulting supernatant (S2 fraction) was collected and the pellet (P2 fraction) was discarded. The P1 fraction was washed once with 500 ml Buffer A and centrifuged 1 minute at 1,300 x g. The P1 fraction was lysed by resuspending in 100 ml Buffer B (3 mM EDTA, 0.2 mM EGTA, Roche cOmplete Protease Inhibitor Cocktail and 1 mM PMSF) and incubating for 30 minutes on ice, followed by centrifugation at 1,700 x g at 4˚C for five minutes. The resulting supernatant (S3 fraction) was separated from the chromatin-enriched pellet (P3 fraction). P3 was washed once with 500 ml Buffer B and resuspended in 400µl SDS sample buffer. All samples were brought to 400 µl in

SDS sample buffer and boiled for five minutes. Equal volumes of each fraction were taken forward for western blotting.

EGFP imaging experiments

U2OS expressing PDPK1-EGFP fusions were plated onto coverslips coated with poly-D lysine and cultured overnight in DMEM. Cells were then treated with 20 nM leptomycin B (LMB) or an equivalent volume of 70% methanol vehicle control in DMEM for four hours. Cells were fixed in 4% paraformaldehyde for 10 min at room temperature then washed three times for five minutes with PBS. Cells were permeabilized in PBS containing 0.1% (v/v) Triton X-100 for five minutes then washed three times for five minutes with PBS. Coverslips were then mounted in ProLong Diamond Antifade Mountant with DAPI. Confocal images were acquired using an Andor DU-897 EMCCD camera mounted on a Nikon Spinning Disk Microscope.

Proximity ligation assay

Retroviral pBabe-puro U2OS cells stably expressing PDPK1-FLAG were plated onto coverslips pretreated with poly D-lysine. After plating, cells were treated overnight with 30μM C6 or C6nc. Cells were fixed in 4% methanol-free formaldehyde and permeabilized with 0.5% Triton X-100. Proximity ligation assays were performed with the Duolink PLA mouse/rabbit kit (Sigma) according to the manufacturer's instructions. Primary antibodies used were mouse anti-FLAG and rabbit anti-WDR5 (Bethyl 429A). Confocal images were acquired using an Andor DU-897 EMCCD camera mounted on a Nikon Spinning Disk Microscope.

Treatment for targeted protein degradation

To deplete cells of FKBP(F36V)-tagged proteins, cells were first plated in normal media, and the next day media was changed to media containing 500 nM dTAG47 bifunctional small molecule, synthesized through the Vanderbilt Chemical Synthesis Core. DMSO vehicle control was 0.01% DMSO. After the time point indicated, cells were collected for the relevant analysis.

Preparation of RNA for RNA-Seq

Cells were plated at sub-confluence and collected after 1-2 days. Where appropriate, media on cells was changed to contain the indicated treatments for the indicated timeframes. Cells were collected in Trizol and RNA was purified with Direct-Zol RNA Miniprep kit (Zymo) with on-column DNaseI treatment. RNA was submitted to Genewiz or the Vanderbilt Technologies for Advanced Genomics Core Laboratory for library preparation and deep sequencing.

RNA extraction and RT-qPCR analysis

Cells were plated at sub-confluence and the next day media was changed to contain the appropriate treatment (ex. 500 nM dTAG47 or 0.01% DMSO vehicle control). Cells were collected in Trizol and RNA was purified with Direct-Zol RNA Miniprep kit (Zymo) with on-column DNaseI treatment. RNA was reverse transcribed with LunaScript RT SuperMix Kit (New England Biolabs) and analyzed by qPCR using gene-specific primers (see **Table 2-2**) and KAPA SYBR FAST qPCR 2x Master Mix.

Table 2-2: Primers for RT-qPCR

Primer name	Primer sequence
CENPE_ mRNA_1	AGCTACAGGCCTACAAACCA
CENPE_ mRNA_2	TGAGCTGTCTTCTCAGATACGC
CENPF_mRNA_1	TGAGCTGGAAGTAGCACGAC
CENPF_mRNA_2	CGGCCTTGAATAGCATCTTCTG
ASPM_mRNA_1	GGAAAGATGTGGGAGAACGTC
ASPM_mRNA_2	AACATAGCCAACCCTGTGAC
SGO2_ mRNA_1	ACCCAAAAATCAGGAATAGGTGATA
SGO2_ mRNA_2	TCTGCTTGTCCGTTCTGAAG
KIF18A_ mRNA_1	GAGAGGCACATGAAGAGAAGT
KIF18A_ mRNA_2	TGTTTTCCGGACGTACACGA
KIF20B_ mRNA_1	AATGGCAGTGAAACACCCTG
KIF20B_ mRNA_2	ACATTTCACCAAGTCCTCCTCC
CCAR1_RNA_1	GGAGGCTGATGGAGAACAGGATG
CCAR1_RNA_2	AGCTCGACTTTCTAATTCTTTTCGG
TOP2A_ mRNA_1	AAGTGTCACCATTGCAGCCT
TOP2A_ mRNA_2	ACCCACATTTGCTGGGTCAC
SMC2_mRNA_1	TTGACAGAAGCTGAAGAGCGA
SMC2_mRNA_2	TTGTTCACCTTTTGCCATGC
SMC3_ mRNA_1	TGTGATTGTGGGCAGAAATGG
SMC3_ mRNA_2	CCGCTGTTCTGGACGAAGAT
SMC4_ mRNA_1	TTGAACAGCATTCCTCCTCCC
SMC4_ mRNA_2	GGAAAAGCGCTTATGGAAAGGT
RPL35_mRNA_1	AACAGCTGGACGACCTGAAG
RPL35_mRNA_2	ACTGTGAGAACACGGGCAAT
GAPDH_mRNA_1	AAGGTGAAGGTCGGAGTCAAC
GAPDH_mRNA_2	GTTGAGGTCAATGAAGGGGTC
RPL14_mRNA_1	GTCTCCTTTGGACCTCATGC
RPL14_mRNA_2	ATGGCCTGTCTCCTCACTTG

Purifying recombinant WDR5 for binding assays

pSUMO plasmids containing N-terminal 6xHis-SUMO tagged WDR5 (amino acids 22-334), WT or F133A mutant, were transformed into Rosetta DE3 competent cells. Bacterial cultures were grown in LB medium supplemented with 50 µg/ml kanamycin. A 50 mL starter culture was grown overnight and used to inoculate a 500 mL culture. When the culture reached OD of approximately 0.8, it was induced with 1 mM isopropyl-beta-D-thiogalactoside (IPTG) for 3 hours. Bacteria were aliquoted, pelleted, and stored at -80˚C. To purify 6xHis-SUMO-WDR5 variants, bacterial pellets were thawed on ice and resuspended in 5 mL SUMO lysis buffer (50 mM NaH_2PO_4, 300 mM NaCl, 3 mM imidazole, adjusted to pH 8.0) supplemented with Roche cOmplete Protease Inhibitor Cocktail and 1 mM PMSF. Bacteria were lysed by sonication and cleared by centrifugation. Proteins were purified by incubating bacterial lysates with Ni-NTA agarose (QIAGEN). After incubation, agarose was washed 3x with 5 mL SUMO lysis buffer. Proteins were either left on beads, or eluted with SUMO elution buffer (1x PBS, 250 mM imidazole, 10% glycerol, 2mM DTT). Protein concentration and purity were assessed by SDS–PAGE and Coomassie Blue staining alongside BSA standards.

Far Western assay

PDPK1-FLAG (WT and R3A) were FLAG immunoprecipitated from pBabe retroviral stable HEK293 cell lines. IP samples were run on an 8% gel and transferred to PVDF. Membrane was stained with Ponceau, destained in water, and imaged before blocking in 5% non-fat dry milk and TBST solution for one hour. Membrane was incubated overnight with recombinant 6xHis-SUMO-WDR5 in 2% non-fat dry milk and TBST solution milk supplemented with 10% glycerol, 1mM DTT, and 0.5mM EDTA. Membrane was washed three times in TBST, then probed with anti-WDR5 antibody.

***In vitro* PDPK1 pulldown**

In vitro transcription and translation of PDPK1 variants was performed using the Takara Human Cell-Free Protein Expression System (Takara #3281) following the manufacturer's

protocol. Yield of the *in vitro* reaction was quantified by western blotting alongside a FLAG-tagged standard. For binding reactions each *in vitro* reaction was incubated with 20 µg of 6xHis-SUMO-WDR5 (22-334) bound to NTA-Ni beads. After combining PDPK1 and WDR5, inputs were removed and binding reactions were performed in a 500µl volume in Kischkel buffer for 2 hours at 4˚C. Beads were washed with 1 ml cold Kischkel buffer four times for two minutes and transferred to new tubes before the last wash. Samples were eluted by boiling in SDS sample buffer supplemented with β-mercaptoethanol and analyzed by western blotting.

Peptide pulldown experiments

Biotinylated peptides were pre-bound to streptavidin agarose by adding an excess of the indicated peptide (60 µg, approximately 3x excess to binding capacity of streptavidin beads) to a 20 µl bed volume of Pierce Streptavidin Agarose and rotating at 4˚C for one hour. Beads were washed three times for five minutes with cold Kischkel buffer and transferred to new tubes. 20 µg of 6xHis-SUMO-WDR5 purified protein was added and samples were rotated for two hours at 4˚C. Beads were washed four times for two minutes with cold Kischkel buffer, eluted in SDS sample buffer supplemented with β-mercaptoethanol, and analyzed by western blotting.

Purification of PDPK1 for MS analysis

HEK293 cells were lysed in Kischkel buffer supplemented with Roche cOmplete Protease Inhibitor Cocktail, 1 mM PMSF, and 5 mM sodium orthovanadate. IP reactions were performed as for an endogenous IP with 5 mg lysate and 10 µg anti-PDPK1 (Bethyl A302-130A) or Normal Rabbit IgG (Cell Signaling Technologies #2729S). Antibodies were incubated with lysates overnight at 4˚C on rotator, and the next day a 20 µl bed volume of BSA-blocked Roche Protein A agarose was added to each IP. IPs were incubated with protein A agarose for 3 hours and then washed four times for five minutes with 1 ml cold Kischkel buffer, transferring to new tubes before last wash. Samples were eluted with SDS sample buffer supplemented with β-mercaptoethanol. Samples were run on a gel and stained with SuperBlue Ultra Coomassie

Stain. The band corresponding to PDPK1 was cut out and taken forward for analysis by mass spectrometry.

Mass spectrometry analysis of endogenous PDPK1

This sample processing and analysis was performed by Dr. Kristie Rose and Salisha Hill at the Vanderbilt University Mass Spectrometry Research Center. Gel band was cut out and diced into 1mm3 cubes. Proteins were treated for 30 minutes with 45 mM DTT, and available Cys residues were carbamidomethylated with 100mM iodoacetamide for 45 minutes. After destaining with 50% MeCN in 25mM ammonium bicarbonate, proteins were digested with trypsin or AspN (10 ng/ul) in 25mM ammonium bicarbonate overnight at 37°C. Peptides were extracted by gel dehydration with 60% MeCN, 0.1% TFA, the extracts were dried by speed vac centrifugation, and reconstituted in 0.1% formic acid for LC-MS/MS. An analytical column was packed with 20cm of C18 reverse phase material (Jupiter, 3 µm beads, 300 Å, Phenomenox) directly into a laser-pulled emitter tip. Peptides were loaded on the capillary reverse phase analytical column using a Dionex Ultimate 3000 nanoLC and autosampler. The mobile phase solvents consisted of 0.1% formic acid, 99.9% water and 0.1% formic acid, 99.9% acetonitrile. Peptides were gradient-eluted at a flow rate of 350 nL/min, using a 90-minute gradient. The gradient consisted of the following: 1-72 min, 2-40% B; 72-78 min, 40-90% B; 78-79 min, 90% B; 79-80 min, 90-2% B; 80-90min (column re-equilibration), 2% B. A Q Exactive Plus mass spectrometer (Thermo Scientific) was used to mass analyze the eluting peptides using a data-dependent method. The instrument method consisted of MS1 using an MS AGC target value of $3x10^6$, followed by up to 16 MS/MS scans of the most abundant ions detected in the preceding MS scan. For identification of peptides, tandem mass spectra were searched with Sequest (Thermo Fisher Scientific) against a Homo sapiens subset database created from the UniprotKB protein database. Variable modification of +15.9949 on Met (oxidation), +57.0214 on Cys (carbamidomethylation), and +42.01056 on the N-terminus (acetylation) were included for database searching. Search results were assembled using Scaffold proteome software.

TR-FRET based peptide competition assays

These assays were performed by Joanna Grace Shaw in the Fesik Group. TR-FRET emissions were recorded on a BioTek Cytation 3 instrument and assays were performed with the indicated peptides. Two or more repeats were obtained, and average K_i values are reported. The PDPK1 and H3 peptides were unlabeled and the KMT2A (MLL1) peptide was a labeled 10-mer-Thr-FAM (ARTEVHLRKS-(Ahx-Ahx)(Lys- (5-FAM))) [34]. 100 nM KMT2A-5FAM peptide, 4 nM 6xHis-tagged WDR5 (24-334) protein and 1 nM anti HisTag-terbium antibody (Cisbio) were combined in FRET Buffer (1X Phosphate Buffered Saline, 300mM NaCl, 0.5mM TCEP, 0.1% CHAPS, pH 7.3). The indicated PDPK1 and H3 peptides were diluted in FRET Buffer and dispensed into 384-well, white, flat-bottom plates in a 10-point, 5x serial dilution scheme. Diluted peptides were incubated with the KMT2A-5FAM/WDR5/anti-His for one hour. The change in TR-FRET signal (Delta F) was measured on the Biotek Cytation 3 equipped with a filter cube containing an Ex 340/30 nM Em 620/10 filter and an Ex 340/30 Em 520 filter. Measurement plates were excited at a wavelength of 340 nm, and emission wavelengths of 495 and 520 nm were used. The 520/495 emission ratios (TR-FRET) were used to calculate an IC50 (peptide concentration at which 50% of the KMT2A-5FAM bound peptide is displaced) by fitting the inhibition data using XLFit software (Guilford, UK) to a four parameter dose-response (variable slope) equation. This was converted into a binding inhibition/displacement constant (K_i) using the formula [175]:

$$\text{Compound } K_i = [I]_{50} / ([L_{50}] / K^{pep}_d + [P]_0 / K^{pep}_d + 1)$$

where $[I]_{50}$ is the concentration of the free peptide at 50% inhibition, $[L]_{50}$ is the concentration of the free labeled ligand at 50% inhibition, $[P]_0$ is the concentration of the free protein at 0% inhibition, and $K_d{}^{pep}$ represents the dissociation constant of the 10-mer-Thr-FAM probe.

Purification of WDR5 for structural studies

These purifications were performed by William G. Payne in the Fesik Group. Human WDR5 (aa: 22–334) was cloned into a modified pET vector (pBG104) with a 6xHis-SUMO tag at the N terminus. The plasmid was then transformed into *E. coli* BL21-Gold (DE3) cells. One

hundred milliliters of LB starter was used to inoculate a 10L fermentation culture (BioFlo 415, New Brunswick Scientific) and grown at 37˚C. Fermentation growth media contained KH_2PO_4 (4 g/L), K_2HPO_4 (6 g/L), Na_2SO_4 (2 g/L), K_2SO_4 (1 g/L), NaCl (0.5 g/L), Yeast Extract (5 g/L), glycerol (2 ml/L), Antifoam (0.2 ml/L), 5% LB medium, glucose (25 g/L), $MgCl_2$ (2 mM), $CaCl_2$ (0.1 mM), NH_4Cl (2.5 g/L), and Kanamycin (50 mg/ml). When the cell density reached OD600 = 2.0, the temperature was lowered to 30˚C, and WDR5 expression induced by treatment with 1 mM isopropyl-beta-D-thiogalactoside (IPTG) overnight. Cell pellets were collected, dissolved in lysis buffer containing 1XPBS plus 300 mM NaCl, 20 mM imidazole, 5 mM BME, and 10% glycerol, and lysed by homogenization (APV-2000, APV). The lysate was cleared by centrifugation, filtered, and then applied to the Ni-column (140 mL, ProBond, Invitrogen). Bound protein was eluted using an imidazole gradient (0–300 mM). The His-SUMO-tag was cleaved by SUMO protease during dialysis and subsequently eliminated through a second Ni-column. WDR5 protein was then purified by size-exclusion chromatography (HiLoad 26/60, Superdex 75, GE Healthcare) using crystallization buffer (20 mM HEPES, pH 7.0, 250 mM NaCl, and 5 mM DTT). The purity of protein was assessed using SDS–PAGE. Purified WDR5 was then concentrated to 10 mg/mL, and stored at -80˚C.

Protein crystallization and data processing

These structural studies were performed by Dr. Bin Zhao in the Fesik Group. Purified WDR5 was crystallized in the presence of a five-fold molar excess of the acetylated PDPK1 15mer peptide under conditions containing 25% PEG 8K, 100 mM Bis-Tris pH 6.0, and 1 mM TCEP. The complex crystallized at 18˚C in the $P2_1$ space group (cell dimensions a=54.52 Å, b=47.23 Å, c=118.97 Å, β=90.92° with 2 molecules in the asymmetric unit). A single flash-cooled crystal diffracted to 2.5 Å, and data were collected on the Life Sciences Collaborative Access Team (LS-CAT) 21-ID-F beamline at the Advanced Photon Source (APS), Argonne National Laboratory. The WDR5–PDPK1 peptide structure was determined by the molecular replacement method using the WDR5-RBBP5 peptide complex (PDB ID: 2XL2) as the search molecule in Phaser [176]. The model was refined to a final R and R-free values of 21% and 25%,

respectively. The refined models and corresponding structure factor amplitudes were deposited in the Research Collaboratory for Structural Biology under accession numbers 6WJQ. Figures were prepared with PyMOL. 6WJQ was aligned with other WDR5 cocrystal structures using the PyMOL 'super' command.

Cell cycle analysis by flow cytometry

U2OS cell lines were plated at approximately 50% confluence and the next day media was exchanged to contain the indicated treatment. At the indicated time point, cells were collected by trypsinization and pelleted by centrifugation. Cell pellet was resuspended in PBS and fixed by adding drop-wise into 70% ethanol. Cells were stored in ethanol at -20˚C for at least 2 hours before washing once in PBS and resuspending in propidium iodide staining buffer (1x PBS, 10 µg/mL propidium iodide (PI), 100 µg/mL RNaseA, 2 mM $MgCl_2$). Samples were stained overnight in the dark at 4˚C before straining through 35 µm nylon Falcon 5 mL Round Bottom Polystyrene Test Tubes. Cell cycle phases were analyzed by DNA content by the Vanderbilt University Flow Cytometry Shared Resource using a Becton Dickinson LSR Fortessa instrument. For each sample, at least 10,000 single cells were analyzed using forward and side scatter to select single cells.

Treatment for cell synchronization

U2OS cells expressing WDR5-FKBP(F36V) were plated at 50% confluence and the next day media was exchanged to contain the appropriate treatment. 1 µM Palbociclib CDK4/6 inhibitor [177] was used to synchronize cells in G1 and 10 µM RO-3306 CDK1 inhibitor [178] was used to synchronize cells in G2/M. Cells were treated for 20 hours with or without simultaneous treatment with 500 nM dTAG47. After treatment cells were collected and taken forward for the appropriate analysis.

Nuclear Run-On RT-qPCR

Protocol was adapted from [179] and optimized by Dr. April M. Weissmiller and Chase M. Woodley. $4x10^6$ U2OS cells expressing WDR5-FKBP(F36V) were plated one day prior to the

experiment. Cells were treated for six hours with 500 nM dTAG47 or DMSO vehicle control. Cells were trypsinized, counted, and resuspended in cold PBS. $4x10^6$ cells were pelleted, and then resuspended in 1 ml NP-40 lysis buffer (10 mM Tris, pH 7.4, 300 mM sucrose, 10 mM KCl, 5 mM $MgCl_2$, 0.5% NP-40, Roche cOmplete Protease Inhibitor Cocktail, and 0.8 U/µl SUPERase•In RNase Inhibitor) and incubated on ice for 5 minutes. Nuclei were pelleted at 300 x g for 4 minutes at 4˚C. Pelleted nuclei were washed once with 1 ml of NP-40 lysis buffer and immediately pelleted again at 300 x g for 4 minutes at 4˚C. Nuclei were resuspended in 40 µl Nuclei Storage Buffer (50 mM Tris, pH 8.0, 25% glycerol, 5 mM $MgCl_2$, 0.1 mM EDTA, Roche cOmplete Protease Inhibitor Cocktail) resulting in a volume of approximately 60 µl. 60 µl of 2x Transcription Buffer (20 mM Tris, pH 8.0, 5 mM $MgCl_2$, 5 mM DTT, 300 mM KCl, 0.5 mM Bio-11-CTP, 1 mM ATP, 1mM GTP, 0.5 mM CTP, 1 mM UTP, 1% sarkosyl, and 0.8 U/µl SUPERase•In RNase Inhibitor) was added to each sample, mixed by pipetting, and incubated at 30˚C for 30 minutes. Samples were resuspended in 300 µl Trizol LS (Thermo Fisher Scientific) and rotated at room temperature for 5 minutes. RNA was extracted using a Direct-Zol RNA Miniprep kit (Zymo) with on-column DNaseI treatment. RNA was eluted in 25 µl of water and stored overnight at -80˚C.

For biotin pulldown, Dynabeads MyOne Streptavidin T1 were first prepared by washing for two minutes at room temperature once with Bead Wash Buffer 1 (0.1 M NaOH, 50 mM NaCl) and then twice with Bead Wash Buffer 2 (100 mM NaCl). Beads were resuspended in Binding Buffer (10 mM Tris, pH 7.4, 300 mM NaCl, 0.1% Triton X-100) and added to RNA samples. RNA samples were rotated at room temperature for 20 minutes. Beads were recovered on a magnetic rack, and the liquid was removed. Beads were washed briefly by resuspending in High Salt Buffer (50 mM Tris, pH 7.4, 2 M NaCl, 0.5% Triton X-100), then Binding Buffer, and finally Low Salt Buffer (5 mM Tris, pH 7.4, 0.1% Triton X-100). In between washes, beads were recovered on a magnetic rack and liquid was removed by aspiration. RNA was extracted from beads by resuspending beads in 300 µl Trizol, rotating five minutes at room temperature, and extracting with 60 µl of chloroform. After recovering the aqueous fraction, bead pellet was

extracted a second time with Trizol and chloroform. Aqueous phases were combined and precipitated with 3x volume of ice cold ethanol and 1 µl Invitrogen Ambion GlycoBlue Coprecipitant. Samples were incubated at -20˚C for at least ten minutes, and then centrifuged at 4˚C for at least 20 minutes at 13,000 rpm. Nucleic acid pellet was washed with 500 µl ice cold 75% ethanol, dried, and then resuspended in 25 µl water. RNA was reverse transcribed with LunaScript RT SuperMix Kit (New England Biolabs), diluted 1:4 in water, and analyzed by qPCR. qPCR was performed using KAPA SYBR FAST qPCR 2x Master Mix and gene-specific primers designed for detection of early transcripts, i.e. primers spanning an intron-exon boundary to avoid contaminating total mRNA (see **Table 2-3** for primer sequences).

Table 2-3: Primers for nuclear run-on RT-qPCR

Primer name	Primer sequence
Run-On CENPE For	TGCGTATGTGTGTTTTGTTT
Run-On CENPE Rev	TGATCTTCTGAACCCATCAT
Run-On CENPF For	ACTGGTTTTAGCAGCCAAACT
Run-On CENPF Rev	ATCTTTGGCCAGACACACCC
Run-On ASPM For	ATAATGTATTGTTTTGATTATAGCC
Run-On ASPM Rev	ATCTCTCTTACTCGGCCTTC
Run-On KIF18A For	GGTGAGAAGTCATTGGAGAC
Run-On KIF18A Rev	TGATACGTTCATCAAAAGCA
Run-On TOP2A For	GGTTAACTGCCTTTGATGAGCTT
Run-On TOP2A Rev	ACATATTTTGCTCCGCCCAG
Run-On KIF20B For	AGGGAAGTAGTGGGCTAGACT
Run-On KIF20B Rev	GTCGAGGTACTCCCTCTTGAT
Run-On SGO2 For	TTTCTTCGCCTAAAGCTAAA
Run-On SGO2 Rev	GCTTCTATAATAATGCAGCTAAAA
Run-On RPL35 For	CTGAGGCACACTCTCTCTTG
Run-On RPL35 Rev	GTCGTCCAGCTGTTTCAG
Run-On RPS24 For	CCTGGATGTACTCTTTTCTCA
Run-On RPS24 Rev	ATTCTGTTCTTGCGTTCCT
Run-On ACTB For	AGCTCATTGTAGAAGGTGTGG
Run-On ACTB Rev	GGCATGGGTCAGAAGGATTC

ChIP from U2OS cells

Cells were fixed with 0.75% formaldehyde for 10 minutes then quenched with 125 mM glycine for ten minutes. Cells were washed twice in PBS then scraped into PBS and pelleted. Cell pellets were resuspended in FALB (50 mM HEPES pH 7.5, 140 mM NaCl, 1 mM EDTA, 1% Triton X-100) supplemented fresh with 1% SDS, Roche cOmplete Protease Inhibitor Cocktail, 1 mM PMSF, and Roche PhosSTOP inhibitor tablet and lysed on ice ten minutes. Cellular material was sonicated in a bioruptor (Diagenode) for 20 minutes 30s on/30s off. Lysates were then clarified by centrifugation for 10 minutes. Chromatin was then diluted ten fold with FALB supplemented with Roche cOmplete Protease Inhibitor Cocktail, 1 mM PMSF, and Roche PhosSTOP inhibitor tablet. Chromatin was aliquoted, snap frozen and stored at -80˚C. Before ChIP, chromatin was thawed on ice. Each ChIP was performed with HA 350 ng anti-HA (Cell Signaling Technologies) or normal rabbit IgG (CST 2729). After incubating overnight with antibody, a 20 µl bed volume of BSA-blocked Roche Protein A agarose was added to each ChIP and rotated for three hours. Beads were then washed 5 minutes each with Low Salt Wash Buffer (20 mM Tris pH 8.0, 150 mM NaCl, 2 mM EDTA, 1% Triton X-100), High Salt Wash Buffer (20 mM Tris pH 8.0, 500 mM NaCl, 2 mM EDTA, 1% Triton X-100), LiCl Wash Buffer (10 mM Tris pH 8.0, 250 mM LiCl, 1 mM EDTA, 1% Triton X-100), and then twice with TE (10 mM Tris pH 8.0, 1 mM EDTA). ChIP samples were then decrosslinked overnight by incubating each bead pellet with 50 µl TE + 0.1% SDS + 20 µg proteinase K. The next day samples were heat inactivated for 20 minutes at 95˚C and then diluted up to 200 µl in TE. Samples were taken forward for qPCR with gene-specific primers (see **Table 2-4** for specific primer sequences).

Table 2-4: Primers for ChIP qPCR

Primer name	Primer sequence	Primer name	Primer sequence
CENPE ChIP-1	TACCTGCTGTTCAGCGGC	TOP2A_ChIP_1	TGACACTTCCATGGTGACGG
CENPE ChIP-2	GCCTGTGAGCCCTGAAGTG	TOP2A_ChIP_2	GAGAGCGAGTCAGGGATTGG
CENPF ChIP-1	TCCAAAACCGCGTCTAGCAT	USP1_1	CTGGAGCCCACCTTTCTTCT
CENPF ChIP-2	GATTGGCCCTTTCGGATGGA	USP1_2	ACCAATTATATCTAGACCAAAG CCA
ASPM ChIP-3	AAGACGCCTCCTCCTCGG	KCNH4-ChIP-1	TGAATAACAGACCCGCCCTC
ASPM ChIP-4	CCAGGAGGGGTCTCGAATCT	KCNH4-ChIP-2	CCTGTGGGTGCTGCGAAATA
KIF18A ChIP-3	CCAGGTTACCGCAACCACTT	GIGYF1-ChIP-1	CGACACGTGACCTGGGC
KIF18A ChIP-4	GGCAGCCAATGAAACGAAGC	GIGYF1-ChIP-2	GCTTCCTGGAGGAAACCGGA
CCAR1_ChIP_1	AAAGGGCCAGGCGTATTGAG	HDAC2-ChIP-1	GCCTGGTAGCCTAGTTTTCT
CCAR1_ChIP_2	CCGGCTAACATCGAAGCCAT	HDAC2-ChIP-2	ACACCTCATACCCATTACGA
KIF20B_ChIP_1	GGACTAAGTGCAGTGGCAGT	SETD3_ChIP_1	GGTTCCAACAATGCTTGGGC
KIF20B_ChIP_2	TCGCGGCTGTCATAAGTACC	SETD3_ChIP_2	GCTCCTTGGCTTTCCTGGTT
SMC2_ChIP_1	AGTGTGCCTAACGCGAACTA	RPL35_ChIP_1	ACAGGCCTAGGTGGCAGATA
SMC2_ChIP_2	CGTCCGGCACTCTATGGTC	RPL35_ChIP_2	ATGGTGAGAGCTGCGGAAT
SMC3_ChIP_1	CCGCCATTTTGTTTGGCTGA	SNHG15_ChIP	CGCCACTGAACCCAATCC
SMC3_ChIP_2	GCGAAGGCCTTACCTGCTTT	SNHG15_ChIP	TCTAGTCATCCACCGCCATC
SMC4_ChIP_1	CTTCCTTCTGCCAACGGACT		
SMC4_ChIP_2	CTGGCAGCGCTTGCTAATTT		

Quantification and statistical analysis

Statistical comparisons between replicates for image quantification, RT-qPCR, and cell cycle profile analysis were performed with GraphPad Prism software 8.0. The n indicates number of biological replicates. The n, error bar representations, and details of statistical tests can be found in the figure legends or under the specific Methods heading.

Analysis of density sedimentation data

Scans of western blots were analyzed in FIJI (ImageJ) [180] by drawing a box around the area of interest, inverting the image, and analyzing the plot profile of the area within the box. Pixel intensities were plotted against pixel distance. Images were unadjusted and boxes of equal pixel size were used for the comparisons of blots.

Image analysis

Statistical comparisons between two groups for proximity ligation assay analyses were performed with GraphPad Prism software using a two-tailed unpaired *t*-test. PDPK1-EGFP localization images were analyzed in batch mode using FIJI (ImageJ) software with the Intensity Ratio Nuclei Cytoplasm Tool. The experiment was performed in triplicate with at least four fields of view analyzed per replicate. Statistical analysis was performed with GraphPad Prism software 8.0.

Ontology and categorization

Gene ontology (GO) enrichment analysis was performed with PANTHER 15.0 with Gene Ontology version 1.2, 2020-02-21 release [181-183]. Unless otherwise stated in the figure legend, analysis type is PANTHER Overrepresentation Test with “GO biological function complete" Annotation Data Set. Analysis was also performed using DAVID Bioinformatic Resource v 6.8 [184, 185]. Protein categorization was performed using PANTHER 15.0 Protein Class ontology tool, 2019_04 reference proteome. Dot plots of the GSEA and GO analyses were generated using Seaborn.

Identifying WIN and WBM motifs

Motifs were identified using the MOTIF2 Search online tool available through GenomeNet at https://www.genome.jp/tools/motif/MOTIF2.html. Patterns used for searches are: WIN motif A-R-[AST]; WBM motif [ED]-[ED]-[IVL]-D-V-[VT].

RNA-Seq Data Analysis

RNA-seq data analysis was performed by Jing Wang. After adapter trimming by Cutadapt [186], RNA-Seq reads were aligned to the hg19 genome using STAR [187] and quantified by featureCounts [188]. Differential analysis were performed by DESeq2 [189], which estimated the $\log_2$ fold changes, Wald test *p*-values, and adjusted *p*-values (FDR) by the Benjamini-Hochberg procedure. The significantly changed genes were chosen with the criteria FDR<0.05.

Chapter III[2]

Impact of WIN site inhibitor on the WDR5 interactome

Introduction

Small molecule WIN site inhibitors obstruct one of the two binding sites on WDR5 and are capable of selectively impairing cancer cell growth. Thus, WIN site inhibitors are a promising anti-cancer strategy, however, the molecular details of what protein interactions are affected by blocking the WIN site are unclear. Studying the protein interactions that change when the WIN site is inhibited has potential to advance understanding of WDR5 biology, reveal interactions that enable moonlighting activities of WDR5, and inform mechanism of action studies for clinical implementation of WIN site inhibitors. Because of the simplicity of the WIN motif—an arginine flanked by residues with small side chains—*in silico* prediction of direct WIN site interactors is not viable. Instead, I took an unbiased SILAC quantitative proteomic approach to delineate how the WDR5 interactome changes when the WIN site of WDR5 is inhibited.

SILAC (stable isotope labeling of amino acids in cell culture) [190, 191] is a mass spectrometry-based technique that enables quantitative detection of differences in protein abundances between biological samples. Two or more samples can be compared by this methodology using different combinations of non-radioactive isotope-labeled amino acids. The most common SILAC comparison is performed between 'light' (the commonly occurring ^{12}C and ^{14}N) and 'heavy' (^{13}C and ^{15}N) isotopes of arginine and lysine. Since the trypsin protease cleaves after arginine and lysine residues, this setup enables consistent labeling of tryptic peptides. In designing an experiment to interrogate WDR5 interaction partners, SILAC was an

---

[2] Parts of Chapter III are adapted with permission from the following publication:
171. Guarnaccia A.D., Rose K.L., Wang J., Zhao B., Popay T.M., Wang C.E., Guerrazzi K., Hill S., Woodley C.M., Hansen T.J., Lorey S.L., Shaw J.G., Payne W.G., Weissmiller A.M., Olejniczak E.T., Fesik S.W., Liu Q., Tansey W.P. Impact of WIN site inhibitor on the WDR5 interactome. Cell Rep. 2021;34(3):108636. PMID: 33472061.

attractive approach because it enabled quantitative comparison of inhibited and uninhibited WDR5. Additionally, the Cortez Laboratory at Vanderbilt University was willing to share their SILAC expertise and isotope-equilibrated HEK293 cell lines, which accelerated my experiments.

Using SILAC together with the C6 WIN site inhibitor developed and characterized by the Tansey-Fesik collaboration [39, 166] enabled me to investigate interaction partners of WDR5 that are affected by WIN site inhibition. I found that, although inhibiting the WIN site broadly impacts the complex-forming capabilities of WDR5, this inhibition does not reduce interaction with known WIN site interaction partners, including HMT enzymes. Instead, WIN site inhibition with C6 mostly alters interaction partners that have yet to be characterized. This unbiased proteome-wide survey expands our understanding of the interaction partners and moonlighting roles for WDR5, and presents WIN site inhibitors as valuable tools for dissecting the biology of WDR5.

Results

Analysis of WDR5 complexes and interacting proteins

As mentioned in the introduction, proteins that interact with WDR5 do so through either a hydrophobic cleft called the "WBM" site, or an arginine-binding pocket called the "WIN" site (**Figure 3-1**), both of which engage motifs in partner proteins [1]. The WBM motif, present in proteins such as MYC and RBBP5, is defined as [ED]-[ED]-[IVL]-D-V-[VT] [16]. The WIN motif, present in SET1/MLL proteins as well as histone H3, KANL1, and KIF2A, is most strictly defined as [GV]-[SCA]-A-R-[AST]-[EKR] [17-19]. Each WDR5 binding site is inactivated by a specific point mutation: L240K for the WBM site and F133A for the WIN site. First I tested the impact of the L240K and F133A WDR5 point mutations on the mobility of WDR5 by using sucrose gradient sedimentation assays and lysates from HEK293 cells stably expressing FLAG-tagged WDR5 variants. Wild-type FLAG-tagged WDR5 migrates well into the gradient, consistent with incorporation into higher molecular weight complexes. In contrast, the F133A mutant WDR5 is

shifted toward lower molecular weight fractions with most F133A WDR5 migrating below the 158 kDa marker, indicating less incorporation into multi-protein complexes. Surprisingly, the L240K mutant shows little if any change in its migration compared to wild-type WDR5 (**Figure 3-2 A and B**). These results indicate that the WIN site is crucial for the ability of WDR5 to form high molecular weight complexes.

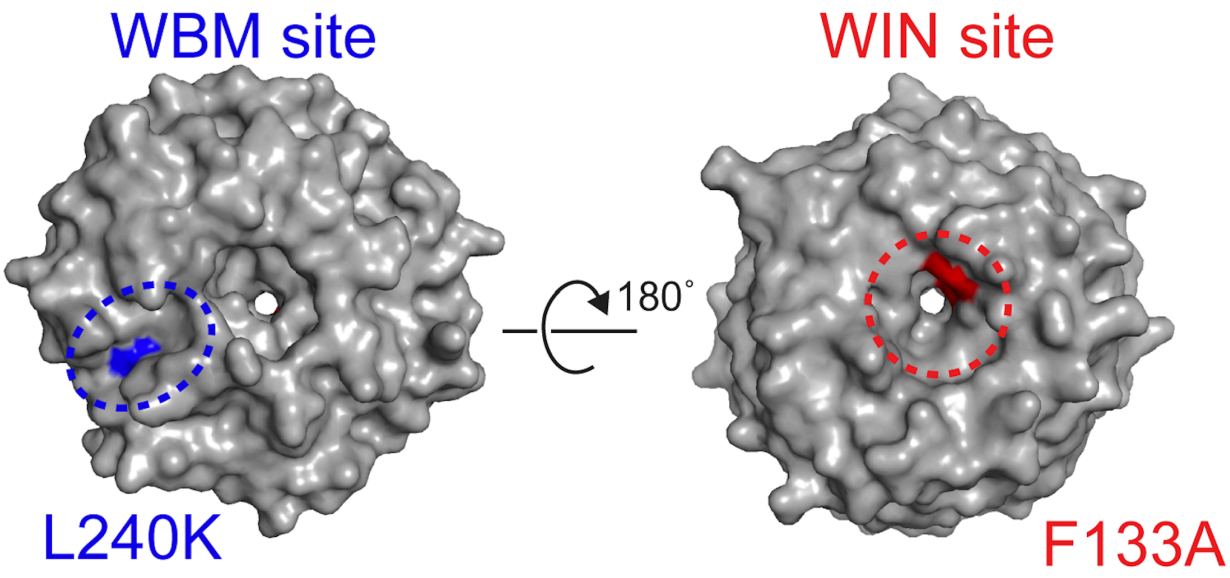

Figure 3-1: Point mutations inactivate the WBM site and the WIN site
Crystal structure of WDR5 (PDB ID: 2H14) outlining the location of the WBM site (blue) and the WIN site (red); locations of the L240K and F133A mutations are also shown.

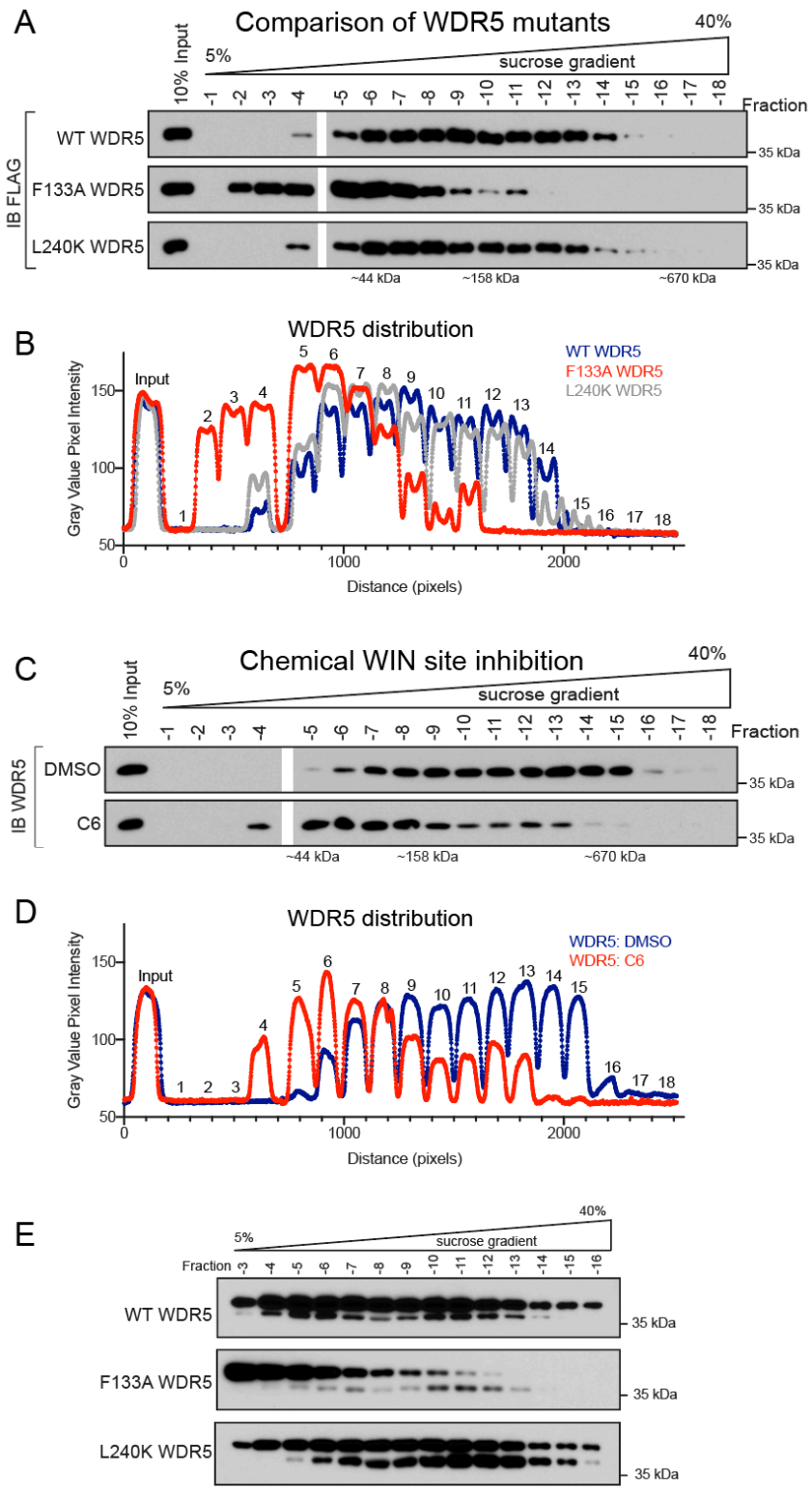

Figure 3-2: Analysis of WDR5 complex formation by density sedimentation
(A) Density sedimentation analysis of HEK293 extracts from cells stably expressing FLAG-tagged WDR5; wild-type (WT) or the F133A or L240K mutants. Immunoblots (IB) were probed with an anti-FLAG antibody. Positions of molecular weight markers are indicated. *n=3* biological

replicates.
(B) Graphical representation of the data from (A) as plot profiles that graph the intensities for each pixel across the IB images.
(C) Density sedimentation analysis of HEK293 cells treated for 5 hours with 30 μM C6 or DMSO. After treatment, cells were lysed and extracts analyzed by sucrose gradient density sedimentation followed by immunoblotting (IB) for WDR5. Positions of molecular weight markers are indicated. *n=3* biological replicates.
(D) Graphical representation of the data from (C) as plot profiles that graph the intensities for each pixel across the IB images.
(E) Density sedimentation analysis of HEK293 extracts from cells stably expressing FLAG-tagged WDR5; wild-type (WT) or the F133A or L240K mutants, as in (A) except IB were probed with an anti-WDR5 antibody and FLAG WDR5 (upper bands) and endogenous WDR5 (lower bands) are visible. Positions of molecular weight markers are indicated.

Both WBM and WIN sites are focal points for drug discovery, but because of the impact of WIN site mutation in the sucrose gradient assay, I asked how WIN site inhibition influences the sedimentation of WDR5. I treated HEK293 cells with WIN site inhibitor C6 [39] or vehicle control and then assayed lysates to assess the mobility of WDR5 in sucrose gradient sedimentation assays. I used a high concentration of C6 in these experiments (30 μM) to ensure maximal inhibition, but only treated cells for five hours to minimize secondary effects. In vehicle-treated HEK293 cells, endogenous WDR5 migrates beyond the 670 kDa marker (**Figure 3-2 C and D**), consistent with assembly into multiprotein complexes. In C6-treated cells, however, WDR5 is absent from fractions above 670 kDa (**Figure 3-2 C and D**), with most WDR5 migrating below the 158 kDa marker. Thus, similar to the WIN site F133A mutant, C6 chemical inhibition of the WIN site causes a reduction in WDR5 sedimentation, indicative of a reduced ability to form stable complexes when the WIN site is inactivated.

I next asked how WIN site inhibition influences the interaction properties of WDR5. Probing C6-treated sucrose gradient experiments I compared WDR5 with KMT2A and KMT2B, two proteins that bind the WIN site and one of which (KMT2A) is enzymatically inhibited by WIN site blockade *in vitro* [32, 39]. Despite the effect on WDR5, the migration of KMT2A/B is only subtly altered by C6, demonstrating that overall integrity of SET1/MLL (KMT2) complexes is not perturbed by WIN site inhibition, and that these complexes play little role in governing the bulk of high molecular weight WDR5 species (**Figure 3-3 A**). Interrogating how WIN site mutation affects KMT2A/B in the same way was not possible since the samples expressing mutant WDR5 also express endogenous wild-type WDR5 that migrates in a similar pattern to wild-type WDR5 (**Figure 3-2 E**).

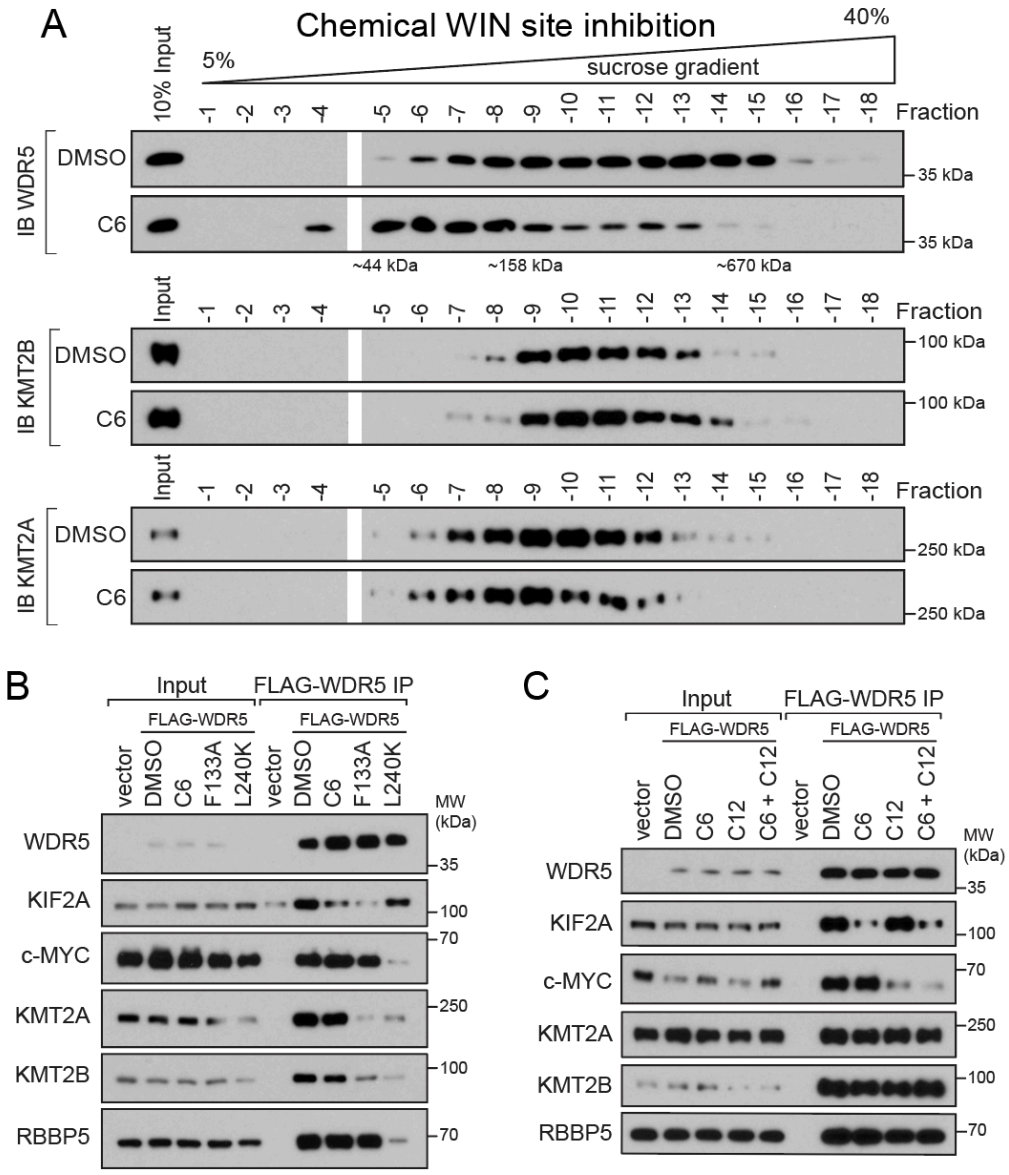

Figure 3-3: WIN site inhibitor C6 selectively displaces proteins from WDR5
(A) Density sedimentation analysis of HEK293 cells treated for five hours with 30 μM C6 or DMSO. After treatment, cells were lysed and extracts analyzed by sucrose gradient density sedimentation followed by immunoblotting (IB) for WDR5 (top), KMT2B (middle), or KMT2A (bottom). WDR5 panel is the same as Figure 3-2 C, shown again for comparison to KMT2A/B. Positions of molecular weight markers are indicated. *n=3* biological replicates.
(B) HEK293 cells stably expressing wild-type (WT) FLAG-tagged WDR5, or the indicated mutant, were treated with DMSO or 30 μM C6 for five hours, WDR5 was recovered by FLAG IP, and the co-precipitating proteins detected by IB. Inputs are 5% for RBBP5 and WDR5, 3% for KMT2A and KMT2B, and 1% for KIF2A and c-MYC; *n=3* biological replicates.
(C) Lysates from cells stably-expressing WT FLAG-tagged WDR5 were treated with DMSO (0.1%), 5 μM C6, 50 μM C12, or both, for five hours, WDR5 recovered by anti-FLAG IP and IB performed for the indicated proteins. Inputs are 5% for RBBP5 and WDR5, 3% for KMT2A and KMT2B, and 0.5% for KIF2A and c-MYC; *n=4* biological replicates.

To further explore the impact of WIN site inhibitor on known WDR5 interaction partners, I used co-immunoprecipitation (co-IP) assays to compare the effects of C6 with mutations in the WBM and WIN sites, both in cells treated with inhibitor (**Figure 3-3 B**) and by treatment of lysates *in vitro* (**Figure 3-3 C**). For the latter, I also tested the WBM site inhibitor C12 [151]. These analyses revealed that not all WDR5 interaction partners comport with expectations. MYC and KIF2A, on one hand, behave as expected. Interaction of MYC with WDR5 is sensitive to genetic (L240K) and chemical (C12) disruption of the WBM site, but insensitive to perturbations (F133A/C6) at the WIN site. And the opposite is true for the WIN site binder KIF2A. SET1/MLL complex members, on the other hand, do not behave as expected. Interaction of WDR5 with KMT2A, KMT2B, and RBBP5 is insensitive to both C6 and C12 (alone or in combination), and although RBBP5 is displaced by the WBM mutation, so too are KMT2A and KMT2B, both of which bind WDR5 through the WIN site. These data show that C6 disrupts WDR5-containing protein complexes and that these are distinct from complexes involving KMT2A/B and RBBP5. By extension, they also suggest that much of the impact of WIN site inhibition on the WDR5 interactome affects interaction partners that have yet to be characterized.

Impact of WIN site inhibitor on the WDR5 interactome

To learn how WIN site inhibition alters the ensemble of proteins with which WDR5 interacts I used SILAC (stable isotope labeling of amino acids in cell culture) [190, 191] to compare WDR5 complexes treated with 5 μM C6 or its inactive analog C6nc [39]. I treated lysates from “heavy” and “light” HEK293 cells expressing FLAG-tagged WDR5, recovered proteins by FLAG IP, and analyzed samples by MudPIT LC-MS/MS in collaboration with the Vanderbilt Mass Spectrometry Research Center (**Figure 3-4 A** and **3-5 A**). The experiment was performed in duplicate, with label swap, and a total of 747 proteins were quantified in both IP samples (**Figures 3-5 B–C)**. Using overexpressed FLAG-WDR5 enabled even and high-yield recovery of WDR5 complexes, and the label swap enabled clear delineation of external

contaminating proteins, such as keratins, that are always “light” because they are not produced in the isotope-cultured cells. My SILAC approach resulted in the identification of hundreds of WDR5-associated proteins (see Guarnaccia et al. [171] supplemental Table 1 for full list of proteins).

Next I evaluated the proteins that are significantly changed upon C6-treatment. Enforcing a two-fold cutoff of SILAC ratios (C6nc/C6), 25 proteins are altered in their ability to interact with WDR5 by C6, 17 of which are reduced and eight of which are increased (**Figure 3-4 B–C**). As predicted from experiments in **Figure 3-3**, most canonical WDR5 interaction partners are recalcitrant to WIN site inhibition, including members of SET1/MLL (KMT2) and NSL complexes (**Figure 3-4 D** and **Figure 3-5 D; Table 3-1**). Also as predicted, most of the WDR5-associated proteins affected by C6 have not been studied in detail. Some of these proteins (e.g., PDPK1, RICTR, SIN1, MSL1, HELB, CYTSB1) were identified in previous large scale screens [100, 192], and CHD8 [87-89] and HSF2 [86] have be shown by low throughput co-IP experiments to interact with WDR5. Others (URFB1, MTMR5, MTMR1, ZC21A, PWP1) are exclusive to this dataset. Within the 17 decreased proteins, seven have relationships that cluster in two nodes: “aminoacyl tRNA ligase activity” and “phosphatidylinositol mediated signaling” (**Figure 3-4 E**). The tRNA ligase node is represented by SYIC, SYEP, and SYRC, which are components of the multi-tRNA synthetase complex [193]. The signaling node is represented by RICTR and SIN1, subunits of the mTORC2 complex [194], and by PDPK1, a kinase that, together with mTORC2, phosphorylates protein kinase B (AKT) [195, 196]. These same themes are reinforced by results of Reactome pathway and ontology analyses (**Figures 3-5 E–F**). The eight enriched proteins, in contrast, have few connections, and represent processes such as DNA replication (CLSPN), transcription (GTF2I, TAF1), ubiquitylation (UBR5), and chromatin remodeling (CHD8).

From these data, I conclude that WIN site inhibition bidirectionally alters the WDR5 interactome, resulting in decreased interactions with some proteins and increased interactions with others. I conclude that a majority of the impact of WIN site inhibitor is on proteins that have

not previously been connected to WDR5 in a substantive way. And I conclude that some proteins displaced from WDR5 by WIN site inhibitor have links to tRNA synthetases or PI3K/AKT signaling.

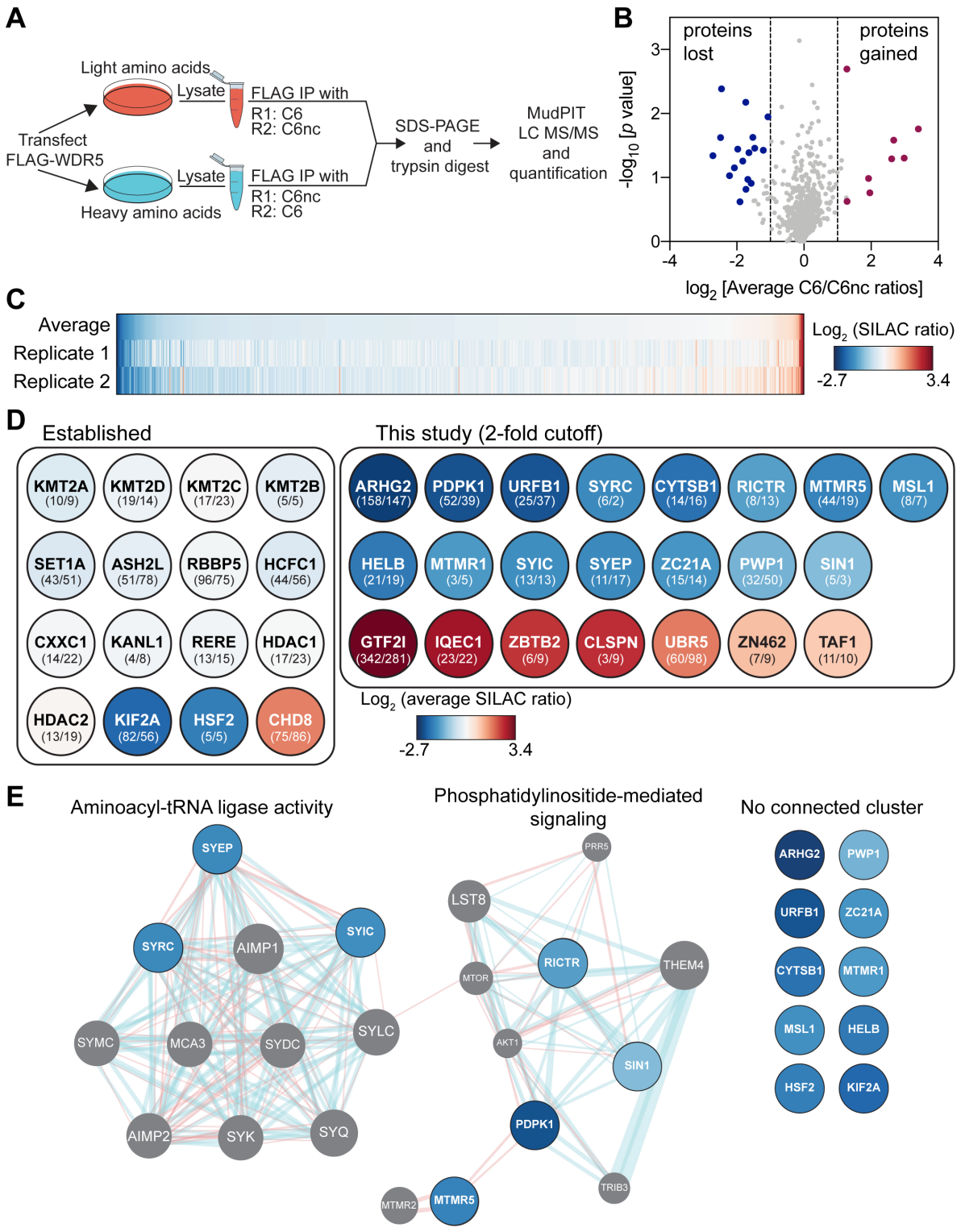

Figure 3-4: Identification of WDR5 interaction partners that are sensitive to WIN site inhibitor

(A) Schematic of SILAC setup. The experiment was performed in duplicate (R1 and R2) with label swap.

(B) Volcano plot of the SILAC data plotting $\log_2$ (average ratio) against the *p* value from one

sample *t*-test. Proteins meeting a two-fold cutoff in both replicates are highlighted.
(C) Heatmap of the log_2-transformed SILAC ratios for the 747 proteins quantified in both SILAC replicates and ranked by average ratio.
(D) Impact of C6 on the interaction of established (left) or novel (right) proteins with WDR5. The color of each circle corresponds to the average log_2 (SILAC ratio) from the heatmap in (C). Numbers in parentheses are spectral counts from the two replicates (R1/R2). UniProt names are used throughout.
(E) GeneMANIA [197] was used to predict functional nodes among depleted proteins, identifying "aminoacyl tRNA ligase activity" (FDR=2.04e-18) and "phosphatidylinositol-mediated signaling" (FDR=4.00e-4). Blue lines represent pathway interactions; red lines indicate physical interactions. Gray circles represent proteins identified by GeneMANIA as connected functionally or physically to the 17 input proteins (blue). Proteins on the right failed to cluster.

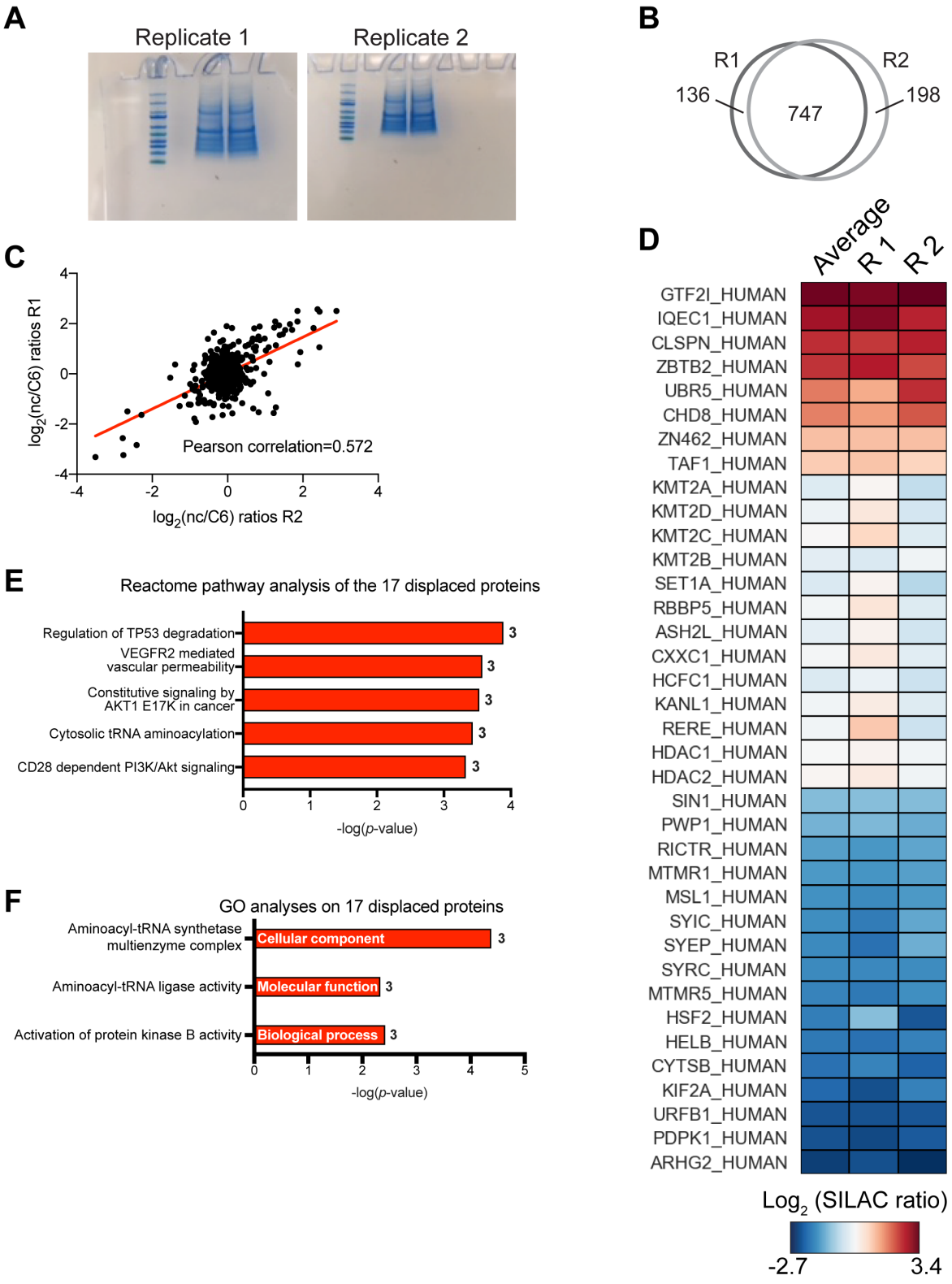

Figure 3-5: Quantitative proteomic analysis of the impact of C6 on the WDR5 interactome
(A) SILAC samples for mass spectrometry. Short stack Coomassie-stained gels of FLAG-WDR5 IP samples prior to trypsin digestion and LC MS/MS. Heavy and Light samples were pooled

before loading in two lanes of each gel.
(B) Venn diagram of the overlap between replicates.
(C) Comparison of SILAC duplicate experiments. Pearson correlation coefficient was calculated with Perseus software.
(D) Heatmap of the subset of proteins represented in Figure 3-4 D.
(E) Reactome pathways analysis of the 17 proteins that are displaced from WDR5 in the presence of C6. These proteins were analyzed using PANTHER Overrepresentation Test with the “Reactome pathways” Annotation Data Set (Reactome version 65 Released 2019-12-22). The five enriched categories are shown; numbers on the right are the number of proteins in each category.
(F) Gene ontology analysis of the 17 displaced proteins. These proteins were analyzing using PANTHER Overrepresentation Tests with “GO biological function complete,” “GO molecular function complete,” and “GO cellular compartment complete" Annotation Data Sets. Only one category was enriched for each of these Annotation Data Sets and each of these categories is described in the graph with the number of proteins in each category listed on the right.

Table 3-1: Summary statistics of key proteins identified in WDR5 SILAC experiment
Replicate values are reported with the slash, represented as R1 / R2.

Protein Name	Total Spectra	Razor + Unique peptides	Molecular Weight (kDa)	Sequence Coverage(%)	Ratio nc/C6 (normalized)	UniProt Accession	Official Gene Symbol
ARHG2_HUMAN	158 / 147	42 / 49	111.5	44 / 58	5.68 / 7.43	Q92974	*ARHGEF2*
KIF2A_HUMAN	82 / 56	30 / 30	79.9	44 / 55	5.67 / 3.62	O00139	*KIF2A*
PDPK1_HUMAN	52 / 39	13 / 13	63.2	28 / 30	5.95 / 5.23	O15530	*PDPK1*
PWP1_HUMAN	32 / 50	5 / 15	55.8	25 / 37	2.2 / 2.43	Q13610	*PWP1*
URFB1_HUMAN	25 / 37	22 / 26	159.5	17 / 24	5.56 / 5.44	Q6BDS2	*UHRF1BP1*
MTMR5_HUMAN	44 / 19	22 / 15	208.3	17 / 12	3.93 / 3.15	O95248	*SBF1*
HELB_HUMAN	21 / 19	16 / 12	123.2	16 / 15	4.23 / 3.62	Q8NG08	*HELB*
CYTSB_HUMAN	14 / 16	9 / 10	118.6	11 / 12	3.54 / 4.86	Q5M775	*SPECC1*
ZC21A_HUMAN	15 / 14	8 / 7	35.1	23 / 21	3.58 / 2.35	Q96GY0	*ZC2HC1A*
SYEP_HUMAN	11 / 17	9 / 14	170.6	7 / 12	4.23 / 2.40	P07814	*EPRS*
SYIC_HUMAN	13 / 13	5 / 8	144.5	4 / 7	3.80 / 2.58	P41252	*IARS*
RICTR_HUMAN	8 / 13	8 / 10	192.2	6 / 8	2.92 / 2.61	Q6R327	*RICTOR*
MSL1_HUMAN	8 / 7	4 / 4	67.1	11 / 11	3.35 / 2.89	Q68DK7	*MSL1*
HSF2_HUMAN	5 / 5	7 / 5	60.3	11 / 9	2.08 / 5.42	Q03933	*HSF2*
SIN1_HUMAN	5 / 3	4 / 2	59.1	8 / 5	2.08 / 2.13	Q9BPZ7	*MAPKAP1*
SYRC_HUMAN	6 / 2	5 / 2	75.4	9 / 3	3.37 / 3.28	P54136	*RARS*
MTMR1_HUMAN	3 / 5	2 / 4	74.7	4 / 9	2.99 / 2.76	Q13613	*MTMR1*
GTF2I_HUMAN	342 / 281	46 / 53	112.4	46 / 58	0.10 / 0.09	P78347	*GTF2I*
CHD8_HUMAN	75 / 86	31 / 37	290.5	15 / 19	0.32 / 0.20	Q9HCK8	*CHD8*
UBR5_HUMAN	60 / 98	29 / 57	309.3	14 / 28	0.35 / 0.16	O95071	*UBR5*
IQEC1_HUMAN	23 / 22	18 / 12	108.3	22 / 16	0.11 / 0.15	Q6DN90	*IQSEC1*
TAF1_HUMAN	11 / 10	8 / 11	212.7	5 / 8	0.43 / 0.49	P21675	*TAF1*
ZN462_HUMAN	7 / 9	6 / 4	284.7	3 / 9	0.41 / 0.41	Q96JM2	*ZNF462*
ZBTB2_HUMAN	6 / 9	5 / 6	57.3	12 / 14	0.14 / 0.19	Q8N680	*ZBTB2*
CLSPN_HUMAN	3 / 9	2 / 8	151.1	2 / 6	0.17 / 0.14	Q9HAW4	*CLSPN*
RBBP5_HUMAN	96 / 78	18 / 24	59.1	35 / 50	0.61 / 1.10	Q15291	*RBBP5*
ASH2L_HUMAN	51 / 78	13 / 19	68.7	24 / 41	0.74 / 1.25	Q9UBL3	*ASH2L*

KMT2A_HUMAN (MLL1)	10 / 9	8 / 5	431.8	2 / 2	0.78 / 1.4	Q03164	*KMT2A*
KMT2D_HUMAN (MLL2)	19 / 14	12 / 11	593.4	3 / 3	0.63 / 1.21	O14686	*KMT2D*
KMT2C_HUMAN (MLL3)	17 / 23	10 / 17	541.4	3 / 5	0.51 / 1.10	Q8NEZ4	*KMT2C*
KMT2B_HUMAN (MLL4)	5 / 5	3 / 3	293.5	2 / 2	1.14 / 0.89	Q9UMN6	*KMT2B*
SET1A_HUMAN	43 / 51	13 / 22	186.0	10 / 17	0.75 / 1.53	O15047	*SETD1A*
HCFC1_HUMAN	44 / 56	13 / 22	208.7	8 / 13	0.92 / 1.31	P51610	*HCFC1*
CXXC1_HUMAN	14 / 22	6 / 9	75.7	11 / 17	0.64 / 1.04	Q9P0U4	*CXXC1*
KANL1_HUMAN	4 / 8	3 / 7	121.0	3 / 9	0.67 / 1.08	Q7Z3B3	*KANSL1*
RERE_HUMAN	13 / 15	8 / 10	172.4	6 / 6	0.44 / 1.31	Q9P2R6	*RERE*
HDAC1_HUMAN	17 / 23	7 / 8	55.1	16 / 17	0.75 / 0.87	Q13547	*HDAC1*
HDAC2_HUMAN	13 / 19	2 / 2	55.4	14 / 15	0.67 / 0.88	Q92769	*HDAC2*

Validation of C6-sensitive WDR5 interaction partners

Because many of the proteins that are lost (**Figure 3-6 A**) or gained (**Figure 3-6 B**) from WDR5 in response to C6 have little to do with the known functions of WDR5, I validated some of the more interesting candidates. I found that IP of endogenous WDR5 from HEK293 cells recovers endogenous PDPK1, HELB, and MTMR1 (**Figure 3-6 C**), as well as RICTR, SIN1, GTF2I, and UBR5 (**Figure 3-6 D**). I confirmed that interaction of FLAG-tagged WDR5 with PDPK1, RICTR, SIN1, HELB, SYRC, SYIC, MTMR1, and KIF2A is sensitive to C6 (**Figure 3-6 E**), and to mutation of the WIN site of WDR5 (**Figure 3-7 A**–**B**). And for these proteins, with the exception of MTMR1 and KIF2A, I saw that interaction with WDR5 is insensitive to ethidium bromide (**Figure 3-6 E**), indicating that they are not bridged by contaminating DNA in the IP samples [198]. By extension, I infer that the MTMR1–WDR5 and KIF2A–WDR5 interaction may be due to DNA contamination, and in my paper I suggest investigators perform such experiments before pursuing proteins in this list of 25.

Because I only recovered two subunits of mTORC2 in the SILAC experiment, I asked whether WDR5 interacts with these subunits alone, or if it is capable of interacting with the remaining mTORC2 components LST8 and MTOR [194]. I suspected that it was our use of Triton X-100, rather than CHAPS, as a detergent that prevented recovery of LST8 and the MTOR kinase [199], and I repeated the FLAG–WDR5 co-IPs in the presence of CHAPS. Now, WDR5 associates with all four mTORC2 components in a manner that is sensitive to C6 (**Figure 3-6 F**) and the F133A mutation (**Figure 3-7 C**). Importantly, WDR5 does not interact with the mTORC1-specific component RPTOR (**Figure 3-6 F**) [200, 201], revealing that WDR5 interacts selectively with mTORC2.

Finally, to understand how C6 promotes association of WDR5 with partner proteins, I looked more closely at three gained interactors—CHD8, GTF2I, and UBR5. I confirmed that all three bind at higher levels to WDR5 upon inhibition or mutation of the WIN site (**Figure 3-6 G**). Interestingly, I also observed that all three interact with WDR5 in a manner that is sensitive to mutation of the WBM site, and that two—CHD8 and UBR5—contain WBM motifs (**Figure 3-7**

D). Thus it appears as though disruption of protein binding to the WIN site of WDR5 can promote selective loading of proteins at the WBM site.

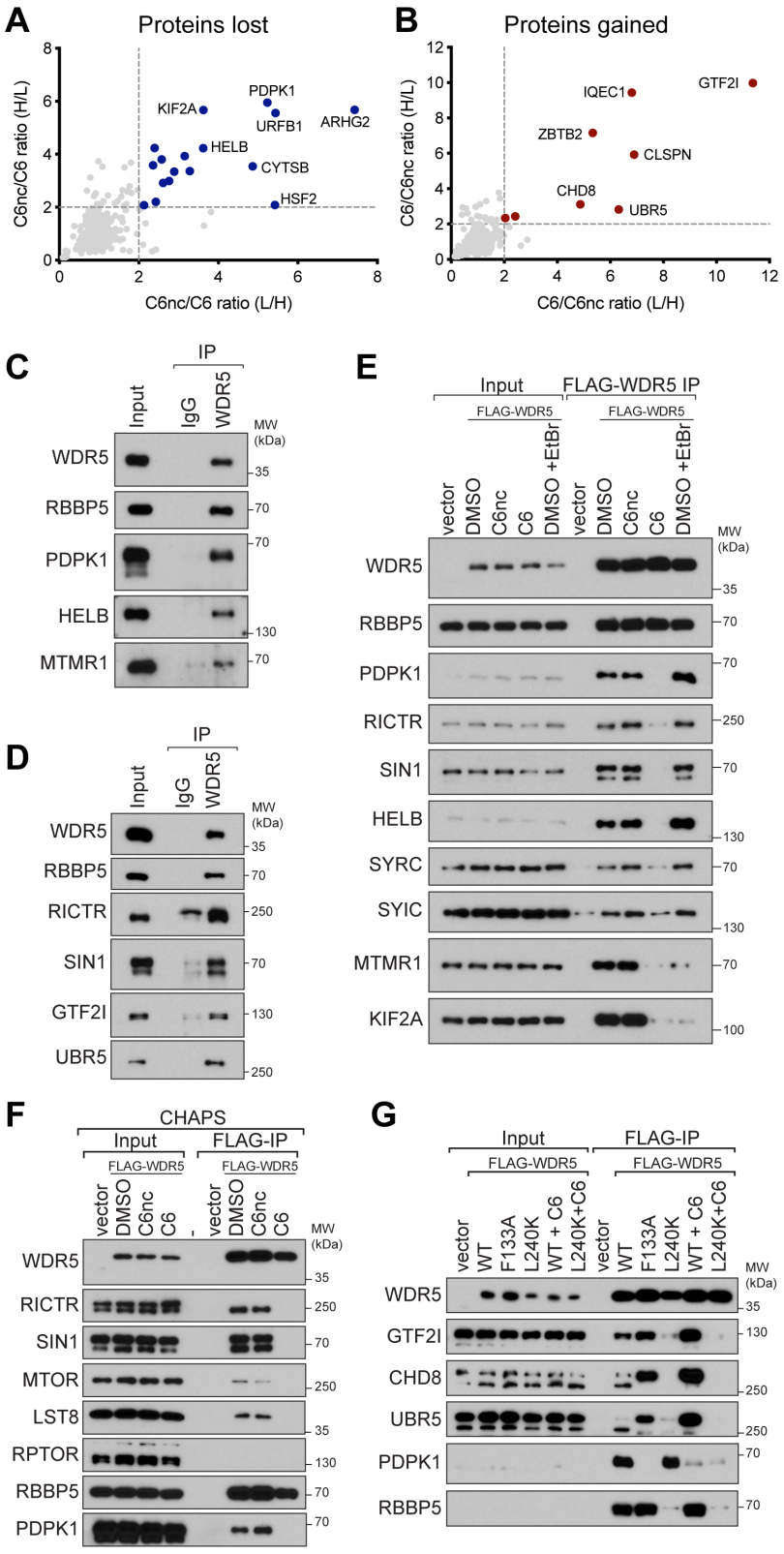

Figure 3-6: Validation of C6-sensitive WDR5 interaction partners
(A) Comparison of C6nc/C6 ratios for the two SILAC replicates. Depleted proteins that met a two-fold cutoff in both replicates are highlighted in blue.

(B) As in (A) except for enriched proteins (red).
(C) Extracts from HEK293 cells were subject to IP with a polyclonal antibody against WDR5 or non-immune IgG. IP samples were probed by IB with antibodies against the indicated endogenous proteins. Inputs are 2% for WDR5 and RBBP5 and 0.3% for others. *n=3* biological replicates.
(D) As in (C) but for different candidate proteins. Inputs are 5% for WDR5, RBBP5, and UBR5, and 0.3% for others. *n=3* biological replicates.
(E) HEK293 cells stably expressing FLAG-tagged WDR5 were treated for four hours with 30 μM C6 or C6nc prior to lysis and subsequent FLAG IP. For ethidium bromide (EtBr) treatment, 200 μg/ml EtBr was added to the lysate for the duration of the experiment. Candidate WDR5 interaction partners were probed by IB. Inputs are 5% for WDR5 and RBBP5, 0.1% for SYRC and SYIC, and 1% for all others; *n=3* biological replicates.
(F) HEK293 cells stably expressing FLAG-tagged WDR5 were treated for four hours with 30 μM C6 or C6nc prior to lysis and subsequent FLAG IP in buffer using CHAPS detergent. IP samples were probed with antibodies against the indicated proteins. Inputs are 10% for WDR5 and RBBP5 and 1% for others; *n=3* biological replicates.
(G) HEK293 cells stably expressing FLAG-tagged WDR5 proteins were treated for four hours with 30 μM C6 (where indicated) prior to lysis and FLAG IP. IP samples were probed with antibodies against the indicated proteins. Inputs are 10% for WDR5 and 1% for others; *n=3* biological replicates.

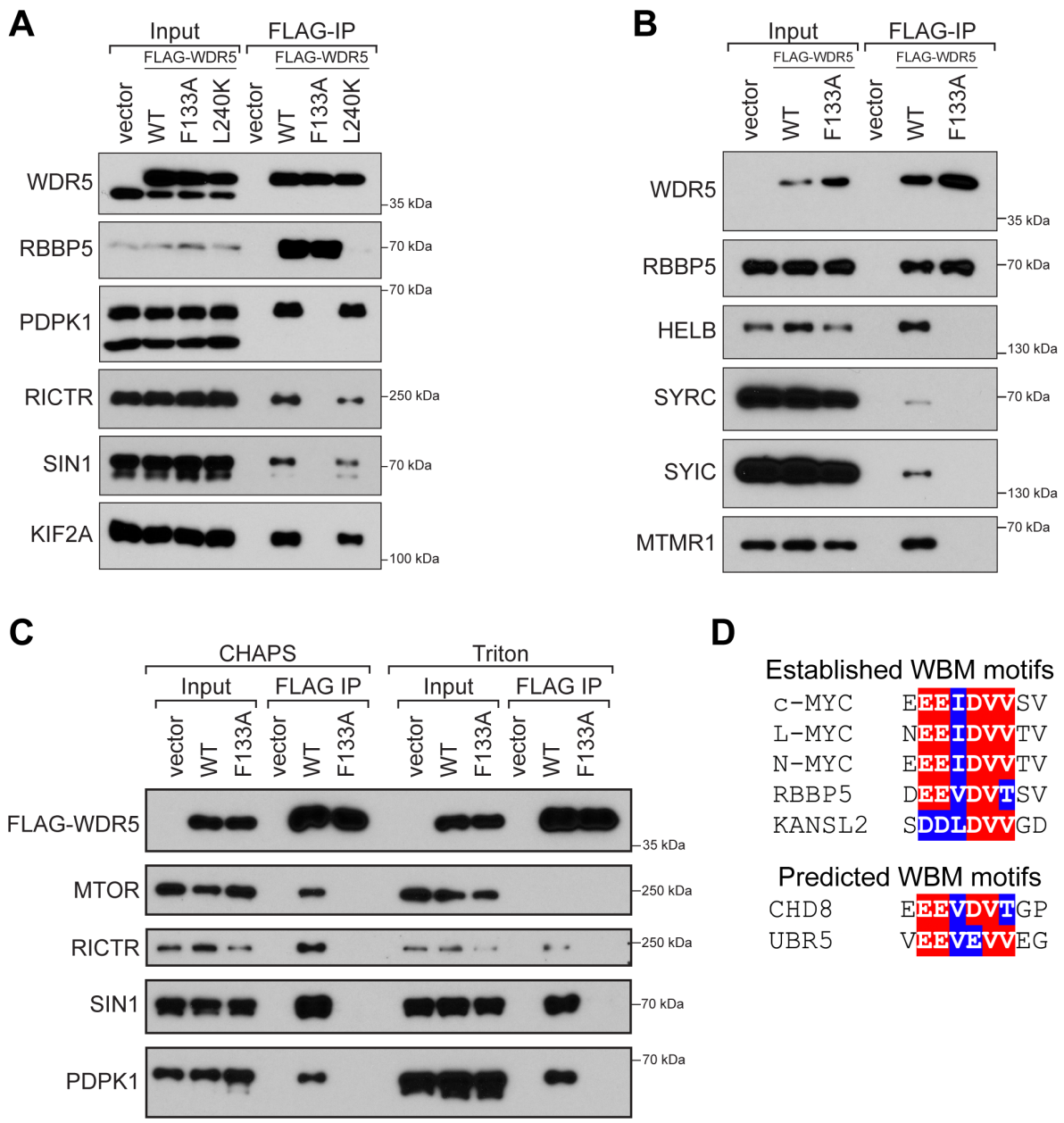

Figure 3-7: Mutation of the WIN site affects protein interactions with WDR5
(A) Genetic validation of WIN site-dependent WDR5 binding proteins identified by SILAC. Immunoblots of co-IP experiments from HEK293 cells stably expressing FLAG-tagged WDR5 variants. Inputs are 20% for WDR5 and 10% for others; *n=3* biological replicates. The antibody used for PDPK1 is Bethyl A302-130A.
(B) As in (A) but for a second set of WDR5-interacting proteins. Inputs are 10% for WDR5 and RBBP5 and 1% for others. *n=3* biological replicates.
(C) mTORC2 components can bind WDR5 in the presence of CHAPS but not Triton X-100. Lysates from HEK293 cells stably expressing FLAG-tagged WDR5 proteins were prepared in buffer containing either CHAPS or Triton X-100 and subject to FLAG IP under those same conditions. IP samples were probed with antibodies against the indicated proteins. Inputs are 10% for WDR5 and 1% for all others; *n=3* biological replicates.
(D) Comparison of established WBM motifs to predicted WBM motifs in CHD8 and UBR5.

Discussion

The development of potent small molecule inhibitors against WDR5 affords opportunity to interrogate the basic biology of WDR5 in ways that were previously not possible. Mutation is inherent and permanent, whereas inhibition only occurs upon exposure to the inhibitor. Chemical inhibitors enable rapid inhibition of a protein and do not rely on ectopic expression of a mutant variant, which is especially important for an essential protein like WDR5 where exclusive expression of mutant WDR5 is unlikely to be viable. Although mutant WDR5 is impaired from the outset as soon as it is translated, chemical inhibition affects WDR5 after it has been localized and interacting with other proteins in the cell. Also, it is possible that certain complexed forms or pools of WDR5 are resistant to inhibitor binding and that an inhibitor may have a different spectrum of influences compared to a mutant. Experimental discrepancies between genetic and chemical manipulations may not be surprising, but they do require careful consideration—and distinction—when evaluating the mechanism of action of a potential therapeutic like WDR5 WIN site inhibitor. In the results described in this chapter I used biochemical approaches to identify WIN site-dependent WDR5-interacting proteins and, in the process, uncovered some differences between genetic mutation and chemical inhibition of WDR5.

WIN site inhibitors, including C6, inhibit the *in vitro* activity of KMT2A [37-39, 156, 158], leading to a common assumption that WIN site inhibitors block interaction of WDR5 with all KMT2 methyltransferase proteins. But my biochemical and proteomic experiments demonstrate that for KMT2 proteins, and for KANL1, C6 does not prevent these known WIN site binding proteins from associating with WDR5. Based on the structure of the C6–WDR5 complex [39] it is unlikely that C6 binding to WDR5 could displace some WIN motifs but not others. Rather, it is possible that multivalent interactions among SET1/MLL complex members retain association of KMT2A/B with WDR5 even when the WIN site is blocked. Indeed, recent biochemical and structural studies describe a network of interactions between ASH2L, RBBP5, WDR5, the SET

domain of KMT2 proteins that hold together these complexes [30, 202, 203]. And interaction of RBBP5 with WDR5 at the WBM site seems to be crucial for methyltransferase complex assembly [36]. Consistent with these observations, I find that both the F133A WIN site mutant and the L240K WBM site mutant are deficient for interaction with KMT2 proteins (**Figure 3-3 B**), indicating that without functional binding sites, these HMT complexes cannot assemble or are less stable and not detected in my assays. Overall, stable complex formation and association of WDR5 with KMT2 proteins seems to rely on multivalent interactions which are not fully disrupted by WIN site inhibitor, but are disabled with WDR5 mutants.

The finding that C6 impairs the catalytic activity of SET1/MLL (KMT2) complexes [39] without disrupting interaction with WDR5 (**Figure 3-3 B and C**) raises an important distinction between complex assembly and complex activity. Just because a complex is assembled does not mean it is catalytically active, and for *in vitro* assays, the detected activity can depend on details of the assay such as what substrate is used [36]. A limitation of the SILAC proteomic approach is that it only detects changes in levels of associated proteins; proteins that remain associated with WDR5 but are impaired in function, like KMT2A, are not revealed. Truly the impact of WDR5 inhibitors is multifaceted and cannot be fully assessed with any single approach.

One puzzling finding is the similarity between wild-type and L240K WDR5 size distributions by sucrose gradients (**Figure 3-2 A**). Because the WBM site mediates so many interactions with WDR5, one would naively expect the L240K mutant would be impaired in its ability to form high molecular weight complexes. But instead the distribution is almost unchanged compared to wild-type. Perhaps the WBM site is not important for forming high molecular weight complexes, but instead stabilizes lower molecular weight complexes. Or perhaps the L240K mutation induces gained interactions that balance out the lost interactions resulting in a net neutral impact on the sucrose gradient migration pattern. We know that the L240K mutant (as well as the F133A mutant) is impaired in its ability to associate with histone methyltransferase complexes (**Figure 3-3 B**), but this impact is not reflected in the sucrose

gradient migration pattern, therefore perhaps histone methyltransferase complexes are not a majority species affecting WDR5 migration. To explicitly understand the interactions that are affected by the L240K (and F133A) mutant of WDR5, additional proteomic experiments would need to be performed.

Assaying WDR5 interactions for their ability to withstand EtBr treatment revealed that the known WIN site binding protein KIF2A [19] fails this test. Interaction between KIF2A and WDR5 is sensitive to EtBr treatment (**Figure 3-6 E**) indicating that this interaction is likely DNA-dependent. Because both C6 and F133A disrupt the KIF2A–WDR5 interaction the WIN site is clearly required for this interaction. But the EtBr-sensitive results challenges KIF2A as a direct WIN site binding protein. Ali et al. proposed that KIF2A interacts directly with WDR5 to mediate spindle localization in mitosis, but many of the assays that interrogated this direct interaction used crudely purified proteins [19]. Additionally, of the nine WIN-site interacting proteins with a mapped WIN motif (**Figure 1-4 A**), KIF2A is the only one without a determined co-crystal structure. More rigorous interrogation of the KIF2A–WDR5 interaction and its role in mitosis is warranted.

Another finding from this SILAC experiment is that certain proteins—including CHD8 and UBR5—load onto WDR5 upon WIN site inhibition and appear to be WBM interacting proteins. Perhaps a steric clash with complexes tethered to the WIN site normally limits interaction of WDR5 with these better binding proteins proteins. These findings establish that WIN site inhibitors influence more than just local protein-protein interactions at the WIN site, revealing crosstalk between the binding sites where what is bound at the WIN site can inform what binds at the WBM site. These observations raise the possibility that actions of WIN site inhibitors are mediated, in part, by promoting association of WDR5 with partner proteins.

CHD8 and UBR5 in particular are interesting because these proteins contain WBM sequences. There are relatively few proteins within the human proteome that contain such sequences, only a few dozen when the sequence is defined as [E,D] [E,D] [L,I,V] [E,D] [V,T] [V,T] (**Table 3-2**). This list of proteins spans a wide variety of cellular functions, from

transcriptional regulation to vesicular transport. It is unlikely that all of these proteins interact with WDR5, but even a subset of proteins from this list would represent an assortment of moonlighting functions. Certain WBM-containing proteins that stand out from this list are the APC/C complex member CDC26 which may be relevant for the recently discovered APC/C–WDR5 interaction [83], and the TGF-β receptor protein TGBR3 which is intriguing given the established connection between WDR5 and TGF-β signaling [123-126]. Interrogation of this list of WBM-containing proteins is an exciting future direction in investigating the WDR5 interactome.

Table 3-2: Human proteins containing WBM-like motifs
List of human proteins containing amino acid sequences that align with the WBM motif, defined as [E,D] [E,D] [L,I,V] [E,D] [V,T] [V,T]. The validated WBM motif-containing proteins are highlighted in blue in the table. TF is an abbreviation for transcription factor.

Protein	Uniprot ID	Function	Motif
MYC_HUMAN	P01106	C-MYC	EEIDVV
MYCN_HUMAN	P04198	N-MYC	EEIDVV
MYCL_HUMAN	P12524	L-MYC	EEIDVV
RBBP5_HUMAN	Q15291	RBBP5	EEVDVT
KANL2_HUMAN	Q9H9L4	KANSL2	DDLDVV
4ET_HUMAN	Q9NRA8	nuclear shuttling protein for eIF4E	DDLDVV
ABRX1_HUMAN	Q6UWZ7	Component of BRCA1-A complex; DDR	DDVEVV
BTBDI_HUMAN	B2RXH4	POZ-domain protein; fused to MLL in ALL	EEIDVV
C144C_HUMAN	Q8IYA2	coiled-coil domain protein	EDIEVV
CDC26_HUMAN	Q8NHZ8	APC component	EDVEVV
CHD8_HUMAN	Q9HCK8	ATP-dependent chromatin remodeling; associated with autism	EEVDVT
COPG1_HUMAN	Q9Y678	vesicular transport	EDLEVT
COPG2_HUMAN	Q9UBF2	vesicular transport	EDLEVT
CPN2_HUMAN	P22792	carboxypeptidase subunit	EDLEVT
DGLA_HUMAN	Q9Y4D2	Sn1-specific diacylglycerol lipase alpha	EEVEVT
DOCK7_HUMAN	Q96N67	Guanine exchange factor for Rho GTPases Rac and Cdc42	DDIEVV
DOCK8_HUMAN	Q8NF50	Guanine exchange factor for Rho GTPases Rac and Cdc42	DDLDVV
DYH10_HUMAN	Q8IVF4	Dynein heavy chain 10	DDVEVV
DYHC2_HUMAN	Q8NCM8	Dynein heavy chain 2	DDLEVT
EMX1_HUMAN	Q04741	TF involved in patterning in the primary visual area	EDIDVT
EMX2_HUMAN	Q04743	TF involved in patterning in the primary visual area	EEIDVT
ERC6L_HUMAN	Q2NKX8	DNA helicase involved in spindle assembly checkpoint	EELDVV
ERF_HUMAN	P50548	Inhibitory TF of the ETS family	EEVEVT
F92A1_HUMAN	A1XBS5	unknown	DELDVT

Protein	Uniprot ID	Function	Motif
HIPL1_HUMAN	Q96JK4	HHIP-like protein; uncharacterized	EEVDVV
IF4A3_HUMAN	P38919	ATP-dependent RNA helicase; splicing	EEVDVT
LAP2A_HUMAN	P42166	Lamina-associated polypeptide 2; nucleus organization	DDLDVT
LAP2B_HUMAN	P42167	Directs assembly of the nuclear lamina	DDLDVT
MAP1B_HUMAN	P46821	microtubule-associated protein	EEVDVT
MYCP1_HUMAN	P12525	MYC-like protein 1	EEIDVT
NEP_HUMAN	P08473	Thermolysis-Like protease	DELEVV
OSGEP_HUMAN	Q9NPF4	Probable tRNA N6-adenosine threonylcarbamoyltransferase	DEVEVT
PARG_HUMAN	Q86W56	Poly(ADP-ribose) glycohydrolase	DEIDVV
PRAME_HUMAN	P78395	Transcriptional repressor	EDLEVT
PRP16_HUMAN	Q92620	RNA helicase; splicing	EDIEVT
PTHD1_HUMAN	Q96NR3	Transmembrane protein associated with autism	DEVDVV
RBG10_HUMAN	B7ZAP0	Rab GTPase-activating protein 1-like	EELEVV
RBG1L_HUMAN	Q5R372	Rab GTPase-activating protein 1-like	EELEVV
REXO4_HUMAN	Q9GZR2	RNA exonuclease; links to transcriptional induction	EELEVV
SIDT1_HUMAN	Q9NXL6	Transmembrane protein	DDLDVV
SPTB1_HUMAN	P11277	Spectrin; cytoskeleton network	EDLEVV
SPTN2_HUMAN	O15020	Spectrin; cytoskeleton network	EDLEVV
SPTN4_HUMAN	Q9H254	Spectrin; cytoskeleton network	DDVEVV
SYNE2_HUMAN	Q8WXH0	Nesprin-2; spectrin-repeat containing protein; nuclear lamina	EDVDVV
TGBR3_HUMAN	Q03167	TGFbeta-receptor	EDLEVV
UBR5_HUMAN	O95071	E3 in N-end rule pathway	EEVEVV
ZZZ3_HUMAN	Q8IYH5	Component of the ATAC complex	EEVDVV

WDR5 has an established connection to biomass accumulation both by interaction with MYC on chromatin at ribosome protein genes [62, 79] and as as a direct regulator of ribosome protein gene expression [82]. Here, I uncover other potential connections between WDR5 and biomass accumulation: WIN site-dependent interactions with mTORC2 and with tRNA ligase proteins. The PI3K/AKT/mTOR pathway promotes biomass accumulation by activating a cascade of pro-growth activities including protein synthesis, motility, proliferation, and metabolic regulation. Many components of this pathway can exist in the nucleus, including AKT [204], PTEN [205], PDPK1 [206-209], mTOR [210-213]. In particular, nuclear RICTR and SIN1 have been observed [211, 213], and at least for RICTR, nuclear accumulation occurs in response to androgen stimulation in prostate cancer cells [213]. Active mTORC2 also interacts with cytosolic ribosomes [214]. Perhaps in disease states deregulated levels of WDR5 or mTORC2 subunits promote oncogenic signals in the nucleus or at the cytosolic ribosome. Notably, both RICTR and SIN1 have WIN motif-like sequences and could directly interact with WDR5. These sequences, in addition to the localization of the WDR5–mTORC2 interaction, should be interrogated in the future.

Transfer RNA (tRNA) ligase (or synthetase) enzymes covalently attach amino acids to tRNA molecules in a process called aminoacylation that preps them for mRNA translation. The tRNA ligases identified in this SILAC screen—SYRC (charges arginine), SYIC (charges isolucine), SYEP (bifunctional for glutamate and proline)—assemble in a multisynthetase complex composed of nine ligases and three auxiliary subunits [193]. Although the vast majority of tRNA ligases are cytoplasmic, a small percentage of tRNA ligases do exist in the nucleus where they aminoacylate newly transcribed tRNAs as a means of quality control ensuring that nonfunctional tRNAs do not impede translation in the cytoplasm [215-218]. Perhaps WDR5 interacts with this nuclear pool of tRNA ligases to regulate nascent tRNA quality control. With only a small percentage of tRNA ligase activity occurring in the nucleus, this nuclear interaction would only require a small amount of WDR5. If WDR5 does function in this way then inhibiting WDR5 would not only impact protein synthesis by reducing transcription of ribosome protein

genes [39, 82], but it might also affect protein synthesis at the level of tRNAs. Still, there are some important unanswered questions regarding the interaction between WDR5 and tRNA ligases. SYRC, SYIC, and SYEP do not contain any WIN motif sequences, so how do they interact with WDR5? Is there an additional unidentified WIN site binding partner? Do they interact together or separately? And is the interaction nuclear or cytosolic? Answering such questions will reveal whether or not the interaction between WDR5 and tRNA synthetases is another layer of protein synthesis regulation by WDR5.

Contributions

The experiments and data presented in this chapter were facilitated by the assistance of some stellar collaborators. Dr. Kristie Rose provided assistance with SILAC proteomic experimental design, proteomic data collection, and proteomic data analysis. Salisha Hill provided assistance with proteomic sample preparation and data analysis. Dr. Tessa Popay provide assistance with analysis of IPs with endogenous proteins. Christina Wang performed and assisted with FLAG-WDR5 IPs. Kiana Guerrazzi performed and assisted with mTORC2 experiments. All other analyses and data were performed and collected by Alissa Guarnaccia.

Chapter IV[3]

PDPK1 is a high affinity WIN site binding protein

Introduction

Taking a quantitative proteomic approach to delineate how the WDR5 interactome changes when its WIN site is inhibited, I identified a collection of WIN site-sensitive WDR5 binders, three of which have links to phosphatidylinositol mediated signaling. Although WDR5 has been shown to be important for cellular responses to signaling [102, 103, 124-130], no physical interactions with activators of cellular signaling networks have been demonstrated. In my dataset, I identify both mTORC2 and PDPK1 as WIN site dependent WDR5 interacting partners. Both are kinases that predominantly function in the cytosol and are the major transducers of PI3K/AKT signaling [219-221]. To better understand the connection of WDR5 to cellular signaling, I focused my efforts on PDPK1 because its role in growth factor signal transduction in the cytosol [222] is disparate from the known functions of WDR5 in the nucleus [1] and, unlike mTORC2, it is a single protein and not a protein complex.

3-Phosphoinositide-dependent kinase 1 (PDPK1) is a master kinase that activates at least 23 other kinases. In cells, PDPK1 is constitutively active and phosphorylates to activate members of the AGC group of kinases including protein kinase B (AKT) [219, 223], p70 S6K [224, 225], SGK [226, 227], and p90 RSK [228] (**Figure 4-1**). Thus downstream of PDPK1 is the activation of a variety of kinases that mediate proliferation, cell growth, survival, glucose uptake and storage—all responses to growth factors and processes that promote biomass accumulation [222, 229]. The most well known function of PDPK1 is in the PI3K/AKT pathway

---

[3] Parts of Chapter IV are adapted with permission from the following publication:
171. Guarnaccia A.D., Rose K.L., Wang J., Zhao B., Popay T.M., Wang C.E., Guerrazzi K., Hill S., Woodley C.M., Hansen T.J., Lorey S.L., Shaw J.G., Payne W.G., Weissmiller A.M., Olejniczak E.T., Fesik S.W., Liu Q., Tansey W.P. Impact of WIN site inhibitor on the WDR5 interactome. Cell Rep. 2021;34(3):108636. PMID: 33472061.

where PDPK1 phosphorylates AKT. In fact, the predominant way that AKT gets activated is by the coordinated actions of both PDPK1 and mTORC2: PDPK1 phosphorylates AKT on T308, and mTORC2 phosphorylates AKT on S473 [196, 221]. Notably, the process of AKT activation occurs largely in the cytosol, mostly at the plasma membrane, where the pleckstrin homology (PH) domains in AKT and PDPK1 are thought to aid in their co-localization [195, 230]. But how and why does a predominantly nuclear protein like WDR5 interact with cytosolic signaling proteins? Although the majority of PDPK1 and mTORC2 are cytosolic, there are reports that many components of the PI3K/AKT pathway can exist in the nucleus, including AKT [204], PTEN [205], PDPK1 [206-209], mTOR [210-213], RICTOR and SIN1[211, 213]. For RICTR and SIN1 the nuclear association is not well studied, but for PDPK1 there are multiple reports of nuclear shuttling of PDPK1, seemingly in response to growth factor signaling [209, 231]. This nuclear shuttling activity is observed in a variety of cell types and involves a nuclear export signal in PDPK1 and CRM1-mediated nuclear export [207, 208]. The association of PDPK1 with WDR5 indicates that perhaps WDR5 works with PDPK1 upon its growth factor-induced nuclear accumulation.

Association of WDR5 with the predominantly cytosolic kinase PDPK1 indicates an area of unexplored WDR5 biology. WDR5 is a predominantly nuclear protein and concordantly many WDR5 interacting proteins are nuclear proteins (**Figure 1-4 A**), but this does not exclude the possibility that moonlighting functions of WDR5 involve engagement with cytosolic players. Understanding how and where the PDPK1–WDR5 interaction occurs could yield new biological insights into the moonlighting capabilities of WDR5. Therefore I initiated biochemical and structural studies of the PDPK1–WDR5 interaction, described below.

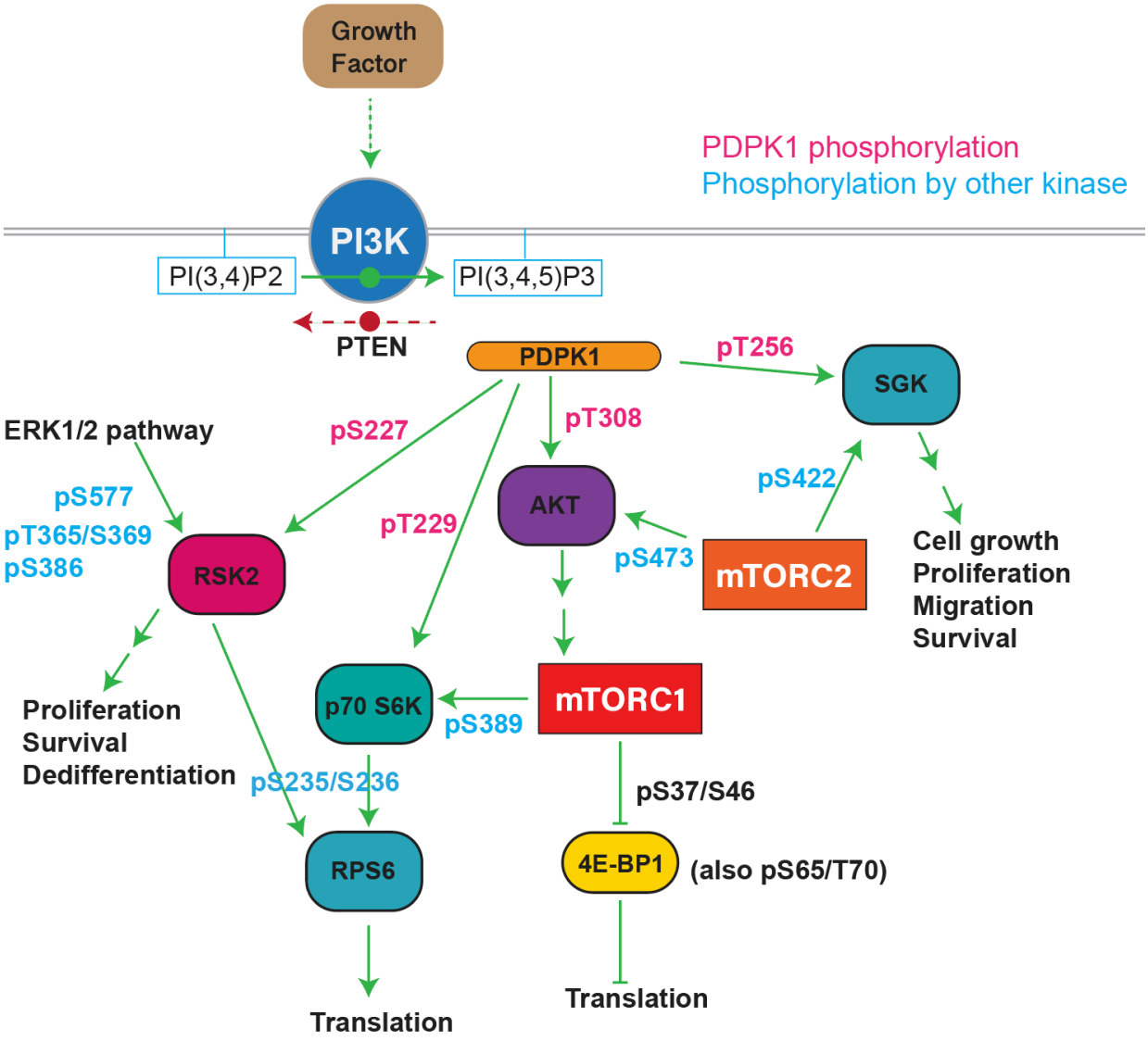

Figure 4-1: PDPK1 phosphorylates to activate a variety of kinases
Many AGC kinases are PDPK1 substrates. Summary of some of the downstream phosphorylation events and cellular processes activated by PDPK1 activity.

Results

PDPK1 binds WDR5 in the nucleus and via an N-terminal WIN motif

To investigate the PDPK1–WDR5 interaction, I performed co-IPs and found that endogenous PDPK1 and WDR5 interact in HEK293, U2OS, K562, and MV4;11 cells (**Figures 4-2 A and B**). I also performed a proximity ligation assay in U2OS cells, and confirmed that WDR5 and PDPK1 associate in cells in a manner that is sensitive to WIN site blockade (**Figures 4-2 C and D**). I also demonstrated that the interaction is unaffected by treatment of cells with the PDPK1 kinase inhibitor GSK2334470 [232] (**Figure 4-2 E**). Interestingly, I found that although PDPK1 and WDR5 are both present in cytosolic (S2) and nuclear (S3 and P3) fractions (**Figure 4-2 F**), the interaction is only detected in IPs from the nuclear fraction (**Figure 4-2 G**). This result is consistent with the proximity ligation assay which demonstrates predominantly nuclear interaction signal. Based on these observations, I conclude that PDPK1 is a bona-fide WDR5 interaction partner and that the interaction likely occurs predominantly in the nucleus.

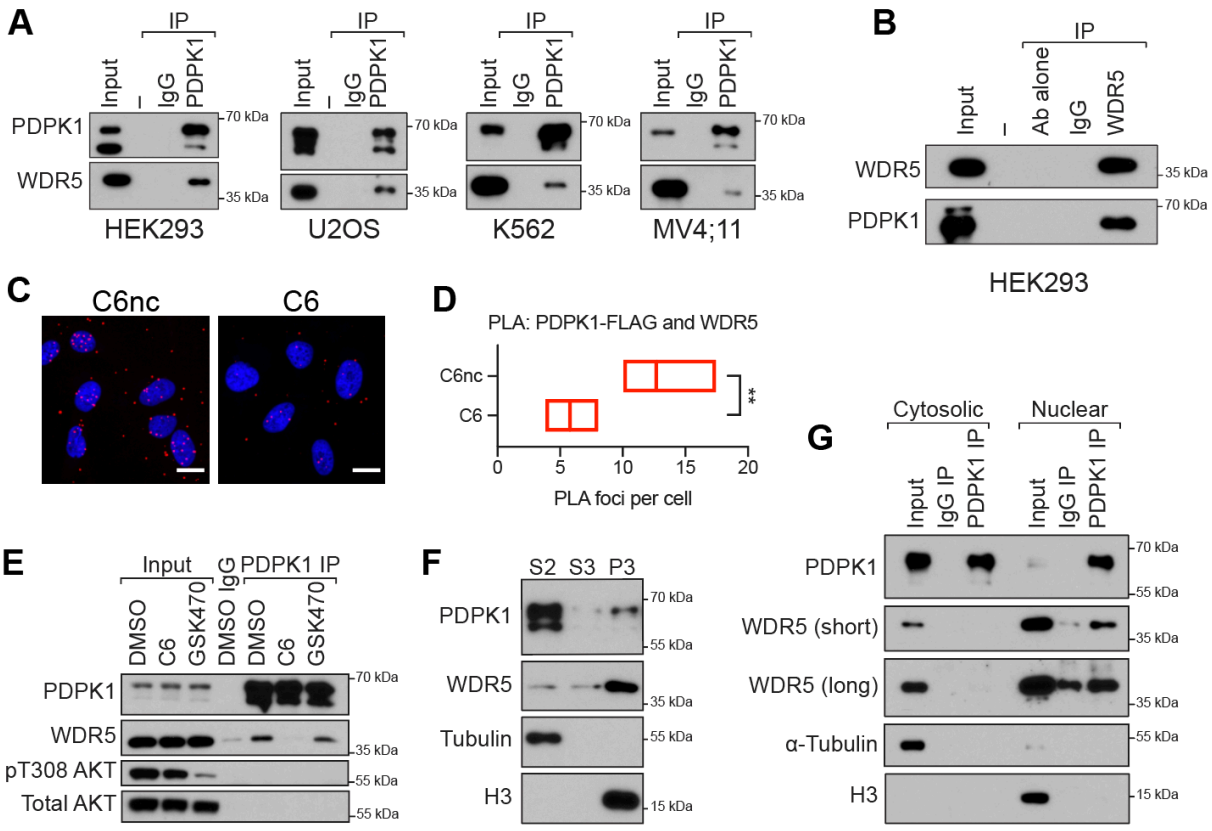

Figure 4-2: Validating the PDPK1–WDR5 interaction

(A) Endogenous PDPK1 was recovered from lysates from the indicated cell lines and probed for co-precipitating WDR5 by Western blotting. Inputs for PDPK1 are 10-20%. Inputs for WDR5 are 1-5%.

(B) Reciprocal coimmunoprecipitation between endogenous WDR5 and PDPK1; performed in HEK293 cells. Input is 5% for WDR5 and 1% for PDPK1. *n=3* biological replicates.

(C) Proximity ligation assay with FLAG and WDR5 antibodies in U2OS cell stably expressing PDPK1–FLAG. Cells were treated overnight and then fixed and assayed; scale bar 20 μm.

(D) Quantification of proximity ligation assay between PDPK1–FLAG and WDR5 in (C). Quantification of foci per cell; line represents the mean, and bars represents the min and max; *n=3*, unpaired two-tailed *t*-test, ***p*= 0.0037.

(E) HEK293 cells were treated overnight with 30 μM C6 or 5 μM GSK2334470 (GSK470), lysates prepared, and a PDPK1 IP performed. Western blots were then performed for the indicated proteins. Inputs are 5% for PDPK1 and 1% for all others. *n=3* biological replicates.

(F) HEK293 cells were fractionated into cytosolic (S2), soluble nuclear (S3), and chromatin-associated (P3) fractions. Equal amounts of each fraction were analyzed by western blotting with the indicated antibodies. H3 and α-tubulin are controls for fractionation.

(G) Cytosolic and nuclear fractions from HEK293 cells were subject to IP with PDPK1 antibody or an IgG control and immunoblotted with the indicated antibodies. *n=3* biological replicates.

Within PDPK1 are two arginine residues that align to established WIN motifs (**Figure 1-4 A**). I tested both of these residues—R3 and R238 (**Figure 4-3 A**)—by generating FLAG-tagged PDPK1 alanine mutants (R3A and R238A) and performing FLAG co-IPs. Mutation of R238 to alanine has no effect on the PDPK1–WDR5 interaction (**Figure 4-3 B**; R238A). Mutation of R3 to alanine, in contrast, reduces interaction with WDR5, suggesting that this amino-terminal WIN-like sequence mediates interaction with WDR5. Consistent with this notion, the R3A mutation disrupts the ability of PDPK1 to interact with WDR5 *in vitro*, as measured by far-western (**Figure 4-3 C**) and by interaction of recombinant WDR5 with *in vitro* translated PDPK1 (**Figure 4-3 D**). Interestingly, I also observed that RBBP5 is recovered in a PDPK1 IP, and that it too is sensitive to the R3A mutation. I conclude that PDPK1 interacts with WDR5 in a manner that depends on the WIN site of WDR5 and the amino-terminal WIN motif of PDPK1. I also conclude that PDPK1 interacts indirectly with RBBP5 via WDR5.

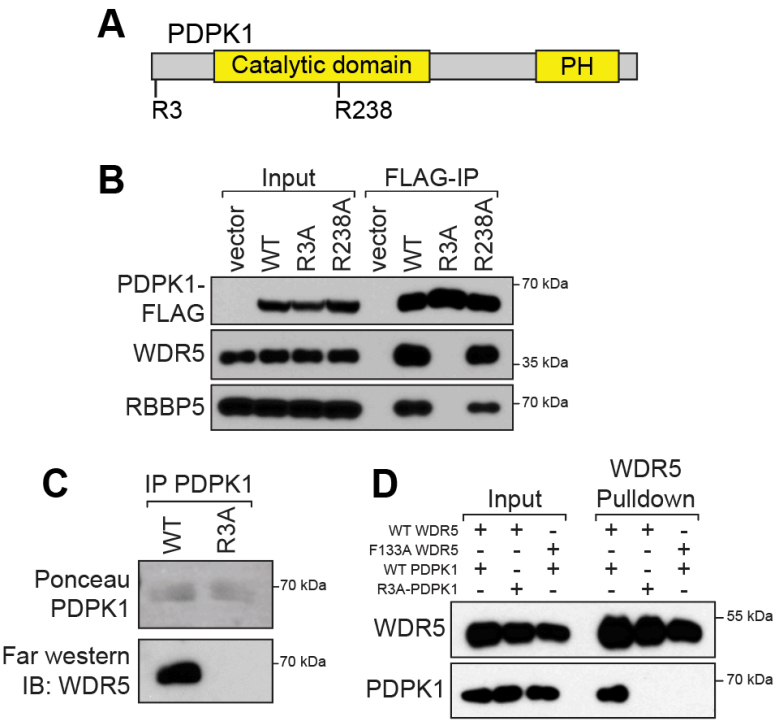

Figure 4-3: PDPK1 binds WDR5 via an N-terminal WIN motif
(A) PDPK1 possess two putative WIN motifs centered on R3 (ART) and R238 (ARA). PH indicates the pleckstrin homology domain.
(B) Variants of PDPK1-FLAG were transiently transfected into HEK293 cells. FLAG co-IPs were performed and analyzed by IB.
(C) PDPK1–FLAG proteins were recovered by FLAG IP, separated by SDS-PAGE and transferred to PVDF. Membranes were incubated with recombinant WDR5 followed by anti-WDR5 IB.
(D) *In vitro*-transcribed and translated PDPK1–FLAG variants were incubated with recombinant 6xHis-SUMO-WDR5 proteins, recovered with Ni-NTA agarose, and analyzed by IB.

Acetylation of the amino-terminus of PDPK1 creates a high affinity WIN motif

The only confirmed WIN site binding protein with an N-terminal WIN motif is histone H3 [28, 43, 45] (**Figure 1-4 A**), which is bereft of an initiator methionine. I asked if the PDPK1 N-terminal WIN-like motif resembles H3. By peptide pulldown assays I confirmed that a PDPK1 N-terminal peptide lacking the initiator methionine binds to recombinant WDR5 *in vitro* (**Figure 4-4 A**). I also purified endogenous PDPK1 from HEK293 cells (**Figure 4-4 B**) and, in collaboration with the Vanderbilt Mass Spectrometry Research Center, analyzed AspN digestion products by tandem mass spectrometry. All spectra that assigned to the N-terminus of PDPK1 carry two modifications: they lack the initiator methionine and carry an amino-terminal acetyl moiety (**Figure 4-4 C**). No other modifications were detected on the N-terminal peptide of PDPK1. We also attempted a trypsin digestion in the hopes that a missed cleavage would produce an N-terminal PDPK1 peptide for analysis, but coverage of the N-terminal arginine was only obtained with AspN digestion (**Figure 4-4 D**).

Ectopic N-terminal acetylation has been shown to increase the affinity of H3 and KMT2A WIN motif peptides for WDR5 *in vitro* [34, 233], and we observe this phenomenon with H3 peptides. In collaboration with team members in the Fesik Group, we performed TR-FRET assays and found that N-terminal acetylation on an H3 peptide has K_i of ~10 nM (**Figure 4-4 E**). But N-terminal acetylation is not a major modification of H3 in cells [234, 235], and the KMT2A WIN motif is not N-terminal. To determine whether a naturally occurring WIN motif is impacted in this way, we measured how N-terminal acetylation influences the affinity of PDPK1 WIN peptides for WDR5 in a TR-FRET displacement assay (**Figure 4-4 F**). Compared to unmodified peptides, which bind WDR5 weakly (K_i = 15–19 μM), acetylated PDPK1 peptides bind tightly (K_i = 0.04–0.05 μM), and in a manner that is sensitive to the R3A mutation. Thus, acetylation of the N-terminal PDPK1 WIN motif increases its affinity for WDR5 by a factor of ~400.

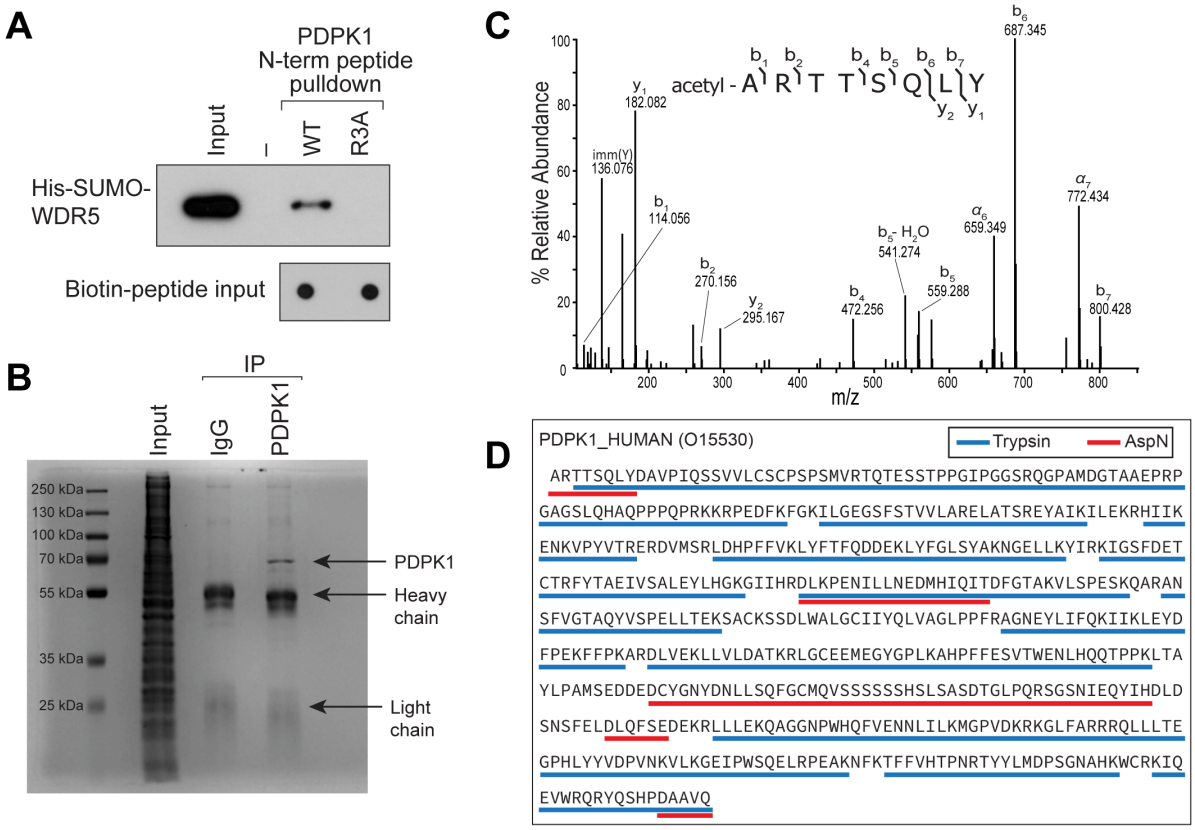

E Affinity measurements: H3 and WDR5

Peptide Name	Sequence	K_i (μM)
Acetyl-H3	Acetyl-ARTKQTARKSTGGK	0.010 ± 0.001
Acetyl-H3(10mer)[+]	Acetyl-ARTKQTARKS	< 0.001
H3 (10mer)[+]	NH2-ARTKQTARKS	15.1 ± 1.3
H3 (14mer)[++]	NH2-ARTKQTARKSTGGK	3.3 ± 0.2
H3 (20mer)[+++]	NH2-ARTKQTARKSTGGKAPRKQL-Y	6.6 ± 1.3
H3 (20mer)[++++]	NH2-ARTKQTARKSTGGKAPRKQL	5.6 ± 1.5
H3 (12mer)[+++++]	NH2-ARTKQTARKSTGG	10.7 ± 0.9

F Affinity measurements: PDPK1 and WDR5

Peptide Name	Sequence	K_i(μM)
PDPK1 (15mer)	NH2-ARTTSQLYDAVPIQS	19.0 ± 1.0
PDPK1 (10mer)	NH2- ARTTSQLYDA	15.0 ± 0.3
Acetyl-PDPK1 (15mer)	Acetyl- ARTTSQLYDAVPIQS	0.05 ± 0.03
Acetyl-PDPK1 (10mer)	Acetyl -ARTTSQLYDA	0.04 ± 0.02
PDPK1 R3A	NH2-A**A**TTSQLYDAVPIQS	>50
Acetyl-PDPK1(R3A)	Acetyl-A**A**TTSQLYDAVPIQS	>50

Figure 4-4: The N-terminus of PDPK1 is acetylated and binds tightly to WDR5

(A) Biotinylated peptides were pre-bound to streptavidin beads and incubated with recombinant 6xHis-SUMO-WDR5. Recovery of WDR5 was analyzed by IB. PDPK1 peptides do not include Met1 and are not acetylated.

(B) Purification of PDPK1 for MS/MS analysis of post-translational modifications. Coomassie-stained gel of endogenous PDPK1 purified by IP from HEK293 cells. Top arrow denotes the PDPK1 band that was cut out and taken forward for analysis. Co-purified immunoglobulin heavy and light chains are indicated.

(C) Tandem mass spectrum of N-terminally acetylated PDPK1 peptide, residues 2-9. The doubly-protonated precursor, $[M+2H]^{+2}$, with m/z 491.2556 was fragmented with higher-energy collisional dissociation. The identified amino acid sequence is provided above the annotated spectrum; brackets indicate sites of dissociation at the peptide backbone. Observed product ions are assigned to their corresponding m/z peaks in the mass spectrum.

(D) PDPK1 sequence coverage by tandem mass spectrometry for trypsin and for AspN cleavages. Coverage with trypsin (75%) is shown as blue underline, and coverage with AspN (15%) is shown as red underline. Although trypsin had high sequence coverage, only AspN had N-terminal coverage.

(E) TR-FRET analysis of acetyl-H3 compared to published affinity values for histone H3

peptides. For the TR-FRET measurement the peptide is amidated at the C terminus; two or more repeats were obtained and average K_i values and standard deviations are reported. Published binding constants: ┼ measured by fluorescence polarization [34]; ┼┼ measured by SPR [45]; ┼┼┼ measured by ITC [43]; ┼┼┼┼ measured by SPR [48]; ┼┼┼┼┼ measured by ITC [49].
(F) Binding constants of PDPK1 peptides were determined using a TR-FRET-based KMT2A peptide competition assay. All peptides are amidated at the C-terminus. Two or more repeats were obtained; average K_i values and standard deviations are reported.

Next, in collaboration with the Fesik group we determined the X-ray crystal structure of WDR5 in complex with an acetylated PDPK1 peptide (**Figures 4-5 A–B; Table 4-1**). We observe electron density for the N-terminal acetyl group and the first nine residues of the PDPK1 peptide (**Figure 4-5 C**). The orientation of the peptide directs the methyl group of PDPK1 A2 into a hydrophobic pocket formed by F133 and F149, and positions the PDPK1 R3 residue into the deep acidic pocket of the WIN site (**Figure 4-5 D**). Within the WIN site, the side chain nitrogens of the PDPK1 R3 residue form electrostatic interactions with backbone carbonyls of WDR5 and the R3 side chain is sandwiched by the aromatic rings from F133 and F263 of WDR5 (**Figures 4-5 D and E**). In general, the WDR5–PDPK1 WIN peptide interaction resembles other WDR5–WIN peptide structures (**Figure 4-5 F**). Like other WDR5–WIN peptide structures [35], residues downstream of R3 lie along a crevice between blades three and four of the WDR5 β-propellor structure (**Figure 4-5 A**), and like other structures the exact conformation of these residues is unique (**Figure 4-5 F**).

The structure of WDR5 in complex with acetylated PDPK1 highlights some important features of this WDR5 interaction. Distinct from other structures, the side chain of L8 of PDPK1 makes contact with side chains of F149 and Y191 of WDR5 (**Figure 4-5 E**). Although residues corresponding to L8 of PDPK1 are often hydrophobic in WIN motif proteins (often L, I, or A; **Figure 4-5 G**) and make backbone contacts with WDR5, this is the only structure, so far, to show to side chain-side chain interactions at this position. Another distinction is regarding the acetyl group of PDPK1. We see that the N-terminal acetyl group of PDPK1 fits into a WIN-site adjacent pocket on WDR5, which is not large enough to accommodate a methionine at this position. Indeed, residues that occupy this position for other WIN site-binding peptides are small: alanine, serine, or cysteine (**Figures 4-5 G**). Importantly, the acetyl group of the PDPK1 peptide forms an intramolecular interaction whereby the carbonyl of the acetyl group makes a hydrogen bond to the amide of T4 (**Figure 4-5 H**). This intramolecular hydrogen bond stabilizes the conformation of the peptide and points the N-terminal amide of PDPK1 A2 toward the carboxylate of WDR5 D107 to form a salt bridge. These characteristics explain how removal of

the initiator methionine and acetylation of the α-amino group of A2 enable the PDPK1 WIN motif to achieve its unusually high affinity.

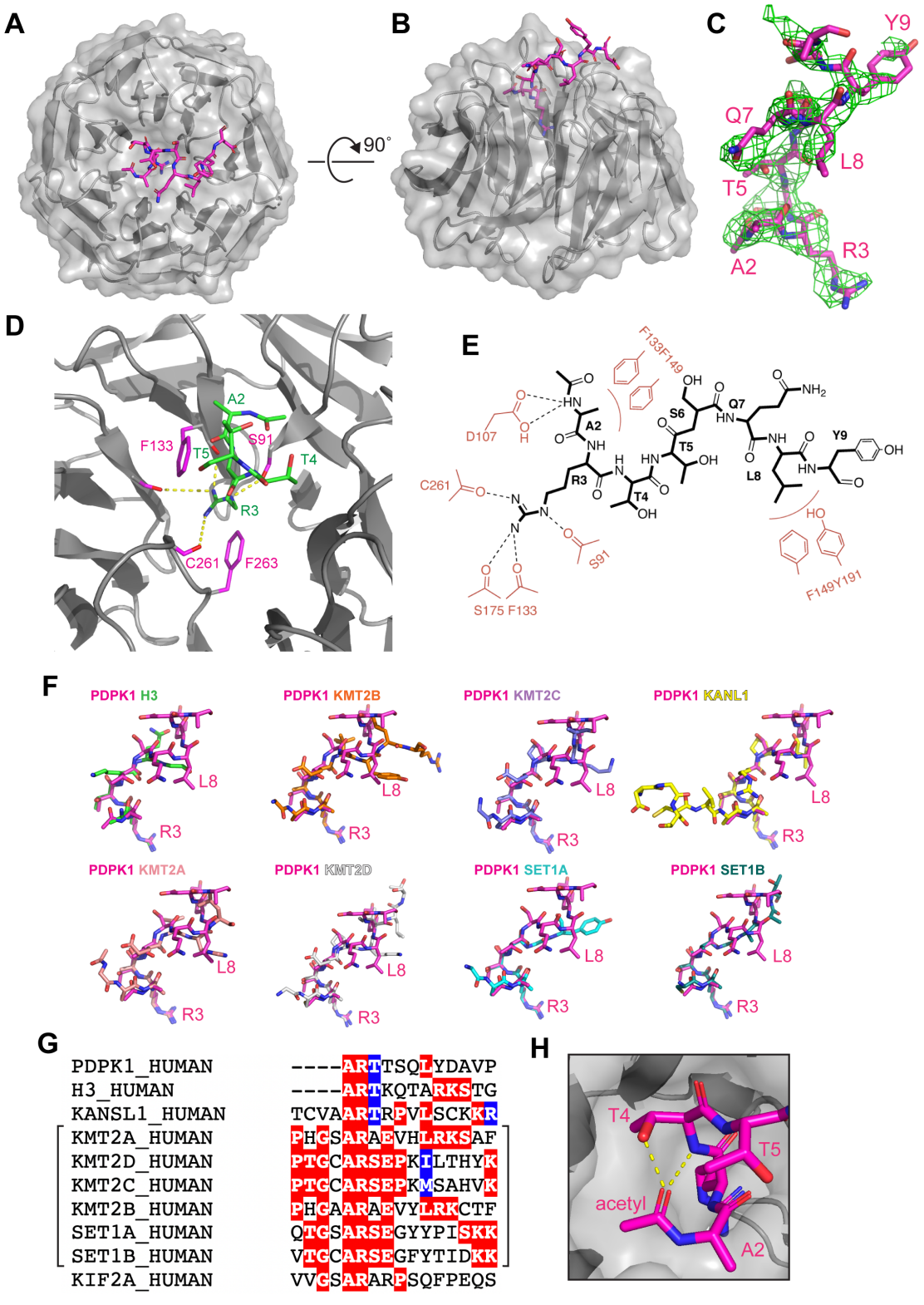

Figure 4-5: Structural analysis of the PDPK1–WDR5 interaction
(A) Structure of WDR5 in complex with the acetylated-PDPK1 WIN peptide. The PDPK1 WIN peptide is shown in stick representation (magenta, colored by atom type); WDR5 is shown as

cartoon with semitransparent surface representation (gray). 2.7 Å resolution.
(B) As in (A) but rotated along a 90˚ axis.
(C) The F_o-F_c omit map of PDPK1 peptide bound with WDR5 domain contoured at 2.0 σ level. PDPK1 peptide is shown in magenta sticks.
(D) Close up of the first three residues of PDPK1 (ART) in the WIN site of WDR5. The PDPK1 peptide is green sticks; WDR5 is gray ribbons. Key WDR5 residues F133, S175, C261, and F263 are indicated in pink stick representation. Yellow dotted lines indicate intermolecular hydrogen bonds.
(E) Summary of residue interactions between WDR5 and the PDPK1 WIN peptide. The PDPK1 peptide is in black and critical WDR5 residues are in red. Hydrophobic contacts are shown as red arcs and polar contacts are shown as black dotted lines.
(F) PDPK1 interacts with WDR5 in a manner similar to other WIN motifs. The figures show superimposition of the PDPK1 (magenta, PDB 6WJQ) with published WIN motif co-crystal structures: unmodified histone H3 (green, PDB 2H9M), KMT2B (orange, PDB 3UVM), KMT2C (lavender, PDB 3UVL), KANL1 (yellow, PDB 4CY2), KMT2A (rose, PDB 3EG6), KMT2D (white, PDB 3UVK), SET1A (cyan, PDB 3UVN), and SET1B (teal, PDB 3UVO).
(G) WIN motif of PDPK1 aligned with established WIN motifs. The related histone methyltransferase enzymes are grouped with brackets.
(H) Intramolecular hydrogen bonding stabilizes the WDR5-acPDPK1 interaction. Co-crystal structure of WDR5 in complex with acetylated PDPK1 peptide shows hydrogen bonding between carboxyl group of the acetyl group and T4 which stabilizes the conformation of the peptide. WDR5 is grey and PDPK1 is pink. Yellow dotted lines denote hydrogen bonds.

Table 4-1: X-ray crystallographic data collection and refinement statistics
PDPK1 peptide (Acetyl-ARTTSQLYDAVPIQS-amidated) in complex with WDR5 (22-334).

Data collection		
Space group		$P2_1$
Cell dimensions		
	a, *b*, *c* (Å)	54.52, 47.23, 118.97
	α, β, γ (°)	90.00, 90.92, 90.00
Resolution (Å)		2.7 (2.7-2.75)[a]
Rsym or Rmerge		0.072/0.063 (0.208/0.209)
I / σI		15.11 (3.21)
Completeness (%)		93.3 (86.2)
Redundancy		2.9 (2.2)
Structure Refinement		
Resolution (Å)		2.71-30.0
No. Reflections		15684
Rwork / Rfree		0.22/0.25
No. atoms		
	Protein	4544
	Ligand	152
	Water	49
B-factors		
	Protein	40
	Ligand	48
	Water	26
RMSD		
	Bond lengths (Å)	0.004
	Bond angles (°)	0.751
Ramachandran		
	Favored (%)	94
	Allowed (%)	5
	Disallowed (%)	0
PDB ID code		6WJQ

[a]Values in parentheses are for highest resolution shell.

Impact of R3 mutation on stable interactions with PDPK1

I next asked if there are any other proteins that bind PDPK1 via its N-terminus, either separate from or together with WDR5. I designed a SILAC experiment to analyze the proteins associated with with wild-type and R3A mutant PDPK1 (**Figure 4-6 A**). I transiently transfected WT or R3A PDPK1-FLAG (C-terminal tag) into 'heavy' and 'light' HEK293 cells, recovered complexes with M2 affinity gel, and analyzed recovered proteins by colloidal coomassie. Most of the protein recovered was PDPK1 (**Figure 4-6 B**). To reduce the chance that PDPK1 would overwhelm the detection of peptides from other co-precipitating proteins, we excluded most of the gel region corresponding to PDPK1 from mass spectrometry analysis. We cut out the gel sections above and below the band corresponding to PDPK1 and analyzed these by MudPIT LC/LC MS/MS.

The experiment was performed in duplicate and the proteins identified in both replicates had high overlap (**Figure 4-6 C**). Overall, there are many other protein kinases detected in both SILAC replicates including protein kinase C variants (delta, zeta, and iota) which are known substrates of PDPK1 [236-238]. Enforcing a two-fold cutoff, only a handful of proteins are impacted by the R3A mutation: five proteins are decreased and four proteins were increased. By far the protein most impacted by the R3A mutation is WDR5 ,showing a 20- to 30-fold decrease in both replicates (R3A/WT ratios 0.037 and 0.048) (**Figure 4-6 D**). To a similar but lesser extent, SET1/MLL complex subunits ASH2L and RBBP5 were also decreased. This result is consistent with the finding that the R3A mutation decreases binding to RBBP5 as well as WDR5 (**Figure 4-3 B**), and indicates that RBBP5 and ASH2L bind PDPK1 indirectly through WDR5. Interestingly, RBBP5 was only detected in one replicate likely because RBBP5 is a similar molecular weight to PDPK1 and excising the PDPK1 band also removed RBBP5. The two other decreased proteins are HNRPR, a protein involved in mRNA processing, and SC16A, an endoplasmic reticulum protein. Finally, of the four proteins that bind R3A PDPK1 better than wild-type, three are proteasome subunits (**Figure 4-6 E**). The other protein, IF2B1, is an mRNA-binding and transport protein. All four of these better-binding proteins have fairly low enrichment,

close to the two-fold cutoff. This SILAC experiment finds very few significantly changed stable interactions with PDPK1 and I conclude that the stable interaction predominantly affected by the R3A mutation is WDR5.

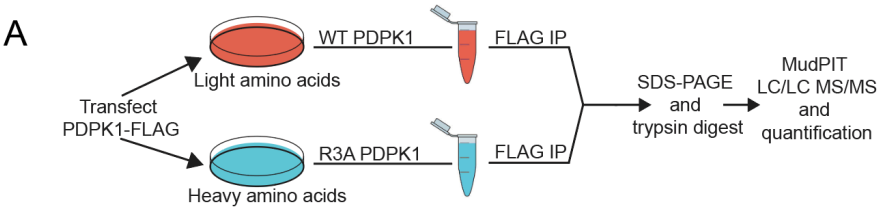

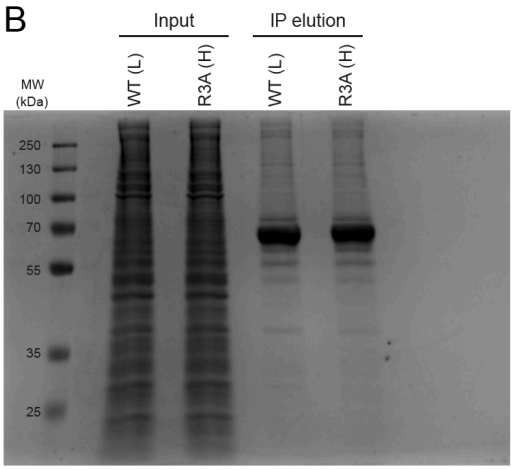

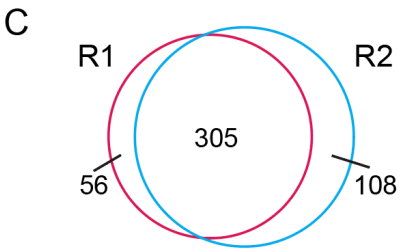

D

PDPK1 SILAC: decreased with R3A mutant

Protein	Replicate	Ratio (R3A/WT)	Uniprot ID	Description
SC16A_HUMAN	R1	0.13	O15027	Protein transport protein Sec16A
ASH2L_HUMAN	R1 and R2	0.12 / 0.19	Q9UBL3	Set1/Ash2 histone methyltransferase complex subunit ASH2
HNRPR_HUMAN	R1	0.11	O43390	Heterogeneous nuclear ribonucleoprotein R
RBBP5_HUMAN	R1	0.076	Q15291	Retinoblastoma-binding protein 5
WDR5_HUMAN	R1 and R2	0.037 / 0.048	P61964	WD repeat-containing protein 5

E

PDPK1 SILAC: gained with R3A mutant

Protein	Replicate	Ratio (R3A/WT)	Uniprot ID	Description
PSA4_HUMAN	R1 and R2	2.5 / 2.1	P25789	Proteasome subunit alpha type-4
IF2B1_HUMAN	R1	2.1	Q9NZI8	Insulin-like growth factor 2 mRNA-binding protein 1
PSMD3_HUMAN	R2	2.2	O43242	26S proteasome non-ATPase regulatory subunit 3
PSA6_HUMAN	R2	2.0	P60900	Proteasome subunit alpha type-6

Figure 4-6: PDPK1 SILAC experiment finds that the R3A mutation is specific for WDR5
(A) Schematic of experimental setup for SILAC experiment on PDPK1. Experiment was performed twice.
(B) Colloidal coomassie-stained gel of WT and R3A PDPK1 immunopurifications. PDPK1-FLAG was recovered from cells with M2 affinity gel, eluted with FLAG peptide, and run on a gel. Most prominent band is PDPK1-FLAG.
(C) Venn diagram of the overlap between replicates.
(D) Table describing the five proteins that met a two-fold threshold as being decreased in association with PDPK1 with the R3A mutation in one or both replicates.
(E) Table describing the four proteins that met a two-fold threshold as being increased in association with PDPK1 with the R3A mutation in one or both replicates.

Discussion

In the results presented in this chapter I interrogate the interaction between the signaling kinase PDPK1 and the nuclear effector WDR5. By focusing my attention PDPK1 I identify a direct WIN site interaction and demonstrate how modification of the amino-terminus of PDPK1 creates an unusually high affinity WIN motif, illuminating features that enable avid WIN site binding. I also find that the R3A mutation is specific to the WDR5–PDPK1 interaction, at least for the proteins that stably associate with PDPK1. These findings establish PDPK1–WDR5 as a direct WIN site interaction partner and validate that the R3A mutation as a tool for disrupting PDPK1 from the WIN site of WDR5.

Modification of the N-terminus of PDPK1 likely occurs co-translationally, and is predicted to be catalyzed by the action of methionine aminopeptidases and the ribosome-anchored NatA N-terminal acetyltransferase complex [239]. Unlike other PTMs, N-terminal acetylation is irreversible, meaning that, for any one molecule of PDPK1, whether or not it can interact tightly with WDR5 is fixed from its moment of synthesis. The proportion of modified PDPK1 molecules in a population, however, could be modulated—NatA complexes are subject to regulation, and are often overexpressed in cancer [240]. Moreover, multiple PDPK1 splice variants have been described, several of which lack the amino-terminal WIN motif [241], suggesting that the interaction of PDPK1 with WDR5 could be controlled via alterations in PDPK1 isoform production. Further study is needed into whether and how the WDR5–PDPK1 interaction is regulated and potentially dysregulated in cancer.

The discovery of PDPK1 as a bonafide WIN site binder enables an intelligent reassessment of the definition of the WIN motif. The WIN motif sequence has previously been defined as G-[SCA]-A-R-[AS]-E [32, 33] and later could be expanded to [GV]-[SCA]-A-R-[AST]-[EKR] [17-19]. With PDPK1 in the mix, the motif can be further expanded to [GV]-[SCA]-A-R-[AST]-[EKRT]. But this motif is largely uninformative for two main reasons. First, this motif does not distinguish between internal WIN motifs and N-terminal ones, which demonstrates that the

first two residues of this motif are not required. Second, the last position, [EKRT], can be polar or positively or negatively charged which does not indicate consistent contribution to interaction with WDR5. Based on our findings, we suggest that definition of the WIN motif be revised to discriminate between those located internally (WIN_I) versus those located at the N-terminus of a protein (WIN_N) (**Figure 4-7**). Because residues at position +5 is quite flexible, and not always resolved in crystal structures, I argue a simple A-R-[AST] captures the flexibility inherent to the WIN site, encompasses the residues most crucial for WIN site interaction, and does not bias discovery efforts. The downside is that this motif is present in 5827 proteins in the human proteome (~30%) and thus does not simplify the search for undiscovered internal WIN motifs. However, the human proteome contains only 67 proteins with potential WIN_N motifs (**Table 4-2**), including PDPK1 and 19 histone H3 variants. Whether any of these WIN_N motifs are capable of tight binding, like PDPK1, depends on removal of the initiator methionine and subsequent acetylation. Large scale proteomic mapping of N-terminal acetylation [235, 242] has not detected this modification in any of these proteins in **Table 4-2**, with exception of a small percentage of H3, perhaps because trypsin (which cleaves after arginine residues) generates WIN_N fragments that are too small for robust detection. But as one-third of all human proteins are subject to this modification [239], chances are high that other high affinity WIN site binding proteins await discovery.

Consensus WIN motif

Position	-3	-2	-1	0	1	2	3	4	5
WIN_N	-	-	**A**	**R**	**AST**	X	X	X	LAIMYQ
WIN_I	GV	SCA	**A**	**R**	**AST**	X	X	X	LAIMYQ

Figure 4-7: Sequence consensus for internal and N-terminal WIN motifs
Summary of consensus sequences for internal (WIN_I) and N-terminal (WIN_N) WIN motifs.

Table 4-2: Human proteins containing N-terminal WIN motif sequences

Protein name	WIN motif(s)	WIN motif position(s)	UniProt Accession	Gene ID
A0A0A6YYL1_HUMAN	ARS	2..4	A0A0A6YYL1	100528021
ACHE_HUMAN	ARA	2..4	Q04844	1145
BCLA3_HUMAN	ARS	2..4	A2AJT9	256643
CALR3_HUMAN	ARA	2..4	Q96L12	125972
CEBOS_HUMAN	ART	2..4	A8MTT3	100505876
CEP72_HUMAN	ARA	2..4	Q9P209	55722
CU058_HUMAN	ARS	2..4	P58505	54058
CXCL2_HUMAN	ARA	2..4	P19875	2920
CYTM_HUMAN	ARS,ARA	2..4,26..28	Q15828	1474
DHB1_HUMAN	ART,ARA	2..4,50..52	P14061	3292
DIK1A_HUMAN	ARS	2..4	Q5T7M9	388650
DIK1C_HUMAN	ARA	2..4	Q0P6D2	125704
DSG2_HUMAN	ARS,ARA	2..4,748..750	Q14126	1829
EPHB3_HUMAN	ARA,ART	2..4,525..527	P54753	2049
GNA15_HUMAN	ARS,ARS	2..4,334..336	P30679	2769
GROA_HUMAN	ARA	2..4	P09341	2919
H3-2, Q5TEC6_HUMAN	ART	2..4	Q5TEC6	440686
H31_HUMAN	ART	2..4	P68431	8350
H31_HUMAN	ART	2..4	P68431	8357
H31_HUMAN	ART	2..4	P68431	8354
H31_HUMAN	ART	2..4	P68431	8356
H31_HUMAN	ART	2..4	P68431	8358
H31_HUMAN	ART	2..4	P68431	8352
H31_HUMAN	ART	2..4	P68431	8351
H31_HUMAN	ART	2..4	P68431	8353
H31_HUMAN	ART	2..4	P68431	8968

Protein name	WIN motif(s)	WIN motif position(s)	UniProt Accession	Gene ID
H31_HUMAN	ART	2..4	P68431	8355
H31T_HUMAN	ART	2..4	Q16695	8290
H32_HUMAN	ART	2..4	Q71DI3	653604
H32_HUMAN	ART	2..4	Q71DI3	126961
H32_HUMAN	ART	2..4	Q71DI3	333932
H33_HUMAN	ART	2..4	P84243	3020
H33_HUMAN	ART	2..4	P84243	3021
H3C_HUMAN	ART	2..4	Q6NXT2	440093
H3Y1_HUMAN	ART	2..4	P0DPK2	391769
H3Y2_HUMAN	ART	2..4	P0DPK5	340096
HELB_HUMAN	ARS,ART	2..4,883..885	Q8NG08	92797
HIPL1_HUMAN	ARA,ARA,ARA	2..4,4..6,618..620	Q96JK4	84439
IFNA7_HUMAN	ARS	2..4	P01567	3444
ITA2B_HUMAN	ARA	2..4	P08514	3674
KLK7_HUMAN	ARS	2..4	P49862	5650
LPP60_HUMAN	ARA,ARA	2..4,51..53	Q86U10	374569
LRC4B_HUMAN	ARA	2..4	Q9NT99	94030
MIA_HUMAN	ARS	2..4	Q16674	8190
NECT2_HUMAN	ARA	2..4	Q92692	5819
NECT3_HUMAN	ART	2..4	Q9NQS3	25945
NPB_HUMAN	ARS	2..4	Q8NG41	256933
NT5C_HUMAN	ARS	2..4	Q8TCD5	30833
PCYXL_HUMAN	ARA	2..4	Q8NBM8	78991
PDIA5_HUMAN	ARA	2..4	Q14554	10954
PDPK1_HUMAN	ART,ARA	2..4,237..239	O15530	5170
PPR3F_HUMAN	ART,ARS	2..4,606..608	Q6ZSY5	89801
PRR25_HUMAN	ART,ART,ARS	2..4,234..236,271..273	Q96S07	388199

Protein name	WIN motif(s)	WIN motif position(s)	UniProt Accession	Gene ID
PTPRU_HUMAN	ARA,ART	2..4,569..571	Q92729	10076
PVR_HUMAN	ARA,ARS	2..4,268..270	P15151	5817
RAMP1_HUMAN	ARA	2..4	O60894	10267
RHXF1_HUMAN	ARS	2..4	Q8NHV9	158800
SHSA8_HUMAN	ARA,ARA,ARA,ARA	2..4,122..124,293..295, 344..346	B8ZZ34	440829
SPIR2_HUMAN	ARA	2..4	Q8WWL2	84501
TM221_HUMAN	ARS,ARA	2..4,176..178	A6NGB7	100130519
TSN4_HUMAN	ARA	2..4	O14817	7106
UD110_HUMAN	ARA	2..4	Q9HAW8	54575
UD17_HUMAN	ARA	2..4	Q9HAW7	54577
UD18_HUMAN	ART	2..4	Q9HAW9	54576
WBP1_HUMAN	ARA	2..4	Q96G27	23559
WDR90_HUMAN	ARA,ART,ART,ARA,ARS	2..4,124..126,345..347, 429..431,696..698	Q96KV7	197335
XPP2_HUMAN	ARA,ARA	2..4,650..652	O43895	7512

A promising candidate for an additional acetylated, high affinity, N-terminal WIN motif is HELB (helicase B), identified and validated in my WIN site SILAC data (**Figure 3-6 C and E**). HELB is a DNA helicase that plays roles in initiating DNA replication, responding to replication stress, and responding to DNA damage [243]. Ellen Fanning's group at Vanderbilt University showed that the subcellular localization of HELB is cell cycle-dependent and controlled by phosphorylation. For most of G1, HELB is predominantly nuclear, but in late G1 and into S phase and G2/M, HELB is phosphorylated by CDK2 and most but not all HELB translocates to the cytoplasm [244, 245]. These results indicate there may be different roles for HELB depending upon cell cycle phase and is intriguing given the known connections of WDR5 to cell cycle regulation. A promising line of research will be investigating how and when HELB interacts with WDR5 and if this interaction is regulated at all by phosphorylation events.

The structural analysis of the PDPK1 acetylated peptide in complex with WDR5 reveals some similarities and differences in the mode of binding for different WIN motif sequences. All WIN motif structures are similar in binding of the central arginine deep into the pocket of the WIN site, with the guanidinium side chain of the arginine clamped by the aromatic rings from F133 and F263 of WDR5. However, beyond this central arginine, certain details of the interaction diverge. One difference is the stabilizing intramolecular interaction within the peptide induced by the acetyl group of the PDPK1 peptide. Most other structures do not display such intramolecular interactions, but an exception is for the KMT2A and SET1A cocrystal structures where the hydroxyl group of a serine at position -2 of these internal WIN sequences may be capable of forming a similar stabilization effect (**Figure 4-5 G**). Interestingly, one study found that KMT2A and SET1A are the only two MLL/SET family members that require interaction with WDR5 for *in vitro* complex formation and catalytic activity [37]. Thus even though on their own these internal WIN peptides do not bind as tightly to WIN site of WDR5 as PDPK1 (~3 μM for KMT2A and ~500 nM for SET1A [33]), perhaps in the context of an assembled methyltransferase complex this stabilization is important for catalytic activity. Another difference between the WDR5–PDPK1 structure and other WDR5–WIN peptide structures is in regard to

the residues C-terminal of the arginine. Even though the sequence alignment of WIN peptides shows some consensus at the +5 position (**Figure 4-5 G**), PDPK1 is the only structure where this +5 residue (L8) makes hydrogen bond contacts with WDR5. In fact, for most of the structures, the C-terminal region of the peptide is not even resolved past position +4 indicating that most of the time these C-terminal residues are not contributing significantly to the interaction with WDR5. And for the structures in which C-terminal residues are resolved, the +4 residue (often tyrosine), not the +5 residue, makes backbone contact with WDR5. Thus another unique aspect of the PDPK1 interaction is that the +5 position is making side-chain interaction with WDR5. However, these structural data are only for peptides, and within the context of full length proteins such interactions could behave differently.

Quantitative proteomic comparison of wild-type and R3A PDPK1 protein interactions reveals less than a dozen changes meeting a two-fold cutoff. PDPK1 is a kinase that is known to phosphorylate many substrates, and we detect some but not all of those substrates in the proteomic data. We detect PKC (β, δ, ζ, and ι) and PKN1, but not AKT, SGK, RSK, or S6K, indicating that some but not all interactions of PDPK1 with its substrates are stable interactions. While none of these detected kinase interactions are affected by the R3A mutation, I cannot rule out the possibility that there are undetected transient interactions with known PDPK1 substrates that are impacted by PDPK1 N-terminal mutation. Overall and as expected, WDR5 is the protein decreased the most with the N-terminal mutant, followed closely by ASH2L and RBBP5. This result indicates that a nearly complete WRAD complex is capable of interacting with PDPK1 through WDR5. Conversely, the majority of increased proteins are proteasome subunits, indicating that the R3A mutant may be prone to ubiquitylation and proteasome-mediated degradation. Whether this destabilization is directly caused by loss of interaction with WDR5 is unlikely, but currently unclear. Overall, these data show that the R3A point mutation functions as a more specific tool for studying the PDPK1–WDR5 interaction than mutation or inhibition of the WIN site.

By characterizing the residues, modification status, and structural details of the WDR5–PDPK1 interaction, I demonstrated how modification of the amino-terminus of PDPK1 creates an unusually high-affinity WIN motif. This finding has potential to extend to other WDR5 interactions, such as HELB, and is significant for understanding different modes of WIN site binding. In the following chapters I interrogate the functional significance of the high affinity WDR5–PDPK1 interaction.

Contributions

The experiments and data presented in this chapter were facilitated by the assistance of stellar collaborators. The R3A mutant was generated by Tyler Hansen. The far western blot experiments were performed by Kiana Guerrazzi. Dr. Kristie Rose and Salisha Hill provided assistance with analyzing the post-translational modification status of PDPK1 by mass spectrometry, as well as the PDPK1-centered SILAC experiment. The TR-FRET displacement assays were performed by J. Grace Shaw. Protein purification for structural studies was performed by William G. Payne. Protein crystallization and structural data processing was performed by Dr. Bin Zhao.

Chapter V[4]

Functional analysis of the PDPK1–WDR5 interaction

Introduction

WDR5 is a predominantly nuclear protein and PDPK1 is a mostly cytosolic protein with nuclear shuttling capability. I determined that the PDPK1–WDR5 interaction is predominantly nuclear (**Figure 4-2 C, D, G**), but since the nuclear functions of PDPK1 are not well defined, this does not provide much insight in to why PDPK1 interacts with WDR5. Here, I begin to interrogate the functional significance of the PDPK1–WDR5 interaction by examining cellular signaling, sub-cellular localization, and gene expression networks.

Similar to how WDR5 is a cellular multitasker, PDPK1 is not simply a cytosolic kinase. In addition to initiating signal transduction by phosphorylating dozens of kinases, PDPK1 also is found to stably associate with other cytosolic proteins including integral membrane proteins [246], the scaffolding protein CARD11 [247] and a hippo pathway kinase complex [248]. And PDPK1 can be nuclear. Inhibiting CRM1-dependent nuclear export with leptomycin B induces an accumulation of PDPK1 [207-209], indicating that PDPK1 shuttles into the nucleus and is actively exported. Cellular stimulation with IGF-1 or insulin also induces nuclear accumulation of PDPK1 [207, 208]. Small molecule inhibition of the PI3K pathway reduces nuclear PDPK1 [208], while hyper-activation of PI3K/AKT signaling by PTEN deletion causes accumulation of nuclear PDPK1 [207]. These results indicate that nuclear PDPK1 is a response to PI3K/AKT growth factor signaling. Nuclear localization of PDPK1 is controlled at least in part by phosphorylation at S396, a residue very near to the canonical nuclear export signal (NES) of PDPK1 [207]. S396

---

[4] Parts of Chapter V are adapted with permission from the following publication:
171. Guarnaccia A.D., Rose K.L., Wang J., Zhao B., Popay T.M., Wang C.E., Guerrazzi K., Hill S., Woodley C.M., Hansen T.J., Lorey S.L., Shaw J.G., Payne W.G., Weissmiller A.M., Olejniczak E.T., Fesik S.W., Liu Q., Tansey W.P. Impact of WIN site inhibitor on the WDR5 interactome. Cell Rep. 2021;34(3):108636. PMID: 33472061.

phosphorylation increases with PDPK1 nuclear localization [208], indicating that this modification blocks recognition of the NES and promotes nuclear PDPK1. Additionally, nuclear shuttling of PDPK1 seems to rely on the phosphatase SHP-1 which, unlike PDPK1, does contain a canonical NLS [209]. Overall, PDPK1 has various multitasking roles in cells and is altered in its interaction partners and its sub cellular localization in response to growth factor signaling.

The PI3K/AKT signaling pathway is one of the most frequently mutated and hyper-activated signaling pathways in cancer [221]. Various components of the PI3K/AKT pathway are deregulated in cancer, including PDPK1 [196]. Like WDR5, PDPK1 does not gain function by activating mutations, but rather by its overexpression [249-254]. In some cancers, PDPK1 overexpression is induced by *PDPK1* copy number gain [255-257]. High levels of PDPK1 promote cell proliferation, anchorage independent growth, and metastasis [254, 258-261]. Notably, deleting PDPK1 in a mouse model of acute myeloid leukemia slows disease progression [262]. Thus both WDR5 and PDPK1 are up-regulated in cancer and promote pro-tumorigenic processes. Increased expression of either protein is is likely to promote the PDPK1–WDR5 interaction, but the functional consequences of enhancing this interaction are still to be discovered.

To study the functional intersection between PDPK1 and WDR5, I used CRISPR to engineer cells in two specific ways. First, I knocked in the R3A mutation at the endogenous *PDPK1* locus to create cells that solely express WDR5 interaction-deficient PDPK1. Second, I implemented the dTAG system for targeted protein degradation [263] to specifically degrade either WDR5 or PDPK1. The dTAG system is a strategy for tagging a protein of interest in cells and inducing its degradation using a bifunctional small molecule. The protein of interest is fused with FKBP(F36V), and this modified epitope binds to one end of the bifunctional dTAG degrader molecule. The other end of the degrader molecule, thalidomide, binds to the E3 ubiquitin ligase CRBN [264]. By inducing proximity between the target protein and CRBN, the dTAG molecule promotes ubiquitylation and proteasome-mediated degradation of the targeted chimeric protein.

This system enables rapid depletion of any tagged protein in cells and is useful for studying common essential gene products like WDR5. I combined the dTAG system with comparative genomics to evaluate the functional overlap between PDPK1 and WDR5 (see below). The results of these analyses establish a role for the PDPK1–WDR5 interaction in controlling transcription of cell cycle-regulated genes.

Results

The PDPK1–WDR5 interaction does not influence PDPK1 signaling or nuclear shuttling

Given the established functions of PDPK1 as a transducer of PI3K/AKT signaling and as nuclear shuttling protein, I asked if disrupting the PDPK1–WDR5 interaction affects these processes. First, I treated cells with C6 and found that chemical disruption of the PDPK1–WDR5 interaction has no obvious effect on growth factor signaling by PDPK1, including AKT phosphorylation in HEK293 cells (**Figure 4-2 E**) and AKT and S6 kinase phosphorylation in CHP134 cells (**Figure 5-1 A**). Second, because PDPK1 and WDR5 interact in the nucleus, I asked whether the nuclear shuttling of PDPK1 [207, 208] is dependent on interaction with WDR5. I inhibited CRM1-dependent nuclear export with leptomycin B (LMB) and quantified the distribution of WT and R3A EGFP-tagged PDPK1 variants in U2OS cells (**Figure 5-1 B–D**). I confirmed that PDPK1-EGFP accumulates in the nucleus upon LMB treatment, but observe no difference in nuclear accumulation of the R3A mutant compared to WT PDPK1. Thus, nuclear shuttling of PDPK1 occurs independent from interaction with WDR5.

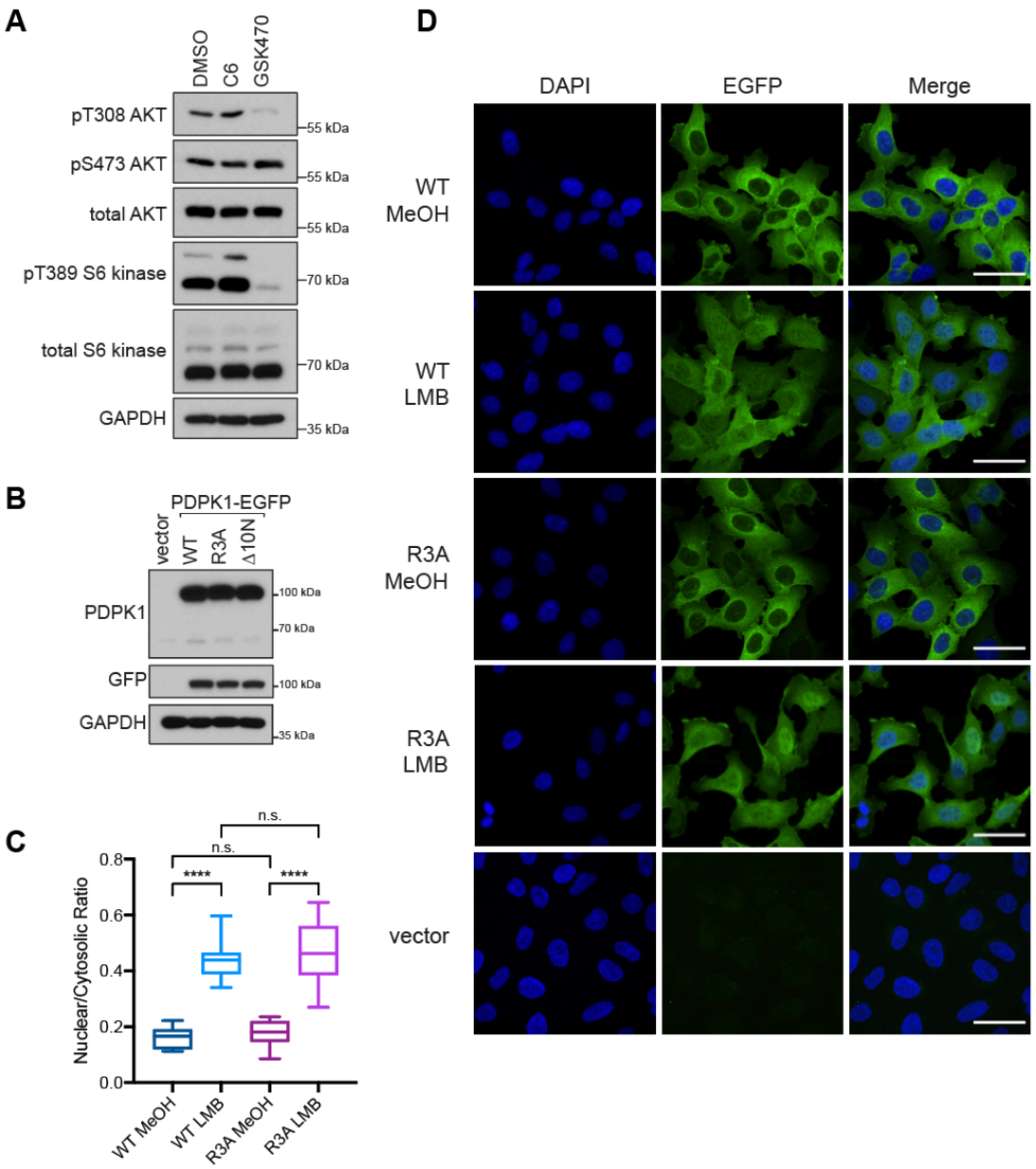

Figure 5-1: The PDPK1–WDR5 interaction does not influence PDPK1 signaling or nuclear shuttling

(A) C6 WIN site inhibition has little if any effect on AKT signaling in CHP134 cells. Cells were treated overnight with 5 μM C6, 2 μM PDPK1 kinase inhibitor GSK2334470, or DMSO vehicle control. Cells were then treated with 50 ng/ml IGF-1 for 30 minutes before lysis in RIPA buffer supplemented phosphatase inhibitors. Lysates were analyzed by western blotting. *n=3* biological replicates.

(B) Overexpression of PDPK1-EGFP fusion proteins. U2OS cells were stably transduced with pBabe-puro vectors to express PDPK1-EGFP-FLAG fusion proteins: wildtype, R3A mutant, or deletion mutant without the first ten amino acids, Δ10.

(C) Representative images from the experiments quantified in (D). Immunofluorescence of the indicated stable cell lines treated for four hours either with 70% methanol vehicle control or with 20 nM leptomycin B. Cells were then fixed, mounted in DAPI-containing media, and imaged. Scale bar is 50 μm.

(D) PDPK1 shuttling capability is not affected by disrupting the interaction with WDR5. Quantification of the nuclear localization of WT and R3A PDPK1 when nuclear export is inhibited by four-hour treatment with 20 nM leptomycin B (LMB) or 70% methanol vehicle control. Plotted as box and whisker plot where the line is at the median, the box represents 25th to 75th percentiles, and whiskers represent min and max; $n=3$, analyzed by unpaired two-tailed *t*-test, **** $p < 0.0001$.

Generating cell lines for targeted protein degradation

To interrogate PDPK1 and WDR5 and examine how these proteins function together, I created cell lines that enable targeted protein degradation using the dTAG system [263]. To create these cell lines I used gene specific targeting vectors and CRISPR/Cas9 ribonucleoprotein complexes. The targeting vectors carry the FKBP(F36V)-2xHA dTAG and a fluorescent marker (mCherry or BFP) flanked by gene-specific homology arms [169]. I introduced targeting vectors and CRISPR reagents into cells by electroporation, and then selected for proper integration events by flow cytometry sorting based on the fluorescent markers. This method enabled me to efficiently tag PDPK1 and WDR5 in U2OS and CHP134 cells, described below.

To tag PDPK1 I designed three separate gRNAs, all of which target the C-terminal region of the *PDPK1* coding sequence (**Figure 5-2 A**). I electroporated targeting vectors and Cas9 ribonucleoprotein complexes into cells, and after cell recovery, I sorted cells by flow cytometry, selecting for fluorescently-marked cells. For PDPK1, the fluorescent signals were fairly weak, low for mCherry and nearly undetectable for BFP (**Figure 5-2 B**). Because of the low BFP signal, I instead sorted for bright mCherry-positive cells (**Figure 5-2 C**), reasoning that brighter cells have multiple alleles of PDPK1 efficiently tagged. Western blot analysis demonstrated high tagging efficiency; even in unsorted cells, a tagged, higher molecular weight version of PDPK1 was detectable (**Figure 5-2 D**). Treatment of the tagged population of cells with the small molecule dTAG47 [265] induces rapid degradation within hours (**Figure 5-2 E**). Importantly, tagging of PDPK1 does not disrupt the PDPK1–WDR5 interaction by co-IP (**Figure 5-2 F**). This depletion is stable over six days (**Figure 5-2 G**), and the cell growth over this time is slowed (**Figure 5-2 H**).

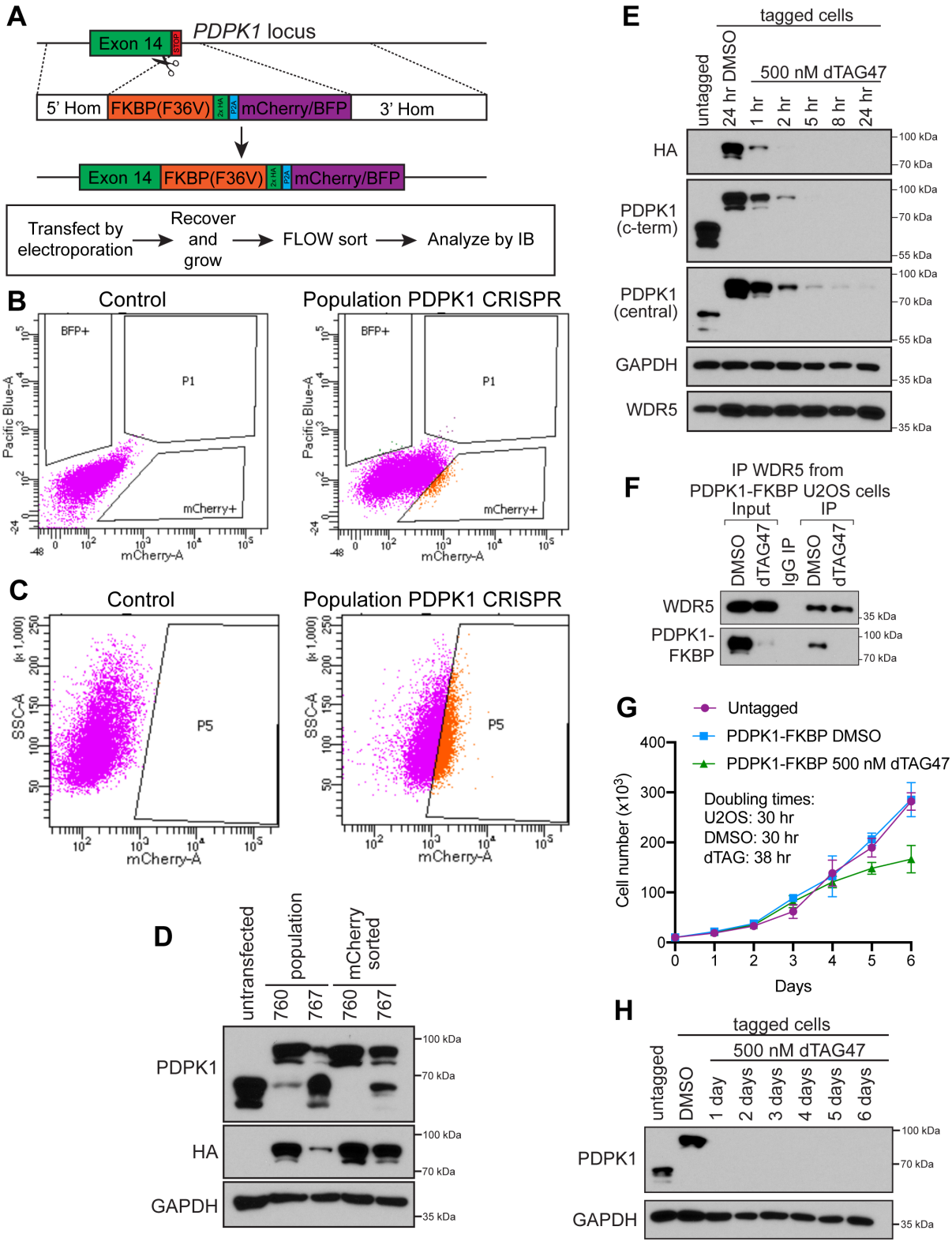

Figure 5-2: Implementing the dTAG system for PDPK1 in U2OS cells
(A) Top, schematic of the CRISPR targeting strategy used to tag endogenous PDPK1 for degradation. Cassettes containing FKBP(F36V)-2xHA-P2A-mCherry (or BFP) were introduced near the stop codon of PDPK1. Bottom, flow chart of tagging strategy.

(B) Representative dot plots from flow cytometry comparing control (untransfected) cells with the population of transfected cells. U2OS cells were sorted for double positive cells (BFP+ and mCherry+) as well as single positive (mCherry+) cells.
(C) Second sort of population of cells gating for bright mCherry positive cells.
(D) Western blot analysis of populations of U2OS cells before and after FLOW sorting, using two gRNAs (760 and 767). This PDPK1 antibody recognizes a C-terminal epitope that is destroyed with the 760 gRNA.The 760 gRNA sample was taken forward for sorting and isolation.
(E) Timecourse analysis of mCherry+ sorted population of PDPK1-tagged U2OS cells. Cells were treated with 500 nM dTAG47 for the indicated time and collected and analyzed by western blotting, here using two different antibodies against PDPK1.
(F) The PDPK1–WDR5 interaction is preserved in PDPK1-FKBP(F36V)-2xHA cells. Co-IP of endogenous proteins from PDPK1-FKBP(F36V)-2xHA cells. Input for WDR5 is 10%. Input for PDPK1 is 1%. *n=3* biological replicates.
(G) Analysis of cell growth of PDPK1-FKBP(F36V)-2xHA cells. Cells were counted every 24 hours, error bars represent standard deviation, *n=3*. The doubling time for a representative experiment is shown.
(H) IB, showing that tagged PDPK1 results in a shift in the apparent molecular weight of the protein, and that knock down by addition of 500 nM dTAG47 is stable for at least six days. Cells were cultured in media containing dTAG47 for the indicated number of days without refreshing the media.

In a similar way I also tagged *WDR5* in U2OS cells (**Figure 5-3 A**). Flow cytometry analysis of the population of *WDR5*-targeted cells showed strong fluorescent signal for both BFP and mCherry (**Figure 5-3 B**). Sorting for double-positive cells (**Figure 5-3 B**) resulted in an enrichment for WDR5-tagged cells, and a second sort that selected for the brightest double positive cells (**Figure 5-3 C**) resulted in a population of cells where >95% of WDR5 protein was tagged (**Figure 5-3 D**). Similar to PDPK1, treating the population of WDR5-FKBP(F36V) tagged cells with dTAG47 induces protein depletion within hours (**Figure 5-3 D**), and tagging WDR5 does not disrupt its interaction with PDPK1 (**Figure 5-3 E**). Depletion is stable over six days in culture, although the small percentage of cells that carry untagged alleles of WDR5 do grow out and are apparent by day 6 in culture (**Figure 5-3 F**). Without WDR5, cells are largely impaired in their proliferation (**Figure 5-3 G**); the small amount of growth that is observed is due to the growth of cells carrying untagged *WDR5*, which is observable by the reappearance of ~35 kDa untagged WDR5 by western blot at six days (**Figure 5-3 F**).

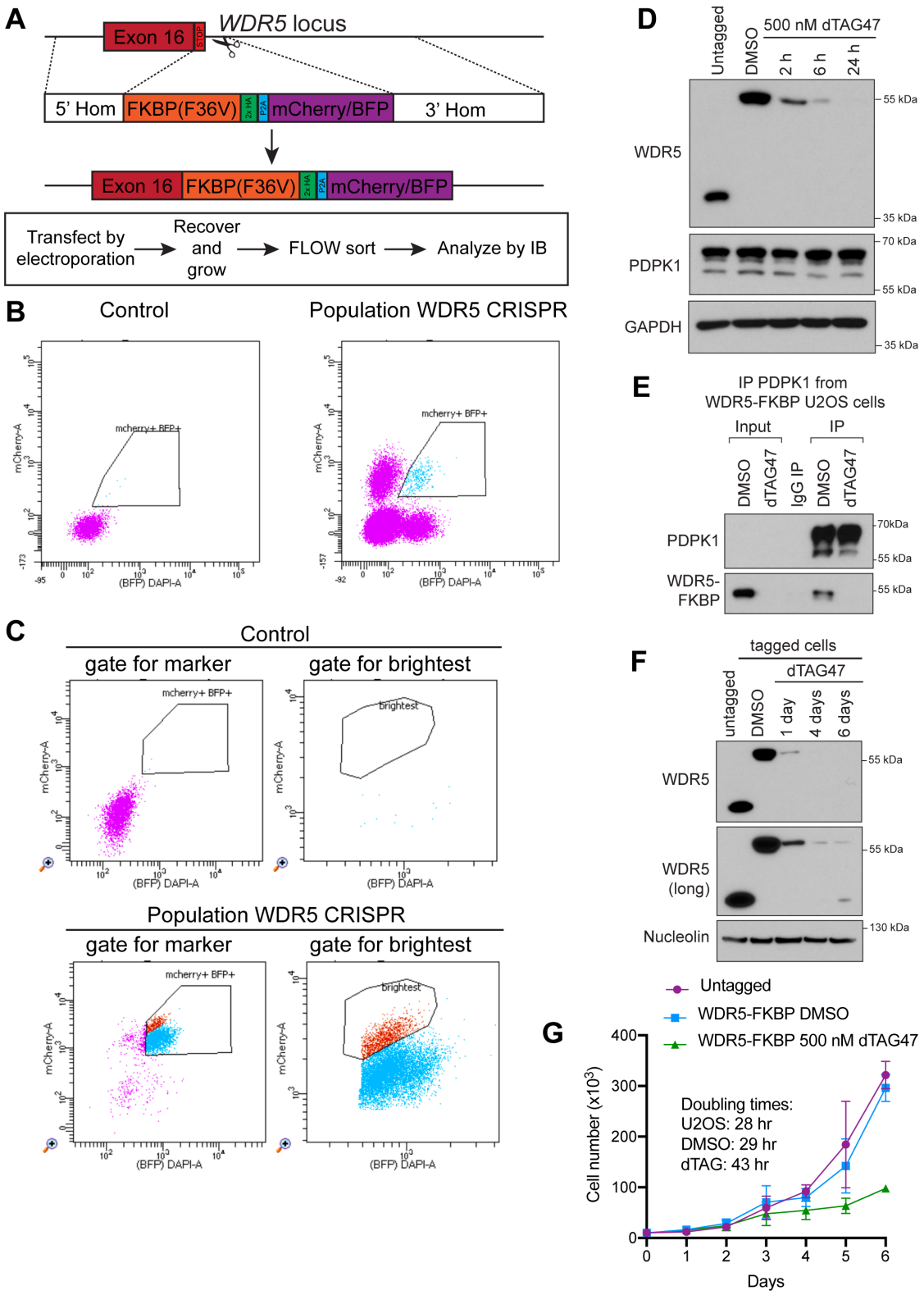

Figure 5-3: Implementing the dTAG system for WDR5 in U2OS cells
(A) Top, schematic of the CRISPR targeting strategy used to tag endogenous WDR5 for degradation. Cassettes containing FKBP(F36V)-2xHA-P2A-mCherry (or BFP) were introduced near the stop codon of PDPK1. Bottom, flow chart of tagging strategy.

(B) Representative dot plots from flow cytometry comparing control (untransfected) cells with the population of transfected cells. U2OS cells were sorted for double positive cells (BFP+ and mCherry+).
(C) Second sort of population of cells gating for brightest double positive cells. Untransfected cells are used as a control.
(D) Timecourse analysis of double positive sorted population of WDR5-tagged U2OS cells. Cells were treated with 500 nM dTAG47 for the indicated time and collected and analyzed by IB.
(E) The PDPK1–WDR5 interaction is preserved in WDR5-FKBP(F36V)-2xHA cells. Co-IP of endogenous proteins from WDR5-FKBP(F36V)-2xHA cells. Input for PDPK1 is 10%. Input for WDR5 is 1%. *n=3* biological replicates.
(F) IB, showing that tagged WDR5 results in a shift in the apparent molecular weight of the protein, and that knock down by addition of 500 nM dTAG47 is stable for at least six days. Note that, by day 6, untagged WDR5 becomes visible in IB (long exposure), which reflects an outgrowth of cells with untagged *WDR5* loci in the population. Cells were cultured in media containing dTAG47 for the indicated number of days without refreshing the media.
(G) Analysis of cell growth of WDR5-FKBP(F36V)-2xHA cells. Cells were counted every 24 hours, error bars represent standard deviation, *n=3*. The doubling time for a representative experiment is shown. The apparent survival of WDR5-depleted cells at day 6 is due to outgrowth of cells with untagged *WDR5* loci in the population.

One interest in the Tansey Lab is in studying N-MYC-amplified neuroblastoma. To assist with this neuroblastoma research I also tagged PDPK1 and WDR5 in the N-MYC-amplified neuroblastoma cell line, CHP134 [266] using the same approach as for U2OS cells. Tagging PDPK1 in CHP134 cells was highly efficient (**Figure 5-4 A**), and sorting for double positive cells yielded a pure population where >95% of PDPK1 is tagged (**Figure 5-4 B**). Tagging WDR5 in CHP134 cells was more challenging. Even though tagging occurred efficiently (**Figure 5-4 C**), sorting for the brightest double-positive cells resulted in a population where only ~60% of WDR5 was tagged (**Figure 5-4 D**). Still, this population of cells was sufficient for experiments needed as part of a manuscript revision, and enabled a direct comparison of WDR5 WIN site inhibition and WDR5 depletion. Inhibiting or depleting WDR5 causes similar cellular responses, most notably induction of p53 and decreased expression of ribosome protein genes [82], indicating on-target action of the inhibitor. Subsequently, to improve the purity of these WDR5-tagged CHP134 cells, I isolated clonal populations of CHP134 cells where all alleles of WDR5 are tagged.

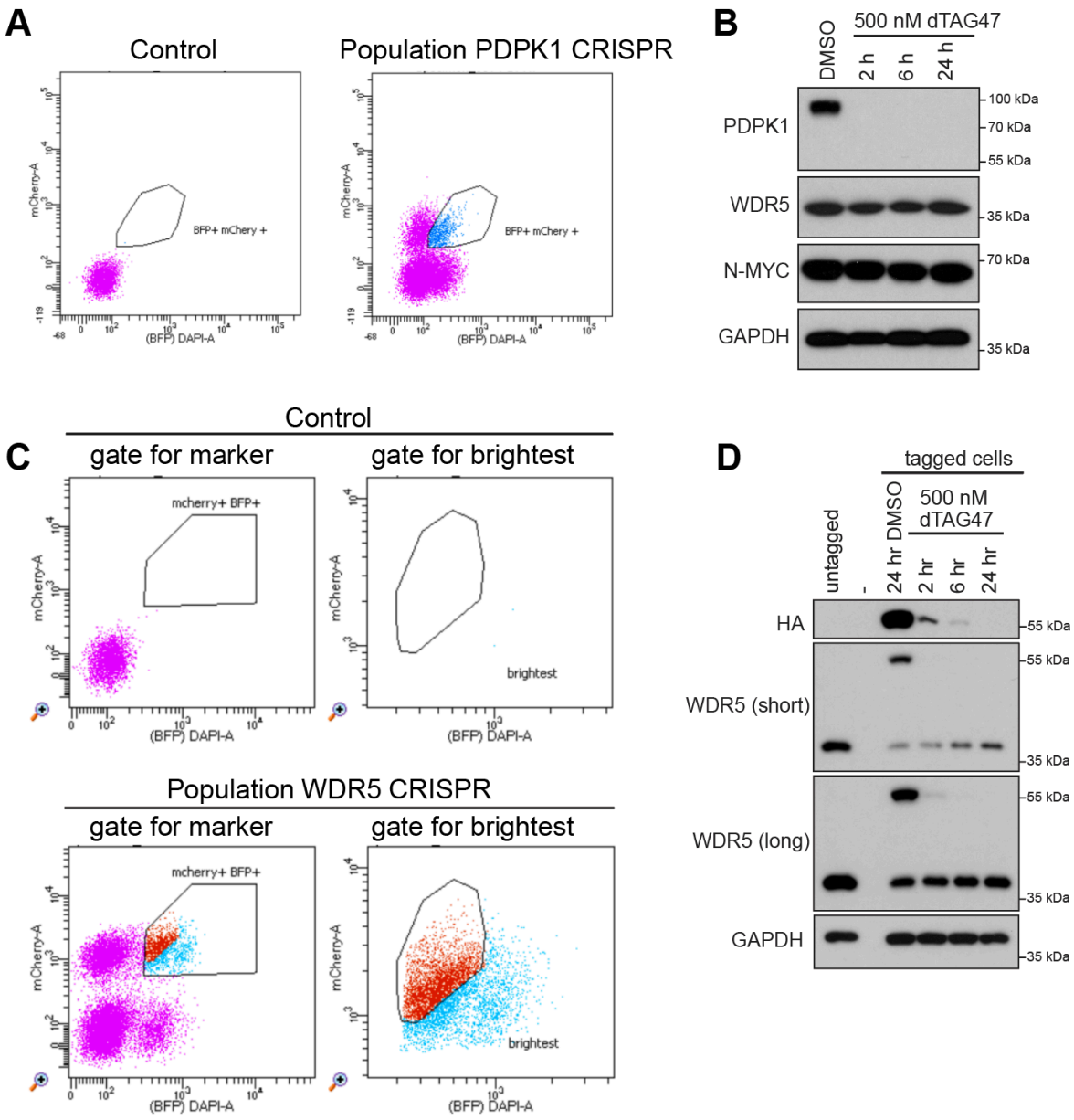

Figure 5-4: Implementing the dTAG system for PDPK1 and WDR5 in CHP134 cells
(A) Representative dot plots from flow cytometry comparing control (untransfected) cells and the population of *PDPK1* CRISPR transfected cells. CHP134 cells were sorted for double positive cells (BFP+ and mCherry+).
(B) IB analysis of sorted PDPK1-FKBP(F36V)-2xHA cells with a dTAG47 time-course analysis.
(C) Representative dot plots from flow cytometry comparing untransfected cells and a *WDR5*-edited population of cells. Sorting was gated for the brightest double positive cells.
(D) IB analysis of sorted WDR5-FKBP(F36V)-2xHA cells with a dTAG47 time-course analysis. Tagging efficiency is only ~60% for this population.

The PDPK1–WDR5 interaction influences G2/M-expressed genes

Interaction of PDPK1 and WDR5 in the nucleus, together with the transcriptional roles of WDR5, prompted me to ask whether PDPK1 and WDR5 influence expression of a common set of genes. Using the U2OS dTAG system cell lines, I performed RNA-Seq after 24 hours of dTAG47 treatment in both PDPK1- and WDR5-tagged cells. PDPK1 depletion results in changes in the expression of ~1,100 genes (**Figures 5-5 A–B, and 5-6 A**). WDR5 depletion has more extensive effects, leading to changes in expression of ~7,400 genes (**Figures 5-5 C–D, and 5-6 B**). The overlap of significant gene expression changes between the two is ~660 (**Figure 5-6 C**). For PDPK1 and WDR5 depletion, (GO) enrichment analysis identified transcript changes consistent with the known functions of both proteins (**Figure 5-5 E–F, and 5-6 D–E**). Interestingly, however, I observed that several of the cell-cycle related GO terms enriched in transcripts decreased by PDPK1 depletion are enriched in transcripts increased by WDR5 depletion (**Figure 5-5 E and F**; red text). Gene set enrichment analysis (GSEA) [267] further strengthened these connections (**Figures 5-5 G–I**). To determine if these reciprocal enrichments are due to changes in a common set of genes, we overlaid gene lists and found that more than 40% (246 count) of genes whose expression is decreased by PDPK1 depletion are induced by depletion of WDR5 (**Figure 5-5 J**). In general, changes in expression of these 246 genes are small (**Figures 5-5 K and 5-6 F**) but significant (**Figure 5-6 G and H**). Importantly, GO analysis on these common genes reinforced cell cycle connections (**Figure 5-5 L**), demonstrating that PDPK1 and WDR5 reciprocally influence the expression of a set of genes linked to the cell cycle.

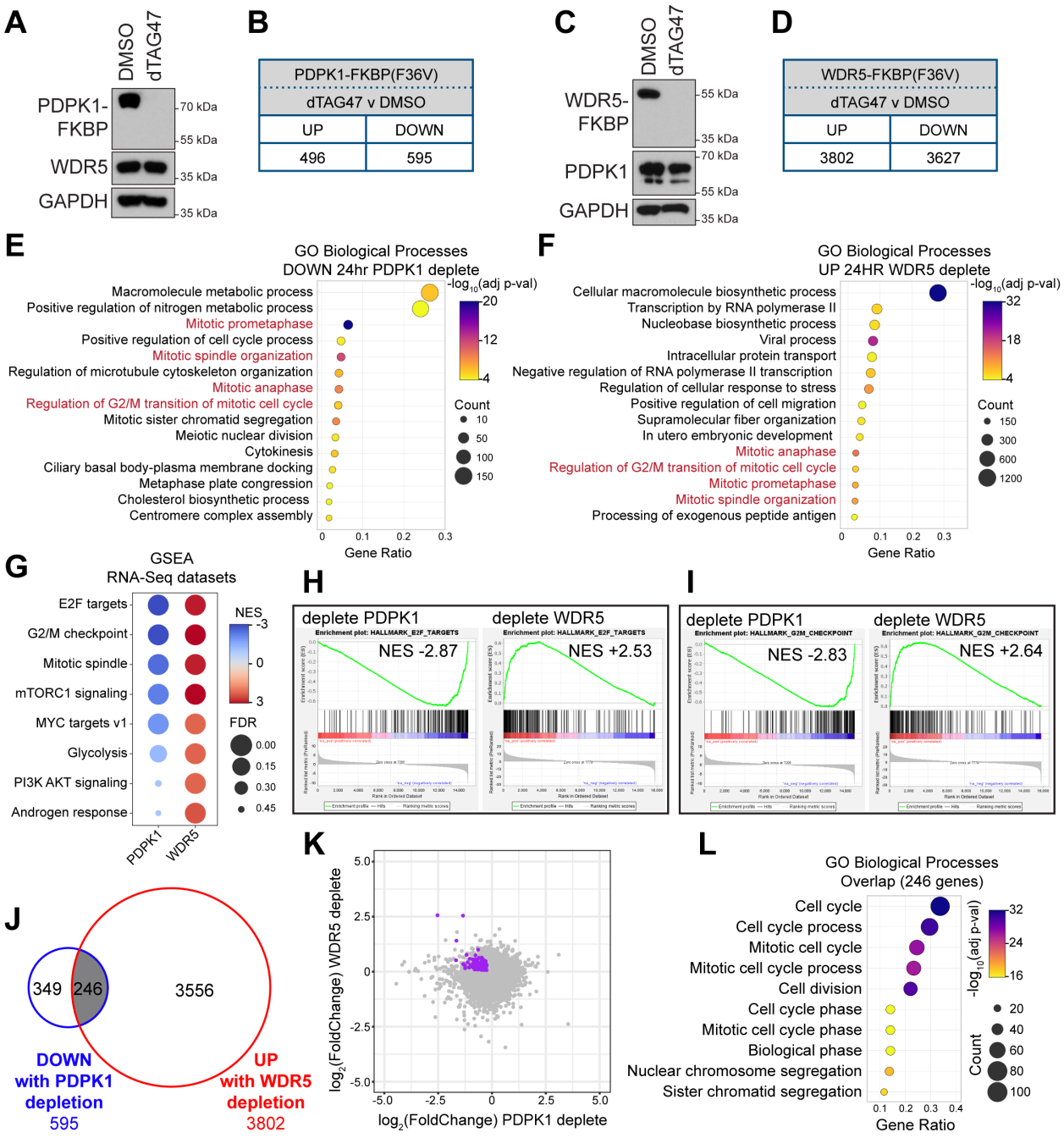

Figure 5-5: PDPK1 and WDR5 oppositely influence the expression of cell cycle genes
(A) U2OS cells expressing PDPK1-FKBP(F36V)-2xHA were treated for 24 hours with 500 nM dTAG47 or DMSO, lysates prepared, and PDPK1, WDR5 and GAPDH levels determined by IB.
(B) Number of transcripts significantly (FDR < 0.05) altered by 24 hour treatment of cells in (A) with 500 nM dTAG47, compared to DMSO control. *n=3* biological replicates.
(C) As in (A) but for the cells expressing WDR5-FKBP(F36V)-2xHA.
(D) Number of transcripts significantly (FDR < 0.05) altered by 24 hour treatment of cells in (C) with 500 nM dTAG47, compared to DMSO control. *n=4* biological replicates.
(E) GO analysis of decreased transcripts identified by RNA-Seq of U2OS cells depleted of PDPK1 for 24 hours. Biological Process GO terms were ranked by adjusted *p*-value, and the 15 most significant enriched terms are presented; the color indicates the Bonferroni-corrected

Fisher Exact *p*-value; the size indicates the number of genes in that category; the x axis the ratio of genes in the category over total analyzed genes.
(F) GO term analysis of increased transcripts identified by RNA-Seq of U2OS cells depleted of WDR5 for 24 hours. Ranking and presentation are as in (E).
(G) Enriched Hallmark gene sets [268], determined by GSEA of RNA-Seq from 24 hour PDPK1 or WDR5 depletion. Eight of the top Hallmarks are shown. Color indicates the normalized enrichment score (NES); size indicates the FDR value.
(H and I) Examples of GSEA enrichment plots summarized in (G). FDR=0.000 for all plots shown.
(J) Overlap of transcripts that are decreased with PDPK1 depletion and increased with WDR5 depletion.
(K) Scatter plot of RNA-Seq data from PDPK1 and WDR5 depletions. The 246 genes from (J) are highlighted in purple.
(L) GO term analysis of the 246 genes represented in (J). Biological Process GO terms were sorted hierarchically, and the most specific subclasses were ranked by adjusted *p*-value. The 10 most significantly enriched subclasses are presented. Presented as in (E).

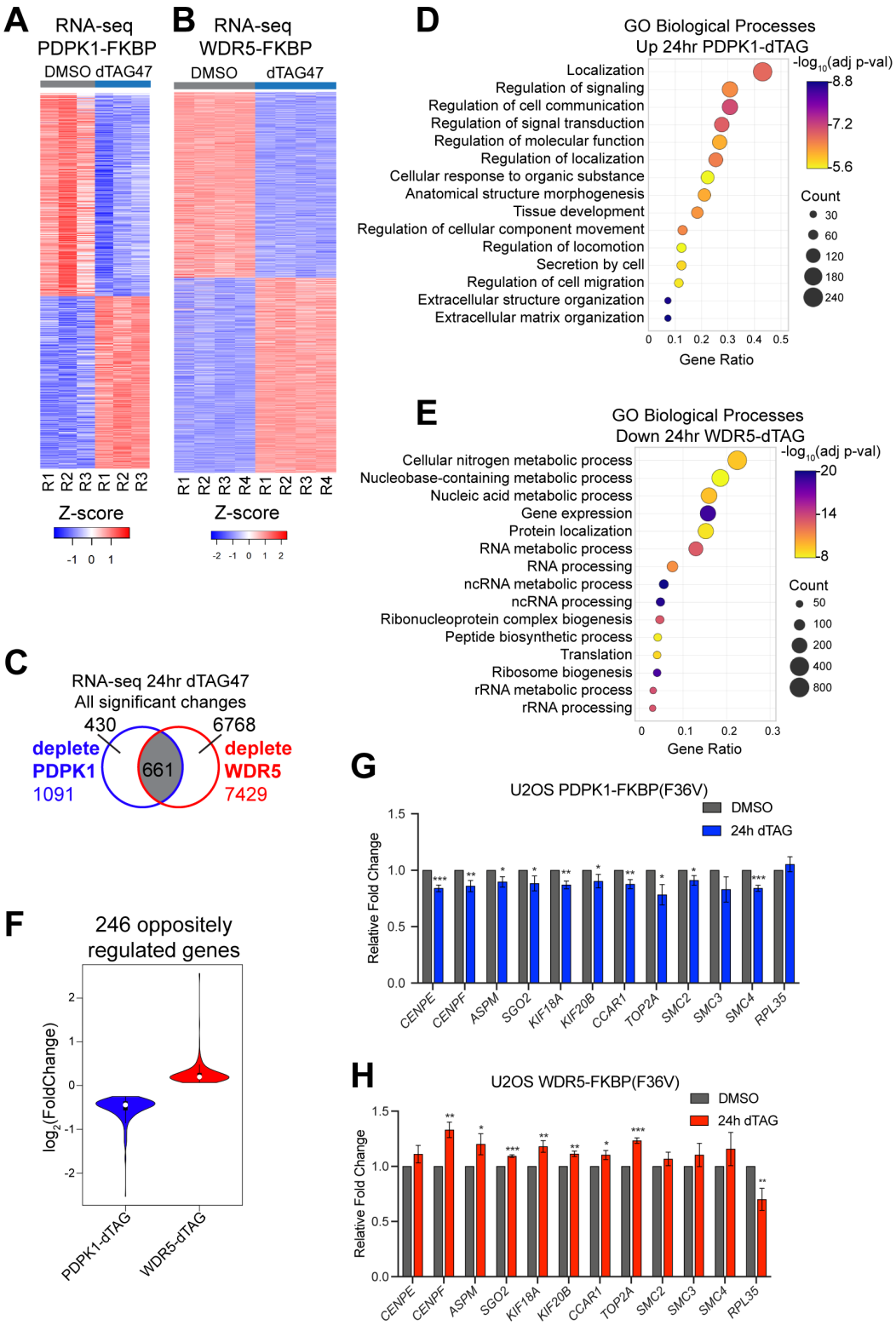

Figure 5-6: Inducible degradation of PDPK1 and WDR5 enables comparative genomic analysis

(A) Heatmap, displaying z-transformed gene expression for significantly changed genes in 24 hr dTAG47 versus DMSO (FDR < 0.05) for three replicates (R1–R3) of RNA-Seq from PDPK1-

FKBP(F36V)-2xHA U2OS cells.
(B) Heatmap, displaying z-transformed gene expression for significantly changed genes in 24 hr dTAG47 versus DMSO (FDR < 0.05) for four replicates (R1–R4) of RNA-Seq from WDR5-FKBP(F36V)-2xHA U2OS cells.
(C) Venn diagram of overlap of significantly changed genes between RNA-Seq from WDR5 depletion and PDPK1 depletion datasets.
(D) GO term analysis of increased transcripts identified by RNA-Seq of U2OS cells depleted of PDPK1 for 24 hours. Biological Process GO terms were ranked by adjusted *p*-value, and the 15 most significant enriched terms are presented; the color indicates the Bonferroni-corrected Fisher Exact *p*- value; the size indicates the number of genes in that category; the x axis the ratio of genes in the category over total analyzed genes.
(E) GO term analysis of decreased transcripts identified by RNA-Seq of U2OS cells depleted of WDR5 for 24 hours. Ranking and presentation are as in (D).
(F) Violin plot of the 246 gene expression changes that are decreased with PDPK1 depletion and increased with WDR5 depletion.
(G) Gene expression analysis by RT-qPCR to validate PDPK1 depletion RNA-Seq results. U2OS PDPK1-FKBP(F36V)- 2xHA cells were treated for 24 hours with 500 nM dTAG47 or DMSO vehicle control, RNA collected, reverse transcribed, and analyzed by qPCR. Signal is normalized to *GAPDH*. Error bars represent standard deviation, *n=3* independent biological replicates. *** $p<0.001$, ** $p<0.01$, * $p<0.05$ by unpaired two-tailed *t*-test.
(H) Gene expression analysis by RT-qPCR to validate WDR5 depletion RNA-Seq results. U2OS WDR5-FKBP(F36V)- 2xHA cells were treated for 24 hours with 500 nM dTAG47 or DMSO vehicle control, RNA collected, reverse transcribed, and analyzed by qPCR. Signal is normalized to *RPL14*. Error bars represent standard deviation, *n=3* independent biological replicates. *** $p<0.001$, ** $p<0.01$, * $p<0.05$ by unpaired two-tailed *t*-test.

To ask if any of these reciprocal gene expression changes are due to disruption of the WDR5–PDPK1 interaction, I introduced the R3A mutation into endogenous *PDPK1* loci in HEK293 cells (**Figures 5-7 A–B**). Unfortunately, mutation of the N-terminus of endogenous PDPK1 is accompanied by a decrease in PDPK1 expression (**Figure 5-7A**), preventing comparison of the R3A and wild-type (WT) parental cell lines. I therefore engineered R3A PDPK1 mutant cells with empty vector, or vectors overexpressing WT PDPK1 or the R3A PDPK1 mutant (**Figure 5-8 A**), and performed RNA-Seq. Compared to the WT PDPK1 reconstitution, I identified 429 significantly-changed transcripts for vector cells and 136 significantly-changed transcripts for R3A PDPK1 cells (**Figures 5-7 C–D**), 110 of which overlap (**Figure 5-8 B**). All 110 genes are increased in expression with the R3A mutant. These transcripts represent genes that are consistently induced by disruption of the PDPK1–WDR5 interaction both with low (vector) or high (R3A) mutant PDPK1 expression. GO analysis on these 110 genes again shows enrichment for cell cycle and mitotic categories (**Figure 5-8 C**), driven in large part by the same genes reciprocally altered by WDR5 and PDPK1 depletion (see below).

Degradation of WDR5 and PDPK1 leads to changes in cell cycle distribution that could produce changes in cell cycle gene expression (**Figure 5-7 E–G**). To separate cause from effect, I arrested cells in G1 with Palbociclib CDK4/6 inhibitor [177], or G2 with RO-3306 CDK1 inhibitor [178] (**Figure 5-7 H**), and examined the impact of WDR5 degradation on the expression of a set of G2/M-induced genes. Here, I observed transcript levels from the G2/M genes are unaffected by WDR5 depletion in G1-arrested cells, but are induced by WDR5 depletion in the G2 arrested state (**Figure 5-7 I**). I also used nuclear run-on to ask if transcription of G2 genes is induced six hours after dTAG47 addition; a timepoint at which most WDR5 is degraded (**Figure 5-8 D**), but there is no impact on cell cycle distribution (**Figure 5-8 E**). By nuclear run-on I find that transcription of seven representative G2 genes is induced by WDR5 degradation (**Figure 5-8 F**), and that this induction is gene-selective, as ribosome protein genes *RPL35* and *RPS24* show the expected decrease in transcription [82]. Together, these data argue that WDR5-

dependent changes in G2/M gene expression drive changes in cell cycle distribution, and not vice-versa.

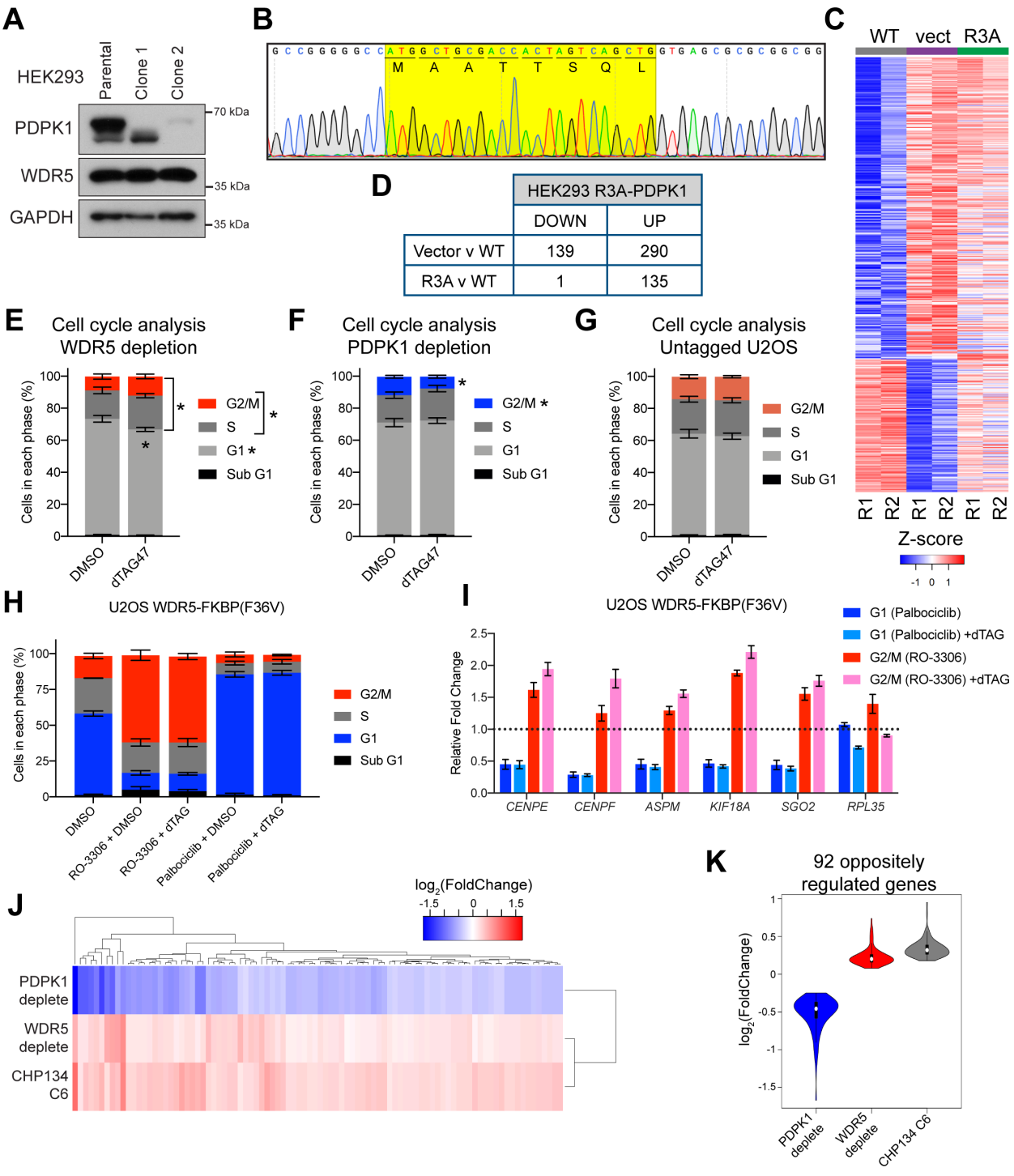

Figure 5-7: Disrupting the PDPK1–WDR5 interaction causes increased gene expression of cell cycle genes

(A) HEK293 cells were engineered with CRISPR/Cas9 and a single stranded template to express only the R3A mutant of PDPK1. IB analysis of two clones compared to unedited cells is shown, demonstrating a lower level of expression. Clone 2 was taken forward for retroviral add-back of PDPK1 variants and analysis by RNA-Seq.

(B) Chromatogram of Sanger sequencing of genomic DNA from Clone 2 in (A). Yellow highlights

the sequence of the first coding intron of PDPK1 and demonstrates efficient integration of the R3A mutation. DNA sequence is at the top, and black letters below indicate the protein sequence.
(C) Heatmap displaying z-transformed gene expression measured by RNA-Seq from the R3A-engineered HEK293 cells. The 429 significantly changed (FDR < 0.05) genes are compared for WT PDPK1 overexpression, low R3A PDPK1 expression (vector), and R3A PDPK1 overexpression in two replicates.
(D) Results of RNA-Seq in HEK293 cells to assess the consequences of the PDPK1 R3A mutant. Table shows the number of transcripts significantly (FDR < 0.05) altered with low (vector) and high R3A PDPK1 expression, compared high WT PDPK1 expression. *n=2* biological replicates for each condition.
(E) Distribution of cell cycle phases as determined by flow cytometry for WDR5-FKBP(F36V)-2xHA U2OS cells treated for 24 hours with 500 nM dTAG47or DMSO vehicle control. Data are presented as mean and error bars are SEM; * $p < 0.05$ by unpaired two-tailed *t*-test. *n=4* biological replicates.
(F) Distribution of cell cycle phases as determined by flow cytometry for PDPK1-FKBP(F36V)-2xHA U2OS cells treated for 24 hours with 500 nM dTAG47 or DMSO vehicle control. Data are presented as mean and error bars are SEM; * $p = 0.016$ by unpaired two-tailed *t*-test. *n=4* biological replicates.
(G) Distribution of cell cycle phases as determined by flow cytometry for untagged U2OS cells treated with 500 nM dTAG47 or DMSO vehicle control for 24 hours. Data are presented as mean and error bars are SEM; *n=3* biological replicates. No significance by unpaired two-tailed *t*-test.
(H) Distribution of cell cycle phases as determined by flow cytometry for WDR5-FKBP(F36V)-2xHA U2OS cells treated for 20 hours with DMSO vehicle control, 1 μM Palbociclib (CDK2/4 inhibitor), 10 μM RO-3306 (CDK1 inhibitor), and 500 nM dTAG47 as indicated. Data are represented as mean ± SEM. *n=3* biological replicates, except for Palbociclib samples where *n=2*.
(I) Gene expression changes are specific to cells in G2/M cell cycle phase. Gene expression analysis by RT-qPCR in U2OS WDR5-FKBP(F36V)-2xHA cells treated for 20 hours with DMSO vehicle control, 1 μM Palbociclib CDK2/4 inhibitor for G1 enrichment, 10 μM RO-3306 CDK1 inhibitor for G2/M enrichment, and 500 nM dTAG47 as indicated. Signal is normalized to *GAPDH*. Data are represented as mean ± SEM; *n=3* biological replicates.
(J) Hierarchical clustering of $\log_2$(fold change) in gene expression over the 92 genes oppositely regulated in the U2OS data and those increased by 24-hour treatment of CHP134 cells with 5 μM C6 (GEO accession GSE136451).
(K) Violin plots compare the distribution of fold change values for the oppositely regulated genes shown in (J).

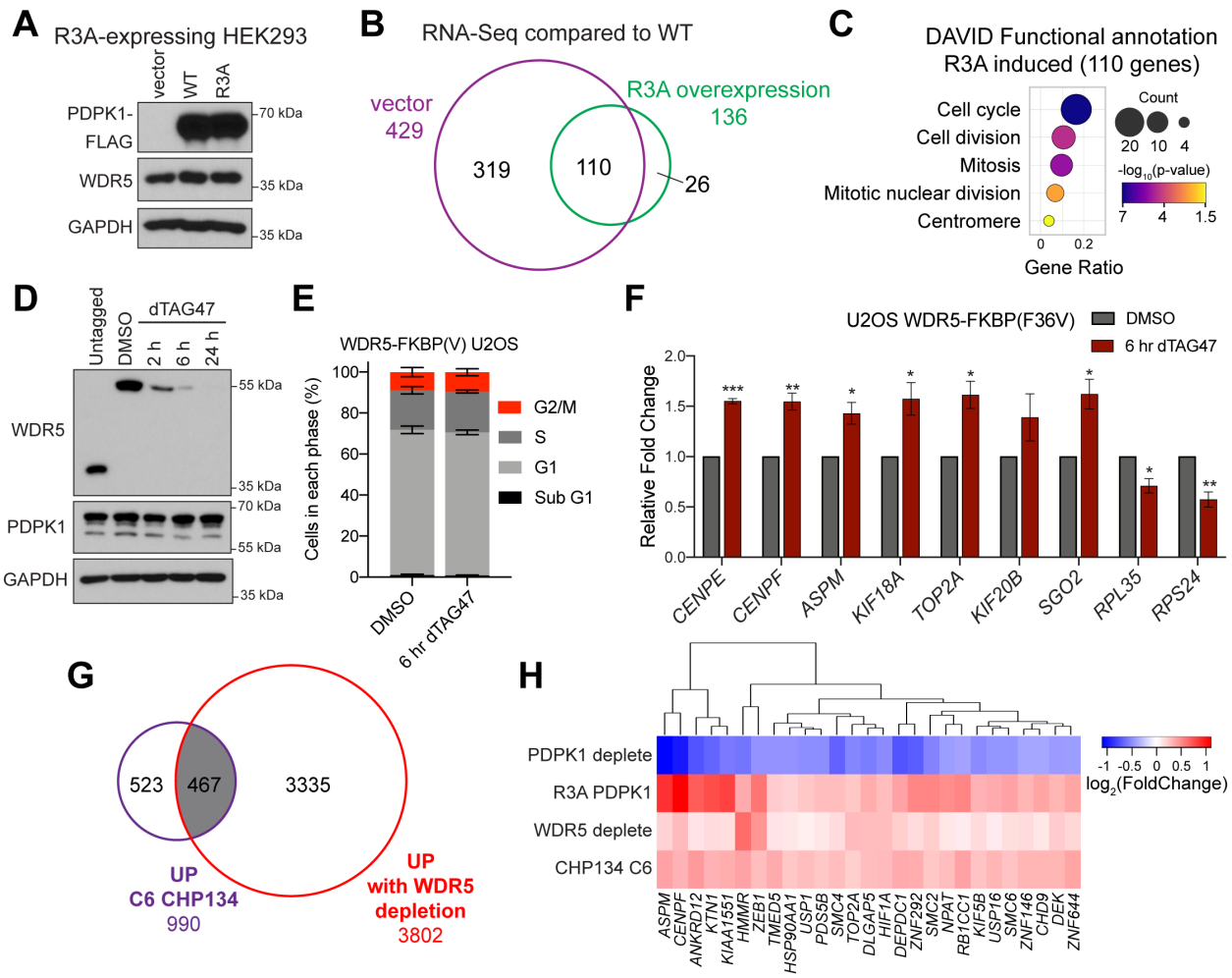

Figure 5-8: Disrupting the PDPK1–WDR5 interaction induces transcription of cell cycle genes

(A) IB of lysates from HEK293 cells expressing the PDPK1 R3A mutant and transduced with vector control, WT, and R3A PDPK1.

(B) Venn diagram of RNA-Seq, comparing low-expressing (vector) and high-expressing R3A PDPK1, normalized to WT PDPK1-expressing cells. All 110 transcripts common to both samples are increased. *n=2* biological replicates for each condition.

(C) GO analysis on the 110 overlapping genes performed using DAVID Bioinformatic Resource [184, 185]; the color indicates the Fisher Exact *p*-value; the dot size indicates the number of genes in that category; the x axis represents the Gene Ratio, the ratio of genes in the category to total analyzed genes.

(D) IB of WDR5 depletion time course with 500 nM dTAG47 in U2OS cells expressing WDR5-FKBP(F36V)-2xHA and compared to untagged cells.

(E) Distribution of cell cycle phases as determined by flow cytometry for WDR5-FKBP(F36V)-2xHA U2OS cells treated for 6 hours with 500 nM dTAG47 or DMSO vehicle control. Data are represented as mean ± SEM; no significance between treatments by unpaired two-tailed *t*-test. *n=3* biological replicates.

(F) Nuclear run-on analysis of nascent transcripts from cells treated with DMSO control or 500 nM dTAG47 for six hours. Signal is normalized to nascent *ACTB* transcripts. Data are represented as mean ± SEM; *n=3* independent biological replicates. *** $p<0.001$, ** $p<0.01$, * $p<0.05$ by unpaired two-tailed *t*-test.

(G) Venn diagram showing the overlap between gene expression changes that are increased

with 24 hour WDR5 depletion in U2OS cells and increased with 24 hour C6 treatment in CHP134 cells [82].
(H) Hierarchical clustering of log_2 (fold change) in gene expression for genes significantly decreased for U2OS PDPK1-FKBP(F36V)-2xHA, and increased for HEK293 R3A PDPK1, U2OS WDR5-FKBP(F36V)-2xHA, and CHP134 24 hour 5 μM C6.

Finally, I asked whether dysregulation of genes controlled by the WDR5–PDPK1 interaction could explain any of aspects of the transcriptional response to WIN site inhibitor. Remarkably, we see that almost half (467) of the genes induced by C6 in CHP134 cells [82] are induced by WDR5 degradation in U2OS cells, despite the different cell lines (**Figure 5-8 G**). Ninety-two of these common genes (**Table 5-1**) show reduced expression in response to PDPK1 depletion (**Figures 5-7 J and 5-7 K**), and 27 are also induced by the R3A mutation in PDPK1 (**Figure 5-8 H**). Many of these 27 genes are connected to the cell cycle and specifically to mitosis, including the mitotic spindle component ASPM, the centromere component CENPF, the segregation-critical topoisomerase TOP2A, and the condensin component SMC2. This analysis reinforces the concept that WDR5 and PDPK1 together control the expression of G2/M connected genes, and demonstrates that part of the response of cells to WIN site inhibitor C6 is due to disruption of the WDR5–PDPK1 interaction.

Table 5-1: Ninety-two oppositely regulated genes
Five high-coverage, representative enriched GO categories are presented; genes present in each category are marked. These genes are from Figures 5-7J and 5-7K: decreased expression with loss of PDPK1, increased expression with loss of WDR5, and increased expression with blockade of the WIN site.

Gene	Regulation of macromolecule metabolic process	Organelle organization	Cell cycle	Mitotic cell cycle	Chromosome segregation
ARL15					
AKAP9	x	x	x	x	
ANKRD12					
ARHGAP5					
ARL6IP1	x	x			
ASF1A	x	x			
ASPM		x	x		
ATP8A1					
BCLAF1	x				
CAPZA1		x			
CCDC88A		x			
CENPE	x	x	x	x	x
CENPF	x	x	x	x	x
CHD9		x			
CYCS	x	x			
DBF4	x		x	x	
DDR2	x				
DEK	x	x			
DEPDC1					
DLGAP5	x	x	x	x	x
DST		x			
ECT2	x		x	x	
EHBP1		x			
EIF4G2	x		x		

Gene	Regulation of macromolecule metabolic process	Organelle organization	Cell cycle	Mitotic cell cycle	Chromosome segregation
FMNL2		x			
FSD1L					
GABPA	x	x			
GLS					
GPBP1	x				
HIF1A	x				
HLTF	x	x			
HMMR					
HSP90AA1	x	x	x	x	
KIAA0586		x			
KIAA1551	x				
KIAA1586					
KIF20B			x		
KIF5B		x			
KITLG	x				
KTN1					
LCORL	x				
LMO3	x				
LPHN3					
MAPK6	x		x		
MEIS1	x				
MMP16					
NCAPG		x	x	x	x
NDC80		x	x	x	x
NIPBL	x	x	x	x	x
NPAT	x		x	x	
ODC1	x				

Gene	Regulation of macromolecule metabolic process	Organelle organization	Cell cycle	Mitotic cell cycle	Chromosome segregation
PAPOLA	x				
PCDH9					
PCM1		x	x	x	
PDS5B		x	x	x	x
PGRMC1					
PHIP	x	x			
PHTF2					
PIK3R3	x				
PSAT1					
PTPLB					
RAD21	x	x	x		x
RAP2A	x	x			
RB1CC1	x	x	x		
RND3		x	x		
SACS					
SCFD1		x			
SEC63					
SEMA3D					
SENP6					
SEPT7		x	x		
SGOL2		x	x	x	x
SHOC2	x				
SMARCA5	x	x			
SMC2		x	x	x	X
SMC4		x	x	x	X
SMC6		x			
STAG2		x	x		x

Gene	Regulation of macromolecule metabolic process	Organelle organization	Cell cycle	Mitotic cell cycle	Chromosome segregation
TBC1D4					
TMED5		x			
TOP2A	x	x	x	x	x
TTK	x	x	x	x	x
UHRF1BP1L					
USP1	x				
USP16	x	x	x	x	
ZEB1	x				
ZHX1	x				
ZNF146	x				
ZNF292	x				
ZNF644	x				
ZNF654	x				
ZNF92	x				

WDR5 binds chromatin at cell cycle genes

To investigate if the cell cycle genes that are induced upon WDR5 depletion are bound by WDR5, I performed ChIP-qPCR experiments. Although the WDR5 peaks identified by ChIP-Seq using a WDR5-specific antibody do not include these genes [39, 62, 82], I reasoned that using the HA epitope might enable more sensitive detection of WDR5 chromatin binding. Indeed, based on percent input, the signal obtained for WDR5 using the HA epitope was five-fold higher than the signal obtained with the anti-WDR5 antibody (~1% input at *SNHG15* with anti-WDR5, and ~5% input with anti-HA) (**Figure 5-9**). Gene specific primers for qPCR were designed to be promoter-proximal and overlapping with detected ChIP-seq peaks for MYC. Analysis by ChIP-qPCR with these gene specific primers for eleven of the genes induced upon WDR5 depletion revealed low levels of WDR5 binding to these loci (**Figure 5-9**). IgG control as well as 24 hour dTAG treatment of cells prior to chromatin collection showed that this signal is specific for WDR5-HA. As a control, the *SETD3* locus has little to no signal for WDR5-HA. I also analyzed three other loci where WDR5 binding is detected at low levels in some ChIP-Seq datasets (*KCNH4*, *GIGYF1*, *HDAC2*) and these loci have similar levels of signal as the cell cycle loci. Together these results demonstrate that the genes that are induced upon WDR5 depletion have low but detectable signal for WDR5 chromatin binding.

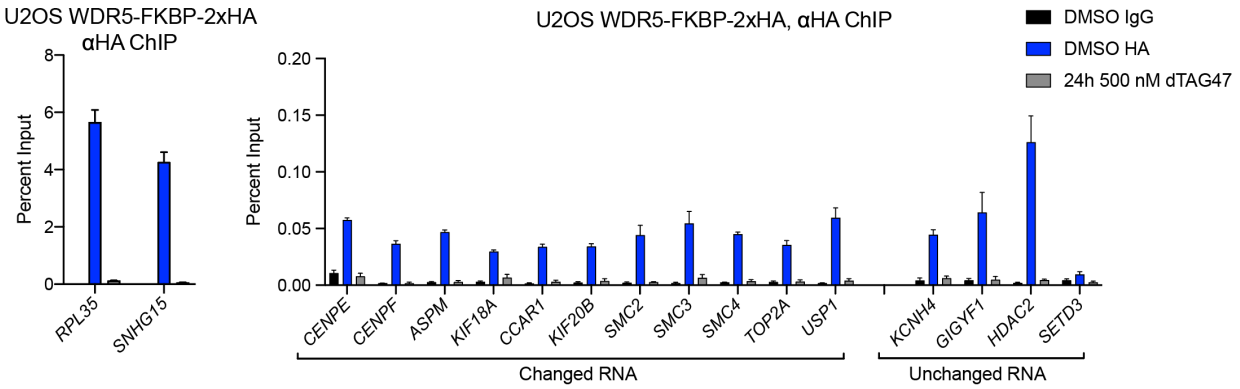

Figure 5-9: WDR5 binds chromatin at cell cycle genes
ChIP-qPCR analysis of WDR5 chromatin binding measured in U2OS WDR5-FKBP(F36V)-2xHA cells using anti-HA antibody. ChIP was performed with pre-immune rabbit IgG or anti-HA antibody in cells treated for 24 hours with DMSO or 500 nM dTAG47. Graphs are data from the same experiment, but shown separately to accommodate the y-axis scale. Graph on the left shows two high-intensity WDR5-bound loci; graph on the right shows loci from eleven genes induced upon WDR5 depletion (Changed RNA), and four control loci (Unchanged RNA). *n=3* biological replicates.

Discussion

By using engineered dTAG system cell lines and R3A mutant cells, I find that disrupting the PDPK1-WDR5 interaction induces the expression of cell cycle genes. Disrupting this interaction does not affect the nuclear shuttling capability of PDPK1 or the main marks of active PI3K/AKT signaling, indicating that WDR5 does not influence these recognized functions of PDPK1. Instead, loss of interaction with WDR5 activates transcription of G2/M genes. And many of the same genes that are increased in expression with loss of WDR5 are decreased in expression with loss of PDPK1, indicating opposing roles for these two pro-cancer proteins. These results are only a preliminary assessment of the cellular function of the PDPK1–WDR5 interaction, but they establish a link to cell cycle regulatory functions that should be further interrogated.

Although the nuclear functions of PDPK1 are not well understood, PDPK1 is known to play an important role in advancing the G2/M phase of the cell cycle [269], and can influence the transcription of G2/M-expressed genes via regulation of FoxM1 [270]. The data presented in this chapter suggest that WDR5 impacts this aspect of PDPK1 function. What is interesting about this idea, however, is that WDR5 inhibits the ability of PDPK1 to activate these genes. Given the role of WDR5 in the control of protein synthesis genes, one possibility is that WDR5 links nuclear functions of PDPK1 to protein synthesis capacity, restricting PDPK1 activity until a sufficient level of ribosome production is achieved, or new ribosome synthesis is completed, during G2. By extension, this notion predicts that WIN site inhibitors could act, at least in part, by allowing cells to enter mitosis without an adequate ribosome inventory. Further experimentation will be needed to determine when and how the WDR5–PDPK1 interaction controls events during G2/M, and how this contributes to the response of cancer cells to WIN site inhibitors.

Alignment of PDPK1 orthologs across various species finds that conservation of the N-terminal WIN motif is limited: mouse, chimp, and fish PDPK1 proteins all contain N-terminal WIN

motifs, but lower-order species do not (**Figure 5-10**). Although the WDR5 interaction capability is not highly conserved, the function of PDPK1 in regulating mitotic integrity is conserved in yeast. Specifically the *Schizosaccharomyces pombe* proteins Ppk21 and Ksg1 are PDPK1 orthologs that have important mitotic functions. Ppk21 localizes to the mitotic spindle and its deletion causes mitotic defects [271]. Ksg1 temperature-sensitive mutants result in cell cycle checkpoint defects where mutant cells arrest in G2 instead of in G1 [272]. One possibility is that as PDPK1 evolved it retained cell cycle regulatory function and acquired an N-terminal WIN motif and the ability to use WDR5 as a regulatory platform for its cell cycle functions. Perhaps in higher order species, the PDPK1–WDR5 interaction functions as a transcriptional checkpoint for the appropriate expression of G2/M genes. Nuclear run-on experiments show that increased expression of G2/M genes is an early response to WDR5 disruption and occurs before changes in cell cycle distribution (**Figure 5-8 F**). Perhaps the PDPK1–WDR5 interaction, promoted by PDPK1 nuclear localization in response to growth factor signaling, initiates this transcriptional checkpoint and helps coordinate growth factor signals and cell growth responses. More experiments are needed to explore this potential regulation, but the conserved function of PDPK1 orthologs in cell cycle integrity is intriguing.

Contributions

The experiments and data presented in this chapter were facilitated by the assistance of stellar collaborators. Dr. Jing Wang and Dr. Qi Liu assisted with the analysis and presentation of RNA-Seq datasets. The nuclear run-on protocol was adapted from [179] and optimized by Dr. April M. Weissmiller and Chase M. Woodley, and performed by Alissa Guarnaccia.

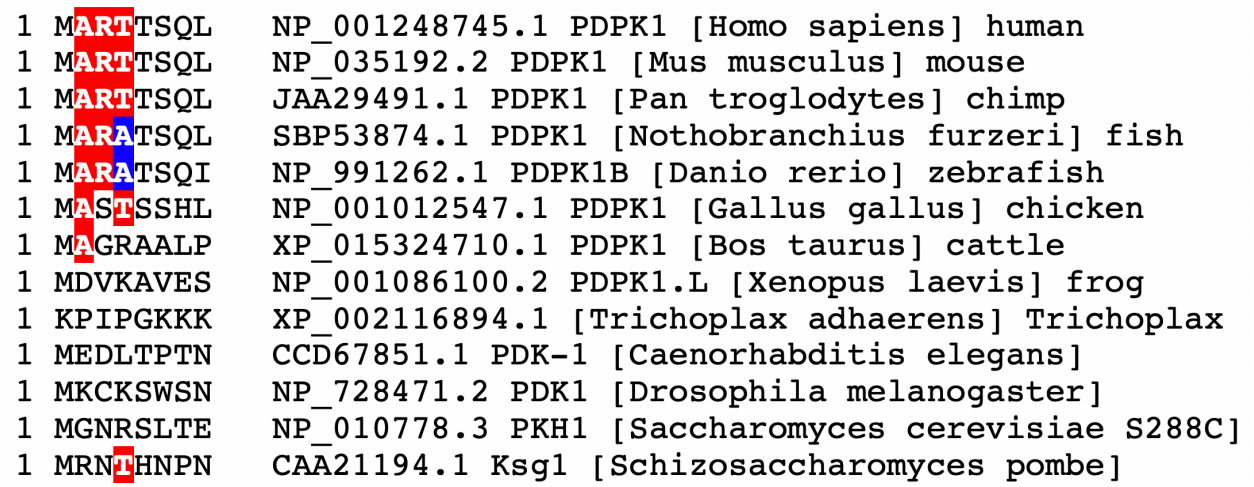

Figure 5-10: Conservation of N-terminal WIN motifs
Alignment of the first eight amino acids from the coding sequences of PDPK1 proteins from the indicated species. Residues matching the human PDPK1 WIN motif are in red; residues consistent with an alternate consensus WIN motif are in blue.

Interaction of WDR5 with the constitutively active kinase PDPK1 raises the possibility that WDR5 functions are modulated by PTMs. High throughput mass spectrometry-based analyses have identified fifteen PTMs on WDR5, several of which are phosphorylation [273]. Five of these modifications occur within the N-terminal tail, two within the WIN site, and two within the WBM site (**Table 5-2**). Phosphorylation, ubiquitylation, SUMOylation, acetylation, or even methylation at or near WDR5 binding sites would likely obstruct certain interactions and could promote others. If PDPK1 phosphorylates WDR5, this could influence WDR5 interaction capabilities and localization. Targeted experiments are needed to address if WDR5 is a substrate for PDPK1 phosphorylation.

Finally, the action of WIN site inhibitors in disrupting the PDPK1–WDR5 interaction might contribute to their anti-cancer action. My RNA-Seq analyses show that disrupting the PDPK1–WDR5 interaction does not result in decreased RPG expression; instead I found increased G2/M cell cycle gene expression. Thus the PDPK1–WDR5 interaction operates separate from the impact of WIN site inhibitors on biomass accumulation and seems to be a transcriptionally repressive function for WDR5 at these specific cell cycle genes. Disrupting the PDPK1–WDR5 interaction could contribute to the cellular sensitivity to WIN site inhibitors by activating cellular checkpoints leading to cell cycle arrest or cell death, at least in cancer cells where those checkpoints are intact. Ultimately, we need to know more and further investigate how the PDPK1–WDR5 interaction contributes to the cellular response to WIN site inhibitors. A direct comparison of the effects of the R3A mutation and WIN site inhibitor in a sensitive cell line such CHP134 would be useful in teasing out the contribution of this interaction to the cellular response to WIN site inhibitors.

Table 5-2: Detected post-translational modifications on WDR5
Post-translational modifications within WDR5 as detected by low-throughput (LTP) or high-throughput (HTP) methods and reported in PhosphoSitePlus [273]. Colored rows indicate specific locations within the protein: red for the N-terminal tail, blue for near the WIN site, green for near the WBM site.

Residue	Modification	Location	LTP	HTP
K7	Acetylation	N-terminal tail	0	1
T18	Phosphorylation	N-terminal tail	0	3
K27	Acetylation	N-terminal tail	0	1
K27	Ubiquitylation	N-terminal tail	0	5
T29-p	Phosphorylation	N-terminal tail	0	1
K32	Ubiquitylation	Outer surface of blade 7	0	4
K38	Monomethylation	Outer surface of blade 7	0	1
K46	SUMOylation	WIN site; blade 1	0	1
S49	Phosphorylation	WIN site; blade 1	1	0
S54	Phosphorylation	Blade 1	0	1
K112	Acetylation	Blade 2	0	2
K120	Ubiquitylation	Blade 2	0	11
Y131	Phosphorylation	WIN site; blade 3	0	2
K159	Ubiquitylation	Blade 3	0	4
K227	Ubiquitylation	WBM site; blade 5	0	3
Y228	Phosphorylation	WBM site; blade 5	0	3

Chapter VI

Investigating MbIIIb-dependent MYC interacting proteins

Introduction

In studying WDR5 another connected goal of my thesis research is to identify proteins that interact with MYC when it is bound to WDR5. Identifying and understanding this class of proteins has potential to bring insight into the broader molecular context of the MYC–WDR5 interaction and what proteins can tether WDR5 to chromatin. MYC is an oncoprotein transcription factor that is overexpressed in the majority of malignancies and is capable of promoting the expression of thousands of genes [55]. What we do not completely understand is the molecular details of how MYC selects its target genes. In pursuing this question, the Tansey laboratory found that MYC directly interacts with WDR5 at chromatin and that the tumorigenic potential of MYC depends on its ability to interact with WDR5 [79]. WDR5 is a cellular multitasker, an essential protein involved with histone modifying complexes, transcriptional regulators, mitotic machinery, and more [1]. Both MYC and WDR5 are highly networked proteins, each interacting with hundreds of other proteins [1, 274]. Additionally we know that small molecule inhibition of WDR5 prevents its chromatin binding, and—for MYC and WDR5 co-bound genes—also prevents MYC chromatin binding [39, 62, 82]. This functional connection presents a possible therapeutic opportunity for targeting MYC in cancer through WDR5. The studies presented in this chapter are centered on MYC and aim to tease out what other proteins, besides WDR5, rely on the WDR5 binding motif (WBM) in MYC.

MYC binds directly to WDR5 via a WBM peptide motif located within one of the highly conserved central portion MYC boxes, MbIIIb (**Figure 1-8**). Structural insights from the cocrystal structure of WDR5 in complex with the WBM MYC peptide enabled the creation of structure-guided mutations in MYC that selectively disrupt interaction with WDR5 [79]. The WBM mutant

form of MYC swaps three hydrophobic residues for acidic residues (EEIDVV to EEEDEE) (**Figure 6-1 A**) and selectively disrupts MbIIIb-dependent interaction with WDR5 but not other MYC interactions such as HCF-1 via MbIV (**Figure 6-1 B**). Although the WBM MYC mutant retains the ability to bind MAX and to interact with naked DNA, it is deficient in binding to target genes and is defective for tumorigenesis [62, 79]. In this chapter I describe experiments that begin to identify and dissect MYC interactions that rely on MbIIIb. In the process, I discover an additional protein complex that interacts with MYC via MbIIIb and identify PDPK1 as a WDR5-mediated MYC-interacting protein. These surprising insights into MYC biology open up exciting avenues for future research on MbIIIb.

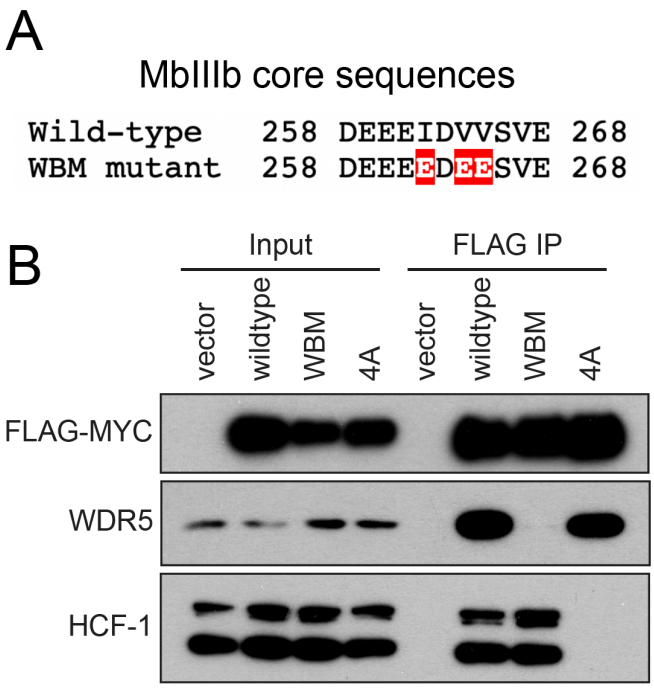

Figure 6-1: Mutation of MbIIIb in MYC disrupts interaction with WDR5
(A) Amino acid sequence of the core of MbIIIb, comparing wild-type (top) and the WBM mutant form (bottom) which is generated by mutating three key hydrophobic residues to glutamic acid. **(B)** Co-IP experiment using FLAG-Gal4-HA-MYC central portion (151-319) comparing Wild-type, WBM mutant, and an additional mutation, 4A, that reduces MbIV-dependent interactions. WDR5 interaction with MYC is affected by the WBM mutant but not the 4A mutant. HCF-1 binds MYC via MbIV and is affected by the 4A mutant but not by the WBM mutant. Similar results are found with full-length FLAG-tagged MYC protein. Antibody used for HCF-1 is specific for the C-terminal region.

Results

Identification of MbIIIb-dependent MYC interactions

To investigate MYC protein interactions that rely on MbIIIb, I designed a SILAC-based [190, 191] proteomic experiment analyzing MbIIIb-centered fragments. I took a fragment-based approach to focus attention on MbIIIb and to simplify the complicated suite of MYC protein interactions that co-precipitate with full-length MYC. I used FLAG-Gal4-HA-tagged MYC fusions carrying three different MbIIIb-encompassing MYC fragments: 251-319 (C-terminal central portion), 151-275 (N-terminal central portion), and 151-319 (central portion) (**Figure 6-2 A**). I transiently transfected wild-type or WBM mutant fusions into 'heavy' or 'light' HEK293 cells, recovered MYC protein complexes by FLAG co-immunoprecipitation, and analyzed samples by MudPIT LC-MS/MS in collaboration with the Vanderbilt Mass Spectrometry Research Center (**Figure 6-2 B**). Validation of these preps by western blotting confirmed loss of WDR5 interaction with the WBM mutant (**Figure 6-2 C**). I performed a total of five replicates: triplicate with 151-275, once with 251-319, and once with 151-319. For each replicate more than 1,400 proteins were identified and quantified with high confidence, and overall the number of identified proteins correlated with the length of the analyzed fragment (**Figure 6-2 D**). Enforcing a two-fold cutoff, I found that the WBM mutation induces both decreases and increases in MYC-associated proteins. Details of the proteins changed beyond two-fold for all five experiments are presented in **Appendix A**. Although the number of changed proteins varies considerably between replicates (**Figure 6-2 D**), WDR5 is consistently a top enriched protein, displaying about five-fold enrichment in all experiments. Therefore WDR5 is a consistent internal control, and these experiments identify proteins other than WDR5 that are impacted by the WBM mutant.

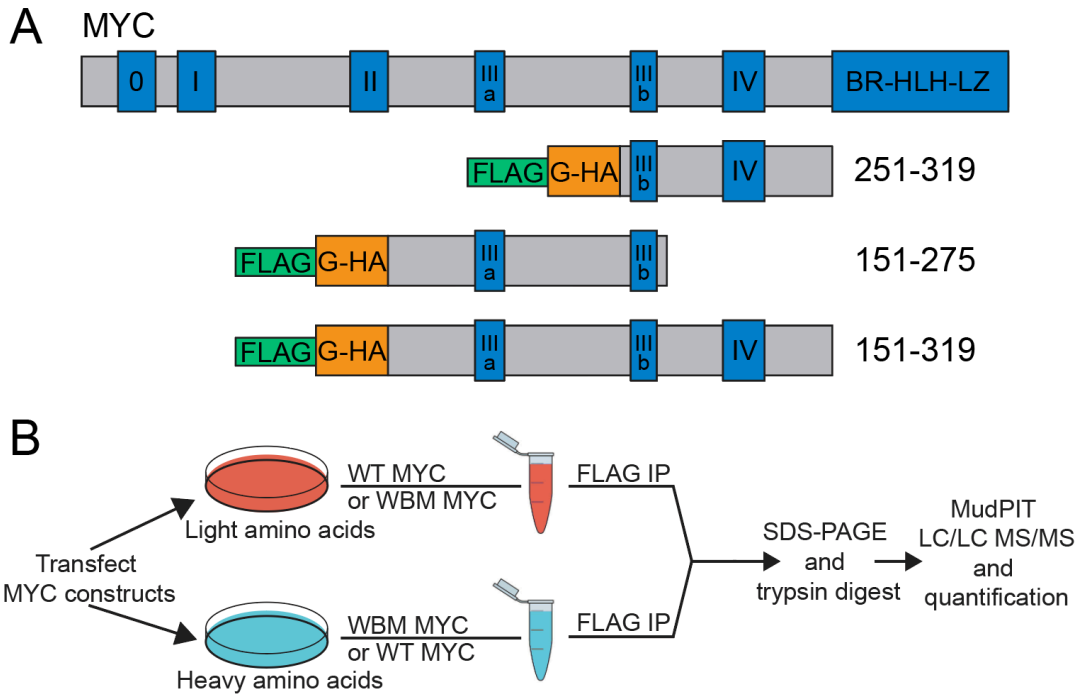

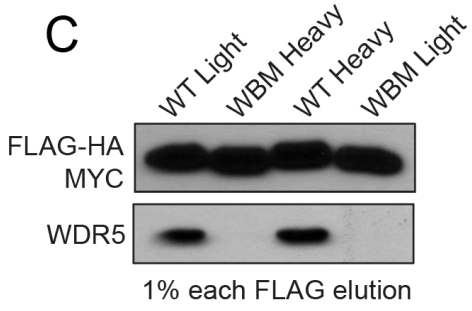

D

Experiment	Total proteins identified	Decreased with WBM mutation	Increased with WBM mutation
151-319	2100	8	5
251-319	1319	21	78
151-275 R1	1673	52	2
151-275 R2	1460	13	38
151-275 R3	1531	4	222

Figure 6-2: MYC-centered proteomic experiments focus on MbIIIb
(A) Schematic of MYC protein (top) with the three different MbIIIb-centered fragments (below) used for proteomic experiments. Each fragment used in SILAC was an N-terminal FLAG-Gal4-HA fusion (FLAG-G-HA). The FLAG epitope was used for protein recovery. Experiment was performed once for 251-319, once for 151-319, and three times for 151-275. **(B)** Schematic of experimental setup for SILAC experiment comparing WT and WBM MYC fragments described in (A). **(C)** Example of western blot validation of FLAG-eluted MYC samples showing even recovery and specificity for WDR5 interaction. Notably, WBM MYC consistently runs slightly faster on the gel. **(D)** Summary of five experiments performed using the MYC constructs depicted in (A). Numbers of proteins decreased and increased reflect a two-fold cutoff. See Appendix A for lists of proteins changed past two-fold cutoffs.

Validation of MbIIIb-dependent MYC interaction partners

Because the number of proteins changed beyond two-fold varies between SILAC replicates, I focused my attention on the proteins that were changed in at least two experiments. This filtering step narrowed the list to 28 increased proteins (**Table 6-1**) and six decreased proteins (**Figure 6-3 A**). The increased proteins are a miscellaneous group, and none of these proteins are present in more than three of the five experiments. I did not investigate these increased proteins further and instead focused on the decreased proteins. The list of decreased proteins is much smaller, includes WDR5, and four of the six proteins are present in three or more replicates. Two things are notable among the six decreased proteins. First, three of the decreased proteins—WDR11, FAM91A1 (F91A1), and NJMU—are known to physically interact and form a complex called the WDR11 complex [275, 276]. Second, PDPK1, which directly binds WDR5 at the WIN site (Chapter IV), is decreased with the WBM mutation, indicating that perhaps PDPK1 is capable of interacting with MYC through WDR5. Given these interesting connections, I next validated these decreased proteins.

Table 6-1: Proteins increased in association with MYC upon WBM mutation
Table summarizing the 28 proteins that were increased in association with MYC with the WBM mutation in at least two of the five experiments.

Protein	Number of experiments	Average Ratio WBM/WT	Uniprot ID	Full protein name
SPTB2_HUMAN	n=3	4.47	Q01082	Spectrin beta chain, brain 1
DREB_HUMAN	n=3	4.01	Q16643	Drebrin
COR1C_HUMAN	n=3	3.98	Q9ULV4	Coronin-1C
EFHD2_HUMAN	n=3	3.34	Q96C19	EF-hand domain-containing protein D2
LIMA1_HUMAN	n=3	3.32	Q9UHB6	LIM domain and actin-binding protein 1
ACTA_HUMAN	n=2	2.87	P62736	Actin
MYH9_HUMAN	n=3	2.83	P35579	Myosin-9
MYH14_HUMAN	n=3	2.78	Q7Z406	Myosin-14
ALDOA_HUMAN	n=3	2.77	P04075	Fructose-bisphosphate aldolase A
ACTN4_HUMAN	n=3	2.73	O43707	Alpha-actinin-4
SPTN2_HUMAN	n=3	2.72	O15020	Spectrin beta chain, non-erythrocytic 2
CALM_HUMAN	n=2	2.63	P62158	Calmodulin
MY18A_HUMAN	n=2	2.46	Q92614	Unconventional myosin-XVIIIa
MYH10_HUMAN	n=3	2.45	P35580	Myosin-10
K0020_HUMAN	n=2	2.44	Q15397	Pumilio domain-containing protein KIAA0020
TMOD3_HUMAN	n=2	2.44	Q9NYL9	Tropomodulin-3
EZRI_HUMAN	n=3	2.38	P15311	Ezrin
NSA2_HUMAN	n=2	2.36	O95478	Ribosome biogenesis protein NSA2 homolog
CXA1_HUMAN	n=2	2.34	P17302	Gap junction alpha-1 protein
LMO7_HUMAN	n=2	2.34	Q8WWI1	LIM domain only protein 7
CSKP_HUMAN	n=2	2.33	O14936	Peripheral plasma membrane protein CASK
LRRF2_HUMAN	n=2	2.33	Q9Y608	Leucine-rich repeat flightless-interacting protein 2
RAB35_HUMAN	n=2	2.32	Q15286	Ras-related protein Rab-35

Protein	Number of experiments	Average Ratio WBM/WT	Uniprot ID	Full protein name
BCLF1_HUMAN	n=2	2.32	Q9NYF8	Bcl-2-associated transcription factor 1
MPRIP_HUMAN	n=2	2.29	Q6WCQ1	Myosin phosphatase Rho-interacting protein
ACINU_HUMAN	n=3	2.24	Q9UKV3	Apoptotic chromatin condensation inducer in the nucleus
CLH1_HUMAN	n=2	2.24	Q00610	Clathrin heavy chain 1
CYTSA_HUMAN	n=2	2.15	Q69YQ0	Cytospin-A

A

Protein	Number of experiments	Average Ratio WBM/WT	Uniprot ID	Full protein name
WDR5_HUMAN	n=5	0.21	P61964	WD repeat-containing protein 5
WDR11_HUMAN	n=5	0.26	Q9BZH6	WD repeat-containing protein 11
F91A1_HUMAN	n=5	0.26	Q658Y4	FAM91A1
PDPK1_HUMAN	n=3	0.27	O15530	3-phosphoinositide-dependent protein kinase 1
NJMU_HUMAN	n=2	0.25	Q9HAS0	Protein NJMU-R1
PERQ2_HUMAN	n=2	0.25	Q6Y7W6	GRB10-interacting GYF protein 2

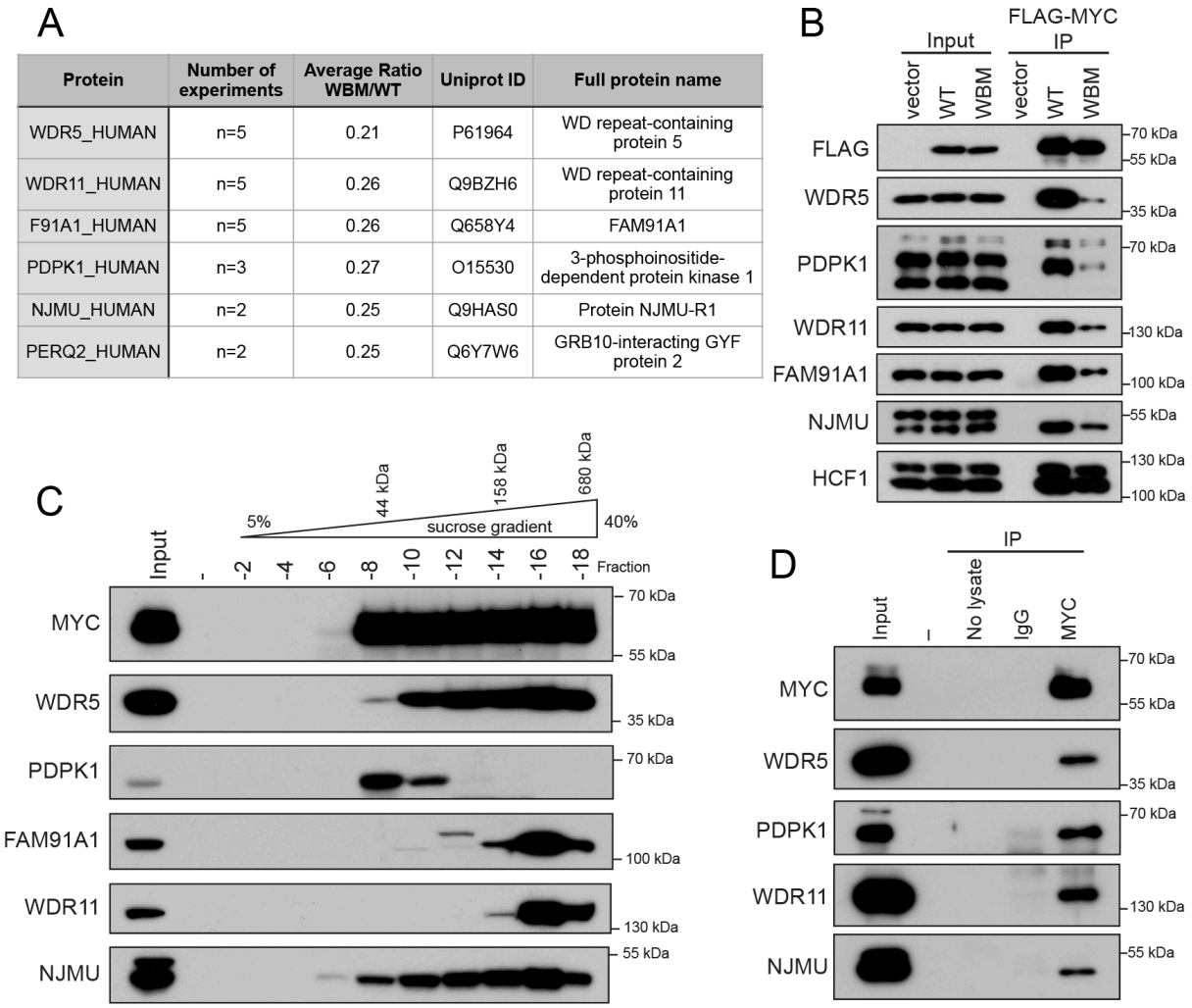

Figure 6-3: Validation and analysis of WBM-dependent MYC interacting proteins
(A) Table summarizing the six proteins that were decreased in association with MYC with the WBM mutation in at least two of the five experiments. **(B)** FLAG-tagged full-length MYC proteins (WT and the WBM mutant) were transiently expressed in HEK293 cells, lysates prepared, and subject to IP with anti-FLAG beads. Immune complexes were probed for FLAG-MYC or candidate proteins from the SILAC proteomic screen: PDPK1, WDR11, FAM91A1, and NJMU. HCF1 is a control for the WBM mutant. **(C)** Density sedimentation analysis using sucrose gradients. HEK293 lysates were separated on sucrose gradients, fractionated, and probed for for candidates from the SILAC experiment. **(D)** Endogenous MYC was recovered from lysates of HEK293 cells and probed for co-precipitating proteins by IB.

To validate the decreased proteins identified in these SILAC datasets I performed FLAG co-immunoprecipitation experiments using FLAG-tagged full-length MYC. I overexpressed WT or WBM mutant MYC in HEK293 cells and analyzed the recovered proteins by immunoblotting. All proteins probed interact with full-length wild-type MYC (**Figure 6-3 B**). Interaction with MYC is decreased with the WBM mutant for WDR5, PDPK1, WDR11, FAM91A1, and NJMU, but not for the MbIV-interacting protein HCF-1. Unfortunately the antibody for PERQ2 did not give clear signal by western blot and was not analyzed further. I next asked if any of the validated proteins might associate together in a single protein complex with MYC. I analyzed lysates from HEK293 cells by density sedimentation using sucrose gradients and probed for the proteins of interest (**Figure 6-3 C**). Both MYC and WDR5 have broad distributions and occupy most of the fractions. In contrast, the candidate proteins PDPK1, WDR11, and FAM91A1 have more narrow distributions. PDPK1 migrates separate from WDR11 and FAM91A1, and NJMU, an auxiliary subunit for the WDR11 complex [276], has a broader distribution that concentrates with WDR11 and FAM91A1. I conclude that the association of PDPK1 with MYC is separate from the association of WDR11 complex members with MYC.

Next, I analyzed these MYC protein interactions by IP with endogenous proteins. I immunoprecipitated MYC from HEK293 cells using a MYC-specific antibody and found that endogenous MYC recovers endogenous WDR5, PDPK1, WDR11, and NJMU (**Figure 6-3 D**), demonstrating that PDPK1 and the WDR11 complex interact with MYC. Together with the transient co-IP experiments, these results validate the WBM-dependent MYC interactions identified by SILAC proteomics.

The WDR11 complex interacts with MYC

The WDR11 complex is composed of WDR11, FAM91A1, and NJMU [276]. Like WDR5, and as its name suggests, WDR11 is a WD repeat-containing protein composed of at least nine WD repeat domains [277]. I wondered if WDR11 is capable of interacting with MYC separate from and in a parallel manner to WDR5. I analyzed FLAG-WDR5 co-IP samples and was unable

to detect WDR11 complex members associating with WDR5; as controls I probed PDPK1 which interacts with WDR5 at the WIN site, and MYC which interacts with WDR5 at the WBM site (**Figure 6-4 A**). I next analyzed the WDR11 complex by IP of endogenous proteins using WDR11 or FAM91A1 antibodies. Pulldown of one WDR11 complex member recovers the other two complex members as well as MYC, but does not recover detectable WDR5 (**Figure 6-4 B and C**). I also did not detect PDPK1 associating with the WDR11 complex members in these experiments. These results indicate that interaction of MYC with the WDR11 complex is separate from, and perhaps mutually exclusive with, interaction with WDR5.

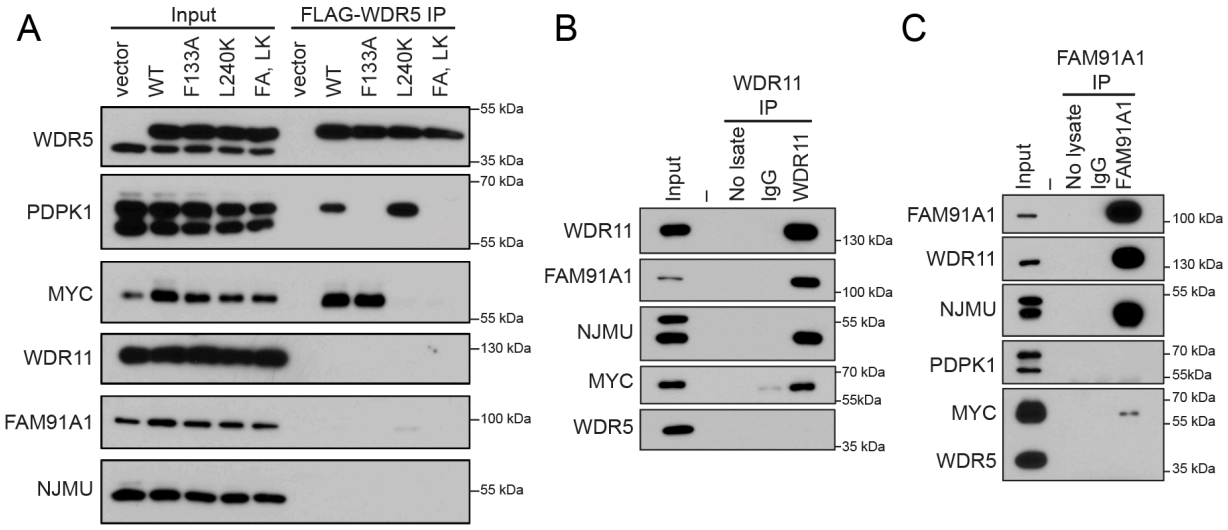

Figure 6-4: The WDR11 complex interacts with MYC and is separate from WDR5
(A) HEK293 cells stably expressing FLAG-tagged WDR5, wild-type or mutants, were lysed and WDR5 complexes recovered by FLAG IP. Candidate WDR5 interaction partners were probed by IB. **(B)** Endogenous WDR11 was recovered from lysates of HEK293 cells and probed for co-precipitating proteins by IB.(C) Endogenous FAM91A1 was recovered from lysates of HEK293 cells and probed for co-precipitating proteins by IB.

PDPK1 interacts with MYC

In the results presented in Chapter IV I established that PDPK1 is a WIN site interacting protein, and here I find that PDPK1 is a MYC-interacting protein. This result is curious because my PDPK1-centered proteomic experiments performed in HEK293 cells did not detect MYC as a PDPK1-interacting protein (**Figure 4-6**). However, because MYC and PDPK1 are similar molecular weights and run at a similar place by gel electrophoresis, it is possible that MYC was excluded along with the predominant PDPK1 band in this proteomic analysis. The identification of PDPK1 as a MYC-interacting protein presents the possibility that WDR5 forms a trimeric complex with MYC at the WBM site and PDPK1 at the WIN site. To examine if WDR5 mediates interaction between PDPK1 and MYC, I performed co-IP experiments with and without WDR5 using cells I engineered to express degradable WDR5. In order to study this interaction in a MYC-driven cancer context and to extend these findings to N-MYC, I used CHP134 neuroblastoma cells expressing WDR5-FKBP(F36V)-2xHA. I treated the cells with DMSO vehicle control or dTAG47 degrader molecule and then immunoprecipitated PDPK1 from lysates using a PDPK1-specific antibody. In this experiment WDR5 interacts with PDPK1 and is efficiently degraded with dTAG47 (**Figure 6-5**). Furthermore, N-MYC only interacts with PDPK1 when WDR5 is present. I conclude that PDPK1 interacts with MYC via WDR5 and that these three proteins are capable of forming a trimeric complex.

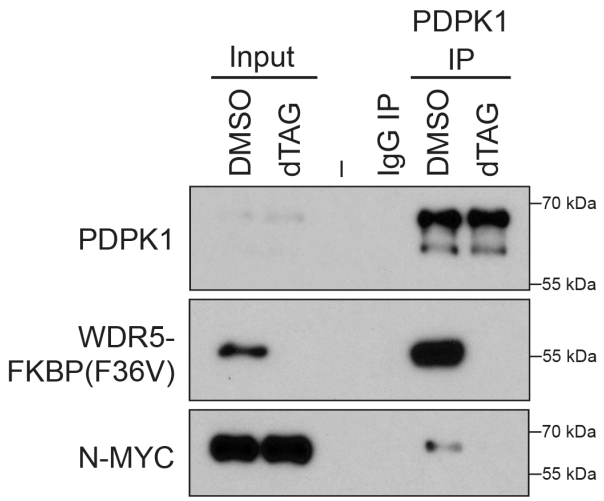

Figure 6-5: PDPK1 depends on WDR5 for interaction with MYC
Endogenous PDPK1 IP from CHP134 cells expressing WDR5-FKBP(F36V)-2xHA. Cells were treated for 24 hours with DMSO vehicle control or 500 nM dTAG47 prior to lysis and IP. Inputs are 10% for PDPK1, 0.1% for WDR5, and 0.2% for N-MYC. *n=2*.

Discussion

In this chapter I describe experiments that interrogate the WBM motif of MbIIIb of MYC. In particular, I focus on the identification and validation of two separate WBM-dependent interactions: PDPK1 and the WDR11 complex. In contrast with one another, the PDPK1 interaction with MYC requires WDR5, and the WDR11 interaction with MYC is separate from WDR5. Seemingly, these interactions with MYC are mutually exclusive. Pinpointing these interactions to MbIIIb of MYC opens up new avenues of research towards understanding the importance of MbIIIb as well as the cellular functions of the WDR11 complex and the WDR5–PDPK1 interaction.

Here I identify WDR11 and its complex members as MYC-interacting proteins. The WDR11 complex is comprised of WDR11, FAM91A1, and NJMU. WDR11 is the most well-studied protein of this trio, and little is known about FAM91A1 and NJMU aside from their association with WDR11. WDR11 is known for being frequently deleted or mutated in a series of developmental disorders that include congenital hypogonadotropic hypogonadism, Kallmann syndrome [277, 278], CHARGE [279], pituitary stalk interruption syndrome [280], and 10q26 deletion syndrome [281, 282]. Patients with these disorders display similar developmental defects including abnormalities in eye and digit formation, delayed puberty, and infertility. *WDR11*-null mice also display a litany of developmental defects—microcephaly, impaired eye development, delayed puberty, infertility, and neuroendocrine and metabolic defects [283]—making it clear that WDR11 is essential for development. In cancer, WDR11 presents as a tumor suppressor [284-286]. Compellingly, overexpression of WDR11 in a mouse model of grade 3 meduloblastoma slows disease progression [286]. MYC is also a crucial developmental regulator and necessary for embryonic development [287, 288], and perhaps interaction with WDR11 regulates MYC activities during development.

WDR11 is a nuclear shuttling protein and has apparent cytosolic and nuclear roles. Treatment of cells with leptomycin B [277, 280, 283] or with hedgehog signaling agonists [283] promotes nuclear accumulation of WDR11. FAM91A1 and NJMU are also probably involved in most if not all functions with WDR11 since the three proteins seem to be consistently in complex with one another and because FAM91A1 is necessary for WDR11 protein stability in cells [275, 276]. In the cytosol, WDR11 localizes to the basal bodies of cilia, is essential for ciliogenesis [283], and plays an important role in vesicular trans Golgi network trafficking [276]. In the nucleus, WDR11 interacts with EMX1 [277, 283], which seems to mediate the transcriptional response to hedgehog signaling [283]. But perhaps MYC is also involved in recognizing nuclear WDR11 and responding in this process. Notably, in meduloblastoma, *MYCN* is an early and likely direct target gene of hedgehog signaling [289], and since WDR11 rapidly responds to hedgehog signaling by nuclear translocation [283], one function of WDR11 could be in regulating the nuclear activity of MYC proteins in response to hedgehog signaling. Another consideration is regarding the anti-tumor effect of the WBM MYC mutation [62, 79]. Because both WDR11 and WDR5 rely on the WBM for interaction with MYC, either one could be partly or fully responsible for disabling MYC-driven tumor formation. Perhaps the WDR11 complex is capable of acting as a cofactor for MYC at chromatin, or influences MYC stability or subnuclear localization. Comparing the effect of inhibiting the MYC–WDR5 interaction with inhibitors to the WBM site of WDR5 could assist in teasing apart the contribution of MYC interactions with WDR5 and with WDR11. Important future questions surrounding the MYC–WDR11 complex interaction involve when and how MYC and WDR11 complex members interact, and what cellular signals and transcriptional networks are affected by this interaction.

In addition to both being WD40 repeat containing proteins, another striking parallel between WDR5 and WDR11 is that they both are known to interact with WBM-containing transcription factors: WDR5 interacts with MYC (WBM: EEIDVV) [79] and WDR11 interacts with EMX1 (WBM: EDIDVT) [277] (**Table 3-2**). Interaction of WDR11 with EMX1 is important for cellular responses to signaling and is disrupted by disease-specific point mutations from

patients with Kallman syndrome including A435T and H690Q [277, 283]. If WDR11 uses this same interaction surface for interaction with WBM motifs of EMX1 and MYC, interaction with MYC should also be affected by these mutations. Testing these WDR11 mutants for interaction with MYC, as well as testing interaction of WDR11 with a WBM mutant form of EMX1, would investigate the potential for direct interaction of WDR11 with the WBM motifs of these transcription factors.

I also identify PDPK1 as a WDR5-dependent MYC-interacting protein and establish the existence of a trimeric MYC–WDR5–PDPK1 complex. But what is the function of such a complex? One possibility is that the MYC–WDR5–PDPK1 complex functions to regulate MYC-driven mitotic gene expression patterns. In particular, N-MYC is known to upregulate G2/M genes [290] including many of the same genes that are increased upon disruption of the WDR5–PDPK1 interaction [171]. Expression of G2/M genes is increased upon overexpression of N-MYC [290], and decreased upon inhibition of N-MYC in CHP134 N-MYC-amplified neuroblastoma cells (unpublished data from Dr. April Weissmiller). Furthermore, many of these genes are bound by N-MYC as measured by ChIP-Seq in CHP134 cells (unpublished data from Dr. April Weissmiller). Perhaps the PDPK1–WDR5 interaction serves to dampen the transcriptional activity of MYC proteins at mitotic target genes, and represents an atypical repressive role for WDR5. Further experiments in CHP134 cells are required to investigate the functional importance of the N-MYC–WDR5–PDPK1 interactions.

Although MbIIIb is a well conserved sequence in the central portion of MYC proteins, until the discovery of the MYC–WDR5 interaction [79] it had no known function. Here I accelerate our understanding of MbIIIb by identifying additional proteins that rely on this sequence. I describe a successful approach for interrogating MYC interactions, and I identify two MYC complexes for future interrogation: interaction with the WDR11 complex and interaction with WDR5–PDPK1. Finally, it is quite possible that these identified proteins are not the full scope of MbIIIb-dependent interactions and other such proteins still lie undiscovered.

Undoubtedly the enigmatic central portion of MYC will provide intriguing research questions and unexpected results for years to come.

Contributions

The experiments and data presented in this chapter were facilitated by the assistance of some stellar collaborators. Dr. Kristie Rose provided assistance with SILAC proteomic experimental design, proteomic data collection, and proteomic data analysis. Salisha Hill provided assistance with proteomic sample preparation and data analysis. Christina Wang performed and assisted with FLAG-WDR5 IPs.

Chapter VII

Discussion and future directions

Conclusions and discussion

WDR5 is a cellular multitasker, an essential cellular protein, and an anti-cancer drug target. Although it is a focus for drug discovery, the extent of the cellular functions of WDR5—and thus the impact of inhibitors against it—is still unknown. WDR5 is best known for its scaffolding role in histone methyltransferase (HMT) complexes. This well-known function leads to assumptions that HMT regulation is the predominant function of WDR5 in cells, and often influences interpretations of the actions of WDR5 inhibitors. But there are many other roles for WDR5 outside of HMT complexes. Indeed, proteomic quantitation finds that WDR5 is up to ten times more abundant in cells than other HMT complex subunits [40], indicating that only a fraction of WDR5 interactions in cells is in HMT complexes. In my dissertation research, I employed quantitative proteomics and a potent inhibitor of WDR5 to investigate the interaction profile of WDR5 and how it is impacted by blocking a key binding site on WDR5.

My SILAC proteomic analysis of WDR5 and the WIN site inhibitor C6 uncovered 25 proteins affected by this inhibition. This group of proteins is unexpected, enriched in proteins connected to cellular signaling, and notably does not include any of the SET1/MLL HMT enzymes. I additionally find that certain proteins bind better to WDR5 when the WIN site is inhibited. These results highlight that WDR5 binding sites are capable of interacting with a variety of proteins. But with this flexibility also comes a potential vulnerability. Studies of WDR5 and viruses indicate that WDR5 might be coopted by viral proteins, and it is easy to imagine how the flexibility of WDR5 binding sites might also be exploited in cancer to interact with mutant proteins. It is also possible that WDR5 has cell type-specific interaction partners or that the ratios and subsets of WDR5-containing complexes vary in different cell types. In such contexts WDR5 inhibitors might be particularly advantageous. As more in-depth studies of

WDR5 interactions are performed, perhaps disease state-specific interactions will be discovered which can be targeted with WDR5 small molecule inhibitors.

For a bulk of my research I concentrated on one of the newly-discovered WDR5 interacting protein, PDPK1. Focused analysis of the PDPK1–WDR5 interaction revealed that N-terminal acetylation of PDPK1 enables nanomolar affinity interaction with the WIN site (~50 nM), the highest affinity WIN site protein interaction to date. Most known WIN site binding proteins contain internal motifs, but these data emphasize N-terminal WIN motifs as a distinct class of WIN motifs that can be influenced by post-translational modification. More broadly, the association of WDR5 with PDPK1 and other enzymes raises the possibility that post-translational modification of WDR5 occurs and can shape the interaction capabilities of WDR5.

My research also uncovered an intriguing connection between the PDPK1–WDR5 interaction and MYC. My data indicate that MYC, PDPK1, and WDR5 form a trimeric complex, and that functionally, these proteins converge on regulation of G2/M gene expression. This result is meaningful because MYC is well-known to regulate cell growth and perhaps the PDPK1–WDR5–MYC complex functions to regulate expression of these genes.

Together, my results indicate that WDR5 is a node in a previously unimagined web of protein interactions involved in various cellular processes. With WDR5 inhibitors coming down the drug discovery pipeline, assaying the impact of such molecules is important for understanding the actions and potential of WDR5 inhibitors as therapy. In particular, WDR5 inhibitors hold promise for targeting MYC in cancer since MYC interacts with WDR5 and is impacted by WDR5 inhibitors. The extent of the interactions affected by WIN site blockade and the functional significance of these interactions is only beginning to be understood. Yet overall, my research advances this effort by enhancing understanding of the impact of inhibiting the WDR5 WIN site. The results presented in this dissertation also open up interesting future directions, discussed below.

Future directions

In-depth proteomic analysis of WDR5 interactions and modifications

SILAC proteomic analysis of the impact of C6 on WDR5 in HEK293 cells identified 25 proteins that are affected by blocking the WIN site in this context. In order to more fully understand WDR5 interactions and how different binding sites are inhibited, additional SILAC comparisons would be informative. I propose three experiments. First, I suggest analysis of WDR5 mutants by SILAC proteomic comparison. The F133A and L240K mutants of WDR5 are often used to interrogate the two binding sites on WDR5 and the behaviors of these mutants are often extrapolated as presumed actions of WDR5 inhibitors. But my C6 SILAC data indicate that interactions disrupted by these mutations are not always disrupted by WDR5 inhibitors, most notably the in the context of SET1/MLL HMT complexes. A set of quantitative proteomic experiments focused on these mutants of WDR5—comparing F133A to wild-type, and L240K to wild-type—would enable a fuller picture of the similarities and differences of specific manipulations of WDR5. Second, I propose analysis of other classes of WIN site inhibitors in the same manner to my analysis fo C6. This would include OICR-9429, MM-401, and C16, the next-generation of C6. Analyzing other WIN site inhibitors, and the WBM site inhibitor C12 [151], in the same manner as C6 by *in vitro* treatment of lysates [171], would enable unbiased analysis of different forms of chemical inhibition of WDR5. One reported discrepancy between WIN site inhibitors is regarding the MYC–WDR5 interaction. Data from our lab demonstrates that C6 does not disrupt the MYC–WDR5 interaction [62, 171], which is in contrast to data from Sun et al. [140] who demonstrate that OICR-9429 disrupts the N-MYC–WDR5 interaction. Since the WBM motifs of c-MYC and N-MYC are identical, this is more likely to be a difference in the WIN site inhibitor than the MYC protein interrogated. One possibility is that OICR-9429 is capable of disrupting WBM site interactions as well as WIN site interactions, perhaps through a conformational change induced by OIR-9429 WIN site engagement. Comparison of the interaction profiles of WDR5 with different WIN site inhibitors would help to clarify this difference and perhaps reveal additional differences in changes in interactions caused by different WIN

site inhibitors. Third and finally, I propose investigating the effect of C6 in a cancer cell context where WIN site inhibitor impairs proliferation. CHP134 cells are a prime context for such studies. I propose introducing an endogenous FLAG tag onto WDR5 in CHP134 cells and performing quantitative proteomic comparison of WDR5-associated proteins with C6 and C6nc treatments. This kind of analysis could reveal if there are interactions that are specific to or impacted more strongly in a sensitive cellular context. Overall, further analysis of changes in WDR5 interactions upon different WIN and WBM site manipulations would enable a more comprehensive assessment of WDR5 interactions and the mutants and inhibitors that affect them.

High throughput studies have established that WDR5 can be post-translationally modified [273]. Based on the structure of WDR5, any modification at or near the WIN site or the WBM site would likely prevent known protein interactions at those surfaces, but it is also possible that PTMs could induce interactions, for example by creating phospho-docking sites. Few WDR5-focused studies have investigated the post-translational modifications (PTMs) WDR5 can carry or the enzymes that deposit such marks, and no study I am aware of has investigated how PTMs on WDR5 influence its interactions. Additionally, my discovery that WDR5 directly interacts with the kinase PDPK1 raises questions about if WDR5 is phosphorylated by PDPK1 in cells and, more broadly, about how phosphorylation might modulate WDR5 functions. Both are valuable areas for future research.

To clarify understanding of PTMs on WDR5, first, I propose a targeted survey of the WDR5 PTMs in HEK293 cells. I propose affinity purification of WDR5 from cells followed by targeted mass spectrometry analysis. Two or three different digestion approaches, each using a different protease, would help to ensure high sequence coverage of WDR5 for robust detection of WDR5 modifications. Next to investigate if PDPK1 is capable of phosphorylating WDR5, an *in vitro* phosphorylation assay coupled with mass spectrometry analysis should be performed. By comparing recombinant WDR5 alone or incubated with wild-type PDPK1 or R3A PDPK1 we might be able to identify sites of modification on WDR5. I have so far been unsuccessful in

detecting phosphorylation of WDR5 by PDPK1 using a phos-tag gel assay, but perhaps detection by mass spectrometry would be successful. If a site of phosphorylation can be detected on WDR5, these sites can then be interrogated with phospho-mimic mutants for how they might influence interactions with WDR5.

Investigate other WDR5-associated proteins as potential direct interactors

The WDR5 SILAC experiment with C6 presented here identifies 25 proteins that are affected by WIN site inhibition. During my time in the lab I was only able to validate a handful of these proteins and interrogate even fewer in further depth. Thus all of these as-of-yet unexplored proteomic hits represent future directions in interrogating the WDR5 interactome. Below I discuss a few that have potential for being direct WDR5 interactions.

mTORC2 is an mTOR-containing protein complex that is most well known for functioning together with PDPK1 to phosphorylate and activate AKT. Other functions and substrates of mTORC2 are not well understood, but overall mTORC2 regulates cell growth and metabolism [291]. Additionally, mTORC2 subunits have been detected in the nucleus [211]. I identified the mTORC2 subunits RICTR and SIN1 as WIN site-dependent WDR5 interacting proteins, and found that mTORC2 subunits MTOR and LST8 are also capable of interaction with WDR5 (Chapter III). RICTR and SIN1 contain WIN motifs that potentially mediate direct interaction with WDR5. Interrogating each of these WIN motifs by alanine mutagenesis could identify a motif that mediates WIN site binding. Since WDR5 is predominantly nuclear and mTORC2 is predominantly cytosolic, determining where this interaction happens in the cell is imperative. Cytosolic functions of mTORC2—including a notable association with ribosomes in response to signaling [214]—are better understood than the nuclear roles, which seem to be oncogenic [213], but most functions for mTORC2 are not well defined. If it is cytosolic, the mTORC2–WDR5 interaction could affect translation by modulating interaction with the ribosome. If it is nuclear, the mTORC2–WDR5 interaction could be oncogenic by directing WDR5 away from important chromatin interactions that regulate transcription. Understanding where the WDR5–

mTORC2 interaction happens in a cell will be useful for informing subsequent analysis of the functional significance of this interaction.

Next I propose analyzing the proteins that bind better to WDR5 when the WIN site is inhibited. Of the eight better binding proteins identified UBR5 and CHD8 are particularly intriguing because they contain WBM-like motifs. UBR5 is an E3 ubiquitin ligase with extensive cellular activities including in ciliogenesis, gene expression, genome stability, and as a component of the N-end rule pathway [292, 293]. UBR5 is frequently overexpressed or mutated in cancer, and can be co-amplified with *MYC* [294, 295]. CHD8 is an ATP-dependent chromatin remodeling protein that functions mainly in transcriptional regulation [296]. Mutant forms of CHD8 are frequently associated with neurodevelopment disorders, and *CHD8* is one of the most commonly mutated genes in autism spectrum disorder [297]. CHD8 has been shown to interact with WDR5 [87-89] and to be important for the recruitment of WDR5 to chromatin [298]. I propose interrogating these WDR5 interactions by mutating the WBM-like sequence motifs in UBR5 and CHD8 and testing their ability to interact with WDR5 both in cells and *in vitro*. Testing these sequence motifs will further validate the interactions and could yield a mutant that would be advantageous for further investigations.

Finally I propose focused efforts on HELB because of its potential to interact with WDR5 via an N-terminal acetylated WIN motif. Similar to PDPK1, HELB also carries an N-terminal WIN motif (M-A-R-S), and I validated that the WDR5–HELB interaction is WIN site-dependent and is detectable with endogenous proteins (**Figure 3-6**). As next experiments I propose testing if the N-terminal arginine of HELB is necessary for interaction with WDR5 and, if so, analyzing the modification status of HELB by mass spectrometry. If HELB is a WDR5 interaction parallel to PDPK1, then the affinity and structural data can be collected and compared. Presumably, an acetylated HELB peptide would also have high affinity for the WIN site. In terms of biological relevance, HELB is fairly well-studied: HELB plays an important role in DNA replication and DNA damage response [243], and can exist in the nucleus or the cytosol depending on cell cycle phase [244, 245]. Perhaps WDR5 interacts with HELB only in a particular cellular compartment,

or in response to DNA damage, or perhaps only during a certain cell cycle phase. Testing these factors and how they apply to the WDR5–HELB interaction could uncover an additional moonlighting function for WDR5.

Investigate the PDPK1–WDR5–MYC interaction

The interaction of WDR5 together with MYC and PDPK1, and the influence on cell cycle gene expression presents the possibility that these proteins work together in cells. The function of the PDPK1–WDR5 interaction seems closely tied to transcriptional regulation, as nuclear run-on assays detect transcriptional changes hours after protein disruption and before any changes in cell cycle distribution [171]. Many of the same G2/M genes that are increased upon disruption of the WDR5–PDPK1 interaction [171] are known to be upregulated by N-MYC [290]. And experiments from the Tansey Lab in CHP134 cells show that many of these same genes are bound by N-MYC as measured by ChIP-Seq, and are decreased in expression upon inhibition of MYC (unpublished data from Dr. April Weissmiller). Together, these data indicate that MYC may work together with PDPK1–WDR5 in regulating a subset of G2/M genes. I propose investigating the N-MYC–WDR5–PDPK1 interaction using genomic analyses in CHP134 neuroblastoma cells.

I have already generated CHP134 neuroblastoma cell lines that enable targeted degradation of WDR5 or PDPK1 with the dTAG system (**Figure 5-4**). I propose using these CHP134 cells to perform RNA-Seq upon depletion of these proteins to understand the transcriptional networks influenced by each protein. Such genomic data in CHP134 cells can be compared to the existing data obtained in U2OS cells to understand commonalities and differences between insensitive and sensitive cell lines, and cells with and without MYC deregulation. I also propose ChIP-Seq, using the HA epitope, introduced with the degradable tag, to understand the DNA binding patterns of WDR5 and PDPK1 in CHP134 cells. The HA epitope produces reliable signal for ChIP-Seq in our lab [62], and can be controlled by comparison to degrader molecule-treated samples where all HA-tagged proteins are destroyed.

I find in U2OS cells that WDR5 binding to chromatin is detectable at a subset of these G2/M genes (**Figure 5-9**), and although we do not know if PDPK1 is capable of associating with chromatin, ChIP-Seq analysis can be used to interrogate this possibility.

Next, to investigate how the PDPK1–WDR5 interaction might influence N-MYC in CHP134 cells, I propose disrupting the PDPK1–WDR5 interaction and analyzing MYC chromatin binding. The most specific tool for disrupting this interaction is the R3A PDPK1 mutant. I propose using inducible expression of R3A PDPK1 (or wild-type) in tandem with PDPK1 dTAG degradation, followed by analysis of N-MYC chromatin binding, WDR5 chromatin binding, and gene expression changes. Dr. April Weissmiller has generated RNA-Seq data in CHP-134 cells upon OmoMYC [299], inhibition of N-MYC (unpublished), and integrating all these datasets will help in defining the genes involved, and overall functional significance of the PDPK1–WDR5–MYC interactions.

Finally, it is also possible that the PDPK1–WDR5 interaction can take multiple forms. I find that both MYC (**Figures 6-3 and 6-5**) and RBBP5 (**Figures 4-3 and 4-6**) are able to associate with PDPK1 through WDR5. Investigating these two separate trimeric complexes is an additional possible future direction in dissecting the PDPK1–WDR5 interaction.

Investigate the interaction between MYC and the WDR11 complex

MYC proteomic experiments present the WDR11 complex (comprised of WDR11, FAM91A1, and NJMU) as an interaction that is dependent on the WBM motif of MYC. The MYC–WDR11 complex interaction appears to be separate from interaction with WDR5, and thus the anti-tumorigenic effects of the WBM mutant form of MYC [62, 79] could stem from disruption of MYC interaction with both WDR5 and the WDR11 complex. I propose experiments to tease out the molecular details and functional significance of the MYC–WDR11 complex interaction.

First, I propose determining if the MYC–WDR11 complex interaction is direct by *in vitro* binding assays with each individual component of the WDR11 complex. This should be possible by *in vitro* transcription/translation of each subunit individually, and incubation with recombinant

purified MYC, but alternatively, over-expressing and immunoprecipitation of each of the WDR11 complex subunits may also indicate which protein might mediate interaction with MYC. If this MYC interaction proves to be direct, I next propose structural analysis of the WDR11 complex by cryogenic electron microscopy (cryo-EM). WDR11 and FAM91A1 are large proteins, and a 1:1:1 ratio of WDR11:FAM91A1:NJMU is predicted to be a 300 kDa complex. Structural insights into the orientation and number of subunits will be especially useful for understanding the WD40 repeat domains (or blades) within WDR11. Because the sequences of WD40 repeat domains are incredibly plastic, they are not substantially conserved and can be difficult to predict [300, 301]. Different predictions have been made about how many blades WDR11 has; nine blades (UniProt Q9BZH6), twelve blades [277], and fourteen blades [276] have all been proposed based on the amino acid sequence. Only structural insights will determine with confidence the orientation of the blades and β-propeller(s) in WDR11. WDR11 complexes are efficiently immunopurified from cells and such purifications could be optimized for structural studies. Additionally, size-exclusion chromatography could aid in purification and give insight into the stoichiometry of the core WDR11 complex. Determining the structural details of WDR11 and the WDR11 complex could guide studies of how disease-causing mutations in WDR11 affect the complex, and how WDR11 might interact with WBM-containing transcription factors EMX1 and MYC.

I next propose investigating EMX1 and MYC as a WBM-containing proteins that interact with WDR11. The WBM of EMX1 (EDIDVT) (**Table 3-2**) could be mutated similarly to mutant WBM MYC (EDEDEE) and then tested for interaction with WDR11 in cells. In the same experiments EMX1 could be tested for WBM-dependent interaction with WDR5. If WBM mutant EMX1 does not interact with WDR11, this would indicate that WDR11 supports WBM-mediated interactions with multiple transcription factors, both MYC and EMX1. Next, I would perform reciprocal mutational analysis using the disease-specific point mutations in WDR11 (A435T and H690Q) found in patients with Kallman syndrome [277, 283]. These mutations have been shown to disrupt interaction with EMX1 [277] and should be tested for their ability to interact with MYC.

Any structural information obtained by cryo-EM could assist in determining the impact of these mutations. Perhaps these disease-associated mutations disrupt the conformation of β-propellers in WDR11, or perhaps they are located directly within a binding site. Discovery of a cleft on WDR11 that could serve as a WBM binding site, parallel to the WBM site of WDR5, would provide a compelling lead for investigating the WBM motif binding specificity of the WDR11 complex.

Lastly, I propose investigating how hedgehog signaling affects the MYC–WDR11 complex interaction and the transcriptional consequences of disrupting this interaction. Activation of hedgehog signaling rapidly induces nuclear translocation of WDR11 [283]. Perhaps this signaling and translocation influences the MYC–WDR11 interaction and promotes nuclear MYC–WDR11 complex interaction. I propose investigating the sub-cellular localization and the level of interaction between MYC and the WDR11 complex upon treatment of cells with hedgehog signaling agonists. I also propose transcriptional analysis by RNA-Seq upon disruption of the MYC–WDR11 complex interaction. Targeted degradation of WDR11 or a MYC interaction-deficient mutant of WDR11 could be used to analyze the transcriptional consequences of disrupting the MYC–WDR11 complex interaction. This kind of transcriptional analysis will be informative for determining the functional relevance of this interaction, such as perhaps a connection to hedgehog signaling.

Summary

In summary, I used a small molecule WIN site inhibitor to interrogate and uncover WDR5 interacting proteins. I identified 25 WDR5 protein interactions that are affected by blocking the WIN site. Focused efforts on the PDPK1–WDR5 interaction revealed that PDPK1 carries an acetylated N-terminal WIN motif that enables high affinity interaction with the WIN site of WDR5. Comparative genomic analyses highlight a cell cycle gene expression pattern that is influenced by the PDPK1–WDR5 interaction. MYC-centered proteomic analysis finds that MYC

also interacts with PDPK1, possibly together with WDR5. Overall, I uncover new insights into the interaction capabilities of WDR5 and pave the way for future WDR5-centered studies.

Appendix A. Proteins identified past two-fold thresholds in MYC SILAC experiments
Related to figure 6-2. Lists of proteins are ordered by SILAC ratio and a dark line separates the decreased and increased proteins.

151-319 MYC: 13 proteins (8 decreased, 5 increased)

UniProt	Protein Name	MW (kDa)	SILAC Ratio H/L (WBM/WT)	Sequence Coverage (%)	Razor + Unique Peptides
Q9ULI0	ATD2B_HUMAN	165	0.12	2	2
P61964	WDR5_HUMAN	37	0.20	43	10
Q658Y4	F91A1_HUMAN	94	0.24	26	18
O15530	PDPK1_HUMAN	63	0.24	13	5
Q9HAS0	NJMU_HUMAN	45	0.24	10	4
Q9BZH6	WDR11_HUMAN	137	0.26	21	18
Q9NS73	MBIP1_HUMAN	39	0.26	8	2
Q8IYH5	ZZZ3_HUMAN	102	0.48	5	3
P34896	GLYC_HUMAN	53	2.03	23	7
P04075	ALDOA_HUMAN	39	2.03	43	16
Q6P2C8	MED27_HUMAN	35	2.04	14	4
P01116	RASK_HUMAN	22	2.06	11	2
Q9NSK0	KLC4_HUMAN	69	3.88	12	2

251-319 MYC: 99 proteins (21 decreased, 78 increased)

UniProt	Protein Name	MW (kDa)	SILAC Ratio H/L (WBM/WT)	Sequence Coverage (%)	Razor + Unique Peptides
Q6PKX4	DOK6_HUMAN	38	0.02	4	2
Q03052	PO3F1_HUMAN	45	0.05	5	3
Q9BZH6	WDR11_HUMAN	137	0.18	10	10
Q6Y7W6	PERQ2_HUMAN	150	0.23	2	2
P61964	WDR5_HUMAN	37	0.23	20	5
Q658Y4	F91A1_HUMAN	94	0.25	11	8
O15530	PDPK1_HUMAN	63	0.29	15	6
P54259	ATN1_HUMAN	125	0.30	2	2
P13693	TCTP_HUMAN	20	0.32	10	2
O95352	ATG7_HUMAN	78	0.37	8	5
Q96PU5	NED4L_HUMAN	112	0.38	5	2
Q9Y3U8	RL36_HUMAN	12	0.43	29	3
P27635	RL10_HUMAN	25	0.44	16	5
Q9UKS6	PACN3_HUMAN	48	0.44	14	5
Q8WZA0	LZIC_HUMAN	21	0.46	10	2

UniProt	Protein Name	MW (kDa)	SILAC Ratio H/L (WBM/WT)	Sequence Coverage (%)	Razor + Unique Peptides
P43686	PRS6B_HUMAN	47	0.46	12	2
Q96DV4	RM38_HUMAN	45	0.46	8	3
P62841	RS15_HUMAN	17	0.47	9	2
Q13200	PSMD2_HUMAN	100	0.48	16	11
P62191	PRS4_HUMAN	49	0.50	8	3
P49366	DHYS_HUMAN	41	0.50	38	10
O14936	CSKP_HUMAN	105	2.00	6	6
Q00013	EM55_HUMAN	52	2.05	9	2
O94973	AP2A2_HUMAN	104	2.07	13	7
Q9UKV3	ACINU_HUMAN	152	2.09	8	8
P15153	RAC2_HUMAN	21	2.11	10	2
O95782	AP2A1_HUMAN	108	2.15	16	14
Q9NYF8	BCLF1_HUMAN	106	2.20	5	4
Q12959	DLG1_HUMAN	100	2.22	7	5
Q96HP0	DOCK6_HUMAN	230	2.22	2	3
Q00610	CLH1_HUMAN	192	2.24	21	25
Q6PJT7	ZC3HE_HUMAN	83	2.25	4	2
P09651	ROA1_HUMAN	39	2.30	36	11
O00443	P3C2A_HUMAN	191	2.35	2	2
Q08945	SSRP1_HUMAN	81	2.35	6	4
Q5T2T1	MPP7_HUMAN	66	2.38	6	3
P48380	RFX3_HUMAN	84	2.39	6	2
P35221	CTNA1_HUMAN	100	2.39	7	5
P36957	ODO2_HUMAN	49	2.41	7	3
Q9Y5B9	SP16H_HUMAN	120	2.45	11	10
O00422	SAP18_HUMAN	18	2.45	14	3
Q92979	NEP1_HUMAN	27	2.49	18	3
O60716	CTND1_HUMAN	108	2.58	14	10
Q9H307	PININ_HUMAN	82	2.63	3	2
P49736	MCM2_HUMAN	102	2.64	3	3
Q15233	NONO_HUMAN	54	2.70	26	13
P35580	MYH10_HUMAN	229	2.71	6	6
Q9NZW5	MPP6_HUMAN	61	2.71	6	3
O43707	ACTN4_HUMAN	105	2.72	14	11

UniProt	Protein Name	MW (kDa)	SILAC Ratio H/L (WBM/WT)	Sequence Coverage (%)	Razor + Unique Peptides
Q4VCS5	AMOT_HUMAN	118	2.73	13	12
Q15386	UBE3C_HUMAN	124	2.80	2	2
P15311	EZRI_HUMAN	69	2.87	3	2
O15020	SPTN2_HUMAN	271	2.87	7	7
O43795	MYO1B_HUMAN	132	2.90	5	5
Q5SNT2	TM201_HUMAN	72	2.94	3	2
Q96PK6	RBM14_HUMAN	69	3.14	22	11
Q2TAY7	SMU1_HUMAN	58	3.17	19	8
P23246	SFPQ_HUMAN	76	3.28	17	8
P14923	PLAK_HUMAN	82	3.30	11	8
P59998	ARPC4_HUMAN	20	3.45	11	2
P04075	ALDOA_HUMAN	39	3.49	21	7
Q9Y2J2	E41L3_HUMAN	121	3.55	8	5
P61158	ARP3_HUMAN	47	3.62	5	2
P62834	RAP1A_HUMAN	21	3.81	20	3
P35579	MYH9_HUMAN	227	3.88	8	13
Q05682	CALD1_HUMAN	93	3.98	3	2
P14635	CCNB1_HUMAN	48	4.01	6	2
Q99816	TS101_HUMAN	44	4.09	6	2
O14950	ML12B_HUMAN	20	4.19	40	6
P35222	CTNB1_HUMAN	85	4.73	9	6
Q96C19	EFHD2_HUMAN	27	4.74	21	6
Q07157	ZO1_HUMAN	195	4.80	1	2
P11171	41_HUMAN	97	4.89	5	3
Q5JWF2	GNAS1_HUMAN	111	4.90	8	5
P35240	MERL_HUMAN	70	4.92	3	2
O00159	MYO1C_HUMAN	122	4.99	6	6
P62070	RRAS2_HUMAN	23	5.02	11	2
Q9UHB6	LIMA1_HUMAN	85	5.10	10	6
O75083	WDR1_HUMAN	66	5.19	13	5
P23470	PTPRG_HUMAN	162	5.35	2	2
Q6S8J3	POTEE_HUMAN	121	5.38	11	2
P50148	GNAQ_HUMAN	42	5.41	14	2
Q16643	DREB_HUMAN	71	5.93	13	8

UniProt	Protein Name	MW (kDa)	SILAC Ratio H/L (WBM/WT)	Sequence Coverage (%)	Razor + Unique Peptides
P07947	YES_HUMAN	61	5.99	16	6
P62879	GBB2_HUMAN	37	6.28	28	9
Q14978	NOLC1_HUMAN	74	6.43	3	2
Q9ULV4	COR1C_HUMAN	53	6.91	35	15
P63096	GNAI1_HUMAN	40	7.05	26	2
Q13813	SPTN1_HUMAN	285	7.13	41	87
P04899	GNAI2_HUMAN	40	7.54	34	10
O94832	MYO1D_HUMAN	116	7.62	6	5
Q01082	SPTB2_HUMAN	275	7.96	27	55
P08754	GNAI3_HUMAN	41	8.64	28	3
Q9UBI6	GBG12_HUMAN	8	9.22	38	2
O75955	FLOT1_HUMAN	47	9.91	28	9
O43491	E41L2_HUMAN	113	10.15	11	10
P29992	GNA11_HUMAN	42	10.57	21	6
Q14254	FLOT2_HUMAN	47	11.12	17	6
Q14126	DSG2_HUMAN	122	11.53	19	13

Replicate 1 151-275 MYC: 54 proteins (52 decreased, 2 increased)

UniProt	Protein Name	MW (kDa)	SILAC Ratio H/L (WBM/WT)	Sequence Coverage (%)	Razor + Unique Peptides
P61964	WDR5_HUMAN	37	0.17	33	11
Q658Y4	F91A1_HUMAN	94	0.22	24	18
Q9UNL2	SSRG_HUMAN	21	0.25	11	2
Q9HAS0	NJMU_HUMAN	45	0.26	4	2
Q13322	GRB10_HUMAN	67	0.26	5	3
Q6Y7W6	PERQ2_HUMAN	150	0.28	2	2
Q9BZH6	WDR11_HUMAN	137	0.28	28	30
O15530	PDPK1_HUMAN	63	0.28	8	3
Q69YQ0	CYTSA_HUMAN	125	0.32	8	7
P13987	CD59_HUMAN	14	0.33	16	2
Q9HAU4	SMUF2_HUMAN	86	0.33	4	3
Q9UHB6	LIMA1_HUMAN	85	0.34	14	9
Q7Z406	MYH14_HUMAN	228	0.35	10	11
Q16643	DREB_HUMAN	71	0.35	14	6
P35580	MYH10_HUMAN	229	0.36	59	108

UniProt	Protein Name	MW (kDa)	SILAC Ratio H/L (WBM/WT)	Sequence Coverage (%)	Razor + Unique Peptides
O43707	ACTN4_HUMAN	105	0.36	3	3
O00159	MYO1C_HUMAN	122	0.36	39	36
Q5JWF2	GNAS1_HUMAN	111	0.37	3	2
O14950	ML12B_HUMAN	20	0.37	55	9
P35579	MYH9_HUMAN	227	0.37	62	137
A6NL28	TPM3L_HUMAN	26	0.39	18	2
Q14156	EFR3A_HUMAN	93	0.39	3	2
Q01082	SPTB2_HUMAN	275	0.39	29	61
Q13813	SPTA2_HUMAN	285	0.39	35	72
Q92614	MY18A_HUMAN	233	0.39	5	11
Q6WCQ1	MPRIP_HUMAN	117	0.39	14	11
P61513	RL37A_HUMAN	10	0.40	52	5
Q9NYL9	TMOD3_HUMAN	40	0.40	23	6
O94832	MYO1D_HUMAN	116	0.40	23	19
Q96C19	EFHD2_HUMAN	27	0.40	18	4
Q15286	RAB35_HUMAN	23	0.40	11	2
P62158	CALM_HUMAN	17	0.41	17	2
Q03252	LMNB2_HUMAN	68	0.41	8	2
O43795	MYO1B_HUMAN	132	0.43	25	25
P06753	TPM3_HUMAN	33	0.43	23	8
P07355	ANXA2_HUMAN	39	0.43	17	4
O75396	SC22B_HUMAN	25	0.43	8	2
Q9ULV4	COR1C_HUMAN	53	0.43	25	11
Q14146	URB2_HUMAN	171	0.44	2	3
O14639	ABLM1_HUMAN	88	0.44	6	4
P62873	GBB1_HUMAN	37	0.45	22	7
O95425	SVIL_HUMAN	248	0.45	1	2
Q9NXV2	KCTD5_HUMAN	26	0.45	39	6
P52907	CAZA1_HUMAN	33	0.46	28	6
Q9UBI6	GBG12_HUMAN	8	0.46	32	2
O43663	PRC1_HUMAN	72	0.47	8	5
O14974	MYPT1_HUMAN	115	0.47	10	8
P08754	GNAI3_HUMAN	41	0.47	24	7
Q4VCS5	AMOT_HUMAN	118	0.48	19	17

UniProt	Protein Name	MW (kDa)	SILAC Ratio H/L (WBM/WT)	Sequence Coverage (%)	Razor + Unique Peptides
Q14254	FLOT2_HUMAN	47	0.48	42	16
O75955	FLOT1_HUMAN	47	0.49	50	18
O75695	XRP2_HUMAN	40	0.49	7	3
P16615	AT2A2_HUMAN	115	2.09	6	4
Q04637	IF4G1_HUMAN	175	2.15	3	4

Replicate 2 151-275 MYC: 51 proteins (13 decreased, 38 increased)

UniProt	Protein Name	MW (kDa)	SILAC Ratio H/L (WBM/WT)	Sequence Coverage (%)	Razor + Unique Peptides
P06702	S10A9_HUMAN	13	0.18	32	3
P61964	WDR5_HUMAN	37	0.24	24	7
Q02413	DSG1_HUMAN	114	0.24	7	4
Q9BZH6	WDR11_HUMAN	137	0.28	23	23
Q658Y4	F91A1_HUMAN	94	0.30	23	16
Q9HCL2	GPAT1_HUMAN	94	0.33	4	3
Q9P016	THYN1_HUMAN	26	0.39	9	2
Q15021	CND1_HUMAN	157	0.41	2	2
Q8WYP5	ELYS_HUMAN	253	0.42	2	3
Q70UQ0	IKIP_HUMAN	39	0.43	6	2
Q9UGN5	PARP2_HUMAN	66	0.48	11	6
Q9BSJ8	ESYT1_HUMAN	123	0.49	2	2
P49916	DNLI3_HUMAN	113	0.50	14	12
Q8WWI1	LMO7_HUMAN	193	2.00	6	7
Q96SB3	NEB2_HUMAN	89	2.02	7	5
Q15286	RAB35_HUMAN	23	2.03	17	3
O14950	ML12B_HUMAN	20	2.06	55	9
P17302	CXA1_HUMAN	43	2.07	8	2
O95478	NSA2_HUMAN	30	2.07	15	3
P11233	RALA_HUMAN	24	2.07	13	2
O14974	MYPT1_HUMAN	115	2.08	14	13
P35240	MERL_HUMAN	70	2.09	3	2
P15311	EZRI_HUMAN	69	2.09	10	5
Q7Z406	MYH14_HUMAN	228	2.18	12	13
Q69YQ0	CYTSA_HUMAN	125	2.20	13	13

UniProt	Protein Name	MW (kDa)	SILAC Ratio H/L (WBM/WT)	Sequence Coverage (%)	Razor + Unique Peptides
Q15397	K0020_HUMAN	74	2.24	6	3
Q9Y608	LRRF2_HUMAN	82	2.31	6	3
P62158	CALM_HUMAN	17	2.33	25	3
Q6WCQ1	MPRIP_HUMAN	117	2.34	17	13
O60292	SI1L3_HUMAN	195	2.35	2	3
P35580	MYH10_HUMAN	229	2.37	60	113
P35579	MYH9_HUMAN	227	2.37	64	145
O95425	SVIL_HUMAN	248	2.38	3	4
Q9Y6J0	CABIN_HUMAN	246	2.41	1	2
Q92614	MY18A_HUMAN	233	2.47	7	14
O15020	SPTN2_HUMAN	271	2.49	14	17
Q9ULV4	COR1C_HUMAN	53	2.50	28	15
P09012	SNRPA_HUMAN	31	2.54	9	3
Q13813	SPTA2_HUMAN	285	2.55	51	111
O43707	ACTN4_HUMAN	105	2.56	13	10
Q9UHB6	LIMA1_HUMAN	85	2.60	30	21
Q01082	SPTB2_HUMAN	275	2.66	50	107
Q9NYL9	TMOD3_HUMAN	40	2.77	20	5
P04075	ALDOA_HUMAN	39	2.80	24	9
Q9BUP0	EFHD1_HUMAN	27	2.92	8	2
Q8WVD3	RN138_HUMAN	28	2.98	20	5
Q6S8J3	POTEE_HUMAN	121	3.03	12	2
Q16643	DREB_HUMAN	71	3.21	28	21
Q96C19	EFHD2_HUMAN	27	3.23	29	7
P62736	ACTA_HUMAN	42	3.42	31	2
O75083	WDR1_HUMAN	66	4.23	6	4

Replicate 3 151-275: 226 proteins (4 decreased, 222 increased)

UniProt	Protein Name	MW (kDa)	SILAC Ratio L/H (WBM/WT)	Sequence Coverage (%)	Razor + Unique Peptides
P61964	WDR5_HUMAN	37	0.20	25	7
Q658Y4	F91A1_HUMAN	94	0.31	17	12
Q9BZH6	WDR11_HUMAN	137	0.32	18	18
P54132	BLM_HUMAN	159	0.34	1	2
Q9BV38	WDR18_HUMAN	47	2.01	6	2

UniProt	Protein Name	MW (kDa)	SILAC Ratio L/H (WBM/WT)	Sequence Coverage (%)	Razor + Unique Peptides
Q9UQ35	SRRM2_HUMAN	300	2.02	6	12
P61353	RL27_HUMAN	16	2.02	43	7
Q9UKM9	RALY_HUMAN	32	2.02	8	3
Q8WWQ0	PHIP_HUMAN	207	2.03	2	3
P62834	RAP1A_HUMAN	21	2.03	30	6
Q15459	SF3A1_HUMAN	89	2.04	5	3
Q9BQ39	DDX50_HUMAN	83	2.05	12	6
O75475	PSIP1_HUMAN	60	2.06	7	4
P61978	HNRPK_HUMAN	51	2.06	44	15
P55072	TERA_HUMAN	89	2.06	4	2
Q9Y4I1	MYO5A_HUMAN	215	2.06	4	7
Q93050	VPP1_HUMAN	96	2.06	3	2
P06748	NPM_HUMAN	33	2.07	53	15
Q96C19	EFHD2_HUMAN	27	2.07	33	8
Q06787	FMR1_HUMAN	71	2.07	6	3
P42766	RL35_HUMAN	15	2.07	24	4
Q8NEJ9	NGDN_HUMAN	36	2.07	11	3
P61254	RL26_HUMAN	17	2.08	28	6
Q8WYP5	ELYS_HUMAN	253	2.08	3	7
Q9BVJ6	UT14A_HUMAN	88	2.08	11	7
Q15269	PWP2_HUMAN	102	2.08	13	9
Q03701	CEBPZ_HUMAN	121	2.09	9	8
Q8IZL8	PELP1_HUMAN	120	2.09	4	3
O60506	HNRPQ_HUMAN	70	2.10	12	3
P09874	PARP1_HUMAN	113	2.10	49	51
Q99959	PKP2_HUMAN	97	2.10	6	6
Q01780	EXOSX_HUMAN	101	2.10	6	5
Q12792	TWF1_HUMAN	40	2.11	10	3
Q69YQ0	CYTSA_HUMAN	125	2.11	15	16
Q96RT1	LAP2_HUMAN	158	2.12	3	4
P26373	RL13_HUMAN	24	2.12	26	6
Q9NYL9	TMOD3_HUMAN	40	2.12	20	6
O60245	PCDH7_HUMAN	116	2.13	2	2
Q5SSJ5	HP1B3_HUMAN	61	2.13	5	3
P36873	PP1G_HUMAN	37	2.14	29	2
Q12906	ILF3_HUMAN	95	2.14	11	8

UniProt	Protein Name	MW (kDa)	SILAC Ratio L/H (WBM/WT)	Sequence Coverage (%)	Razor + Unique Peptides
O15213	WDR46_HUMAN	68	2.14	5	3
Q15149	PLEC_HUMAN	532	2.15	15	63
Q6DKI1	RL7L_HUMAN	29	2.15	15	5
Q9UIG0	BAZ1B_HUMAN	171	2.15	5	8
P42696	RBM34_HUMAN	49	2.16	10	4
Q9HAC8	UBTD1_HUMAN	26	2.16	12	2
Q99569	PKP4_HUMAN	132	2.16	13	12
Q14156	EFR3A_HUMAN	93	2.17	4	3
Q1KMD3	HNRL2_HUMAN	85	2.17	4	3
Q14642	I5P1_HUMAN	48	2.17	10	3
P15311	EZRI_HUMAN	69	2.18	3	2
P46778	RL21_HUMAN	19	2.19	18	4
P62277	RS13_HUMAN	17	2.20	44	7
P62424	RL7A_HUMAN	30	2.20	36	12
P62805	H4_HUMAN	11	2.22	54	10
Q9UN86	G3BP2_HUMAN	54	2.22	6	2
Q14160	SCRIB_HUMAN	175	2.23	11	15
Q9H6F5	CCD86_HUMAN	40	2.23	11	4
P40429	RL13A_HUMAN	24	2.23	23	5
P62753	RS6_HUMAN	29	2.23	23	5
P35579	MYH9_HUMAN	227	2.23	60	136
P18124	RL7_HUMAN	29	2.23	36	10
Q6WCQ1	MPRIP_HUMAN	117	2.24	24	17
Q00610	CLH1_HUMAN	192	2.24	20	26
Q96PY5	FMNL2_HUMAN	123	2.24	12	12
P05388	RLA0_HUMAN	34	2.25	36	9
P50914	RL14_HUMAN	23	2.25	27	7
Q8NI36	WDR36_HUMAN	105	2.25	9	8
P62750	RL23A_HUMAN	18	2.25	40	8
P68431	H31_HUMAN	15	2.25	35	8
P26599	PTBP1_HUMAN	57	2.26	17	8
P35580	MYH10_HUMAN	229	2.26	59	111
P49916	DNLI3_HUMAN	113	2.26	13	11
Q9UKV3	ACINU_HUMAN	152	2.26	8	9
O75367	H2AY_HUMAN	40	2.27	30	9
O75369	FLNB_HUMAN	278	2.27	8	17

UniProt	Protein Name	MW (kDa)	SILAC Ratio L/H (WBM/WT)	Sequence Coverage (%)	Razor + Unique Peptides
Q9UHB6	LIMA1_HUMAN	85	2.28	41	31
P62917	RL8_HUMAN	28	2.28	20	7
P11388	TOP2A_HUMAN	174	2.28	17	25
Q7Z406	MYH14_HUMAN	228	2.29	16	17
Q9BY77	PDIP3_HUMAN	46	2.30	11	4
P61313	RL15_HUMAN	24	2.31	22	5
Q9UM54	MYO6_HUMAN	150	2.31	23	29
Q07020	RL18_HUMAN	22	2.32	26	4
Q5QJE6	TDIF2_HUMAN	84	2.33	10	5
P62736	ACTA_HUMAN	42	2.33	27	2
Q9Y3C1	NOP16_HUMAN	21	2.33	20	4
Q07157	ZO1_HUMAN	195	2.34	13	20
Q9NVX2	NLE1_HUMAN	53	2.34	7	3
Q9NUP9	LIN7C_HUMAN	22	2.34	14	3
P07948	LYN_HUMAN	59	2.34	25	12
P49207	RL34_HUMAN	13	2.35	28	4
O75494	SRS10_HUMAN	31	2.35	9	2
Q9Y608	LRRF2_HUMAN	82	2.36	4	2
Q13151	ROA0_HUMAN	31	2.37	18	5
P18887	XRCC1_HUMAN	69	2.39	5	3
P27105	STOM_HUMAN	32	2.39	14	3
P28290	SSFA2_HUMAN	138	2.40	5	6
O00159	MYO1C_HUMAN	122	2.40	32	32
P52272	HNRPM_HUMAN	78	2.40	34	25
Q9NR30	DDX21_HUMAN	87	2.40	39	25
P23246	SFPQ_HUMAN	76	2.41	23	9
P38159	RBMX_HUMAN	42	2.42	36	13
P36578	RL4_HUMAN	48	2.44	34	16
Q7L9B9	EEPD1_HUMAN	62	2.44	10	5
O00566	MPP10_HUMAN	79	2.44	5	3
O43491	E41L2_HUMAN	113	2.44	28	24
Q15717	ELAV1_HUMAN	36	2.45	23	5
Q9NYF8	BCLF1_HUMAN	106	2.45	12	11
Q8WXX5	DNJC9_HUMAN	30	2.45	20	4
P62070	RRAS2_HUMAN	23	2.46	36	6
Q14676	MDC1_HUMAN	227	2.46	6	9

UniProt	Protein Name	MW (kDa)	SILAC Ratio L/H (WBM/WT)	Sequence Coverage (%)	Razor + Unique Peptides
Q92614	MY18A_HUMAN	233	2.46	9	17
Q9Y2D5	AKAP2_HUMAN	95	2.47	5	3
Q9BUP0	EFHD1_HUMAN	27	2.47	27	5
Q03164	MLL1_HUMAN	432	2.47	1	3
Q08211	DHX9_HUMAN	141	2.48	17	21
Q86V48	LUZP1_HUMAN	120	2.49	3	2
Q08945	SSRP1_HUMAN	81	2.50	20	12
Q13595	TRA2A_HUMAN	33	2.50	19	3
P07910	HNRPC_HUMAN	34	2.50	33	12
Q9BR76	COR1B_HUMAN	54	2.51	6	3
P19022	CADH2_HUMAN	100	2.52	8	5
P28289	TMOD1_HUMAN	41	2.53	11	3
Q9ULV4	COR1C_HUMAN	53	2.54	41	19
Q9NQ55	SSF1_HUMAN	53	2.55	12	7
P62995	TRA2B_HUMAN	34	2.55	23	6
Q9Y5B9	SP16H_HUMAN	120	2.55	25	25
Q9NVP1	DDX18_HUMAN	75	2.55	18	11
Q9Y5J1	UTP18_HUMAN	62	2.55	4	2
P55060	XPO2_HUMAN	110	2.57	3	3
P46013	KI67_HUMAN	359	2.57	10	24
Q9NZI8	IF2B1_HUMAN	63	2.57	12	7
P09471	GNAO_HUMAN	40	2.57	23	5
Q14137	BOP1_HUMAN	84	2.57	21	12
O43166	SI1L1_HUMAN	200	2.59	3	4
Q9NZW5	MPP6_HUMAN	61	2.60	6	3
Q9Y2W1	TR150_HUMAN	109	2.60	8	7
P62879	GBB2_HUMAN	37	2.61	27	4
Q02880	TOP2B_HUMAN	183	2.62	11	10
P17302	CXA1_HUMAN	43	2.62	7	2
P84090	ERH_HUMAN	12	2.62	16	2
Q15286	RAB35_HUMAN	23	2.63	17	3
P18077	RL35A_HUMAN	13	2.63	39	5
Q7L2E3	DHX30_HUMAN	134	2.63	4	5
P35222	CTNB1_HUMAN	85	2.63	15	9
Q16629	SRSF7_HUMAN	27	2.63	27	8
P16403	H12_HUMAN	21	2.64	38	4

UniProt	Protein Name	MW (kDa)	SILAC Ratio L/H (WBM/WT)	Sequence Coverage (%)	Razor + Unique Peptides
Q9UBI6	GBG12_HUMAN	8	2.64	38	2
Q9H307	PININ_HUMAN	82	2.64	10	7
Q15397	K0020_HUMAN	74	2.64	7	4
O95478	NSA2_HUMAN	30	2.65	12	3
Q9BZE4	NOG1_HUMAN	74	2.65	25	14
O14936	CSKP_HUMAN	105	2.65	5	4
Q14980	NUMA1_HUMAN	238	2.67	21	34
P55769	NH2L1_HUMAN	14	2.67	25	3
Q96GQ7	DDX27_HUMAN	90	2.67	16	12
Q8WWI1	LMO7_HUMAN	193	2.68	9	12
P46777	RL5_HUMAN	34	2.68	19	5
P63092	GNAS2_HUMAN	46	2.68	32	12
P08754	GNAI3_HUMAN	41	2.68	50	13
Q13247	SRSF6_HUMAN	40	2.70	23	10
Q96PK6	RBM14_HUMAN	69	2.71	21	13
P29992	GNA11_HUMAN	42	2.73	28	10
Q7Z5G4	GOGA7_HUMAN	16	2.74	19	2
P62241	RS8_HUMAN	24	2.74	35	7
Q15424	SAFB1_HUMAN	103	2.75	7	6
P51991	ROA3_HUMAN	40	2.76	19	4
P19338	NUCL_HUMAN	77	2.77	41	32
P84103	SRSF3_HUMAN	19	2.78	38	6
Q96A72	MGN2_HUMAN	17	2.78	25	4
Q14344	GNA13_HUMAN	44	2.79	18	5
O15020	SPTN2_HUMAN	271	2.80	16	23
P04899	GNAI2_HUMAN	40	2.80	36	5
O94832	MYO1D_HUMAN	116	2.80	25	24
P07305	H10_HUMAN	21	2.81	26	6
P56537	IF6_HUMAN	27	2.81	20	3
Q01082	SPTB2_HUMAN	275	2.81	48	107
O75695	XRP2_HUMAN	40	2.81	18	8
O76021	RL1D1_HUMAN	55	2.82	35	19
Q07955	SRSF1_HUMAN	28	2.84	51	14
P10412	H14_HUMAN	22	2.85	44	14
Q13813	SPTA2_HUMAN	285	2.85	52	115
O43795	MYO1B_HUMAN	132	2.88	33	35

UniProt	Protein Name	MW (kDa)	SILAC Ratio L/H (WBM/WT)	Sequence Coverage (%)	Razor + Unique Peptides
Q16643	DREB_HUMAN	71	2.89	29	20
P62873	GBB1_HUMAN	37	2.89	37	10
O43707	ACTN4_HUMAN	105	2.90	14	11
Q13243	SRSF5_HUMAN	31	2.91	18	5
Q4VCS5	AMOT_HUMAN	118	2.92	31	28
P62158	CALM_HUMAN	17	2.94	17	3
Q9NW13	RBM28_HUMAN	86	2.96	13	10
Q9UKD2	MRT4_HUMAN	28	2.99	11	2
P46087	NOP2_HUMAN	89	3.01	22	16
O75955	FLOT1_HUMAN	47	3.06	29	10
Q9UMY1	NOL7_HUMAN	29	3.08	7	2
Q99848	EBP2_HUMAN	35	3.18	10	3
Q15050	RRS1_HUMAN	41	3.20	24	7
Q9H6R4	NOL6_HUMAN	128	3.25	2	2
Q8IY81	RRMJ3_HUMAN	97	3.28	14	12
Q68CQ4	DIEXF_HUMAN	87	3.29	3	2
Q14254	FLOT2_HUMAN	47	3.31	25	10
P22626	ROA2_HUMAN	37	3.33	38	13
P16402	H13_HUMAN	22	3.37	33	4
P08670	VIME_HUMAN	54	3.43	66	35
O43818	U3IP2_HUMAN	52	3.43	12	5
Q9H9Y2	RPF1_HUMAN	40	3.44	7	2
Q9UNL2	SSRG_HUMAN	21	3.47	12	2
P63096	GNAI1_HUMAN	40	3.51	37	5
Q9H501	ESF1_HUMAN	99	3.51	2	2
Q9H7B2	RPF2_HUMAN	36	3.53	10	3
Q5M775	CYTSB_HUMAN	119	3.64	4	4
Q9GZR2	REXO4_HUMAN	47	3.66	6	2
O75037	KI21B_HUMAN	183	3.67	2	2
P14923	PLAK_HUMAN	82	3.70	23	16
P13987	CD59_HUMAN	14	3.75	25	3
Q01130	SRSF2_HUMAN	25	3.85	18	4
Q14126	DSG2_HUMAN	122	3.95	23	20
Q14692	BMS1_HUMAN	146	4.04	2	3
P09651	ROA1_HUMAN	39	4.13	19	8
P19086	GNAZ_HUMAN	41	4.33	13	3

UniProt	Protein Name	MW (kDa)	SILAC Ratio L/H (WBM/WT)	Sequence Coverage (%)	Razor + Unique Peptides
Q8TDN6	BRX1_HUMAN	41	4.41	8	3
Q9UKS6	PACN3_HUMAN	48	4.50	9	3
P17096	HMGA1_HUMAN	12	4.54	33	3
P22087	FBRL_HUMAN	34	4.68	16	6
Q14978	NOLC1_HUMAN	74	5.36	11	9

References

1. Guarnaccia A.D., Tansey W.P. Moonlighting with WDR5: A Cellular Multitasker. J Clin Med. 2018;7(2). PMID: 29385767.
2. Jeffery C.J. Moonlighting proteins. Trends Biochem Sci. 1999;24(1):8-11. PMID: 10087914.
3. Somma M.P., Andreyeva E.N., Pavlova G.A., Pellacani C., Bucciarelli E., Popova J.V., Bonaccorsi S., Pindyurin A.V., Gatti M. Moonlighting in Mitosis: Analysis of the Mitotic Functions of Transcription and Splicing Factors. Cells. 2020;9(6). PMID: 32604778.
4. Gori F., Divieti P., Demay M.B. Cloning and characterization of a novel WD-40 repeat protein that dramatically accelerates osteoblastic differentiation. J Biol Chem. 2001;276(49):46515-46522. PMID: 11551928.
5. Gori F., Friedman L.G., Demay M.B. Wdr5, a WD-40 protein, regulates osteoblast differentiation during embryonic bone development. Dev Biol. 2006;295(2):498-506. PMID: 16730692.
6. Gori F., Demay M.B. BIG-3, a novel WD-40 repeat protein, is expressed in the developing growth plate and accelerates chondrocyte differentiation in vitro. Endocrinology. 2004;145(3):1050-1054. PMID: 14657013.
7. Gori F., Zhu E.D., Demay M.B. Perichondrial expression of Wdr5 regulates chondrocyte proliferation and differentiation. Dev Biol. 2009;329(1):36-43. PMID: 19217897.
8. Zhu S., Zhu E.D., Provot S., Gori F. Wdr5 is required for chick skeletal development. J Bone Miner Res. 2010;25(11):2504-2514. PMID: 20533303.
9. Miller T., Krogan N.J., Dover J., Erdjument-Bromage H., Tempst P., Johnston M., Greenblatt J.F., Shilatifard A. COMPASS: a complex of proteins associated with a trithorax-related SET domain protein. Proc Natl Acad Sci U S A. 2001;98(23):12902-12907. PMID: 11687631.
10. Roguev A., Schaft D., Shevchenko A., Pijnappel W.W., Wilm M., Aasland R., Stewart A.F. The Saccharomyces cerevisiae Set1 complex includes an Ash2 homologue and methylates histone 3 lysine 4. EMBO J. 2001;20(24):7137-7148. PMID: 11742990.
11. Wysocka J., Swigut T., Milne T.A., Dou Y., Zhang X., Burlingame A.L., Roeder R.G., Brivanlou A.H., Allis C.D. WDR5 associates with histone H3 methylated at K4 and is essential for H3 K4 methylation and vertebrate development. Cell. 2005;121(6):859-872. PMID: 15960974.
12. Ang Y.S., Tsai S.Y., Lee D.F., Monk J., Su J., Ratnakumar K., Ding J., Ge Y., Darr H., Chang B., Wang J., Rendl M., Bernstein E., Schaniel C., Lemischka I.R. Wdr5 mediates self-renewal and reprogramming via the embryonic stem cell core transcriptional network. Cell. 2011;145(2):183-197. PMID: 21477851.
13. Schuetz A., Allali-Hassani A., Martin F., Loppnau P., Vedadi M., Bochkarev A., Plotnikov A.N., Arrowsmith C.H., Min J. Structural basis for molecular recognition and presentation of histone H3 by WDR5. EMBO J. 2006;25(18):4245-4252. PMID: 16946699.
14. Berman H.M., Westbrook J., Feng Z., Gilliland G., Bhat T.N., Weissig H., Shindyalov I.N., Bourne P.E. The Protein Data Bank. Nucleic Acids Res. 2000;28(1):235-242. PMID: 10592235.
15. Orchard S., Ammari M., Aranda B., Breuza L., Briganti L., Broackes-Carter F., Campbell N.H., Chavali G., Chen C., del-Toro N., Duesbury M., Dumousseau M., Galeota E., Hinz U., Iannuccelli M., Jagannathan S., Jimenez R., Khadake J., Lagreid A., Licata L., Lovering R.C., Meldal B., Melidoni A.N., Milagros M., Peluso D., Perfetto L., Porras P., Raghunath A., Ricard-Blum S., Roechert B., Stutz A., Tognolli M., van Roey K., Cesareni G., Hermjakob H. The MIntAct project--IntAct as a common curation platform for 11 molecular interaction databases. Nucleic Acids Res. 2014;42(Database issue):D358-363. PMID: 24234451.
16. Odho Z., Southall S.M., Wilson J.R. Characterization of a novel WDR5-binding site that recruits RbBP5 through a conserved motif to enhance methylation of histone H3 lysine 4 by mixed lineage leukemia protein-1. J Biol Chem. 2010;285(43):32967-32976. PMID: 20716525.

17. Song J.J., Kingston R.E. WDR5 interacts with mixed lineage leukemia (MLL) protein via the histone H3-binding pocket. J Biol Chem. 2008;283(50):35258-35264. PMID: 18840606.
18. Dias J., Van Nguyen N., Georgiev P., Gaub A., Brettschneider J., Cusack S., Kadlec J., Akhtar A. Structural analysis of the KANSL1/WDR5/KANSL2 complex reveals that WDR5 is required for efficient assembly and chromatin targeting of the NSL complex. Genes Dev. 2014;28(9):929-942. PMID: 24788516.
19. Ali A., Veeranki S.N., Chinchole A., Tyagi S. MLL/WDR5 Complex Regulates Kif2A Localization to Ensure Chromosome Congression and Proper Spindle Assembly during Mitosis. Dev Cell. 2017;41(6):605-622 e607. PMID: 28633016.
20. Schuettengruber B., Martinez A.M., Iovino N., Cavalli G. Trithorax group proteins: switching genes on and keeping them active. Nat Rev Mol Cell Biol. 2011;12(12):799-814. PMID: 22108599.
21. Hughes C.M., Rozenblatt-Rosen O., Milne T.A., Copeland T.D., Levine S.S., Lee J.C., Hayes D.N., Shanmugam K.S., Bhattacharjee A., Biondi C.A., Kay G.F., Hayward N.K., Hess J.L., Meyerson M. Menin associates with a trithorax family histone methyltransferase complex and with the Hoxc8 locus. Mol Cell. 2004;13(4):587-597. PMID: 14992727.
22. Yokoyama A., Wang Z., Wysocka J., Sanyal M., Aufiero D.J., Kitabayashi I., Herr W., Cleary M.L. Leukemia proto-oncoprotein MLL forms a SET1-like histone methyltransferase complex with menin to regulate Hox gene expression. Mol Cell Biol. 2004;24(13):5639-5649. PMID: 15199122.
23. Lee J.H., Skalnik D.G. CpG-binding protein (CXXC finger protein 1) is a component of the mammalian Set1 histone H3-Lys4 methyltransferase complex, the analogue of the yeast Set1/COMPASS complex. J Biol Chem. 2005;280(50):41725-41731. PMID: 16253997.
24. Glaser S., Schaft J., Lubitz S., Vintersten K., van der Hoeven F., Tufteland K.R., Aasland R., Anastassiadis K., Ang S.L., Stewart A.F. Multiple epigenetic maintenance factors implicated by the loss of Mll2 in mouse development. Development. 2006;133(8):1423-1432. PMID: 16540515.
25. Mo R., Rao S.M., Zhu Y.J. Identification of the MLL2 complex as a coactivator for estrogen receptor alpha. J Biol Chem. 2006;281(23):15714-15720. PMID: 16603732.
26. Lee J.H., Tate C.M., You J.S., Skalnik D.G. Identification and characterization of the human Set1B histone H3-Lys4 methyltransferase complex. J Biol Chem. 2007;282(18):13419-13428. PMID: 17355966.
27. Ernst P., Vakoc C.R. WRAD: enabler of the SET1-family of H3K4 methyltransferases. Brief Funct Genomics. 2012;11(3):217-226. PMID: 22652693.
28. Dou Y., Milne T.A., Ruthenburg A.J., Lee S., Lee J.W., Verdine G.L., Allis C.D., Roeder R.G. Regulation of MLL1 H3K4 methyltransferase activity by its core components. Nat Struct Mol Biol. 2006;13(8):713-719. PMID: 16878130.
29. Shinsky S.A., Monteith K.E., Viggiano S., Cosgrove M.S. Biochemical reconstitution and phylogenetic comparison of human SET1 family core complexes involved in histone methylation. J Biol Chem. 2015;290(10):6361-6375. PMID: 25561738.
30. Li Y., Han J., Zhang Y., Cao F., Liu Z., Li S., Wu J., Hu C., Wang Y., Shuai J., Chen J., Cao L., Li D., Shi P., Tian C., Zhang J., Dou Y., Li G., Chen Y., Lei M. Structural basis for activity regulation of MLL family methyltransferases. Nature. 2016;530(7591):447-452. PMID: 26886794.
31. Patel A., Dharmarajan V., Cosgrove M.S. Structure of WDR5 bound to mixed lineage leukemia protein-1 peptide. J Biol Chem. 2008;283(47):32158-32161. PMID: 18829459.
32. Patel A., Vought V.E., Dharmarajan V., Cosgrove M.S. A conserved arginine-containing motif crucial for the assembly and enzymatic activity of the mixed lineage leukemia protein-1 core complex. J Biol Chem. 2008;283(47):32162-32175. PMID: 18829457.
33. Dharmarajan V., Lee J.H., Patel A., Skalnik D.G., Cosgrove M.S. Structural basis for WDR5 interaction (Win) motif recognition in human SET1 family histone methyltransferases. J Biol Chem. 2012;287(33):27275-27289. PMID: 22665483.
34. Karatas H., Townsend E.C., Bernard D., Dou Y., Wang S. Analysis of the binding of mixed lineage leukemia 1 (MLL1) and histone 3 peptides to WD repeat domain 5 (WDR5) for

the design of inhibitors of the MLL1-WDR5 interaction. J Med Chem. 2010;53(14):5179-5185. PMID: 20575550.
35. Zhang P., Lee H., Brunzelle J.S., Couture J.F. The plasticity of WDR5 peptide-binding cleft enables the binding of the SET1 family of histone methyltransferases. Nucleic Acids Res. 2012;40(9):4237-4246. PMID: 22266653.
36. Kwon M., Park K., Hyun K., Lee J.H., Zhou L., Cho Y.W., Ge K., Skalnik D.G., Muir T.W., Kim J. H2B ubiquitylation enhances H3K4 methylation activities of human KMT2 family complexes. Nucleic Acids Res. 2020;48(10):5442-5456. PMID: 32365172.
37. Alicea-Velazquez N.L., Shinsky S.A., Loh D.M., Lee J.H., Skalnik D.G., Cosgrove M.S. Targeted Disruption of the Interaction between WD-40 Repeat Protein 5 (WDR5) and Mixed Lineage Leukemia (MLL)/SET1 Family Proteins Specifically Inhibits MLL1 and SETd1A Methyltransferase Complexes. J Biol Chem. 2016;291(43):22357-22372. PMID: 27563068.
38. Cao F., Townsend E.C., Karatas H., Xu J., Li L., Lee S., Liu L., Chen Y., Ouillette P., Zhu J., Hess J.L., Atadja P., Lei M., Qin Z.S., Malek S., Wang S., Dou Y. Targeting MLL1 H3K4 methyltransferase activity in mixed-lineage leukemia. Mol Cell. 2014;53(2):247-261. PMID: 24389101.
39. Aho E.R., Wang J., Gogliotti R.D., Howard G.C., Phan J., Acharya P., Macdonald J.D., Cheng K., Lorey S.L., Lu B., Wenzel S., Foshage A.M., Alvarado J., Wang F., Shaw J.G., Zhao B., Weissmiller A.M., Thomas L.R., Vakoc C.R., Hall M.D., Hiebert S.W., Liu Q., Stauffer S.R., Fesik S.W., Tansey W.P. Displacement of WDR5 from Chromatin by a WIN Site Inhibitor with Picomolar Affinity. Cell Rep. 2019;26(11):2916-2928 e2913. PMID: 30865883.
40. van Nuland R., Smits A.H., Pallaki P., Jansen P.W., Vermeulen M., Timmers H.T. Quantitative dissection and stoichiometry determination of the human SET1/MLL histone methyltransferase complexes. Mol Cell Biol. 2013;33(10):2067-2077. PMID: 23508102.
41. Strahl B.D., Allis C.D. The language of covalent histone modifications. Nature. 2000;403(6765):41-45. PMID: 10638745.
42. Jenuwein T., Allis C.D. Translating the histone code. Science. 2001;293(5532):1074-1080. PMID: 11498575.
43. Couture J.F., Collazo E., Trievel R.C. Molecular recognition of histone H3 by the WD40 protein WDR5. Nat Struct Mol Biol. 2006;13(8):698-703. PMID: 16829960.
44. Han Z., Guo L., Wang H., Shen Y., Deng X.W., Chai J. Structural basis for the specific recognition of methylated histone H3 lysine 4 by the WD-40 protein WDR5. Mol Cell. 2006;22(1):137-144. PMID: 16600877.
45. Ruthenburg A.J., Wang W., Graybosch D.M., Li H., Allis C.D., Patel D.J., Verdine G.L. Histone H3 recognition and presentation by the WDR5 module of the MLL1 complex. Nat Struct Mol Biol. 2006;13(8):704-712. PMID: 16829959.
46. Guccione E., Bassi C., Casadio F., Martinato F., Cesaroni M., Schuchlautz H., Luscher B., Amati B. Methylation of histone H3R2 by PRMT6 and H3K4 by an MLL complex are mutually exclusive. Nature. 2007;449(7164):933-937. PMID: 17898714.
47. Hyllus D., Stein C., Schnabel K., Schiltz E., Imhof A., Dou Y., Hsieh J., Bauer U.M. PRMT6-mediated methylation of R2 in histone H3 antagonizes H3 K4 trimethylation. Genes Dev. 2007;21(24):3369-3380. PMID: 18079182.
48. Migliori V., Muller J., Phalke S., Low D., Bezzi M., Mok W.C., Sahu S.K., Gunaratne J., Capasso P., Bassi C., Cecatiello V., De Marco A., Blackstock W., Kuznetsov V., Amati B., Mapelli M., Guccione E. Symmetric dimethylation of H3R2 is a newly identified histone mark that supports euchromatin maintenance. Nat Struct Mol Biol. 2012;19(2):136-144. PMID: 22231400.
49. Lorton B.M., Harijan R.K., Burgos E.S., Bonanno J.B., Almo S.C., Shechter D. A Binary Arginine Methylation Switch on Histone H3 Arginine 2 Regulates Its Interaction with WDR5. Biochemistry. 2020. PMID: 32207970.
50. Su J., Wang F., Cai Y., Jin J. The Functional Analysis of Histone Acetyltransferase MOF in Tumorigenesis. Int J Mol Sci. 2016;17(1). PMID: 26784169.

51. Smith E.R., Cayrou C., Huang R., Lane W.S., Cote J., Lucchesi J.C. A human protein complex homologous to the Drosophila MSL complex is responsible for the majority of histone H4 acetylation at lysine 16. Mol Cell Biol. 2005;25(21):9175-9188. PMID: 16227571.
52. Mendjan S., Taipale M., Kind J., Holz H., Gebhardt P., Schelder M., Vermeulen M., Buscaino A., Duncan K., Mueller J., Wilm M., Stunnenberg H.G., Saumweber H., Akhtar A. Nuclear pore components are involved in the transcriptional regulation of dosage compensation in Drosophila. Mol Cell. 2006;21(6):811-823. PMID: 16543150.
53. Cai Y., Jin J., Swanson S.K., Cole M.D., Choi S.H., Florens L., Washburn M.P., Conaway J.W., Conaway R.C. Subunit composition and substrate specificity of a MOF-containing histone acetyltransferase distinct from the male-specific lethal (MSL) complex. J Biol Chem. 2010;285(7):4268-4272. PMID: 20018852.
54. Raja S.J., Charapitsa I., Conrad T., Vaquerizas J.M., Gebhardt P., Holz H., Kadlec J., Fraterman S., Luscombe N.M., Akhtar A. The nonspecific lethal complex is a transcriptional regulator in Drosophila. Mol Cell. 2010;38(6):827-841. PMID: 20620954.
55. Tansey W.P. Mammalian MYC Proteins and Cancer. New Journal of Science. 2014;2014:1-27.
56. Marinkovic D., Marinkovic T., Mahr B., Hess J., Wirth T. Reversible lymphomagenesis in conditionally c-MYC expressing mice. Int J Cancer. 2004;110(3):336-342. PMID: 15095297.
57. Shachaf C.M., Kopelman A.M., Arvanitis C., Karlsson A., Beer S., Mandl S., Bachmann M.H., Borowsky A.D., Ruebner B., Cardiff R.D., Yang Q., Bishop J.M., Contag C.H., Felsher D.W. MYC inactivation uncovers pluripotent differentiation and tumour dormancy in hepatocellular cancer. Nature. 2004;431(7012):1112-1117. PMID: 15475948.
58. Lawlor E.R., Soucek L., Brown-Swigart L., Shchors K., Bialucha C.U., Evan G.I. Reversible kinetic analysis of Myc targets in vivo provides novel insights into Myc-mediated tumorigenesis. Cancer Res. 2006;66(9):4591-4601. PMID: 16651409.
59. Soucek L., Whitfield J.R., Sodir N.M., Masso-Valles D., Serrano E., Karnezis A.N., Swigart L.B., Evan G.I. Inhibition of Myc family proteins eradicates KRas-driven lung cancer in mice. Genes Dev. 2013;27(5):504-513. PMID: 23475959.
60. Herbst A., Hemann M.T., Tworkowski K.A., Salghetti S.E., Lowe S.W., Tansey W.P. A conserved element in Myc that negatively regulates its proapoptotic activity. EMBO Rep. 2005;6(2):177-183. PMID: 15678160.
61. Kalkat M., Resetca D., Lourenco C., Chan P.K., Wei Y., Shiah Y.J., Vitkin N., Tong Y., Sunnerhagen M., Done S.J., Boutros P.C., Raught B., Penn L.Z. MYC Protein Interactome Profiling Reveals Functionally Distinct Regions that Cooperate to Drive Tumorigenesis. Mol Cell. 2018;72(5):836-848 e837. PMID: 30415952.
62. Thomas L.R., Adams C.M., Wang J., Weissmiller A.M., Creighton J., Lorey S.L., Liu Q., Fesik S.W., Eischen C.M., Tansey W.P. Interaction of the oncoprotein transcription factor MYC with its chromatin cofactor WDR5 is essential for tumor maintenance. Proc Natl Acad Sci U S A. 2019;116(50):25260-25268. PMID: 31767764.
63. Blackwood E.M., Eisenman R.N. Max: a helix-loop-helix zipper protein that forms a sequence-specific DNA-binding complex with Myc. Science. 1991;251(4998):1211-1217. PMID: 2006410.
64. Amati B., Brooks M.W., Levy N., Littlewood T.D., Evan G.I., Land H. Oncogenic activity of the c-Myc protein requires dimerization with Max. Cell. 1993;72(2):233-245. PMID: 8425220.
65. Brenner C., Deplus R., Didelot C., Loriot A., Vire E., De Smet C., Gutierrez A., Danovi D., Bernard D., Boon T., Pelicci P.G., Amati B., Kouzarides T., de Launoit Y., Di Croce L., Fuks F. Myc represses transcription through recruitment of DNA methyltransferase corepressor. EMBO J. 2005;24(2):336-346. PMID: 15616584.
66. Peukert K., Staller P., Schneider A., Carmichael G., Hanel F., Eilers M. An alternative pathway for gene regulation by Myc. EMBO J. 1997;16(18):5672-5686. PMID: 9312026.
67. Staller P., Peukert K., Kiermaier A., Seoane J., Lukas J., Karsunky H., Moroy T., Bartek J., Massague J., Hanel F., Eilers M. Repression of p15INK4b expression by Myc through association with Miz-1. Nat Cell Biol. 2001;3(4):392-399. PMID: 11283613.

68. Herold S., Wanzel M., Beuger V., Frohme C., Beul D., Hillukkala T., Syvaoja J., Saluz H.P., Haenel F., Eilers M. Negative regulation of the mammalian UV response by Myc through association with Miz-1. Mol Cell. 2002;10(3):509-521. PMID: 12408820.
69. Cheng S.W., Davies K.P., Yung E., Beltran R.J., Yu J., Kalpana G.V. c-MYC interacts with INI1/hSNF5 and requires the SWI/SNF complex for transactivation function. Nat Genet. 1999;22(1):102-105. PMID: 10319872.
70. Weissmiller A.M., Wang J., Lorey S.L., Howard G.C., Martinez E., Liu Q., Tansey W.P. Inhibition of MYC by the SMARCB1 tumor suppressor. Nat Commun. 2019;10(1):2014. PMID: 31043611.
71. Kurland J.F., Tansey W.P. Myc-mediated transcriptional repression by recruitment of histone deacetylase. Cancer Res. 2008;68(10):3624-3629. PMID: 18483244.
72. McMahon S.B., Van Buskirk H.A., Dugan K.A., Copeland T.D., Cole M.D. The novel ATM-related protein TRRAP is an essential cofactor for the c-Myc and E2F oncoproteins. Cell. 1998;94(3):363-374. PMID: 9708738.
73. Liu X., Tesfai J., Evrard Y.A., Dent S.Y., Martinez E. c-Myc transformation domain recruits the human STAGA complex and requires TRRAP and GCN5 acetylase activity for transcription activation. J Biol Chem. 2003;278(22):20405-20412. PMID: 12660246.
74. Richart L., Carrillo-de Santa Pau E., Rio-Machin A., de Andres M.P., Cigudosa J.C., Lobo V.J.S., Real F.X. BPTF is required for c-MYC transcriptional activity and in vivo tumorigenesis. Nat Commun. 2016;7:10153. PMID: 26729287.
75. Gerlach J.M., Furrer M., Gallant M., Birkel D., Baluapuri A., Wolf E., Gallant P. PAF1 complex component Leo1 helps recruit Drosophila Myc to promoters. Proc Natl Acad Sci U S A. 2017;114(44):E9224-E9232. PMID: 29078288.
76. Thomas L.R., Foshage A.M., Weissmiller A.M., Popay T.M., Grieb B.C., Qualls S.J., Ng V., Carboneau B., Lorey S., Eischen C.M., Tansey W.P. Interaction of MYC with host cell factor-1 is mediated by the evolutionarily conserved Myc box IV motif. Oncogene. 2016;35(27):3613-3618. PMID: 26522729.
77. Popay T.M., Wang J., Adams C.M., Howard G.C., Codreanu S.G., Sherrod S.D., McLean J.A., Thomas L.R., Lorey S.L., Machida Y.J., Weissmiller A.M., Eischen C.M., Liu Q., Tansey W.P. MYC regulates ribosome biogenesis and mitochondrial gene expression programs through its interaction with host cell factor-1. Elife. 2021;10. PMID: 33416496.
78. Eberhardy S.R., Farnham P.J. Myc recruits P-TEFb to mediate the final step in the transcriptional activation of the cad promoter. J Biol Chem. 2002;277(42):40156-40162. PMID: 12177005.
79. Thomas L.R., Wang Q., Grieb B.C., Phan J., Foshage A.M., Sun Q., Olejniczak E.T., Clark T., Dey S., Lorey S., Alicie B., Howard G.C., Cawthon B., Ess K.C., Eischen C.M., Zhao Z., Fesik S.W., Tansey W.P. Interaction with WDR5 promotes target gene recognition and tumorigenesis by MYC. Mol Cell. 2015;58(3):440-452. PMID: 25818646.
80. Lorenzin F., Benary U., Baluapuri A., Walz S., Jung L.A., von Eyss B., Kisker C., Wolf J., Eilers M., Wolf E. Different promoter affinities account for specificity in MYC-dependent gene regulation. Elife. 2016;5. PMID: 27460974.
81. Thomas L.R., Adams C.M., Fesik S.W., Eischen C.M., Tansey W.P. Targeting MYC through WDR5. Mol Cell Oncol. 2020;7(2):1709388. PMID: 32158922.
82. Bryan A.F., Wang J., Howard G.C., Guarnaccia A.D., Woodley C.M., Aho E.R., Rellinger E.J., Matlock B.K., Flaherty D.K., Lorey S.L., Chung D.H., Fesik S.W., Liu Q., Weissmiller A.M., Tansey W.P. WDR5 is a conserved regulator of protein synthesis gene expression. Nucleic Acids Res. 2020. PMID: 31996893.
83. Oh E., Mark K.G., Mocciaro A., Watson E.R., Prabu J.R., Cha D.D., Kampmann M., Gamarra N., Zhou C.Y., Rape M. Gene expression and cell identity controlled by anaphase-promoting complex. Nature. 2020;579(7797):136-140. PMID: 32076268.
84. Wu M.Z., Tsai Y.P., Yang M.H., Huang C.H., Chang S.Y., Chang C.C., Teng S.C., Wu K.J. Interplay between HDAC3 and WDR5 is essential for hypoxia-induced epithelial-mesenchymal transition. Mol Cell. 2011;43(5):811-822. PMID: 21884981.

85. Malek R., Gajula R.P., Williams R.D., Nghiem B., Simons B.W., Nugent K., Wang H., Taparra K., Lemtiri-Chlieh G., Yoon A.R., True L., An S.S., DeWeese T.L., Ross A.E., Schaeffer E.M., Pienta K.J., Hurley P.J., Morrissey C., Tran P.T. TWIST1-WDR5-Hottip Regulates Hoxa9 Chromatin to Facilitate Prostate Cancer Metastasis. Cancer Res. 2017;77(12):3181-3193. PMID: 28484075.
86. Hayashida N. Set1/MLL complex is indispensable for the transcriptional ability of heat shock transcription factor 2. Biochem Biophys Res Commun. 2015;467(4):805-812. PMID: 26478434.
87. Thompson B.A., Tremblay V., Lin G., Bochar D.A. CHD8 is an ATP-dependent chromatin remodeling factor that regulates beta-catenin target genes. Mol Cell Biol. 2008;28(12):3894-3904. PMID: 18378692.
88. Yates J.A., Menon T., Thompson B.A., Bochar D.A. Regulation of HOXA2 gene expression by the ATP-dependent chromatin remodeling enzyme CHD8. FEBS Lett. 2010;584(4):689-693. PMID: 20085832.
89. Zhao C., Dong C., Frah M., Deng Y., Marie C., Zhang F., Xu L., Ma Z., Dong X., Lin Y., Koenig S., Nait-Oumesmar B., Martin D.M., Wu L.N., Xin M., Zhou W., Parras C., Lu Q.R. Dual Requirement of CHD8 for Chromatin Landscape Establishment and Histone Methyltransferase Recruitment to Promote CNS Myelination and Repair. Dev Cell. 2018;45(6):753-768 e758. PMID: 29920279.
90. Wang L., Du Y., Ward J.M., Shimbo T., Lackford B., Zheng X., Miao Y.L., Zhou B., Han L., Fargo D.C., Jothi R., Williams C.J., Wade P.A., Hu G. INO80 facilitates pluripotency gene activation in embryonic stem cell self-renewal, reprogramming, and blastocyst development. Cell Stem Cell. 2014;14(5):575-591. PMID: 24792115.
91. Schulz Y., Freese L., Manz J., Zoll B., Volter C., Brockmann K., Bogershausen N., Becker J., Wollnik B., Pauli S. CHARGE and Kabuki syndromes: a phenotypic and molecular link. Hum Mol Genet. 2014;23(16):4396-4405. PMID: 24705355.
92. Yan S., Thienthanasit R., Chen D., Engelen E., Bruhl J., Crossman D.K., Kesterson R., Wang Q., Bouazoune K., Jiao K. CHD7 regulates cardiovascular development through ATP-dependent and -independent activities. Proc Natl Acad Sci U S A. 2020;117(46):28847-28858. PMID: 33127760.
93. Bode D., Yu L., Tate P., Pardo M., Choudhary J. Characterization of Two Distinct Nucleosome Remodeling and Deacetylase (NuRD) Complex Assemblies in Embryonic Stem Cells. Mol Cell Proteomics. 2016;15(3):878-891. PMID: 26714524.
94. Ee L.S., McCannell K.N., Tang Y., Fernandes N., Hardy W.R., Green M.R., Chu F., Fazzio T.G. An Embryonic Stem Cell-Specific NuRD Complex Functions through Interaction with WDR5. Stem Cell Reports. 2017;8(6):1488-1496. PMID: 28528697.
95. Basta J., Rauchman M. The nucleosome remodeling and deacetylase complex in development and disease. Transl Res. 2015;165(1):36-47. PMID: 24880148.
96. Suganuma T., Gutierrez J.L., Li B., Florens L., Swanson S.K., Washburn M.P., Abmayr S.M., Workman J.L. ATAC is a double histone acetyltransferase complex that stimulates nucleosome sliding. Nat Struct Mol Biol. 2008;15(4):364-372. PMID: 18327268.
97. Wang Y.L., Faiola F., Xu M., Pan S., Martinez E. Human ATAC Is a GCN5/PCAF-containing acetylase complex with a novel NC2-like histone fold module that interacts with the TATA-binding protein. J Biol Chem. 2008;283(49):33808-33815. PMID: 18838386.
98. Gao Z., Zhang J., Bonasio R., Strino F., Sawai A., Parisi F., Kluger Y., Reinberg D. PCGF homologs, CBX proteins, and RYBP define functionally distinct PRC1 family complexes. Mol Cell. 2012;45(3):344-356. PMID: 22325352.
99. Qin J., Whyte W.A., Anderssen E., Apostolou E., Chen H.H., Akbarian S., Bronson R.T., Hochedlinger K., Ramaswamy S., Young R.A., Hock H. The polycomb group protein L3mbtl2 assembles an atypical PRC1-family complex that is essential in pluripotent stem cells and early development. Cell Stem Cell. 2012;11(3):319-332. PMID: 22770845.
100. Hauri S., Comoglio F., Seimiya M., Gerstung M., Glatter T., Hansen K., Aebersold R., Paro R., Gstaiger M., Beisel C. A High-Density Map for Navigating the Human Polycomb Complexome. Cell Rep. 2016;17(2):583-595. PMID: 27705803.

101. Aranda S., Mas G., Di Croce L. Regulation of gene transcription by Polycomb proteins. Sci Adv. 2015;1(11):e1500737. PMID: 26665172.
102. Vilhais-Neto G.C., Fournier M., Plassat J.L., Sardiu M.E., Saraf A., Garnier J.M., Maruhashi M., Florens L., Washburn M.P., Pourquie O. The WHHERE coactivator complex is required for retinoic acid-dependent regulation of embryonic symmetry. Nat Commun. 2017;8(1):728. PMID: 28959017.
103. Chung C.Y., Sun Z., Mullokandov G., Bosch A., Qadeer Z.A., Cihan E., Rapp Z., Parsons R., Aguirre-Ghiso J.A., Farias E.F., Brown B.D., Gaspar-Maia A., Bernstein E. Cbx8 Acts Non-canonically with Wdr5 to Promote Mammary Tumorigenesis. Cell Rep. 2016;16(2):472-486. PMID: 27346354.
104. Shen S.M., Zhang C., Ge M.K., Dong S.S., Xia L., He P., Zhang N., Ji Y., Yang S., Yu Y., Zheng J.K., Yu J.X., Xia Q., Chen G.Q. PTENalpha and PTENbeta promote carcinogenesis through WDR5 and H3K4 trimethylation. Nat Cell Biol. 2019;21(11):1436-1448. PMID: 31685992.
105. Wang K.C., Yang Y.W., Liu B., Sanyal A., Corces-Zimmerman R., Chen Y., Lajoie B.R., Protacio A., Flynn R.A., Gupta R.A., Wysocka J., Lei M., Dekker J., Helms J.A., Chang H.Y. A long noncoding RNA maintains active chromatin to coordinate homeotic gene expression. Nature. 2011;472(7341):120-124. PMID: 21423168.
106. Yang Y.W., Flynn R.A., Chen Y., Qu K., Wan B., Wang K.C., Lei M., Chang H.Y. Essential role of lncRNA binding for WDR5 maintenance of active chromatin and embryonic stem cell pluripotency. Elife. 2014;3:e02046. PMID: 24521543.
107. Gomez J.A., Wapinski O.L., Yang Y.W., Bureau J.F., Gopinath S., Monack D.M., Chang H.Y., Brahic M., Kirkegaard K. The NeST long ncRNA controls microbial susceptibility and epigenetic activation of the interferon-gamma locus. Cell. 2013;152(4):743-754. PMID: 23415224.
108. Sun T.T., He J., Liang Q., Ren L.L., Yan T.T., Yu T.C., Tang J.Y., Bao Y.J., Hu Y., Lin Y., Sun D., Chen Y.X., Hong J., Chen H., Zou W., Fang J.Y. LncRNA GClnc1 Promotes Gastric Carcinogenesis and May Act as a Modular Scaffold of WDR5 and KAT2A Complexes to Specify the Histone Modification Pattern. Cancer Discov. 2016;6(7):784-801. PMID: 27147598.
109. Gu P., Chen X., Xie R., Han J., Xie W., Wang B., Dong W., Chen C., Yang M., Jiang J., Chen Z., Huang J., Lin T. lncRNA HOXD-AS1 Regulates Proliferation and Chemo-Resistance of Castration-Resistant Prostate Cancer via Recruiting WDR5. Mol Ther. 2017;25(8):1959-1973. PMID: 28487115.
110. Wang Y.Y., Liu L.J., Zhong B., Liu T.T., Li Y., Yang Y., Ran Y., Li S., Tien P., Shu H.B. WDR5 is essential for assembly of the VISA-associated signaling complex and virus-triggered IRF3 and NF-kappaB activation. Proc Natl Acad Sci U S A. 2010;107(2):815-820. PMID: 20080758.
111. Bailey J.K., Fields A.T., Cheng K., Lee A., Wagenaar E., Lagrois R., Schmidt B., Xia B., Ma D. WD repeat-containing protein 5 (WDR5) localizes to the midbody and regulates abscission. J Biol Chem. 2015;290(14):8987-9001. PMID: 25666610.
112. Kulkarni S.S., Griffin J.N., Date P.P., Liem K.F., Jr., Khokha M.K. WDR5 Stabilizes Actin Architecture to Promote Multiciliated Cell Formation. Dev Cell. 2018;46(5):595-610 e593. PMID: 30205038.
113. Ali A., Veeranki S.N., Tyagi S. A SET-domain-independent role of WRAD complex in cell-cycle regulatory function of mixed lineage leukemia. Nucleic Acids Res. 2014;42(12):7611-7624. PMID: 24880690.
114. Zaidi S., Choi M., Wakimoto H., Ma L., Jiang J., Overton J.D., Romano-Adesman A., Bjornson R.D., Breitbart R.E., Brown K.K., Carriero N.J., Cheung Y.H., Deanfield J., DePalma S., Fakhro K.A., Glessner J., Hakonarson H., Italia M.J., Kaltman J.R., Kaski J., Kim R., Kline J.K., Lee T., Leipzig J., Lopez A., Mane S.M., Mitchell L.E., Newburger J.W., Parfenov M., Pe'er I., Porter G., Roberts A.E., Sachidanandam R., Sanders S.J., Seiden H.S., State M.W., Subramanian S., Tikhonova I.R., Wang W., Warburton D., White P.S., Williams I.A., Zhao H., Seidman J.G., Brueckner M., Chung W.K., Gelb B.D., Goldmuntz E., Seidman C.E., Lifton R.P.

De novo mutations in histone-modifying genes in congenital heart disease. Nature. 2013;498(7453):220-223. PMID: 23665959.
115. Kulkarni S.S., Khokha M.K. WDR5 regulates left-right patterning via chromatin-dependent and -independent functions. Development. 2018;145(23). PMID: 30377171.
116. Lundby A., Lage K., Weinert B.T., Bekker-Jensen D.B., Secher A., Skovgaard T., Kelstrup C.D., Dmytriyev A., Choudhary C., Lundby C., Olsen J.V. Proteomic analysis of lysine acetylation sites in rat tissues reveals organ specificity and subcellular patterns. Cell Rep. 2012;2(2):419-431. PMID: 22902405.
117. Ma D., George C.X., Nomburg J.L., Pfaller C.K., Cattaneo R., Samuel C.E. Upon Infection, Cellular WD Repeat-Containing Protein 5 (WDR5) Localizes to Cytoplasmic Inclusion Bodies and Enhances Measles Virus Replication. J Virol. 2018;92(5). PMID: 29237839.
118. Zhou Y., Su J.M., Samuel C.E., Ma D. Measles Virus Forms Inclusion Bodies with Properties of Liquid Organelles. J Virol. 2019;93(21). PMID: 31375591.
119. Yang B., Liu X.J., Yao Y., Jiang X., Wang X.Z., Yang H., Sun J.Y., Miao Y., Wang W., Huang Z.L., Wang Y., Tang Q., Rayner S., Britt W.J., McVoy M.A., Luo M.H., Zhao F. WDR5 Facilitates Human Cytomegalovirus Replication by Promoting Capsid Nuclear Egress. J Virol. 2018;92(9). PMID: 29437978.
120. Gao W., Jia Z., Tian Y., Yang P., Sun H., Wang C., Ding Y., Zhang M., Zhang Y., Yang D., Tian Z., Zhou J., Ruan Z., Wu Y., Ni B. HBx Protein Contributes to Liver Carcinogenesis by H3K4me3 Modification Through Stabilizing WD Repeat Domain 5 Protein. Hepatology. 2020;71(5):1678-1695. PMID: 31544250.
121. Qin S., Liu Y., Tempel W., Eram M.S., Bian C., Liu K., Senisterra G., Crombet L., Vedadi M., Min J. Structural basis for histone mimicry and hijacking of host proteins by influenza virus protein NS1. Nat Commun. 2014;5:3952. PMID: 24853335.
122. Wang R.N., Green J., Wang Z., Deng Y., Qiao M., Peabody M., Zhang Q., Ye J., Yan Z., Denduluri S., Idowu O., Li M., Shen C., Hu A., Haydon R.C., Kang R., Mok J., Lee M.J., Luu H.L., Shi L.L. Bone Morphogenetic Protein (BMP) signaling in development and human diseases. Genes Dis. 2014;1(1):87-105. PMID: 25401122.
123. Tian W., Fan Z., Li J., Hao C., Li M., Xu H., Wu X., Zhou B., Zhang L., Fang M., Xu Y. Myocardin-related transcription factor A (MRTF-A) plays an essential role in hepatic stellate cell activation by epigenetically modulating TGF-beta signaling. Int J Biochem Cell Biol. 2016;71:35-43. PMID: 26693892.
124. Chen H., Lorton B., Gupta V., Shechter D. A TGFbeta-PRMT5-MEP50 axis regulates cancer cell invasion through histone H3 and H4 arginine methylation coupled transcriptional activation and repression. Oncogene. 2017;36(3):373-386. PMID: 27270440.
125. Punzi S., Balestrieri C., D'Alesio C., Bossi D., Dellino G.I., Gatti E., Pruneri G., Criscitiello C., Lovati G., Meliksetyan M., Carugo A., Curigliano G., Natoli G., Pelicci P.G., Lanfrancone L. WDR5 inhibition halts metastasis dissemination by repressing the mesenchymal phenotype of breast cancer cells. Breast Cancer Res. 2019;21(1):123. PMID: 31752957.
126. Shimoda H., Doi S., Nakashima A., Sasaki K., Doi T., Masaki T. Inhibition of the H3K4 methyltransferase MLL1/WDR5 complex attenuates renal senescence in ischemia reperfusion mice by reduction of p16(INK4a). Kidney Int. 2019;96(5):1162-1175. PMID: 31570196.
127. Tan X., Chen S., Wu J., Lin J., Pan C., Ying X., Pan Z., Qiu L., Liu R., Geng R., Huang W. PI3K/AKT-mediated upregulation of WDR5 promotes colorectal cancer metastasis by directly targeting ZNF407. Cell Death Dis. 2017;8(3):e2686. PMID: 28300833.
128. Huang D., Chen X., Chen X., Qu Y., Wang Y., Yang Y., Cheng Y. WDR5 Promotes Proliferation and Correlates with Poor Prognosis in Oesophageal Squamous Cell Carcinoma. Onco Targets Ther. 2020;13:10525-10534. PMID: 33116631.
129. Kikani C.K., Wu X., Paul L., Sabic H., Shen Z., Shakya A., Keefe A., Villanueva C., Kardon G., Graves B., Tantin D., Rutter J. Pask integrates hormonal signaling with histone modification via Wdr5 phosphorylation to drive myogenesis. Elife. 2016;5. PMID: 27661449.

130. Kikani C.K., Wu X., Fogarty S., Kang S.A.W., Dephoure N., Gygi S.P., Sabatini D.M., Rutter J. Activation of PASK by mTORC1 is required for the onset of the terminal differentiation program. Proc Natl Acad Sci U S A. 2019;116(21):10382-10391. PMID: 31072927.
131. Tsherniak A., Vazquez F., Montgomery P.G., Weir B.A., Kryukov G., Cowley G.S., Gill S., Harrington W.F., Pantel S., Krill-Burger J.M., Meyers R.M., Ali L., Goodale A., Lee Y., Jiang G., Hsiao J., Gerath W.F.J., Howell S., Merkel E., Ghandi M., Garraway L.A., Root D.E., Golub T.R., Boehm J.S., Hahn W.C. Defining a Cancer Dependency Map. Cell. 2017;170(3):564-576 e516. PMID: 28753430.
132. Broad D. DepMap 20Q4 Public2020.
133. Dai B., Xiao Z., Zhu G., Mao B., Huang H., Guan F., Lin Z., Peng W., Liang X., Zhang B., Hu Z. WD Repeat Domain 5 Promotes Invasion, Metastasis and Tumor Growth in Glioma Through Up-Regulated Zinc Finger E-Box Binding Homeobox 1 Expression. Cancer Manag Res. 2020;12:3223-3235. PMID: 32440219.
134. Xu W., Wang L., An Y., Ye J. Expression of WD Repeat Domain 5 (WDR5) is Associated with Progression and Reduced Prognosis in Papillary Thyroid Carcinoma. Med Sci Monit. 2019;25:3762-3770. PMID: 31107859.
135. Neilsen B.K., Chakraborty B., McCall J.L., Frodyma D.E., Sleightholm R.L., Fisher K.W., Lewis R.E. WDR5 supports colon cancer cells by promoting methylation of H3K4 and suppressing DNA damage. BMC Cancer. 2018;18(1):673. PMID: 29925347.
136. Wu Y., Diao P., Li Z., Zhang W., Wang D., Wang Y., Cheng J. Overexpression of WD repeat domain 5 associates with aggressive clinicopathological features and unfavorable prognosis in head neck squamous cell carcinoma. J Oral Pathol Med. 2018;47(5):502-510. PMID: 29569374.
137. Dai X., Guo W., Zhan C., Liu X., Bai Z., Yang Y. WDR5 Expression Is Prognostic of Breast Cancer Outcome. PLoS One. 2015;10(9):e0124964. PMID: 26355959.
138. Cui Z., Li H., Liang F., Mu C., Mu Y., Zhang X., Liu J. Effect of high WDR5 expression on the hepatocellular carcinoma prognosis. Oncol Lett. 2018;15(5):7864-7870. PMID: 29731905.
139. Wang F., Zhang J., Ke X., Peng W., Zhao G., Peng S., Xu J., Xu B., Cui H. WDR5-Myc axis promotes the progression of glioblastoma and neuroblastoma by transcriptional activating CARM1. Biochem Biophys Res Commun. 2020;523(3):699-706. PMID: 31948749.
140. Sun Y., Bell J.L., Carter D., Gherardi S., Poulos R.C., Milazzo G., Wong J.W., Al-Awar R., Tee A.E., Liu P.Y., Liu B., Atmadibrata B., Wong M., Trahair T., Zhao Q., Shohet J.M., Haupt Y., Schulte J.H., Brown P.J., Arrowsmith C.H., Vedadi M., MacKenzie K.L., Huttelmaier S., Perini G., Marshall G.M., Braithwaite A., Liu T. WDR5 Supports an N-Myc Transcriptional Complex That Drives a Protumorigenic Gene Expression Signature in Neuroblastoma. Cancer Res. 2015;75(23):5143-5154. PMID: 26471359.
141. Chen X., Xie W., Gu P., Cai Q., Wang B., Xie Y., Dong W., He W., Zhong G., Lin T., Huang J. Upregulated WDR5 promotes proliferation, self-renewal and chemoresistance in bladder cancer via mediating H3K4 trimethylation. Sci Rep. 2015;5:8293. PMID: 25656485.
142. Sun W., Guo F., Liu M. Up-regulated WDR5 promotes gastric cancer formation by induced cyclin D1 expression. J Cell Biochem. 2018;119(4):3304-3316. PMID: 29125890.
143. Ge Z., Song E.J., Kawasawa Y.I., Li J., Dovat S., Song C. WDR5 high expression and its effect on tumorigenesis in leukemia. Oncotarget. 2016;7(25):37740-37754. PMID: 27192115.
144. Kim J.Y., Banerjee T., Vinckevicius A., Luo Q., Parker J.B., Baker M.R., Radhakrishnan I., Wei J.J., Barish G.D., Chakravarti D. A role for WDR5 in integrating threonine 11 phosphorylation to lysine 4 methylation on histone H3 during androgen signaling and in prostate cancer. Mol Cell. 2014;54(4):613-625. PMID: 24793694.
145. Penalosa-Ruiz G., Bousgouni V., Gerlach J.P., Waarlo S., van de Ven J.V., Veenstra T.E., Silva J.C.R., van Heeringen S.J., Bakal C., Mulder K.W., Veenstra G.J.C. WDR5, BRCA1, and BARD1 Co-regulate the DNA Damage Response and Modulate the Mesenchymal-to-Epithelial Transition during Early Reprogramming. Stem Cell Reports. 2019;12(4):743-756. PMID: 30880078.

146. Yao R., Wang Y., Han D., Ma Y., Ma M., Zhao Y., Tan J., Lu J., Xu G., Li X. Lysines 207 and 325 methylation of WDR5 catalyzed by SETD6 promotes breast cancer cell proliferation and migration. Oncol Rep. 2018;40(5):3069-3077. PMID: 30226578.
147. Grebien F., Vedadi M., Getlik M., Giambruno R., Grover A., Avellino R., Skucha A., Vittori S., Kuznetsova E., Smil D., Barsyte-Lovejoy D., Li F., Poda G., Schapira M., Wu H., Dong A., Senisterra G., Stukalov A., Huber K.V.M., Schonegger A., Marcellus R., Bilban M., Bock C., Brown P.J., Zuber J., Bennett K.L., Al-Awar R., Delwel R., Nerlov C., Arrowsmith C.H., Superti-Furga G. Pharmacological targeting of the Wdr5-MLL interaction in C/EBPalpha N-terminal leukemia. Nat Chem Biol. 2015;11(8):571-578. PMID: 26167872.
148. Bennett R.L., Licht J.D. Targeting Epigenetics in Cancer. Annu Rev Pharmacol Toxicol. 2018;58:187-207. PMID: 28992434.
149. Carugo A., Genovese G., Seth S., Nezi L., Rose J.L., Bossi D., Cicalese A., Shah P.K., Viale A., Pettazzoni P.F., Akdemir K.C., Bristow C.A., Robinson F.S., Tepper J., Sanchez N., Gupta S., Estecio M.R., Giuliani V., Dellino G.I., Riva L., Yao W., Di Francesco M.E., Green T., D'Alesio C., Corti D., Kang Y., Jones P., Wang H., Fleming J.B., Maitra A., Pelicci P.G., Chin L., DePinho R.A., Lanfrancone L., Heffernan T.P., Draetta G.F. In Vivo Functional Platform Targeting Patient-Derived Xenografts Identifies WDR5-Myc Association as a Critical Determinant of Pancreatic Cancer. Cell Rep. 2016;16(1):133-147. PMID: 27320920.
150. Macdonald J.D., Chacon Simon S., Han C., Wang F., Shaw J.G., Howes J.E., Sai J., Yuh J.P., Camper D., Alicie B.M., Alvarado J., Nikhar S., Payne W., Aho E.R., Bauer J.A., Zhao B., Phan J., Thomas L.R., Rossanese O.W., Tansey W.P., Waterson A.G., Stauffer S.R., Fesik S.W. Discovery and Optimization of Salicylic Acid-Derived Sulfonamide Inhibitors of the WD Repeat-Containing Protein 5-MYC Protein-Protein Interaction. J Med Chem. 2019;62(24):11232-11259. PMID: 31724864.
151. Chacon Simon S., Wang F., Thomas L.R., Phan J., Zhao B., Olejniczak E.T., Macdonald J.D., Shaw J.G., Schlund C., Payne W., Creighton J., Stauffer S.R., Waterson A.G., Tansey W.P., Fesik S.W. Discovery of WD Repeat-Containing Protein 5 (WDR5)-MYC Inhibitors Using Fragment-Based Methods and Structure-Based Design. J Med Chem. 2020;63(8):4315-4333. PMID: 32223236.
152. Karatas H., Townsend E.C., Cao F., Chen Y., Bernard D., Liu L., Lei M., Dou Y., Wang S. High-affinity, small-molecule peptidomimetic inhibitors of MLL1/WDR5 protein-protein interaction. J Am Chem Soc. 2013;135(2):669-682. PMID: 23210835.
153. Karatas H., Li Y., Liu L., Ji J., Lee S., Chen Y., Yang J., Huang L., Bernard D., Xu J., Townsend E.C., Cao F., Ran X., Li X., Wen B., Sun D., Stuckey J.A., Lei M., Dou Y., Wang S. Discovery of a Highly Potent, Cell-Permeable Macrocyclic Peptidomimetic (MM-589) Targeting the WD Repeat Domain 5 Protein (WDR5)-Mixed Lineage Leukemia (MLL) Protein-Protein Interaction. J Med Chem. 2017;60(12):4818-4839. PMID: 28603984.
154. Thiel A.T., Blessington P., Zou T., Feather D., Wu X., Yan J., Zhang H., Liu Z., Ernst P., Koretzky G.A., Hua X. MLL-AF9-induced leukemogenesis requires coexpression of the wild-type Mll allele. Cancer Cell. 2010;17(2):148-159. PMID: 20159607.
155. Chen Y., Anastassiadis K., Kranz A., Stewart A.F., Arndt K., Waskow C., Yokoyama A., Jones K., Neff T., Lee Y., Ernst P. MLL2, Not MLL1, Plays a Major Role in Sustaining MLL-Rearranged Acute Myeloid Leukemia. Cancer Cell. 2017;31(6):755-770 e756. PMID: 28609655.
156. Senisterra G., Wu H., Allali-Hassani A., Wasney G.A., Barsyte-Lovejoy D., Dombrovski L., Dong A., Nguyen K.T., Smil D., Bolshan Y., Hajian T., He H., Seitova A., Chau I., Li F., Poda G., Couture J.F., Brown P.J., Al-Awar R., Schapira M., Arrowsmith C.H., Vedadi M. Small-molecule inhibition of MLL activity by disruption of its interaction with WDR5. Biochem J. 2013;449(1):151-159. PMID: 22989411.
157. Bolshan Y., Getlik M., Kuznetsova E., Wasney G.A., Hajian T., Poda G., Nguyen K.T., Wu H., Dombrovski L., Dong A., Senisterra G., Schapira M., Arrowsmith C.H., Brown P.J., Al-Awar R., Vedadi M., Smil D. Synthesis, Optimization, and Evaluation of Novel Small Molecules as Antagonists of WDR5-MLL Interaction. ACS Med Chem Lett. 2013;4(3):353-357. PMID: 24900672.

158. Getlik M., Smil D., Zepeda-Velazquez C., Bolshan Y., Poda G., Wu H., Dong A., Kuznetsova E., Marcellus R., Senisterra G., Dombrovski L., Hajian T., Kiyota T., Schapira M., Arrowsmith C.H., Brown P.J., Vedadi M., Al-Awar R. Structure-Based Optimization of a Small Molecule Antagonist of the Interaction Between WD Repeat-Containing Protein 5 (WDR5) and Mixed-Lineage Leukemia 1 (MLL1). J Med Chem. 2016;59(6):2478-2496. PMID: 26958703.
159. Li D.D., Chen W.L., Wang Z.H., Xie Y.Y., Xu X.L., Jiang Z.Y., Zhang X.J., You Q.D., Guo X.K. High-affinity small molecular blockers of mixed lineage leukemia 1 (MLL1)-WDR5 interaction inhibit MLL1 complex H3K4 methyltransferase activity. Eur J Med Chem. 2016;124:480-489. PMID: 27598236.
160. Li D.D., Wang Z.H., Chen W.L., Xie Y.Y., You Q.D., Guo X.K. Structure-based design of ester compounds to inhibit MLL complex catalytic activity by targeting mixed lineage leukemia 1 (MLL1)-WDR5 interaction. Bioorg Med Chem. 2016;24(22):6109-6118. PMID: 27720555.
161. Chen W.L., Li D.D., Wang Z.H., Xu X.L., Zhang X.J., Jiang Z.Y., Guo X.K., You Q.D. Design, synthesis, and initial evaluation of affinity-based small molecular probe for detection of WDR5. Bioorg Chem. 2017;76:380-385. PMID: 29241110.
162. Zhu J., Sammons M.A., Donahue G., Dou Z., Vedadi M., Getlik M., Barsyte-Lovejoy D., Al-awar R., Katona B.W., Shilatifard A., Huang J., Hua X., Arrowsmith C.H., Berger S.L. Gain-of-function p53 mutants co-opt chromatin pathways to drive cancer growth. Nature. 2015;525(7568):206-211. PMID: 26331536.
163. Lin T.B., Lai C.Y., Hsieh M.C., Ho Y.C., Wang H.H., Yang P.S., Cheng J.K., Chen G.D., Ng S.C., Peng H.Y. Inhibiting MLL1-WDR5 interaction ameliorates neuropathic allodynia by attenuating histone H3 lysine 4 trimethylation-dependent spinal mGluR5 transcription. Pain. 2020. PMID: 32345914.
164. Cao Q., Wang W., Williams J.B., Yang F., Wang Z.J., Z. Y. Targeting histone K4 trimethylation for treatment of cognitive and synaptic deficits in mouse models of Alzheimer's disease. Sci Adv. 2020;6(50).
165. Han X., Xiang J., Li C., Wang J., Wang C., Zhang Y., Li Z., Lu Z., Yue Y., Li X. MLL1 combined with GSK3 and MAP2K inhibition improves the development of in vitro-fertilized embryos. Theriogenology. 2020;146:58-70. PMID: 32059151.
166. Wang F., Jeon K.O., Salovich J.M., Macdonald J.D., Alvarado J., Gogliotti R.D., Phan J., Olejniczak E.T., Sun Q., Wang S., Camper D., Yuh J.P., Shaw J.G., Sai J., Rossanese O.W., Tansey W.P., Stauffer S.R., Fesik S.W. Discovery of Potent 2-Aryl-6,7-dihydro-5 H-pyrrolo[1,2-a]imidazoles as WDR5-WIN-Site Inhibitors Using Fragment-Based Methods and Structure-Based Design. J Med Chem. 2018;61(13):5623-5642. PMID: 29889518.
167. Tian J., Teuscher K.B., Aho E.R., Alvarado J.R., Mills J.J., Meyers K.M., Gogliotti R.D., Han C., Macdonald J.D., Sai J., Shaw J.G., Sensintaffar J.L., Zhao B., Rietz T.A., Thomas L.R., Payne W.G., Moore W.J., Stott G.M., Kondo J., Inoue M., Coffey R.J., Tansey W.P., Stauffer S.R., Lee T., Fesik S.W. Discovery and Structure-Based Optimization of Potent and Selective WD Repeat Domain 5 (WDR5) Inhibitors Containing a Dihydroisoquinolinone Bicyclic Core. J Med Chem. 2020;63(2):656-675. PMID: 31858797.
168. Morgenstern J.P., Land H. Advanced mammalian gene transfer: high titre retroviral vectors with multiple drug selection markers and a complementary helper-free packaging cell line. Nucleic Acids Res. 1990;18(12):3587-3596. PMID: 2194165.
169. Weintraub A.S., Li C.H., Zamudio A.V., Sigova A.A., Hannett N.M., Day D.S., Abraham B.J., Cohen M.A., Nabet B., Buckley D.L., Guo Y.E., Hnisz D., Jaenisch R., Bradner J.E., Gray N.S., Young R.A. YY1 Is a Structural Regulator of Enhancer-Promoter Loops. Cell. 2017;171(7):1573-1588 e1528. PMID: 29224777.
170. Ran F.A., Hsu P.D., Wright J., Agarwala V., Scott D.A., Zhang F. Genome engineering using the CRISPR-Cas9 system. Nat Protoc. 2013;8(11):2281-2308. PMID: 24157548.
171. Guarnaccia A.D., Rose K.L., Wang J., Zhao B., Popay T.M., Wang C.E., Guerrazzi K., Hill S., Woodley C.M., Hansen T.J., Lorey S.L., Shaw J.G., Payne W.G., Weissmiller A.M., Olejniczak E.T., Fesik S.W., Liu Q., Tansey W.P. Impact of WIN site inhibitor on the WDR5 interactome. Cell Rep. 2021;34(3):108636. PMID: 33472061.

172. Cox J., Mann M. MaxQuant enables high peptide identification rates, individualized p.p.b.-range mass accuracies and proteome-wide protein quantification. Nat Biotechnol. 2008;26(12):1367-1372. PMID: 19029910.
173. Tyanova S., Temu T., Sinitcyn P., Carlson A., Hein M.Y., Geiger T., Mann M., Cox J. The Perseus computational platform for comprehensive analysis of (prote)omics data. Nat Methods. 2016;13(9):731-740. PMID: 27348712.
174. Mendez J., Stillman B. Chromatin association of human origin recognition complex, cdc6, and minichromosome maintenance proteins during the cell cycle: assembly of prereplication complexes in late mitosis. Mol Cell Biol. 2000;20(22):8602-8612. PMID: 11046155.
175. Nikolovska-Coleska Z., Wang R., Fang X., Pan H., Tomita Y., Li P., Roller P.P., Krajewski K., Saito N.G., Stuckey J.A., Wang S. Development and optimization of a binding assay for the XIAP BIR3 domain using fluorescence polarization. Anal Biochem. 2004;332(2):261-273. PMID: 15325294.
176. McCoy A.J., Grosse-Kunstleve R.W., Adams P.D., Winn M.D., Storoni L.C., Read R.J. Phaser crystallographic software. J Appl Crystallogr. 2007;40(Pt 4):658-674. PMID: 19461840.
177. Fry D.W., Harvey P.J., Keller P.R., Elliott W.L., Meade M., Trachet E., Albassam M., Zheng X., Leopold W.R., Pryer N.K., Toogood P.L. Specific inhibition of cyclin-dependent kinase 4/6 by PD 0332991 and associated antitumor activity in human tumor xenografts. Mol Cancer Ther. 2004;3(11):1427-1438. PMID: 15542782.
178. Vassilev L.T., Tovar C., Chen S., Knezevic D., Zhao X., Sun H., Heimbrook D.C., Chen L. Selective small-molecule inhibitor reveals critical mitotic functions of human CDK1. Proc Natl Acad Sci U S A. 2006;103(28):10660-10665. PMID: 16818887.
179. Roberts T.C., Hart J.R., Kaikkonen M.U., Weinberg M.S., Vogt P.K., Morris K.V. Quantification of nascent transcription by bromouridine immunocapture nuclear run-on RT-qPCR. Nat Protoc. 2015;10(8):1198-1211. PMID: 26182239.
180. Schindelin J., Arganda-Carreras I., Frise E., Kaynig V., Longair M., Pietzsch T., Preibisch S., Rueden C., Saalfeld S., Schmid B., Tinevez J.Y., White D.J., Hartenstein V., Eliceiri K., Tomancak P., Cardona A. Fiji: an open-source platform for biological-image analysis. Nat Methods. 2012;9(7):676-682. PMID: 22743772.
181. Mi H., Thomas P. PANTHER pathway: an ontology-based pathway database coupled with data analysis tools. Methods Mol Biol. 2009;563:123-140. PMID: 19597783.
182. Mi H., Muruganujan A., Ebert D., Huang X., Thomas P.D. PANTHER version 14: more genomes, a new PANTHER GO-slim and improvements in enrichment analysis tools. Nucleic Acids Res. 2019;47(D1):D419-D426. PMID: 30407594.
183. Mi H., Muruganujan A., Huang X., Ebert D., Mills C., Guo X., Thomas P.D. Protocol Update for large-scale genome and gene function analysis with the PANTHER classification system (v.14.0). Nat Protoc. 2019;14(3):703-721. PMID: 30804569.
184. Huang da W., Sherman B.T., Lempicki R.A. Bioinformatics enrichment tools: paths toward the comprehensive functional analysis of large gene lists. Nucleic Acids Res. 2009;37(1):1-13. PMID: 19033363.
185. Huang da W., Sherman B.T., Lempicki R.A. Systematic and integrative analysis of large gene lists using DAVID bioinformatics resources. Nat Protoc. 2009;4(1):44-57. PMID: 19131956.
186. Martin M. Cutadapt removes adapter sequences from high-throughput sequencing reads. EMBnetjournal. 2011;17(1):10-12.
187. Dobin A., Davis C.A., Schlesinger F., Drenkow J., Zaleski C., Jha S., Batut P., Chaisson M., Gingeras T.R. STAR: ultrafast universal RNA-seq aligner. Bioinformatics. 2013;29(1):15-21. PMID: 23104886.
188. Liao Y., Smyth G.K., Shi W. featureCounts: an efficient general purpose program for assigning sequence reads to genomic features. Bioinformatics. 2014;30(7):923-930. PMID: 24227677.
189. Love M.I., Huber W., Anders S. Moderated estimation of fold change and dispersion for RNA-seq data with DESeq2. Genome Biol. 2014;15(12):550. PMID: 25516281.

190. Ong S.E., Blagoev B., Kratchmarova I., Kristensen D.B., Steen H., Pandey A., Mann M. Stable isotope labeling by amino acids in cell culture, SILAC, as a simple and accurate approach to expression proteomics. Mol Cell Proteomics. 2002;1(5):376-386. PMID: 12118079.
191. Chen X., Wei S., Ji Y., Guo X., Yang F. Quantitative proteomics using SILAC: Principles, applications, and developments. Proteomics. 2015;15(18):3175-3192. PMID: 26097186.
192. Huttlin E.L., Bruckner R.J., Paulo J.A., Cannon J.R., Ting L., Baltier K., Colby G., Gebreab F., Gygi M.P., Parzen H., Szpyt J., Tam S., Zarraga G., Pontano-Vaites L., Swarup S., White A.E., Schweppe D.K., Rad R., Erickson B.K., Obar R.A., Guruharsha K.G., Li K., Artavanis-Tsakonas S., Gygi S.P., Harper J.W. Architecture of the human interactome defines protein communities and disease networks. Nature. 2017;545(7655):505-509. PMID: 28514442.
193. Rajendran V., Kalita P., Shukla H., Kumar A., Tripathi T. Aminoacyl-tRNA synthetases: Structure, function, and drug discovery. Int J Biol Macromol. 2018;111:400-414. PMID: 29305884.
194. Saxton R.A., Sabatini D.M. mTOR Signaling in Growth, Metabolism, and Disease. Cell. 2017;169(2):361-371. PMID: 28388417.
195. Mora A., Komander D., van Aalten D.M., Alessi D.R. PDK1, the master regulator of AGC kinase signal transduction. Semin Cell Dev Biol. 2004;15(2):161-170. PMID: 15209375.
196. Gagliardi P.A., Puliafito A., Primo L. PDK1: At the crossroad of cancer signaling pathways. Semin Cancer Biol. 2018;48:27-35. PMID: 28473254.
197. Warde-Farley D., Donaldson S.L., Comes O., Zuberi K., Badrawi R., Chao P., Franz M., Grouios C., Kazi F., Lopes C.T., Maitland A., Mostafavi S., Montojo J., Shao Q., Wright G., Bader G.D., Morris Q. The GeneMANIA prediction server: biological network integration for gene prioritization and predicting gene function. Nucleic Acids Res. 2010;38(Web Server issue):W214-220. PMID: 20576703.
198. Lai J.S., Herr W. Ethidium bromide provides a simple tool for identifying genuine DNA-independent protein associations. Proc Natl Acad Sci U S A. 1992;89(15):6958-6962. PMID: 1495986.
199. Sarbassov D.D., Ali S.M., Kim D.H., Guertin D.A., Latek R.R., Erdjument-Bromage H., Tempst P., Sabatini D.M. Rictor, a novel binding partner of mTOR, defines a rapamycin-insensitive and raptor-independent pathway that regulates the cytoskeleton. Curr Biol. 2004;14(14):1296-1302. PMID: 15268862.
200. Hara K., Maruki Y., Long X., Yoshino K., Oshiro N., Hidayat S., Tokunaga C., Avruch J., Yonezawa K. Raptor, a binding partner of target of rapamycin (TOR), mediates TOR action. Cell. 2002;110(2):177-189. PMID: 12150926.
201. Kim D.H., Sarbassov D.D., Ali S.M., King J.E., Latek R.R., Erdjument-Bromage H., Tempst P., Sabatini D.M. mTOR interacts with raptor to form a nutrient-sensitive complex that signals to the cell growth machinery. Cell. 2002;110(2):163-175. PMID: 12150925.
202. Park S.H., Ayoub A., Lee Y.T., Xu J., Kim H., Zheng W., Zhang B., Sha L., An S., Zhang Y., Cianfrocco M.A., Su M., Dou Y., Cho U.S. Cryo-EM structure of the human MLL1 core complex bound to the nucleosome. Nat Commun. 2019;10(1):5540. PMID: 31804488.
203. Xue H., Yao T., Cao M., Zhu G., Li Y., Yuan G., Chen Y., Lei M., Huang J. Structural basis of nucleosome recognition and modification by MLL methyltransferases. Nature. 2019;573(7774):445-449. PMID: 31485071.
204. Martelli A.M., Tabellini G., Bressanin D., Ognibene A., Goto K., Cocco L., Evangelisti C. The emerging multiple roles of nuclear Akt. Biochim Biophys Acta. 2012;1823(12):2168-2178. PMID: 22960641.
205. Baker S.J. PTEN enters the nuclear age. Cell. 2007;128(1):25-28. PMID: 17218252.
206. Salinas M., Lopez-Valdaliso R., Martin D., Alvarez A., Cuadrado A. Inhibition of PKB/Akt1 by C2-ceramide involves activation of ceramide-activated protein phosphatase in PC12 cells. Mol Cell Neurosci. 2000;15(2):156-169. PMID: 10673324.
207. Lim M.A., Kikani C.K., Wick M.J., Dong L.Q. Nuclear translocation of 3'-phosphoinositide-dependent protein kinase 1 (PDK-1): a potential regulatory mechanism for PDK-1 function. Proc Natl Acad Sci U S A. 2003;100(24):14006-14011. PMID: 14623982.

208. Scheid M.P., Parsons M., Woodgett J.R. Phosphoinositide-dependent phosphorylation of PDK1 regulates nuclear translocation. Mol Cell Biol. 2005;25(6):2347-2363. PMID: 15743829.
209. Sephton C.F., Zhang D., Lehmann T.M., Pennington P.R., Scheid M.P., Mousseau D.D. The nuclear localization of 3'-phosphoinositide-dependent kinase-1 is dependent on its association with the protein tyrosine phosphatase SHP-1. Cell Signal. 2009;21(11):1634-1644. PMID: 19591923.
210. Kim J.E., Chen J. Cytoplasmic-nuclear shuttling of FKBP12-rapamycin-associated protein is involved in rapamycin-sensitive signaling and translation initiation. Proc Natl Acad Sci U S A. 2000;97(26):14340-14345. PMID: 11114166.
211. Rosner M., Hengstschlager M. Cytoplasmic and nuclear distribution of the protein complexes mTORC1 and mTORC2: rapamycin triggers dephosphorylation and delocalization of the mTORC2 components rictor and sin1. Hum Mol Genet. 2008;17(19):2934-2948. PMID: 18614546.
212. Yadav R.B., Burgos P., Parker A.W., Iadevaia V., Proud C.G., Allen R.A., O'Connell J.P., Jeshtadi A., Stubbs C.D., Botchway S.W. mTOR direct interactions with Rheb-GTPase and raptor: sub-cellular localization using fluorescence lifetime imaging. BMC Cell Biol. 2013;14:3. PMID: 23311891.
213. Audet-Walsh E., Dufour C.R., Yee T., Zouanat F.Z., Yan M., Kalloghlian G., Vernier M., Caron M., Bourque G., Scarlata E., Hamel L., Brimo F., Aprikian A.G., Lapointe J., Chevalier S., Giguere V. Nuclear mTOR acts as a transcriptional integrator of the androgen signaling pathway in prostate cancer. Genes Dev. 2017;31(12):1228-1242. PMID: 28724614.
214. Zinzalla V., Stracka D., Oppliger W., Hall M.N. Activation of mTORC2 by association with the ribosome. Cell. 2011;144(5):757-768. PMID: 21376236.
215. Popenko V.I., Ivanova J.L., Cherny N.E., Filonenko V.V., Beresten S.F., Wolfson A.D., Kisselev L.L. Compartmentalization of certain components of the protein synthesis apparatus in mammalian cells. Eur J Cell Biol. 1994;65(1):60-69. PMID: 7889996.
216. Lund E., Dahlberg J.E. Proofreading and aminoacylation of tRNAs before export from the nucleus. Science. 1998;282(5396):2082-2085. PMID: 9851929.
217. Nathanson L., Deutscher M.P. Active aminoacyl-tRNA synthetases are present in nuclei as a high molecular weight multienzyme complex. J Biol Chem. 2000;275(41):31559-31562. PMID: 10930398.
218. Fu G., Xu T., Shi Y., Wei N., Yang X.L. tRNA-controlled nuclear import of a human tRNA synthetase. J Biol Chem. 2012;287(12):9330-9334. PMID: 22291016.
219. Alessi D.R., James S.R., Downes C.P., Holmes A.B., Gaffney P.R., Reese C.B., Cohen P. Characterization of a 3-phosphoinositide-dependent protein kinase which phosphorylates and activates protein kinase Balpha. Curr Biol. 1997;7(4):261-269. PMID: 9094314.
220. Sarbassov D.D., Guertin D.A., Ali S.M., Sabatini D.M. Phosphorylation and regulation of Akt/PKB by the rictor-mTOR complex. Science. 2005;307(5712):1098-1101. PMID: 15718470.
221. Jiang N., Dai Q., Su X., Fu J., Feng X., Peng J. Role of PI3K/AKT pathway in cancer: the framework of malignant behavior. Mol Biol Rep. 2020;47(6):4587-4629. PMID: 32333246.
222. Bayascas J.R. PDK1: the major transducer of PI 3-kinase actions. Curr Top Microbiol Immunol. 2010;346:9-29. PMID: 20563709.
223. Stokoe D., Stephens L.R., Copeland T., Gaffney P.R., Reese C.B., Painter G.F., Holmes A.B., McCormick F., Hawkins P.T. Dual role of phosphatidylinositol-3,4,5-trisphosphate in the activation of protein kinase B. Science. 1997;277(5325):567-570. PMID: 9228007.
224. Alessi D.R., Kozlowski M.T., Weng Q.P., Morrice N., Avruch J. 3-Phosphoinositide-dependent protein kinase 1 (PDK1) phosphorylates and activates the p70 S6 kinase in vivo and in vitro. Curr Biol. 1998;8(2):69-81. PMID: 9427642.
225. Pullen N., Dennis P.B., Andjelkovic M., Dufner A., Kozma S.C., Hemmings B.A., Thomas G. Phosphorylation and activation of p70s6k by PDK1. Science. 1998;279(5351):707-710. PMID: 9445476.
226. Kobayashi T., Cohen P. Activation of serum- and glucocorticoid-regulated protein kinase by agonists that activate phosphatidylinositide 3-kinase is mediated by 3-phosphoinositide-

dependent protein kinase-1 (PDK1) and PDK2. Biochem J. 1999;339 (Pt 2):319-328. PMID: 10191262.
227. Park J., Leong M.L., Buse P., Maiyar A.C., Firestone G.L., Hemmings B.A. Serum and glucocorticoid-inducible kinase (SGK) is a target of the PI 3-kinase-stimulated signaling pathway. EMBO J. 1999;18(11):3024-3033. PMID: 10357815.
228. Jensen C.J., Buch M.B., Krag T.O., Hemmings B.A., Gammeltoft S., Frodin M. 90-kDa ribosomal S6 kinase is phosphorylated and activated by 3-phosphoinositide-dependent protein kinase-1. J Biol Chem. 1999;274(38):27168-27176. PMID: 10480933.
229. Arencibia J.M., Pastor-Flores D., Bauer A.F., Schulze J.O., Biondi R.M. AGC protein kinases: from structural mechanism of regulation to allosteric drug development for the treatment of human diseases. Biochim Biophys Acta. 2013;1834(7):1302-1321. PMID: 23524293.
230. Anderson K.E., Coadwell J., Stephens L.R., Hawkins P.T. Translocation of PDK-1 to the plasma membrane is important in allowing PDK-1 to activate protein kinase B. Curr Biol. 1998;8(12):684-691. PMID: 9637919.
231. Kikani C.K., Dong L.Q., Liu F. "New"-clear functions of PDK1: beyond a master kinase in the cytosol? J Cell Biochem. 2005;96(6):1157-1162. PMID: 16187290.
232. Najafov A., Sommer E.M., Axten J.M., Deyoung M.P., Alessi D.R. Characterization of GSK2334470, a novel and highly specific inhibitor of PDK1. Biochem J. 2011;433(2):357-369. PMID: 21087210.
233. Avdic V., Zhang P., Lanouette S., Voronova A., Skerjanc I., Couture J.F. Fine-tuning the stimulation of MLL1 methyltransferase activity by a histone H3-based peptide mimetic. FASEB J. 2011;25(3):960-967. PMID: 21135039.
234. Huang H., Sabari B.R., Garcia B.A., Allis C.D., Zhao Y. SnapShot: histone modifications. Cell. 2014;159(2):458-458 e451. PMID: 25303536.
235. Yeom J., Ju S., Choi Y., Paek E., Lee C. Comprehensive analysis of human protein N-termini enables assessment of various protein forms. Sci Rep. 2017;7(1):6599. PMID: 28747677.
236. Dutil E.M., Toker A., Newton A.C. Regulation of conventional protein kinase C isozymes by phosphoinositide-dependent kinase 1 (PDK-1). Curr Biol. 1998;8(25):1366-1375. PMID: 9889098.
237. Le Good J.A., Ziegler W.H., Parekh D.B., Alessi D.R., Cohen P., Parker P.J. Protein kinase C isotypes controlled by phosphoinositide 3-kinase through the protein kinase PDK1. Science. 1998;281(5385):2042-2045. PMID: 9748166.
238. Balendran A., Hare G.R., Kieloch A., Williams M.R., Alessi D.R. Further evidence that 3-phosphoinositide-dependent protein kinase-1 (PDK1) is required for the stability and phosphorylation of protein kinase C (PKC) isoforms. FEBS Lett. 2000;484(3):217-223. PMID: 11078882.
239. Ree R., Varland S., Arnesen T. Spotlight on protein N-terminal acetylation. Exp Mol Med. 2018;50(7):1-13. PMID: 30054468.
240. Koufaris C., Kirmizis A. N-Terminal Acetyltransferases Are Cancer-Essential Genes Prevalently Upregulated in Tumours. Cancers (Basel). 2020;12(9). PMID: 32942614.
241. Dong L.Q., Ramos F.J., Wick M.J., Lim M.A., Guo Z., Strong R., Richardson A., Liu F. Cloning and characterization of a testis and brain-specific isoform of mouse 3'-phosphoinositide-dependent protein kinase-1, mPDK-1 beta. Biochem Biophys Res Commun. 2002;294(1):136-144. PMID: 12054753.
242. Lange P.F., Huesgen P.F., Nguyen K., Overall C.M. Annotating N termini for the human proteome project: N termini and Nalpha-acetylation status differentiate stable cleaved protein species from degradation remnants in the human erythrocyte proteome. J Proteome Res. 2014;13(4):2028-2044. PMID: 24555563.
243. Hazeslip L., Zafar M.K., Chauhan M.Z., Byrd A.K. Genome Maintenance by DNA Helicase B. Genes (Basel). 2020;11(5). PMID: 32455610.

244. Gu J., Xia X., Yan P., Liu H., Podust V.N., Reynolds A.B., Fanning E. Cell cycle-dependent regulation of a human DNA helicase that localizes in DNA damage foci. Mol Biol Cell. 2004;15(7):3320-3332. PMID: 15146062.
245. Guler G.D., Liu H., Vaithiyalingam S., Arnett D.R., Kremmer E., Chazin W.J., Fanning E. Human DNA helicase B (HDHB) binds to replication protein A and facilitates cellular recovery from replication stress. J Biol Chem. 2012;287(9):6469-6481. PMID: 22194613.
246. Chun J., Kwon T., Lee E.J., Hyun S., Hong S.K., Kang S.S. The subcellular localization of 3-phosphoinositide-dependent protein kinase is controlled by caveolin-1 binding. Biochem Biophys Res Commun. 2005;326(1):136-146. PMID: 15567163.
247. Lee K.Y., D'Acquisto F., Hayden M.S., Shim J.H., Ghosh S. PDK1 nucleates T cell receptor-induced signaling complex for NF-kappaB activation. Science. 2005;308(5718):114-118. PMID: 15802604.
248. Fan R., Kim N.G., Gumbiner B.M. Regulation of Hippo pathway by mitogenic growth factors via phosphoinositide 3-kinase and phosphoinositide-dependent kinase-1. Proc Natl Acad Sci U S A. 2013;110(7):2569-2574. PMID: 23359693.
249. Scortegagna M., Ruller C., Feng Y., Lazova R., Kluger H., Li J.L., De S.K., Rickert R., Pellecchia M., Bosenberg M., Ronai Z.A. Genetic inactivation or pharmacological inhibition of Pdk1 delays development and inhibits metastasis of Braf(V600E)::Pten(-/-) melanoma. Oncogene. 2014;33(34):4330-4339. PMID: 24037523.
250. Yang Z., Wu Z., Liu T., Han L., Wang C., Yang B., Zheng F. Upregulation of PDK1 associates with poor prognosis in esophageal squamous cell carcinoma with facilitating tumorigenicity in vitro. Med Oncol. 2014;31(12):337. PMID: 25416048.
251. Zabkiewicz J., Pearn L., Hills R.K., Morgan R.G., Tonks A., Burnett A.K., Darley R.L. The PDK1 master kinase is over-expressed in acute myeloid leukemia and promotes PKC-mediated survival of leukemic blasts. Haematologica. 2014;99(5):858-864. PMID: 24334295.
252. Bai X., Li P., Xie Y., Guo C., Sun Y., Xu Q., Zhao D. Overexpression of 3-phosphoinositide-dependent protein kinase-1 is associated with prognosis of gastric carcinoma. Tumour Biol. 2016;37(2):2333-2339. PMID: 26373731.
253. Wang J., Liu F., Ao P., Li X., Zheng H., Wu D., Zhang N., She J., Yuan J., Wu X. Correlation of PDK1 expression with clinicopathologic features and prognosis of hepatocellular carcinoma. Onco Targets Ther. 2016;9:5597-5602. PMID: 27672330.
254. Jing P., Zhou S., Xu P., Cui P., Liu X., Liu X., Liu X., Wang H., Xu W. PDK1 promotes metastasis by inducing epithelial-mesenchymal transition in hypopharyngeal carcinoma via the Notch1 signaling pathway. Exp Cell Res. 2020;386(2):111746. PMID: 31778670.
255. Maurer M., Su T., Saal L.H., Koujak S., Hopkins B.D., Barkley C.R., Wu J., Nandula S., Dutta B., Xie Y., Chin Y.R., Kim D.I., Ferris J.S., Gruvberger-Saal S.K., Laakso M., Wang X., Memeo L., Rojtman A., Matos T., Yu J.S., Cordon-Cardo C., Isola J., Terry M.B., Toker A., Mills G.B., Zhao J.J., Murty V.V., Hibshoosh H., Parsons R. 3-Phosphoinositide-dependent kinase 1 potentiates upstream lesions on the phosphatidylinositol 3-kinase pathway in breast carcinoma. Cancer Res. 2009;69(15):6299-6306. PMID: 19602588.
256. Choucair K.A., Guerard K.P., Ejdelman J., Chevalier S., Yoshimoto M., Scarlata E., Fazli L., Sircar K., Squire J.A., Brimo F., Cunha I.W., Aprikian A., Gleave M., Lapointe J. The 16p13.3 (PDPK1) Genomic Gain in Prostate Cancer: A Potential Role in Disease Progression. Transl Oncol. 2012;5(6):453-460. PMID: 23401739.
257. Ebrahimizadeh W., Guerard K.P., Rouzbeh S., Bramhecha Y.M., Scarlata E., Brimo F., Patel P.G., Jamaspishvili T., Aprikian A.G., Berman D., Bartlett J.M.S., Chevalier S., Lapointe J. Design and Development of a Fully Synthetic Multiplex Ligation-Dependent Probe Amplification-Based Probe Mix for Detection of Copy Number Alterations in Prostate Cancer Formalin-Fixed, Paraffin-Embedded Tissue Samples. J Mol Diagn. 2020;22(10):1246-1263. PMID: 32763409.
258. Zeng X., Xu H., Glazer R.I. Transformation of mammary epithelial cells by 3-phosphoinositide-dependent protein kinase-1 (PDK1) is associated with the induction of protein kinase Calpha. Cancer Res. 2002;62(12):3538-3543. PMID: 12068001.

259. Xie Z., Yuan H., Yin Y., Zeng X., Bai R., Glazer R.I. 3-phosphoinositide-dependent protein kinase-1 (PDK1) promotes invasion and activation of matrix metalloproteinases. BMC Cancer. 2006;6:77. PMID: 16551362.
260. Gagliardi P.A., di Blasio L., Orso F., Seano G., Sessa R., Taverna D., Bussolino F., Primo L. 3-phosphoinositide-dependent kinase 1 controls breast tumor growth in a kinase-dependent but Akt-independent manner. Neoplasia. 2012;14(8):719-731. PMID: 22952425.
261. Emmanouilidi A., Fyffe C.A., Ferro R., Edling C.E., Capone E., Sestito S., Rapposelli S., Lattanzio R., Iacobelli S., Sala G., Maffucci T., Falasca M. Preclinical validation of 3-phosphoinositide-dependent protein kinase 1 inhibition in pancreatic cancer. J Exp Clin Cancer Res. 2019;38(1):191. PMID: 31088502.
262. Hu T., Li C., Zhang Y., Wang L., Peng L., Cheng H., Wang W., Chu Y., Xu M., Cheng T., Yuan W. Phosphoinositide-dependent kinase 1 regulates leukemia stem cell maintenance in MLL-AF9-induced murine acute myeloid leukemia. Biochem Biophys Res Commun. 2015;459(4):692-698. PMID: 25769952.
263. Nabet B., Roberts J.M., Buckley D.L., Paulk J., Dastjerdi S., Yang A., Leggett A.L., Erb M.A., Lawlor M.A., Souza A., Scott T.G., Vittori S., Perry J.A., Qi J., Winter G.E., Wong K.K., Gray N.S., Bradner J.E. The dTAG system for immediate and target-specific protein degradation. Nat Chem Biol. 2018;14(5):431-441. PMID: 29581585.
264. Asatsuma-Okumura T., Ito T., Handa H. Molecular mechanisms of cereblon-based drugs. Pharmacol Ther. 2019;202:132-139. PMID: 31202702.
265. Huang H.T., Seo H.S., Zhang T., Wang Y., Jiang B., Li Q., Buckley D.L., Nabet B., Roberts J.M., Paulk J., Dastjerdi S., Winter G.E., McLauchlan H., Moran J., Bradner J.E., Eck M.J., Dhe-Paganon S., Zhao J.J., Gray N.S. MELK is not necessary for the proliferation of basal-like breast cancer cells. Elife. 2017;6. PMID: 28926338.
266. Morrison L.J., Cochran A.J., Gibson A.A., Willoughby M.L., More I.A. Establishment and characterization of human neuroblastoma and ganglioneuroblastoma cell lines. Br J Cancer. 1982;45(4):531-542. PMID: 7073944.
267. Subramanian A., Tamayo P., Mootha V.K., Mukherjee S., Ebert B.L., Gillette M.A., Paulovich A., Pomeroy S.L., Golub T.R., Lander E.S., Mesirov J.P. Gene set enrichment analysis: a knowledge-based approach for interpreting genome-wide expression profiles. Proc Natl Acad Sci U S A. 2005;102(43):15545-15550. PMID: 16199517.
268. Liberzon A., Birger C., Thorvaldsdottir H., Ghandi M., Mesirov J.P., Tamayo P. The Molecular Signatures Database (MSigDB) hallmark gene set collection. Cell Syst. 2015;1(6):417-425. PMID: 26771021.
269. Nakamura K., Sakaue H., Nishizawa A., Matsuki Y., Gomi H., Watanabe E., Hiramatsua R., Tamamori-Adachi M., Kitajima S., Noda T., Ogawa W., Kasuga M. PDK1 regulates cell proliferation and cell cycle progression through control of cyclin D1 and p27Kip1 expression. J Biol Chem. 2008;283(25):17702-17711. PMID: 18430722.
270. Wang Z., Ahmad A., Li Y., Banerjee S., Kong D., Sarkar F.H. Forkhead box M1 transcription factor: a novel target for cancer therapy. Cancer Treat Rev. 2010;36(2):151-156. PMID: 20022709.
271. Bimbo A., Liu J., Balasubramanian M.K. Roles of Pdk1p, a fission yeast protein related to phosphoinositide-dependent protein kinase, in the regulation of mitosis and cytokinesis. Mol Biol Cell. 2005;16(7):3162-3175. PMID: 15857958.
272. Niederberger C., Schweingruber M.E. A Schizosaccharomyces pombe gene, ksg1, that shows structural homology to the human phosphoinositide-dependent protein kinase PDK1, is essential for growth, mating and sporulation. Mol Gen Genet. 1999;261(1):177-183. PMID: 10071224.
273. Hornbeck P.V., Zhang B., Murray B., Kornhauser J.M., Latham V., Skrzypek E. PhosphoSitePlus, 2014: mutations, PTMs and recalibrations. Nucleic Acids Res. 2015;43(Database issue):D512-520. PMID: 25514926.
274. Tu W.B., Helander S., Pilstal R., Hickman K.A., Lourenco C., Jurisica I., Raught B., Wallner B., Sunnerhagen M., Penn L.Z. Myc and its interactors take shape. Biochim Biophys Acta. 2015;1849(5):469-483. PMID: 24933113.

275. Bassik M.C., Kampmann M., Lebbink R.J., Wang S., Hein M.Y., Poser I., Weibezahn J., Horlbeck M.A., Chen S., Mann M., Hyman A.A., Leproust E.M., McManus M.T., Weissman J.S. A systematic mammalian genetic interaction map reveals pathways underlying ricin susceptibility. Cell. 2013;152(4):909-922. PMID: 23394947.
276. Navarro Negredo P., Edgar J.R., Manna P.T., Antrobus R., Robinson M.S. The WDR11 complex facilitates the tethering of AP-1-derived vesicles. Nat Commun. 2018;9(1):596. PMID: 29426865.
277. Kim H.G., Ahn J.W., Kurth I., Ullmann R., Kim H.T., Kulharya A., Ha K.S., Itokawa Y., Meliciani I., Wenzel W., Lee D., Rosenberger G., Ozata M., Bick D.P., Sherins R.J., Nagase T., Tekin M., Kim S.H., Kim C.H., Ropers H.H., Gusella J.F., Kalscheuer V., Choi C.Y., Layman L.C. WDR11, a WD protein that interacts with transcription factor EMX1, is mutated in idiopathic hypogonadotropic hypogonadism and Kallmann syndrome. Am J Hum Genet. 2010;87(4):465-479. PMID: 20887964.
278. Quaynor S.D., Kim H.G., Cappello E.M., Williams T., Chorich L.P., Bick D.P., Sherins R.J., Layman L.C. The prevalence of digenic mutations in patients with normosmic hypogonadotropic hypogonadism and Kallmann syndrome. Fertil Steril. 2011;96(6):1424-1430 e1426. PMID: 22035731.
279. Kim H.G., Layman L.C. The role of CHD7 and the newly identified WDR11 gene in patients with idiopathic hypogonadotropic hypogonadism and Kallmann syndrome. Mol Cell Endocrinol. 2011;346(1-2):74-83. PMID: 21856375.
280. McCormack S.E., Li D., Kim Y.J., Lee J.Y., Kim S.H., Rapaport R., Levine M.A. Digenic Inheritance of PROKR2 and WDR11 Mutations in Pituitary Stalk Interruption Syndrome. J Clin Endocrinol Metab. 2017;102(7):2501-2507. PMID: 28453858.
281. Choucair N., Abou Ghoch J., Fawaz A., Megarbane A., Chouery E. 10q26.1 Microdeletion: Redefining the critical regions for microcephaly and genital anomalies. Am J Med Genet A. 2015;167A(11):2707-2713. PMID: 26114870.
282. Sutani A., Shima H., Hijikata A., Hosokawa S., Katoh-Fukui Y., Takasawa K., Suzuki E., Doi S., Shirai T., Morio T., Fukami M., Kashimada K. WDR11 is another causative gene for coloboma, cardiac anomaly and growth retardation in 10q26 deletion syndrome. Eur J Med Genet. 2020;63(1):103626. PMID: 30711679.
283. Kim Y.J., Osborn D.P., Lee J.Y., Araki M., Araki K., Mohun T., Kansakoski J., Brandstack N., Kim H.T., Miralles F., Kim C.H., Brown N.A., Kim H.G., Martinez-Barbera J.P., Ataliotis P., Raivio T., Layman L.C., Kim S.H. WDR11-mediated Hedgehog signalling defects underlie a new ciliopathy related to Kallmann syndrome. EMBO Rep. 2018;19(2):269-289. PMID: 29263200.
284. Chernova O.B., Hunyadi A., Malaj E., Pan H., Crooks C., Roe B., Cowell J.K. A novel member of the WD-repeat gene family, WDR11, maps to the 10q26 region and is disrupted by a chromosome translocation in human glioblastoma cells. Oncogene. 2001;20(38):5378-5392. PMID: 11536051.
285. Jonsson G., Staaf J., Olsson E., Heidenblad M., Vallon-Christersson J., Osoegawa K., de Jong P., Oredsson S., Ringner M., Hoglund M., Borg A. High-resolution genomic profiles of breast cancer cell lines assessed by tiling BAC array comparative genomic hybridization. Genes Chromosomes Cancer. 2007;46(6):543-558. PMID: 17334996.
286. Wei L., Murphy B.L., Wu G., Parker M., Easton J., Gilbertson R.J., Zhang J., Roussel M.F. Exome sequencing analysis of murine medulloblastoma models identifies WDR11 as a potential tumor suppressor in Group 3 tumors. Oncotarget. 2017;8(39):64685-64697. PMID: 29029386.
287. Charron J., Malynn B.A., Fisher P., Stewart V., Jeannotte L., Goff S.P., Robertson E.J., Alt F.W. Embryonic lethality in mice homozygous for a targeted disruption of the N-myc gene. Genes Dev. 1992;6(12A):2248-2257. PMID: 1459450.
288. Davis A.C., Wims M., Spotts G.D., Hann S.R., Bradley A. A null c-myc mutation causes lethality before 10.5 days of gestation in homozygotes and reduced fertility in heterozygous female mice. Genes Dev. 1993;7(4):671-682. PMID: 8458579.
289. Oliver T.G., Grasfeder L.L., Carroll A.L., Kaiser C., Gillingham C.L., Lin S.M., Wickramasinghe R., Scott M.P., Wechsler-Reya R.J. Transcriptional profiling of the Sonic

hedgehog response: a critical role for N-myc in proliferation of neuronal precursors. Proc Natl Acad Sci U S A. 2003;100(12):7331-7336. PMID: 12777630.
290. Ryl T., Kuchen E.E., Bell E., Shao C., Florez A.F., Monke G., Gogolin S., Friedrich M., Lamprecht F., Westermann F., Hofer T. Cell-Cycle Position of Single MYC-Driven Cancer Cells Dictates Their Susceptibility to a Chemotherapeutic Drug. Cell Syst. 2017;5(3):237-250 e238. PMID: 28843484.
291. Fu W., Hall M.N. Regulation of mTORC2 Signaling. Genes (Basel). 2020;11(9). PMID: 32899613.
292. Tasaki T., Sriram S.M., Park K.S., Kwon Y.T. The N-end rule pathway. Annu Rev Biochem. 2012;81:261-289. PMID: 22524314.
293. Shearer R.F., Iconomou M., Watts C.K., Saunders D.N. Functional Roles of the E3 Ubiquitin Ligase UBR5 in Cancer. Mol Cancer Res. 2015;13(12):1523-1532. PMID: 26464214.
294. Qiao X., Liu Y., Prada M.L., Mohan A.K., Gupta A., Jaiswal A., Sharma M., Merisaari J., Haikala H.M., Talvinen K., Yetukuri L., Pylvanainen J.W., Klefstrom J., Kronqvist P., Meinander A., Aittokallio T., Hietakangas V., Eilers M., Westermarck J. UBR5 Is Coamplified with MYC in Breast Tumors and Encodes an Ubiquitin Ligase That Limits MYC-Dependent Apoptosis. Cancer Res. 2020;80(7):1414-1427. PMID: 32029551.
295. Schukur L., Zimmermann T., Niewoehner O., Kerr G., Gleim S., Bauer-Probst B., Knapp B., Galli G.G., Liang X., Mendiola A., Reece-Hoyes J., Rapti M., Barbosa I., Reschke M., Radimerski T., Thoma C.R. Identification of the HECT E3 ligase UBR5 as a regulator of MYC degradation using a CRISPR/Cas9 screen. Sci Rep. 2020;10(1):20044. PMID: 33208877.
296. Sood S., Weber C.M., Hodges H.C., Krokhotin A., Shalizi A., Crabtree G.R. CHD8 dosage regulates transcription in pluripotency and early murine neural differentiation. Proc Natl Acad Sci U S A. 2020;117(36):22331-22340. PMID: 32839322.
297. Barnard R.A., Pomaville M.B., O'Roak B.J. Mutations and Modeling of the Chromatin Remodeler CHD8 Define an Emerging Autism Etiology. Front Neurosci. 2015;9:477. PMID: 26733790.
298. Subtil-Rodriguez A., Vazquez-Chavez E., Ceballos-Chavez M., Rodriguez-Paredes M., Martin-Subero J.I., Esteller M., Reyes J.C. The chromatin remodeller CHD8 is required for E2F-dependent transcription activation of S-phase genes. Nucleic Acids Res. 2014;42(4):2185-2196. PMID: 24265227.
299. Masso-Valles D., Soucek L. Blocking Myc to Treat Cancer: Reflecting on Two Decades of Omomyc. Cells. 2020;9(4). PMID: 32260326.
300. Stirnimann C.U., Petsalaki E., Russell R.B., Muller C.W. WD40 proteins propel cellular networks. Trends Biochem Sci. 2010;35(10):565-574. PMID: 20451393.
301. Schapira M., Tyers M., Torrent M., Arrowsmith C.H. WD40 repeat domain proteins: a novel target class? Nat Rev Drug Discov. 2017;16(11):773-786. PMID: 29026209.